# A Distributive Approach of Microgrid Control based on System Frequency

Ashil Thomas

Delft University of Technology

TU Delft
Delft University of Technology

Challenge the future

*This page is intentionally left blank.*

# A Distributive Approach of Microgrid Control based on System Frequency

By

**Ashil Thomas**

in partial fulfilment of the requirements for the degree of

**Master of Science**
in Sustainable Energy Technology
*Electrical Sustainable Energy*

at the Delft University of Technology,
to be defended publicly on Tuesday August 30, 2017 at 02:00 PM.

| | | |
|---|---|---|
| Student number: | 4508254 | |
| Supervisor: | Prof. Dr.ir. P. Bauer | TU Delft |
| Daily Supervisor: | Dr. S. Izadkhast | TU Delft |
| | Rick Scharrenberg | DNV-GL |
| Thesis committee: | Dr.ir. J. Dong | TU Delft |
| | Dr.ir. M. Popov | TU Delft |
| | Dr. Ir. Jos van der Burgt | DNV-GL |

*This page is intentionally left blank.*

# Abstract

The world at large is passing through a phase of energy transformation – from a traditional centralized unidirectional to a decentralized and distributed bidirectional power system, with consumers becoming prosumers. Facilitated by the technological advancements in power electronics and growing concerns over climatic changes, this transformation lead to increasing deployment of renewable energy sources. All these converge to the evolution of a concept – *Microgrid*, which empowers *Smart Grid of the Future.*

In the thesis, the concept of *Cell*, a microgrid comprising of Distributed renewable energy sources like solar, wind etc., Battery energy storage systems and Controllable loads is conceived. Devoid of use of any communication equipment, the Cell relies on measurements of local variables for evaluating the State of Energy and Power. The primary focus is on the formulation of control strategy based on droop control that enables a seamless (dis)connection of Cell with External Grid, with still maintaining the operation of converter in voltage source mode. This control scheme is further extended for connection and disconnection of multiple Cells interconnected through a Backbone bus, referred to as Interconnected mode. Adding to this, a decision-making algorithm is developed for an autonomous operation of Cells, that determines the switching instants between Stand-alone and Interconnected modes.

The developed control strategy and automated decision-making algorithm was simulated in DIgSILENT PowerFactory software for varied scenarios to evaluate the performance and the overall stability of the system. The simulations show a seamless transition between different operating modes – Stand-alone, Interconnected and Grid-connected and the automated decision-making algorithm succeeded in achieving overall stability, increasing the reliability of power to end consumers. Experiments were performed on a standard converter to prove the practical implementation capability of the developed control scheme as an intermediate interface. The modular and distributed nature of the developed controls and algorithm, makes it's advantageous to apply such Cells to electrify remote areas, which have limited or no access to power. The system can be easily scaled and expanded by adding more Cells, to build a strong and robust microgrid network.

**Keywords:** Microgrid, Smart Grid, Distributed Renewable Energy Sources, Battery Energy Storage System, Droop Control, Voltage Source Converter, PowerFactory, Stand-alone, Grid-connected and Interconnected mode

*This page is intentionally left blank.*

# Acknowledgement

This report is the outcome of nine months of research work on CSGriP project, conducted as a partial fulfilment of the requirements for degree of Master of Science in Sustainable Energy Technology at TU Delft. The thesis was conducted in TU Delft and in DNV GL – Energy.

I would like to express my sincere gratitude to Prof. Pavol Bauer, for introducing me to the CSGriP project and the consortium and giving me guidance and advice throughout my graduation project. Also, special thanks to Seyedmahdi Izadkhast, my postdoc supervisor in TU Delft for all the long hours of discussion and providing me with interesting inputs and feedback on the work.

Furthermore, I would like to extend my thanks to Jos van der Burgt, my company supervisor, for giving me an opportunity to work in the prestigious company and for all his support and guidance. Working with company gave me a valuable international experience and the diverse field of expertise of the company enriched my knowledge on the sector. My heartfelt thanks to Rick Scharrenberg who assisted me during the entire phase of the graduation project, starting from familiarization of company and the project. I would also like to appreciate his effort to address my queries and guide me through the process.

Moreover, a special credit to Ballard Asare Bediako for supporting me to perform the tests for validation of the developed control algorithm at HAN University. Also, I would thank all the partners of CSGriP project and employees in DNV-GL for their valuable remarks and input.

Additionally, I would like to thank Nikolaos Bilidis and Thijs Vral for the cooperation in transferring their knowledge and expertise about the developed models for the project. Their input was commendable for completion of my thesis.

Finally, I am in debt to my family and friends who gave all the support and encouragement during the good and tough times. I would like to express my heartfelt thanks to all of them for their support and prayers through all times.

*Ashil Thomas*
*Delft, August 2017*

*This page is intentionally left blank.*

# Contents

List of Figures ........ xiii
List of Tables ........ xvii
List of Abbreviations ........ xix

**1 INTRODUCTION ........ 1**

1.1 Motivation ........ 1
1.2 Problem Definition ........ 1
1.3 Research Objective & Questions ........ 3
1.4 Research Approach & Methodology ........ 3
1.5 Thesis Outline ........ 4

**2 THEORETICAL BACKGROUND ........ 5**

2.1 Introduction ........ 5
2.2 Microgrid ........ 5
2.2.1 Distributed Generation ........ 6
2.2.2 Role of ESS ........ 7
2.2.3 Interfacing power converters ........ 7
2.3 Control Schemes of Converters ........ 8
2.4 MG Control Architecture ........ 9
2.4.1 Hierarchical control ........ 10
2.4.2 Centralized Vs Decentralized control ........ 11
2.5 Demand Side Management ........ 14
2.6 Supply Side Management ........ 15
2.7 Transition of Operating modes of MG ........ 16
2.8 Identified gaps and challenges ........ 17
2.9 Summary ........ 17

**3 MODELLING OF MICROGRID ........ 19**

3.1 Introduction ........ 19
3.2 MG Architecture ........ 19
3.3 Battery Energy Storage System ........ 21
3.4 Voltage Source Converter ........ 23
3.5 LCL Filter ........ 24
3.6 DRES ........ 26
3.7 Load ........ 28
3.8 Cables & lines ........ 31
3.9 Summary ........ 32

**4 CONTROL FOR SEAMLESS (DIS)CONNECTION ........ 33**

4.1 Introduction ........ 33
4.2 Droop Control ........ 34
4.3 Frequency – Voltage Control ........ 35
4.3.1 Normal Controller ........ 36

4.3.2 Connection Controller ..... 39
4.3.3 Disconnection Controller ..... 41
4.3.4 Set point calculation ..... 42
4.3.5 Switching Logic ..... 43
4.4 Summary ..... 44

**5 AUTOMATED DECISION ALGORITHM ..... 45**

5.1 Introduction ..... 45
5.2 Decision-making algorithm ..... 45
5.2.1 MG Structure, Control & Objective ..... 45
5.2.2 Defining Limits ..... 47
5.2.3 Need Help State ..... 48
5.2.4 RH State ..... 50
5.2.5 DISC State ..... 51
5.3 Modelling & Control flow ..... 52
5.3.1 NH flow diagram ..... 53
5.3.2 RH flow diagram ..... 59
5.3.3 DISC flow diagram ..... 63
5.3.4 Mode Change ..... 65
5.4 Summary ..... 65

**6 SIMULATIONS & RESULTS ..... 67**

6.1 Introduction ..... 67
6.2 Sizing and Selection of parameters ..... 67
6.3 Simulation results – Seamless (dis)connection ..... 68
6.3.1 Case I: Single Cell transition between SA & GC mode ..... 68
6.3.2 Case II: Multiple cells transition between SA & IC mode ..... 81
6.4 Simulation results – Automated Decision algorithm ..... 88
6.4.1 Case I: 2 Cells Low SoC, No Cells High SoC ..... 89
6.4.2 Case II: No Cells Low SoC, 2 Cells High SoC ..... 90
6.4.3 Case III: 2 Cells Low SoC, 2 Cells High SoC ..... 91
6.4.4 Case IV: 1 Cell Very High SoC ..... 93
6.4.5 Case V: Past/forecasted energy profile ..... 96
6.4.6 Case VI: 2 Cells Low SoC, 1 Cell High SoC ..... 99
6.4.7 Case VII: MG Case in Netherlands ..... 103
6.5 Summary ..... 106

**7 VALIDATION ..... 109**

7.1 Introduction ..... 109
7.2 Experimental Set-up ..... 109
7.2.1 Single Line Diagram ..... 110
7.2.2 Limitations ..... 111
7.2.3 VACON converter ..... 111
7.3 Testing ..... 114
7.3.1 Parameters ..... 114
7.3.2 Test A – Stand-alone mode ..... 115

7.3.3 Test B – Grid connected mode – Internal Sync ........ 116
7.3.4 Test C – Grid connected mode – Manual Sync ........ 116
7.4 Summary ........ 117
**8 CONCLUSIONS AND FUTURE WORK ........ 119**
8.1 Conclusions ........ 119
8.2 Future work ........ 120
**BIBLIOGRAPHY ........ 121**
**APPENDICES ........ 125**

*This page is intentionally left blank.*

# List of Figures


Figure 1.2: SOPRA Cell [6] .... 2
Figure 1.3: Multiple cells interconnected through a Backbone [6] .... 2
Figure 1.4: Multiple cells interconnected with main External Grid [6] .... 2
Figure 1.5: Individual cell connected to main External Grid .... 3
Figure 2.1: General MG architecture [11] .... 5
Figure 2.2: Grid-forming converter [5] .... 8
Figure 2.3: Grid-feeding converter [5] .... 9
Figure 2.4: Grid-supporting converter – current source [5] .... 9
Figure 2.5: Grid-supporting converter – voltage source [5] .... 9
Figure 2.6: Three-level hierarchical control [3] .... 10
Figure 2.7: Primary and Secondary response of hierarchical control [29] .... 10
Figure 2.8: Tertiary response of hierarchical control [29] .... 11
Figure 2.9: Equivalent circuit for power flow through a line [34] .... 13
Figure 3.1: Single Cell Architecture .... 19
Figure 3.2: Multiple Cells interconnected through Backbone bus .... 20
Figure 3.3: Multiple Cells interconnected through Backbone bus with External Grid .... 20
Figure 3.4: Equivalent circuit of battery [34] .... 21
Figure 3.5: Terminal voltage dependency on SoC [45] .... 22
Figure 3.6: Battery model .... 22
Figure 3.7: PWM Converter – Equivalent circuit [46] .... 23
Figure 3.8: Input and Output signals of PWM Converter in PowerFactory [46] .... 23
Figure 3.9: Basic filter topologies [49] .... 24
Figure 3.10: Damped LCL filter with series resistor [49] .... 25
Figure 3.11: LCL filter per phase model [51] .... 25
Figure 3.12: Static generator – Current source model [55] .... 27
Figure 3.13: DRES curtailment profile [34] .... 27
Figure 3.14: DRES over-frequency power control .... 28
Figure 3.15: Load shedding profiles[34] .... 30
Figure 3.16: Load under-frequency power control .... 31
Figure 3.17: π-model representation of single phase cable [60] .... 32
Figure 4.1: VSC Control Algorithm .... 33
Figure 4.2: Active power – frequency droop curve [61] .... 34
Figure 4.3: Reactive power – Voltage droop curve [61] .... 35
Figure 4.4: Frequency – Voltage Control .... 36
Figure 4.5: Normal Controller - Frequency .... 36
Figure 4.6: f - SoC curve .... 37
Figure 4.7: Normal Controller - Voltage .... 38
Figure 4.8: Connection controller .... 39
Figure 4.9: Connection criteria .... 41
Figure 4.10: Disconnection controller .... 42
Figure 4.11: Disconnection criteria .... 42
Figure 4.12: Set point Calculation .... 43
Figure 5.1: Multiple Cells interconnected through Backbone bus .... 46
Figure 5.2: $fsoc$ curve .... 47

Figure 5.3: Need Help State ........................................................................................... 49
Figure 5.4: Ready Help State ......................................................................................... 50
Figure 5.5: Disconnect State .......................................................................................... 51
Figure 5.6: Decision-making module................................................................................ 52
Figure 5.7: Live bus function.......................................................................................... 53
Figure 5.8: Need Help Set conditions .............................................................................. 54
Figure 5.9: Need Help Doconnect function ....................................................................... 55
Figure 5.10: Need Help Connect function ........................................................................ 55
Figure 5.11: Need Help Reset conditions ......................................................................... 56
Figure 5.12: Need Help state flow diagram ....................................................................... 57
Figure 5.13: Need Help Reset & Need Help Actual Reset .................................................. 58
Figure 5.14: Need Help Forced & Need Help Forced Reset values ...................................... 58
Figure 5.15: Ready Help Connect function ....................................................................... 59
Figure 5.16: Ready Help Set conditions ........................................................................... 60
Figure 5.17: Ready Help Reset conditions......................................................................... 61
Figure 5.18: Ready Help state flow diagram ...................................................................... 62
Figure 5.19: Ready Help Reset & Ready Help Forced signals .............................................. 62
Figure 5.20: Disconnect functions ................................................................................... 63
Figure 5.21: Disconnect state flow diagram ...................................................................... 64
Figure 5.22: System Control ........................................................................................... 66
Figure 6.1: Single Cell architecture .................................................................................. 68
Figure 6.2: Frequency of Cell and External Grid - Connection ........................................... 69
Figure 6.3: Voltage of Cell and External Grid - Connection ............................................... 69
Figure 6.4: Triggering and mode switching command for Connection ................................. 70
Figure 6.5: Voltage waveforms of Cell and External Grid at instant of connection ................ 70
Figure 6.6: Frequency setpoint signals for connection ....................................................... 71
Figure 6.7: Voltage setpoint signals for connection............................................................ 71
Figure 6.8: Power delivered/absorbed by the converter of battery ....................................... 72
Figure 6.9: Frequency of Cell and External Grid – Connection: Inverter overloading ............ 72
Figure 6.10: Voltage of Cell and External Grid – Connection: Inverter overloading............... 73
Figure 6.11: Converter power and SoC of battery – Overloading ......................................... 73
Figure 6.12: Frequency profile of Cell with PI connection controller ................................... 74
Figure 6.13: Frequency profile of Cell with PID connection controller ................................ 74
Figure 6.14: Frequency of Cell and External Grid – Intentional Disconnection ..................... 75
Figure 6.15: Voltage of Cell and External Grid – Intentional Disconnection......................... 76
Figure 6.16: Active and reactive power flow – External grid............................................... 76
Figure 6.17: Triggering and mode switching command for Disconnection ........................... 76
Figure 6.18: Frequency setpoint signals for disconnection.................................................. 77
Figure 6.19: Voltage setpoint signals for disconnection...................................................... 77
Figure 6.20: Power flow – Unintentional Disconnection: SoC 10 % .................................... 78
Figure 6.21: Frequency of Cell and External Grid – Unintentional Disconnection: SoC 10 % ........... 79
Figure 6.22: Voltage of Cell and External Grid – Unintentional Disconnection: SoC 10 %................ 79
Figure 6.23: Power flow – Unintentional Disconnection: SoC 90 % .................................... 80
Figure 6.24: Frequency of Cell and External Grid – Unintentional Disconnection: SoC 90 % ........... 80
Figure 6.25: Voltage of Cell and External Grid – Unintentional Disconnection: SoC 90 %................ 80
Figure 6.26: Layout of Interconnection of multiple Cells through BB bus ............................ 81
Figure 6.27: Frequency of multiple Cells – Connection at different time instants ................. 82

Figure 6.28: Voltage of multiple Cells – Connection at different time instants ..................................82
Figure 6.29: State of multiple Cells – Connection at different time instants.......................................82
Figure 6.30: Power of multiple Cells – Connection at different time instants.....................................83
Figure 6.31: Frequency of multiple Cells – Disconnection at different time instants ..........................83
Figure 6.32: Voltage of multiple Cells – Disconnection at different time instants..............................83
Figure 6.33: State of multiple Cells – Disconnection at different time instants ..................................84
Figure 6.34: Power of multiple Cells – Disconnection at different time instants ................................84
Figure 6.35: Frequency of multiple Cells – Connection at same time instant .....................................85
Figure 6.36: Voltage of multiple Cells – Connection at same time instant .........................................85
Figure 6.37: State of multiple Cells – Connection at same time instant .............................................85
Figure 6.38: Power of multiple Cells – Connection at same time instant............................................86
Figure 6.39: Frequency of multiple Cells – Disconnection at same time instant.................................86
Figure 6.40: Voltage of multiple Cells – Disconnection at same time instant.....................................86
Figure 6.41: State of multiple Cells – Disconnection at same time instant .........................................87
Figure 6.42: Power of multiple Cells – Disconnection at same time instant .......................................87
Figure 6.43: Microgrid layout for automated decision-making algorithm...........................................88
Figure 6.44: Graphs for Case I.............................................................................................................89
Figure 6.45: Graphs for Case II ...........................................................................................................90
Figure 6.46: Graphs for Case III: Simulation time – 200s...................................................................92
Figure 6.47: Graphs for Case III: Simulation time – 1500s.................................................................93
Figure 6.48: Graphs for Case IV.A: Simulation time – 600s...............................................................94
Figure 6.49: Graphs for Case IV.A: Simulation time – 1500s.............................................................95
Figure 6.50: Graphs for Case IV.B ......................................................................................................96
Figure 6.51: Graphs for Case V: No inclusion of past/forecasted energy profile................................97
Figure 6.52: Graphs for Case V: Inclusion of past/forecasted energy profile......................................98
Figure 6.53: Graphs for Case VI: Simulation time – 360 s..................................................................99
Figure 6.54: Graphs for Case VI: Simulation time – 1500 s (25 min)...............................................100
Figure 6.55: Graphs for Case VI: Simulation time – 2700 s (45 min)...............................................101
Figure 6.56: Graphs for Case VI: Simulation time – 5400 s (1.5 hrs) ...............................................102
Figure 6.57: Graphs for Case VI: Simulation time – 10800 s (3 hrs) ................................................102
Figure 6.58: Load and Generation profile for a week.........................................................................104
Figure 6.59: Graphs for Case VII: State and SoC (with decision-making algorithm)........................105
Figure 6.60: Graphs for Case VII: State and SoC (w/o decision-making algorithm) ........................106
Figure 7.1: Experimental set-up at HAN University .........................................................................110
Figure 7.2: Single Line Diagram.........................................................................................................110
Figure 7.3: AFE mode.........................................................................................................................111
Figure 7.4: Island mode ......................................................................................................................112
Figure 7.5: Microgrid mode................................................................................................................112
Figure 7.6: D7 card measurement – External Grid [70].....................................................................113
Figure 7.7: D7 card measurement - Microgrid [70]............................................................................113
Figure 7.8: Frequency Droop curve [70] ............................................................................................114

*This page is intentionally left blank.*

# List of Tables

Table 2.1: Line parameters [35] ........ 13
Table 3.1: Exponents defining Load Type [57] ........ 29
Table 6.1: Sizing of components in Cell ........ 67
Table 6.2: Case II.A Parameters – SoC & Connection trigger command ........ 81
Table 6.3: Case II.B Parameters – SoC & Disconnection trigger command ........ 83
Table 6.4: Case II.C Parameters – SoC & Connection trigger command ........ 84
Table 6.5: Case II.D Parameters – SoC & Disconnection trigger command ........ 86
Table 6.6: Sizing of components in Cell for automated decision-making algorithm ........ 88
Table 6.7: Limits definition for automated decision-making algorithm ........ 88
Table 6.8: Definition of terms for simulated cases ........ 89
Table 6.9: SoC for Case I ........ 89
Table 6.10: SoC for Case II ........ 90
Table 6.11: SoC for Case III ........ 91
Table 6.12: SoC for Case IV.A ........ 93
Table 6.13: SoC for Case IV.B ........ 95
Table 6.14: SoC and Net power profile for Case V ........ 96
Table 6.15: SoC for Case VI ........ 99
Table 6.16: Sizing of MG components for Case VII in the Netherlands ........ 103
Table 6.17: Comparison of results with and without Decision-making algorithm ........ 106
Table 7.1: Stand-alone mode w/o Load ........ 115
Table 7.2: Stand-alone Mode with Load ........ 115
Table 7.3: Grid Connected Mode - Internal Sync command ........ 116
Table 7.4: Grid Connected Mode – Manual Sync ........ 117

*This page is intentionally left blank.*

# List of Abbreviations

| | |
|---|---|
| AC | Alternating Current |
| BB | Backbone |
| BESS | Battery Energy Storage System |
| CF | Curtailment Factor |
| CSGriP | Cellular Smart Grid Platform |
| CSI | Current Source Inverter |
| DC | Direct Current |
| DG | Distributed Generation |
| DISC | Disconnect |
| DRES | Distributed Renewable Energy Sources |
| DSM | Demand Side Management |
| EG | External Grid |
| ESS | Energy Storage System |
| GC | Grid-connected mode |
| HECN | High Energy Consumption in Need |
| HECR | High Energy Consumption in Ready |
| HMI | Human Machine Interface |
| HV | High Voltage |
| IC | Interconnected mode |
| ICT | Information Communication Technology |
| ID | Intentional Disconnection |
| LECN | Low Energy Consumption in Need |
| LECR | Low Energy Consumption in Ready |
| LV | Low Voltage |
| LVRT | Low-Voltage Ride Through |
| MG | Microgrid |
| MGCC | Microgrid Central Controller |
| MV | Medium Voltage |
| NH | Need Help |
| NHA | Need Help Actual |
| NHAD | Need Help Actual Disconnect |
| NHF | Need Help Forced |
| NHFD | Need Help Forced Disconnect |
| NHFR | Need Help Forced Reset |
| NHR | Need Help Reset |
| NHS | Need Help Set |
| PbbND | Power Backbone Need Disconnect |
| PbbRD | Power Backbone Ready Disconnect |
| PCC | Point of Common Coupling |
| PI | Proportional Integral |

| | |
|---|---|
| PID | Proportional Integral Derivative |
| PLC | Programmable Logic Control |
| PMS | Power Management System |
| PWM | Pulse Width Modulation |
| RES | Renewable Energy Sources |
| RH | Ready Help |
| RHD | Ready Help Disconnect |
| RHF | Ready Help Forced |
| RHFD | Ready Help Forced Disconnect |
| RHFR | Ready Help Forced Reset |
| RHR | Ready Help Reset |
| RHS | Ready Help Set |
| SA | Stand-alone mode |
| SEP | State of Energy & Power |
| ShF | Shedding Factor |
| SLD | Single Line Diagram |
| SoC | State of Charge |
| SoCC | SoC Critical |
| SoCLL | SoC Lower Limit |
| SoCNH | SoC Need Help |
| SoCRH | SoC Ready Help |
| SoCUL | SoC Upper Limit |
| SOPRA | Sustainable Off-grid Power station for Rural Applications |
| SSM | Supply Side Management |
| T&D | Transmission & Distribution |

# 1 Introduction

## 1.1 Motivation

The world at large is passing through a phase of energy transformation and revolution. Though consistent efforts are pursued by countries over the past few years to enhance the global electrification rate, still around 1.1 billion people have no access to electricity. An additional 1 billion people have access to only limited and unreliable electricity. Of the people with no electricity access, nearly 87% live in rural areas where extension of the main grid is often expensive and technically challenging [1].

Historically, over decades, electricity is generated in centralized power plants based on fossil fuels, situated far off from the end consumers. Consequently, power has to be transmitted over long transmission lines, giving rise to high Transmission & Distribution (T&D) losses [2]. Further with rising demand in power, the congestion on the existing transmission network is growing at a rapid pace. Upgrading the existing network implies a huge investment which turns out be economically unviable. [3]. The conventional fossil fuel based power generation leads to emission of $CO_2$, having a significant impact over the climate change. Growing concerns of climate change coupled with the fact that the fossil-fuel reserves are depleting has resulted in declining trend of these conventional power plants. With the advancements in the field of renewable technologies and power electronics, the traditional unidirectional electric grid has started transforming into a bidirectional distributed grid, known as '*Smart Grid of the Future*' [3].

In this context, Distributed Generation (DG) has been widely applied and the concept of Micro Grid (MG) is becoming popular with its decentralized production of energy, particularly through Renewable Energy Sources (RES). MG can be visualized as a small power system, a controllable part of the Smart Grid, capable of both island and grid-connected modes of operation. RES mainly comprises of, but are not limited to, solar, wind, biomass, biogas, combined heat and power, fuel cells etc. All these micro sources are linked to the MG through interface inverter, hence the control performance of these inverter play a vital role in maintaining the overall stability of MG [4]. Rapid deployment of DG along with incorporation of Energy Storage Systems (ESS) and controllable loads unleash new horizons for MG expansion into the electrical power system [5]. Integration of RES in MGs is an ideal solution for electrifying areas which lacks public grid and for ensuring secure and reliable power supply in areas where the public grid is weak. Since the inception of MG concept, the electrical grid has observed a revolution in the control philosophy, but extensive research is essential for a total transformation [2].

## 1.2 Problem Definition

For a clear understanding and articulation of the problem, it's imperative to have a background knowledge of Cellular Smart Grid Platform (CSGriP) philosophy. The *CSGriP project* is aimed at developing a smart grid concept to electrify remote areas with no or weak grid connection by maximally integrating RES. However, the intermittent and unpredictable nature of RES makes it challenging to have a robust and reliable power system. Several partners are involved in this consortium project - Alfen, Alliander, HAN University, DNV GL, ACRRES and TU Delft. ACRRES or Application Centre for Renewable Resources is the national centre for applied research on renewable energy and green resources. Recently, ACRRES is focussing on system integration projects of solar, wind energy, storage and smart-grid applications. ACRRES regarded CSGriP as an opportunity and have conceived the idea of a pilot demonstration installation of the CSGriP in the existing electrical network.

The concept of the *CSGriP* is based on its predecessor – Sustainable Off-grid Power station for Rural Applications (SOPRA). The primary objective of *SOPRA* was to develop a viable stand-alone system to supply power to remote areas in a secure and reliable manner. *SOPRA* uses renewable energy sources, a storage system - battery and intelligent control system for stable operation of the stand-alone grid. The entire control system along with batteries is housed in a single container called *SOPRA* cell. The cell receives input from RES and supply power to loads as depicted in the Figure 1.1. A possible grid connection is also anticipated for future connection to External Grid. The prominent feature of the system is that the cell is independent of costly and often unreliable or absence of Information communication technology (ICT) equipment, meaning that there is no communication infrastructure involved. The control and operation of SOPRA cell was merely based on frequency signal, which conveys state of the system.

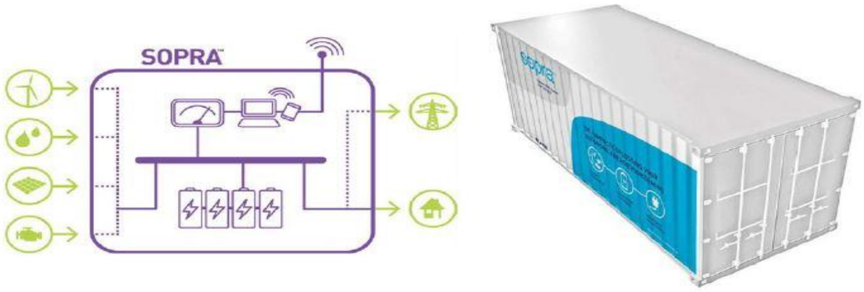


***Figure 1.1:*** *SOPRA Cell* [6]

The goal of CSGriP is to take SOPRA a step further and build a stronger, robust and reliable grid by using Frequency Based Control of SOPRA cell. In CSGriP, ways of interconnection of multiple SOPRA cells to form a stronger grid are explored, so that each cell can either work independently or in interconnected mode. The Figure 1.2 shows how multiple cells can be interconnected through a backbone. When multiple cells are connected with each other through a backbone network, it is termed as Interconnected mode. This kind of structure and philosophy for building a stronger microgrid is applicable in rural areas particularly, in the developing countries.

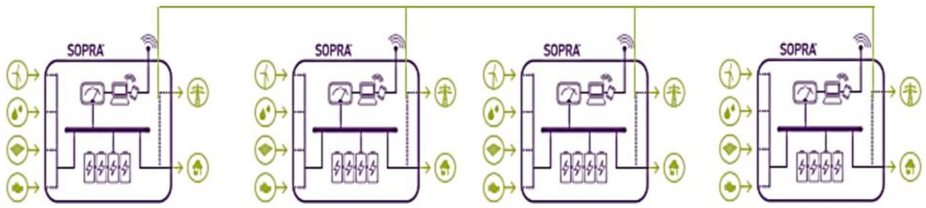


***Figure 1.2:*** *Multiple cells interconnected through a Backbone* [6]

Further, this Interconnected network of multiple cells can be connected to main External grid as in Figure 1.3 or even each individual cell may be connected to the main External grid as in Figure 1.4.

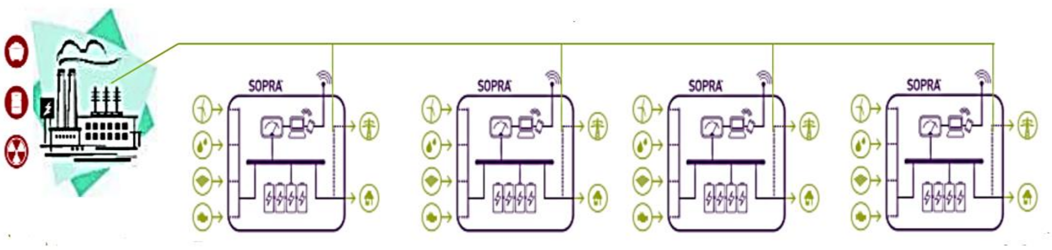


***Figure 1.3:*** *Multiple cells interconnected with main External Grid* [6]

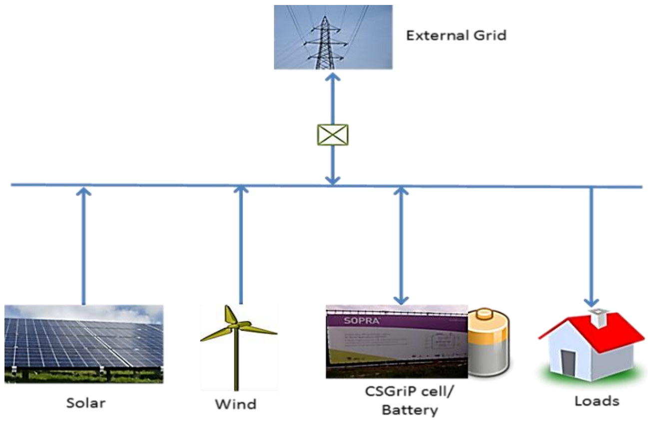


***Figure 1.4:*** *Individual cell connected to main External Grid*

When the cell operates on its own i.e. in a stand-alone condition, the frequency and voltage of the internal AC bus is defined by a grid-forming component, probably the converter of the battery, in the network. As the cell is connected to main External grid, the frequency and voltage is then regulated by the main grid and the grid-forming component would switch its mode into that of grid-feeding element. But in this thesis, due to absence of any kind of communication equipment, the cell would not be able to distinguish whether it's connected to another cell or to the main External Grid. Hence, it's preferred to operate the cell as a grid forming element even when connected to the main Grid. Furthermore, when multiple cells are interconnected with each other to build a strong grid, each cell trying to impose its frequency on the connected bus as a grid forming element share power in between the cells. So, in this mode of operation, some cells may supply power and others may absorb power. However, prolonged delivery of power from a cell may hamper its stable operation in stand-alone mode.

## 1.3 Research Objective & Questions

The objective of this thesis is a to develop a distributive approach of Microgrid control based on system frequency without relying on any communication signals.

The major research questions that were formulated to address the problems defined are describe below.

- What control strategy is required to achieve a seamless transition of a Cell between Grid-connected to Stand-alone mode and vice -versa without changing operating mode of the converter?
- How can this control scheme be practically implemented in an Inverter for a technology demonstration?
- What algorithm is needed to decide the switching states of a Cell between Stand-alone and Interconnected modes for an autonomous and stable operation, in a distributive manner?

## 1.4 Research Approach & Methodology

The first step in the thesis is to model the basic architecture of the MG or the Cell with all its components in PowerFactory simulation software, provided by the company DIgSILENT Gmbh. The steady-state behaviour of the cell is then evaluated both in Stand-alone and Grid-connected modes.

In the second stage, focus is laid on the development of the control schemes to achieve the seamless transition between Stand-alone and Grid-connected modes without changing the operating philosophy of the converter. The lack of ICT equipment compelled to rely only on frequency as the interfacing signal for formulating these schemes. The developed control algorithm was simulated in PowerFactory to study the dynamic behaviour of the system in case of Connection, Intentional Disconnection and Unintentional Disconnection to External grid. To prove the universal application of the proposed control algorithm, the developed philosophy is further applied to realize seamless transition between Stand-alone and Interconnected modes at different and same instants.

For the CSGriP project, a standard inverter was chosen rather than designing one from scratch, due to cost implications involved. In the next phase, the practical application of the proposed control philosophy as an interface to the standard inverter chosen is assessed. This involved field experiments on the inverter to comprehend its operating philosophy and adaptation of the control strategy for possible interfacing with the inverter for pilot demonstration.

Lastly, a decision-making module is developed to decide between the switching behaviour of the cell between Stand-alone and Interconnected modes for ensuring a stable and autonomous operation. For definition of the proposed algorithm, different states are formulated, which are explained in detail in the following chapters, and using these states, the cell performs its desired switching operation.

## 1.5 Thesis Outline

The outline of the document is as follows: Chapter 2 furnishes the theoretical definition of MG, and its various components. Since the converter is the main component in the cell, the existing control schemes of the converter and control architecture are addressed. Special focus is given to the droop control for regulation of frequency and voltage in the MG. Furthermore, some information regarding the transition of operating modes is presented and finally the gaps and challenges are identified.

Chapter 3 describes various MG architectures and describes how each of the components in the MG are modelled in PowerFactory software. In Chapter 4, the first research question is addressed. Initially, the control for Stand-alone operation is formulated and later, the control schemes are devised for seamless connection and disconnection of the cell to an External grid. The control algorithm is extensively deliberated not only for Grid-connected operation but also for Interconnected operation of cells. Chapter 5 stipulates the proposed decision-making algorithm to decide the switching instants between Stand-alone and Interconnected modes. In the process, new limits and states are defined and detailed flow diagrams of each of these states are depicted for performing the switching operation. Lastly, the overall system control is presented for the MG.

In Chapter 6, various cases are simulated and results are analysed for the performance of the devised control algorithm and automated decision-making logic. The chapter comprises of mainly two types of simulations. One focusses on shorter timescale for evaluating the grid dynamics for seamless connection and disconnection. The second on much larger scale for gauging the effectiveness of the decision-making algorithm to maintain a stable operation. Chapter 7 emphasizes on the experiments performed on a converter to show the practical applicability of the proposed control philosophy. Finally, Chapter 8 discusses the conclusion that arose from the analysis and recommends a scope for future work, that would be an appealing addition to current research for practical realization of CSGriP project.

# 2 Theoretical Background

## 2.1 Introduction

In this section, some concepts pertaining to the CSGriP project are discussed. A brief overview of the Micro Grid and Distributed Generation is explained to have an insight into basic structure of the project. Furthermore, some study regarding the different modes of control of inverters and the droop control philosophy are performed, which enlightens the control and operation of Microgrid in islanded and interconnected mode. Lastly, demand side management and supply side management are also researched for the implementation of the control strategy.

## 2.2 Microgrid

In the recent past, the growing concern over climatic changes coupled with the technological developments have resulted in a shift towards DG primarily renewables [7]. The Distributed Renewable Energy Sources (DRES) such as PV, wind, biogas etc. were naturally favored in comparison to the old, polluting traditional conventional power plants, which constitutes the current conventional grid. In this grid, large centralized power plants were used to supply the energy demand of the end consumers [8]. However, owing to the intermittent behaviour of DRES, the application of ESS as a buffer system to maintain the power balance at any moment of time gained significance in this context, thus ensuring higher power quality [9].All these developments paved the path towards the evolution of a very popular area of research, Microgrid.

The MG as defined by [10] is “an integrated energy system consisting of distributed energy resource and multiple electrical loads operating as a single, autonomous grid either in parallel to or islanded from the existing utility power grid”.

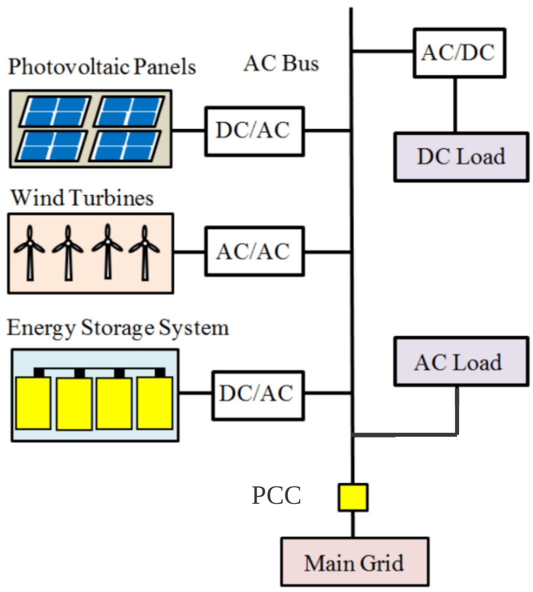


***Figure 2.1:*** *General MG architecture* [11]

The Figure 2.1 shows a generalized structure of MG interconnected to the utility grid at the Point of Common Coupling (PCC) through an isolating device. This device establishes whether the MG is operating in stand-alone and grid-connected mode [3]. In simpler terms, the MG is a small energy system consisting of DRES, ESS and controllable loads, operating at low or medium voltage networks. The system can operate autonomously in different modes of operation – islanded and grid-connected mode [12]. The MG is the evolution of the conventional unidirectional, passive distribution network into a smart, bidirectional, active distribution network with keen involvement of end-consumer in the distributed generation [5].

One of the many benefits of a MG is that it enables DG and helps enhancing the penetration of renewable energy sources [13], [14]. So, in a way, a MG with DRES alleviate environmental impact due to conventional fossil fuel power plants. The proximity of DRES to consumer locations decreases the transmission and distribution losses and also helps in improving the voltage profile of the system.[3]. Regardless of the innumerable advantages of a MG architecture, it also possesses various challenges. One of the most important challenges is the MG protection. The conventional philosophy of protection is no longer viable owing to bidirectional power flow and topological changes associated with islanding or stand-alone operation [15]. Other significant issues involved are power imbalance, active and reactive power control, Inverters for DC-AC conversion and controllers for regulating power flow, which are addressed in Section 2.3 [16]. To further comprehend the challenges, let's discuss about the building blocks of a MG.

### 2.2.1 Distributed Generation

The existing conventional grid comprises of few centralized power producers and long transmission and distribution network involving high maintenance cost, which makes even more challenging to achieve a proper load sharing [17]. Additionally, the depletion of fossil fuels and the negative impact on environment caused by burning these fuels has raised concerns for nations to keep a track over $CO_2$ emissions. The key issues faced by the centralized power system are mentioned below [15].

- *Rising power demand and lack of reliable electric power*
- *Limited scope of power system expansion*
- *High investment in transmission and distribution network*
- *Risks of bulk power outages*
- *Environmental impact*

All the above concerns necessitate the incorporation of DG into the current electrical grid. DG can be defined as small modular power generating units, generally located close to consumers end and permit interconnection to the power grid at any point [8], [18]. The DG has significantly multiple advantages over the current distribution network. The deployment of DG in the present congested distribution or transmission network reduces the need for upgrading the current system, which is investment-intensive and time-consuming [19]. Remote areas with no access to the public grid could be easily electrified with the MG involving DG. The extra cost involved in expanding the main grid and construction of new transmission lines would no longer be a hindrance to the electrification of these remote areas [20]. Additionally, MG provide ancillary services to the main grid. The key attribute of a MG, Islanded mode of operation, would also prevent catastrophic events due to grid faults, outages and power quality problems [21].

However, large-scale and random deployment of DG may raise as many issues as solved. DG units either generate a DC or a variable frequency AC output and hence demand power electronic interface for integrating to the grid [22]. As MG involves bidirectional power flow, the protection systems of the conventional grid may no longer be valid in a grid with high penetration of DRES. The protection mechanisms need to be adapted to MG topology and the short-circuit capacity of the network [23]. The fluctuating output of DRES with changing weather conditions is another concern when DG units are used [24]. The micro DG units have very low or no inertia and thus creating imbalances between generation and load in case of sudden jump in the load [22]. So, to maintain the power balance in the MG, ESS are generally employed in the MG architecture.

### 2.2.2 *Role of ESS*

Due to intermittent behaviour of electricity generation from DRES, the fluctuations arising from variable DRES output and nonlinear loads will have significant repercussions on the operation of MG. The above concern can be easily addressed by ESS and proves to be a preferable solution [16]. ESS offsets the power deviations in the MG and maintains the balance between generation and load in the event of islanding operation. These are also used for controlling the power flow to and from the main electrical grid [3]. Thus, ESS plays a critical role in maintaining the power balance and thus regulating the frequency and voltage of the network. All these enhances the stability of the MG [16].

Further, ESS may provide ancillary services like low-voltage ride through, load shifting and peak shaving and operating reserves [25]. Generally, when a MG is comprised of DRES and ESS, the ESS behaves as the grid forming source regulating the MG AC bus, while DRES inject power to MG [26]. There exist various technologies for storing energy and some of the major ESS comprises of batteries, flywheels, pumped hydro storage, compressed air energy storage, super capacitor, superconducting magnetic energy storage etc. However, most of these units necessitate the use of power electronic device for interface [15].

### 2.2.3 *Interfacing power converters*

Most DG units are small generating units either producing a DC or a variable frequency AC output. For instance, a Solar Photovoltaic (PV) array generates a variable DC output based on the irradiance, which then has to be converted to fixed frequency AC signal for interconnecting to the low-voltage (LV) bus of the MG, generally 400V. On the contrary, in general, variable speed Wind turbine generates a variable frequency AC signal. This signal is then passed through a back-to-back converter, where the variable AC signal is first transformed to DC and then converted back to fixed frequency AC signal. For the case of ESS, it's similar to that of the solar PV system. The DC output of the ESS is linked to the AC network through the interfacing power electronic devices. These devices enhance the flexibility, adaptability and integration of DG and ESS into the MG architecture [22].

The performance of these power converters may vary for different DG and ESS and even behave differently for topological changes associated with whether MG is islanded or grid-connected state. When a MG is grid-connected, the power converters of both DG and ESS could inject power to the main grid-based on the DRES output and set points respectively. However, in islanded condition, the MG cannot establish AC LV bus by its own, it requires a grid forming device. In general, the power converters of ESS forms the grid and the remaining power converters of DRES inject power to the MG. So, it all depends on the control philosophy behind the converters and it may differ from application to application. A proper understanding of the control scheme of the inverters is beneficial for comprehending the overall system behaviour of the MG and this will be dealt in detail in the further sections.

The general layout of MG architecture as seen in Figure 2.1 encompasses all these building blocks, DG, ESS and Interfacing power converters, and the way in which each of these blocks are integrated defines the operating behaviour and overall stability of the MG in all conditions, i.e. in islanded or grid connected modes. With all these, the concept of MG is widely becoming more popular and plays a significant role in the evolution of future *Smart Grid*. A few objectives that can be achieved by use of a MG are summarized below [3].

- *Reliability of electric supply*
- *Reduction of environmental impact of fossil-fuel based power generation*
- *Lower investment in plant and equipment*
- *Diversity of energy supply*
- *Remote site electrification*

The future *Smart Grid* is envisaged to be a well-structured and designed plug-and-play integration of microgrids interconnected for exchange of power.

## 2.3 Control Schemes of Converters

The MG, as stated in Section 2.1, has 2 modes of operation – either grid-connected or islanded. When the MG operates in islanded mode, the voltage and the frequency shall be defined by the MG with the help of a synchronous generator or a ESS through a Voltage Source Converter (VSC). In Grid-connected mode, the VSC is responsible for charging or discharging of battery and the frequency of the system is imposed by the External grid [27]. The converter acts as an interface between the Direct Current (DC) and Alternating Current (AC) to facilitate the power flow from DRES & ESS to loads and Grid. Hence, depending on the role each converter plays in a MG, the inverters are classified as Grid-forming, Grid-feeding and Grid-supporting [5].

a) ***Grid-forming converters*:** In this mode, the converter behaves as an ideal voltage source with a low output impedance or in other words it's a Voltage Source Inverter (VSI). This inverter is responsible for setting the frequency and voltage of MG with the help of a control loop as shown in Figure 2.2. The power delivered by such a VSI is entirely dependent on the loads connected to MG. These converters can operate in parallel, for which a proper synchronization technique is required. The ESS inverter is a good example of VSI as it defines the grid parameters i.e. Voltage and Frequency of the network in stand-alone operation.

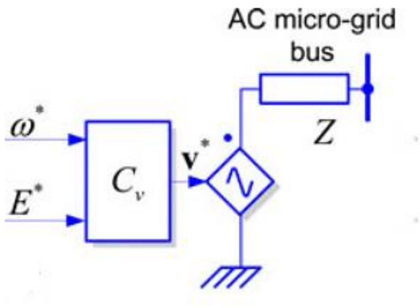


***Figure 2.2:*** *Grid-forming converter* [5]

b) ***Grid-feeding converters:*** These converters behave like an ideal current source parallel with a high output-impedance, also known as Current Source Inverter (CSI). This inverter cannot directly influence the grid parameters but deliver power to an energized grid. The general layout of the grid-feeding converter is depicted in Figure 2.3. A CSI is unable to operate in islanded mode, unless it's connected to the External grid or a MG supported by a Grid-forming inverter. Such converters shall be properly synchronized with AC voltage of MG for accurate active and reactive power-sharing. DRES inverters are interfaced with the grid using this mode of operation.

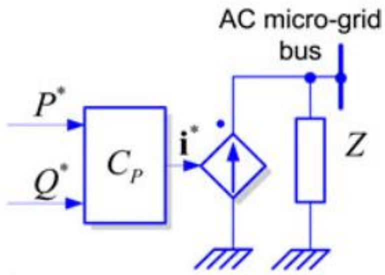


***Figure 2.3:*** *Grid-feeding converter* [5]

**c)** ***Grid-supporting converters:*** A grid-supporting converter is a hybrid of the above-mentioned converter, which means that these can be professed as current sources or voltage sources, based on the mode of control. If the converter is designed as a current source as shown in Figure 2.4, it requires the existence of at least one grid-forming element. On the other hand, if controlled as a voltage source as in Figure 2.5, it can work in island and grid-connected mode.

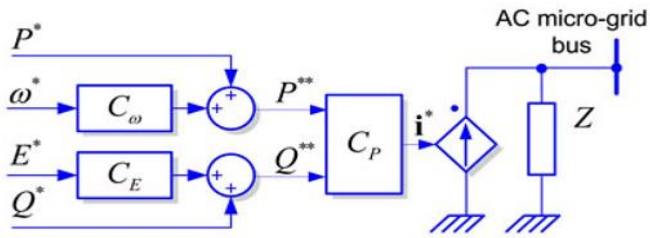


***Figure 2.4:*** *Grid-supporting converter – current source* [5]

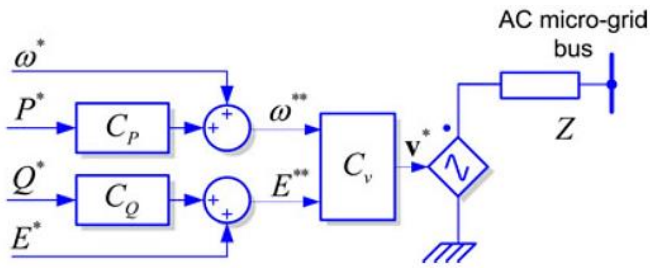


***Figure 2.5:*** *Grid-supporting converter – voltage source* [5]

From the above analysis, it's evident that a MG requires at least an inverter with Grid-forming capabilities to facilitate its operation in island mode.

## 2.4 MG Control Architecture

In a MG, the magnitude and frequency of voltage signal can be modified by using numerous control strategies. In an islanded system, any disturbance or change in the active power requirement will have an impact on the frequency of the AC bus in the MG. The effect of such a change is similar to that of the conventional system. In other words, as the net power demand (difference of power required by load and generator) increases, the frequency of the MG AC bus decreases to meet the power requirement. On the contrary, when the net power demand decreases, the frequency of the MG AC bus decreases. So, there exists an inverse relationship between net power demand and frequency. However, in case of an islanded MG system, the surplus power needs to be stored in ESS like batteries, capacitors etc., or needs to be curtailed [28].

### 2.4.1 Hierarchical control

Conventionally, a hierarchical control is utilized in the existing power grid for regulation of voltage and frequency and to maintain the power balance. The structure of the control scheme is depicted in Figure 2.6 and comprises of Primary control, Secondary control and Tertiary control.

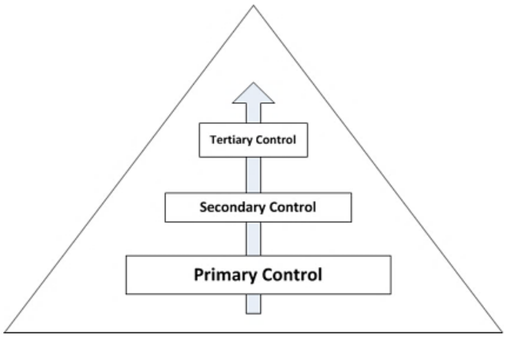


***Figure 2.6:*** *Three-level hierarchical control* [3]

This three-level hierarchical control stands applicable in a MG as well. The functionality of these levels of control differ from each other and are explained below.

a) ***Primary control:*** This is the first level of control whose primary objective to maintain the power balance in the network upon variations in the load dynamics. Because of which, the frequency of the AC voltage deviates from the nominal value and settles at a different value. This control primarily depends on measurement of local variables and has a very fast response [28]. Hence this control is beneficial for load sharing between converters and regulation of output voltage and frequency, thus augmenting the MG stability [3].

b) ***Secondary control:*** The principal function of this control is to ensure power quality by minimizing the deviations in the magnitude and frequency of the voltage, caused by the primary control. The response of the secondary control is slower compared to that of primary control and hence it determines the new reference values for primary control. This iteration is continued till the magnitude of frequency and voltage is settled back to its nominal value. This control demands the use of low bandwidth communication for measuring global variables [28].

c) ***Tertiary control:*** This is third level of control, with a response slower than that of the secondary control. Tertiary control is employed for ensuring the optimum power flow between MG and utility grid and thus sends voltage and frequency reference signals to secondary control. So this control is profoundly dependent on communication infrastructure for evaluation MG system behaviour [3], [28].

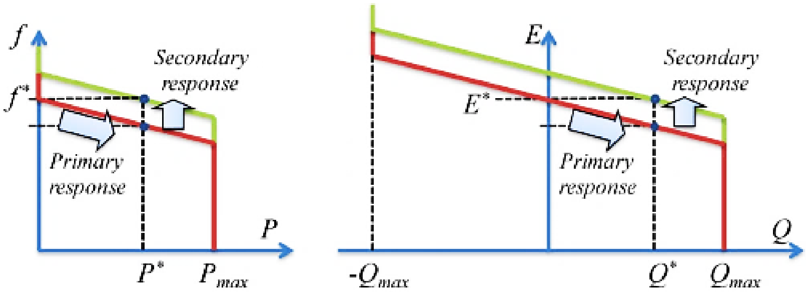


***Figure 2.7:*** *Primary and Secondary response of hierarchical control* [29]

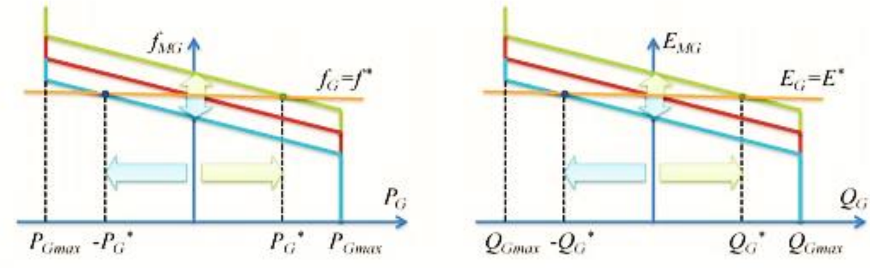


***Figure 2.8:*** *Tertiary response of hierarchical control* [29]

The Figure 2.7 and Figure 2.8 demonstrations a typical response of a three-level hierarchical control to variation in system dynamics in a MG.

### *2.4.2 Centralized Vs Decentralized control*

The control of a MG is either possible in a centralized or a distributed way. In some cases, a hybrid control is chosen for better optimization [2]. However, one of the converters of the MG need to be a grid-forming element for stable operating condition in islanded mode. The choice of whether a centralized or a decentralized controller is chosen varies from case to case.

A centralized controller conceptualizes the fact that it receives signals and commands from each of its agents and makes the decision and sends the signal to all the actors involved through a dedicated communication network. A dedicated communication network means extra cost of investment and greater probability of failure. The failure of centralized controller or any of its components would hamper the entire system operation and if a redundant controller is maintained to tackle this issue would increase the overall cost of the system. On the flip side, the controller can receive all the relevant information of the system and the participating actors, so the system could work as much close to the optimum working point [30].

In the decentralized mode of control, the decisions are made based on the locally available parameters i.e. Grid Frequency and Voltage. The application of such kind of control eliminates the need for external communication network and benefits the systems in terms of cost and higher availability [31]. Hence the entire system becomes less complex and easy to control. Each of the devices in the MG has a distributed controller linked to it and hence failure of any one device would not lead to catastrophic events. Furthermore, due to modular nature of the decentralized control, the system is easily scalable and expandable if necessary. It’s also worth mentioning that each of these decentralized controllers could work autonomously or work in parallel with other controllers [29].

For parallel operation of various MGs or converters within the same MG, different control techniques are found in literature. These can be classified into two major groups based on the interconnecting communication network.

a) *Active Load Sharing*
b) *Droop based control*

The active load sharing techniques are derived from the control schemes of parallel converters such as Centralized, Master-Slave (MS), Average Load Sharing (ALS) and Circular Chain Control (3C). Despite these control techniques are successful in regulation of output voltage and current sharing, it demands critical communication lines among the various actors involved, thus indirectly diminishing reliability of the system. The second control technique is based on droop method which adjusts the magnitude and frequency of the output voltage based on the power delivered by the converter. As the control relies on local measurements, there is high reliability and modularity in respect to location of the actors in the MG [32].

The most prominent feature of the CSGriP project is that the system shall operate without the use of external communication network or devoid of any ICT equipment[6]. So only local grid signals – voltage and frequency of the network are available for control, thus pushing the need for a decentralized mode of control. This enhances the plug and play design of the CSGriP cell into the distribution network without the requirement of extra ICT equipment and can be easily integrated to the existing network even in remote areas. Hence droop control is a natural choice for control of the MG network.

***Droop control***

The operation of the inverter with the droop control can be compared that of a synchronous generator, where, delivered Active Power (*P*) is a function of Grid frequency (*f*). The active power of the generator is decreased as the frequency increases and vice versa. Similarly, the Reactive Power (Q) is a function of Grid Voltage (*V*). These are referred to *P/f* and *Q/V* Droop curves respectively [5].

In MG, the conventional synchronous generators are replaced by power electronics interfaced static generators with VSI. As explained in the Section 2.2, the power supplied by the VSI is dependent on the load on the MG and cannot be controlled by the inverter themselves. Hence while applying the droop concepts to a VSI in a MG, the philosophy of operation is reversed. That is to control the grid frequency as a function of the power of inverter. This is done by measuring the active power flow of the inverter and subsequently calculating the desired frequency of the MG based on the droop curves [33]. In a similar manner, the voltage set point of the inverter is calculated by measuring the reactive power. The frequency and voltage set points as determined by Eqns. (2.1) & (2.2) are given as inputs to VSI.

$$f = f0 - k_p P \tag{2.1}$$

$$V = V_0 - k_Q Q \tag{2.2}$$

Where $P$ & $Q$ are Active and Reactive power delivered by the inverter, $k_p$ & $k_Q$ the droop coefficients and $f0$ & $V_0$ the zero-power frequency and voltage of the droop curves.

An inverter that is grid-connected cannot fix the grid frequency and voltage as these values are imposed by the grid. Such inverters behave as CSI and inject active & reactive power according to Eqns. (2.3) & (2.4).

$$f_g = f_0 - k_p P \tag{2.3}$$

$$V_g = V_0 - k_Q Q \tag{2.4}$$

where $f_g$ & $V_g$ are grid frequency & voltage.

Application of droop curves also aids active & reactive power-sharing in the case where multiple VSI are in parallel operation, feeding the same MG. The frequency (Δf) and voltage (ΔV) variations depend on the interaction between the inverters and can be calculated by Eqns. (2.5) & (2.6).

$$\Delta f = k_{pi} \Delta P_i \tag{2.5}$$

$$\Delta V = k_{Qi} \Delta Q_i \tag{2.6}$$

where ΔP & ΔQ are active and reactive power variations.

To further understand the real and reactive power flow, consider the equivalent circuit of a voltage source inverter connected to a distribution network with an impedance Z (R+jX) between them. The equivalent circuit for power flow and the associated phasor diagram is shown in Figure 2.9.

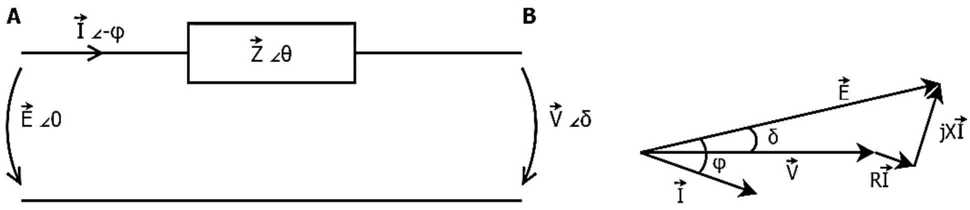


***Figure 2.9:*** *Equivalent circuit for power flow through a line* [34]

The active and reactive power delivered by the inverter are given by the Eqns. (2.7) & (2.8).

$$P = \frac{E}{R^2 + X^2} \left[ R \left( E - V cos\delta \right) + XV sin\delta \right] \tag{2.7}$$

$$Q = \frac{E}{R^2 + X^2} \left[ X \left( E - V cos\delta \right) - RV sin\delta \right] \tag{2.8}$$

where P and Q represent the active and reactive power respectively that the inverter (A) delivers to the grid (B). E and V are the magnitudes of the voltages at the two terminals (inverter and grid), δ represents the phase-angle difference between the voltages and R is the resistance of the connecting line, while X is the reactance of the connecting line[5].

*Influence of Line Impedance*

From the Eqns. (2.7) & (2.8) , it's clear that the line impedance has a strong influence over the delivered active & reactive power. The Table 2.1 shows the typical line parameters and the R/X ratio for LV and HV lines [35].

***Table 2.1****: Line parameters* [35]

| Type of Line | R (Ω/km) | X (Ω/km) | R/X |
|---|---|---|---|
| Low Voltage | 0.642 | 0.083 | 7.7 |
| High Voltage | 0.06 | 0.191 | 0.31 |

*High Voltage Grid*: As the R/X ratio of HV are small, the value of R may be neglected, indicating inductive behaviour. Further, the phase angle difference δ is typically a small value, allowing to the assumption that sin δ = δ and cos δ = 1. The Eqns. (2.7) & (2.8) can now be reformulated as

$$P = \frac{E.V}{X} \delta \tag{2.9}$$

$$Q = \frac{E.(E - V)}{X} \tag{2.10}$$

The active power is proportional to the phase angle difference δ, and the reactive power is proportional to the difference in voltage magnitudes. This is known as the conventional droop curve [35].

*Low Voltage Grid*: Similarly, the R/X ratio of LV lines are so high that, the value of X can be neglected, indicating a resistive behaviour. With the assumption that sin δ = δ and cos δ = 1, as in the previous case, the Eqns. (2.7) & (2.8) become

$$Q = \frac{E.V}{R}\,\delta \tag{2.11}$$

$$P = \frac{E.(E-V)}{R} \tag{2.12}$$

In this case, the voltage depends on active power and the frequency depends on reactive power, and hence called the inverse or opposite droop. But such a system would be incompatible with the higher grid and conventional big power plants [35].

The conventional droop could be applied in a LV grid by emulating the inductive behaviour with the implementation of virtual impedance in the controller or by connecting an inductor to the inverter Adding a virtual impedance to the controller without the need of physically connecting a passive component eliminates the actual loss in the system [36]. However, the voltage drop across the virtual inductor ($V_L$) is subtracted from the current voltage reference to derive the new voltage set point for the inverter. So by implementing this virtual impedance, the active and reactive power flows are decoupled resulting in a satisfactory behaviour of conventional droop curve [35]. This will make the system inherently compatible with the rotating machines and the main grid.

Moreover, due to the voltage drop over the resistances of the connecting lines, the sharing of reactive power is not perfect and this is unavoidable when using a system with no ICT equipment [37].

## 2.5 Demand Side Management

The main source of energy supplies in a MG, particularly the CSGriP is DRES. Due to fluctuating nature of these sources, this energy supply cannot be used directly without any buffer system or control between source and load. In CSGriP, consider the case where the load is connected when the SoC of the BSES is low, this would create disturbance and result in decrease of MG frequency. Because of this momentary mismatch between the power production and consumption in MG results in inducing an instability in the grid. To stabilize the grid behaviour, different measures need to be adopted.

As explained in the Section 2.2, power balance has to be maintained in a MG at any moment of time. The first solution is to install buffer capacity like the battery to match the misbalance between the power demand and supply. But oversizing the buffer system for stabilizing the grid in case of disturbances is financially unattractive because of the increased system cost. Another option is the use of diesel generator when demand of the loads cannot be fulfilled by DRES and batteries. This is not preferred due to running costs and $CO_2$ emissions. The third option is application of Demand Side Management (*DSM*).

DSM involves a combination of measures that focus on changing the behaviour of the end-user in order to stabilize or unburden the public grid, by modifying or reducing the end-user's energy demand. By actively controlling the power consumption by the end-users at times of over-or underproduction of power, the grid can be stabilized without oversizing of the buffer system. The dynamic response of the loads can be achieved by Load shifting and Load shedding [38].

***Load shifting*:** To address the mismatch between the peaks of generation from DRES and peak in load demand, it is desirable to shift some of the loads in the evening peak to moments where supply peaks (noon in case for solar). This can be realized by dividing the loads into 2 groups – Shift & Non-shift loads and operating these shift loads when the MG is in Energy Surplus state. However, sometimes these shiftable loads, for instance a water pump, will have to consume energy during critical stages. Normally, the water pump will supply the buffer tank only when the grid is surplus energy state. However, when the water level reaches a critical state, the pump has to run, even if it drives to grid to unstable condition [34].

***Load shedding*:** Load shedding can be applied in situations, where the power consumed by the loads exceed the generation and that supplied by the batteries. This means that some of the undesirable loads can be switched off to lower the power consumption and achieve a stable operation of the grid. This is very crucial in areas where the public grid is weak or do not exists. To implement load shedding, load needs to be categorized based on their priorities and switched off accordingly in response to grid frequency. Different load shedding profiles for stable operation of the grid are adopted in the CSGriP, which shall be explained in detail in design of the load controller.

***Load priority*:** Prioritization of all possible loads would allow a phased and controlled way of load shedding, thereby disconnecting the lowest priority loads initially, and hopefully avoiding the need of disconnecting loads with higher priority. The consumers have the option of connecting, for example, the basic lighting devices to higher priority supply when load shedding is applied to meet the basic requirement. However, loads such as hospitals, telecom towers shall be given the highest priority and never be switched off [34].

## 2.6 Supply Side Management

Another control mechanism to maintain power balance on the grid and thus ensuring the stability of the grid is the application of Supply Side Management (*SSM*). This is similar to DSM; however, the control is applied on the generation source rather than on the end consumer load profile. The application of SSM is very broad, covering the entire supply chain – generation, transmission and distribution – all driving towards successful delivery of this electricity [38]. In this project, SSM scheme is limited to curtailing the output power of DRES when there is an overproduction state.

The act of curtailment refers to a situation where the full potential DRES is not used in order to maintain or return to grid stability. Considering the limited scale of penetration of DRES, particularly in areas where the grid is weak, curtailing is not required at most time and full generation from DRES could be harvested. But the scenario is not same everywhere. For instance, the German grid, due to large penetration of DRES, stability issues may arise when the production is higher than consumption. As the power injected to the grid increases, the grid frequency also increases. Thus, by monitoring the grid frequency, the state of overproduction can be recognized and steps for reducing the power generated from DRES are carried out, thus offering a means of regaining the grid stability.

Once the grid attains the stable condition, the generation of DRES may be retained to its original state, however, a sudden jump in the generation may lead to a disturbance and subsequently stability issues. So, the output power DRES has to be regulated properly which copes with handling the stability issues. The German grid standard VDE-AR-N 4105 is used for this project, which would be detailed in the design of generation controller.

SSM can provide ancillary services to the grid, For example, Low-Voltage Ride Through (LVRT) function in a Wind farm ensures that DRES are connected to the grid in case of voltage dip, which may otherwise lead to a severe blackout [34]. Additionally, the demand response of loads, as explained in DSM, could also aid in the process of attaining grid stability. So, in a way the DSM & SSM schemes work in tandem for a stable operating regime.

## 2.7 Transition of Operating modes of MG

Commonly, a MG has two main operating modes, namely, Islanded and Grid-connected modes. Transition between these modes define the operating behaviour of the MG. However, in this thesis, there are three operating modes viz. Islanded/Stand-alone, Interconnected and Grid-connected modes.

To describe about the different modes: Islanded mode means that the MG is in isolated from the main external electrical grid, Grid-connected mode refers to the situation where the MG is linked to the external grid through an isolating switch and third mode i.e. Interconnected mode refers to the case where multiple MGs are connected to each other through a LV backbone bus without the presence of external grid.

a) ***Grid-connected mode***: In this mode, the MG can exchange power with the external grid to maintain the supply in the local MG. Since the MG is connected to the external grid, deviations in frequency and power in MG are borne by the main grid, being a very stiff one. Hence, the DRES and ESS in the MG do not contribute to frequency and voltage regulation. The result of which, the interfacing converters are controlled by Active-Reactive (P/Q) method to deliver power according to a reference point [39]. This means that in grid-connected mode, these sources behave like a current source supplying to the MG.

b) ***Islanded/Stand-alone mode***: There are two main challenges in this mode, one is to maintain desired magnitude and frequency of voltage and the other to maintain the power balance in the MG. In such scenarios, there shall be one minimum grid forming converter in the MG and for which the V/f control strategy is commonly used. The frequency is regulated by the active power and voltage is adjusted by the reactive power [39]. Usually the converter of ESS is set to follow the V/f control while the converter of DRES units still follow P/Q method to supply power according to the reference.

c) ***Interconnected mode***: An Interconnected mode can be considered as stronger and bigger MG in islanded state. Similar to the islanded mode, in Interconnected mode, there shall be minimum of one grid-forming element and others as grid-feeding elements, following the master-slave configuration. However, due to application of decentralized control and absence of any ICT equipment, each smaller MG in the whole bigger network would have one grid-forming converter, meaning that in this mode there occurs parallel operation of various grid-forming converters.

To summarize, the DG units with intermittent behaviour like PV, wind etc. are always controlled by the P/Q method and the ESS like the battery are controlled by the P/Q or V/f method based on the operating mode of the MG, whether it’s Grid-connected or Islanded mode. So, a change in operating mode involves a transition of the control philosophies. A systematic approach of defining the controllers is proposed in [40], where both the grid-connected and islanded mode controllers continuously evaluate the operation set points but only one controller is active based on the island detection command. An agent control strategy is investigated in [12] for switching between modes through a MG central switch.

However, these recommended methods rely on exchanging information between agents in MG and external grid.

## 2.8 Identified gaps and challenges

The underlying feature of this thesis is that it does not depend on any communication infrastructure for exchange of data and control. Due to this, it is impracticable for the MG to detect whether it is connected to main external grid or another MG. In other words, it is hard to distinguish between Grid-connected and Interconnected mode.

As discussed before, in Interconnected mode, the converter of ESS is controlled by V/f strategy in each of the MGs. Following this, it is proposed to maintain the control strategy to V/f method even when the MG is connected to the main grid. Meaning that the converter of ESS will always be controlled by V/f method. So, it demands the formulation of a new decentralized control strategy functioning based on local measurable variables for seamless transition between Islanded and Grid-connected modes. Further, it's also worth to mention that the proposed control strategy shall be applicable for Interconnected mode, implying safe and stable operation between the three modes of operation: Islanded, Interconnected and Grid-connected modes.

Another aspect which demands further research is the development of a decision-making algorithm to define the switching instants for state change. A Microgrid central controller (MGCC) could perform this task-based on the input parameters of each MG and external grid and send commands for mode change. In this thesis, rather than focusing on the centralized approach due to reason specified before, it is devised to follow a decentralized approach in formulation of algorithm, supplementing the modularity and expandability feature of the project.

## 2.9 Summary

An elaborative literature study is performed in this chapter on MG, its comprising components. The varied control architectures and different operating modes of the MG are discussed in detail. Furthermore, the control schemes which are currently prevalent are evaluated with respect to the project and gaps and challenges are identified, which would be addressed in this thesis.

# 3 Modelling of Microgrid

## 3.1 Introduction

A MG is a cluster of Distributed Generators , Energy Storage Systems and controllable loads, primarily operating in Low Voltage (LV) or Medium Voltage (MV) networks and having the capability of operating in parallel to utility grid or as an isolated system [9], [12]. The Microgrid modelling is based on the system architecture and various components that form the integral part of the network. The components of MG are either directly connected to the AC network or linked through a power electronics interface, The control strategy associated with ESS in the MG ensures its interoperability behaviour of Grid-connected or Stand-alone mode [3]. A brief overview of DRES and Load control is also discussed to have an insight into how these respond to deviations in MG parameters. The SSM and DSM schemes, which have been proposed in [34], have been adopted in this thesis. This chapter briefly discusses the adopted MG architecture and components and how each of these components are modelled in the PowerFactory software.

## 3.2 MG Architecture

The generalized structure of the Microgrid as depicted in Figure 2.1 in Section 2.2, consists of an isolating device which interconnects the system to utility grid at Point of Common Coupling (PCC). In this thesis, a CSGriP Cell, as explained in Section 1.2, can be considered a MG which have the flexibility to operate as a Stand-alone (SA) / islanded or Interconnected (IC) or Grid-connected (GC) mode. Due to above fact, the terms MG or Cell are interchangeable and is applicable in all the sections of the thesis. The adopted architecture for studying the dynamics involved in connection and disconnection of a CSGriP Cell to the utility grid, referred to as External Grid (EG), is shown in Figure 3.1.

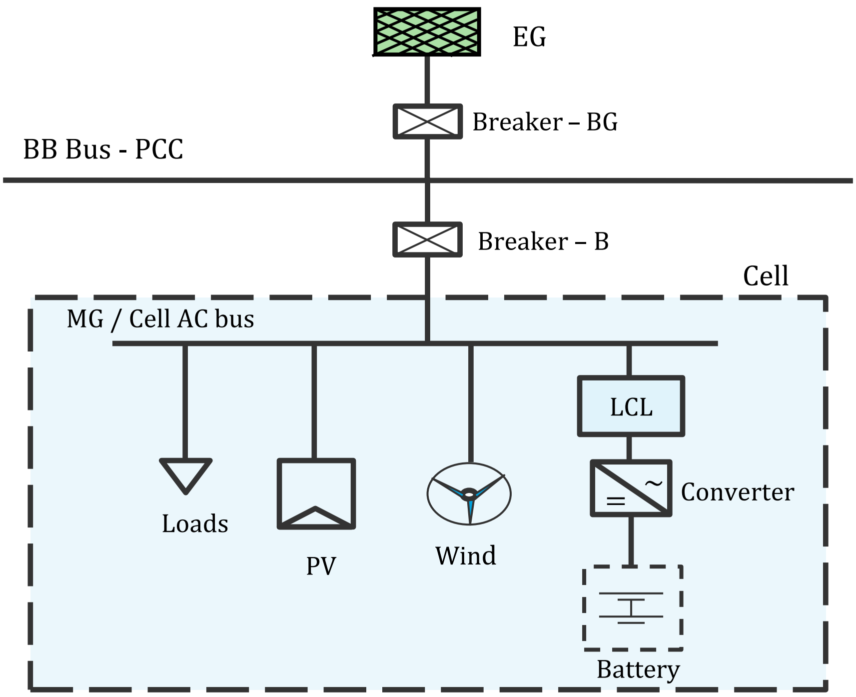


***Figure 3.1:*** *Single Cell Architecture*

A single Cell typically consists of DG, ESS and Loads – controllable and uncontrollable. DG, also referred as Distributed Renewable Energy Source (DRES) – Photovoltaic & Wind, are major sources of generation in the MG to supply the energy demand of the connected loads. Battery is the ESS unit considered for the project, further referred to as Battery Energy Storage System (BESS). BESS is crucial to maintain the power balance in the MG in all modes of operation. The Loads, DRES and Battery, through Converter and LCL filter, are all connected to MG/ Cell AC Bus. This Cell/MG bus is further linked to a Backbone (BB) bus through an isolating device – Breaker (B). The BB bus is coupled with the External Grid through the switch – Breaker BG. In the initial phase of the thesis, the BB is assumed always energized by closing breaker BG and the system is evaluated for ensuring a seamless connection and disconnection to EG by closing and opening breaker B. This means that the system would have 2 modes of operation – SA & GC mode.

As the Cell is modular in nature, the number of cells may be augmented to build a stronger, robust MG network as depicted in Figure 3.2. Each Cell can function as an islanded network or may be interconnected to other Cells through the BB bus by closing its own breaker. In this architecture, the system would also have 2 modes of operation – SA & IC mode.

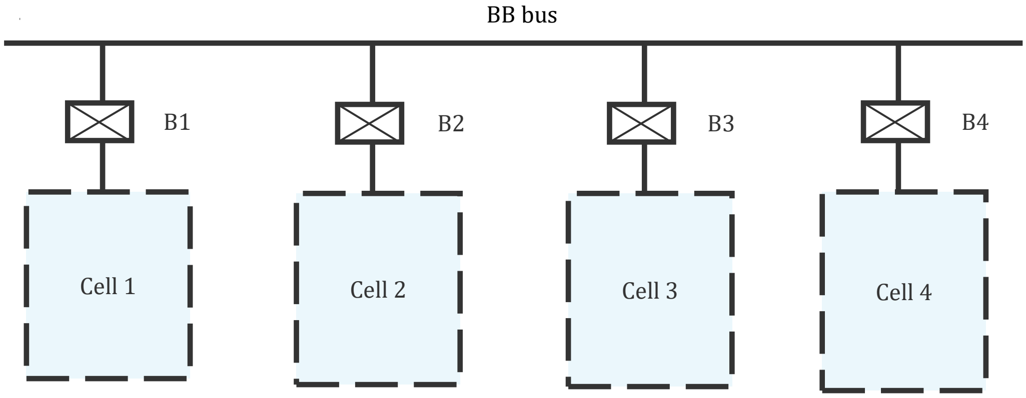


***Figure 3.2:*** *Multiple Cells interconnected through Backbone bus*

A third MG architecture, a combination of both above architectures, implies 3 different operating modes – SA, IC & GC modes. The layout of the system is shown in Figure 3.3. Though each Cell can have three modes of operation, due to lack of ICT equipment, the cell cannot distinguish whether it's connected to another cell or to EG through the BB bus.

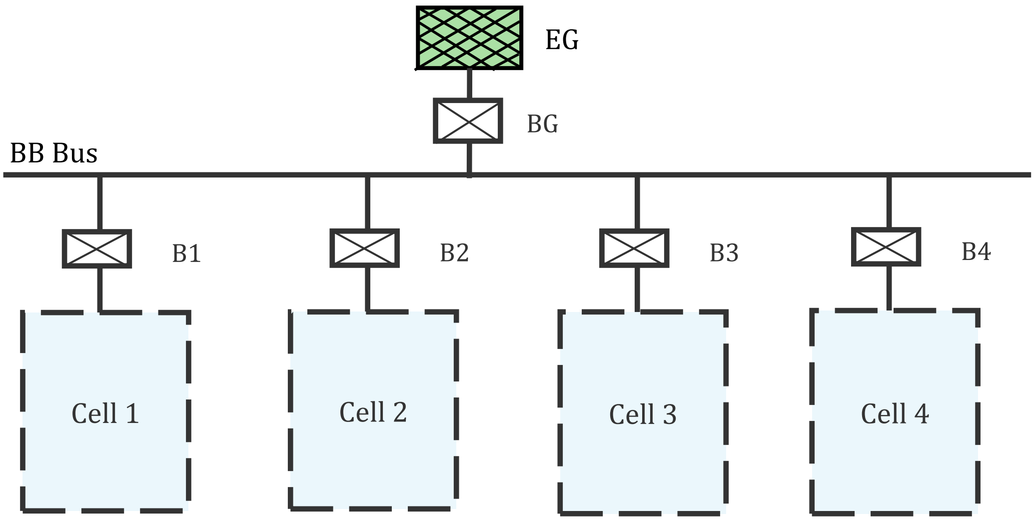


***Figure 3.3:*** *Multiple Cells interconnected through Backbone bus with External Grid*

## 3.3 Battery Energy Storage System

For the modelling of the battery, different approaches – mathematical battery models and circuit-oriented battery models, are proposed in literature. The mathematical models aid in predicting system behaviour like efficiency, age, capacity and provide accurate results for specific applications. Whereas, circuit-oriented models are based on a combination of electrical elements like voltage sources, resistors, capacitors etc. These models are generally used for simulation with other electrical network for instance a MG. Both these modelling approaches have developed over time to efficiently evaluate battery electrochemical characteristics while taking into consideration age, life cycle and charge/discharge rates [41].

The battery system is a cluster of batteries in series and parallel combinations. Based on the number of the batteries in series, the terminal voltage of the battery system is defined. In other words, the voltage of the bank is calculated by multiplying the number of cells in series with the open-circuit voltage ($V_{OC}$) of each battery. The Ampere-hour (Ah) rating of the battery system depends on the number of batteries in parallel strings, i.e. Total Ah rating of system is computed by multiplying individual battery Ah rating and number of parallel strings.

As the design of the battery is not the major focus of thesis, a simple battery model design is utilized in our system design for estimating the voltage of the battery system and State of Charge (SoC). To model the battery, a variable DC voltage source is applied in series with an internal resistance [42]. The voltage of the battery is dependent on $V_{OC}$ and internal resistance.

The SoC of the battery system is computed by measuring the current flowing through the bank using the following Eqn. (3.1) , taking into consideration the initial capacity of the battery system [9].

$$SoC(t) = \frac{Q_o - \int_{to}^{t} I_{bat}}{Q_{bat}} \tag{3.1}$$

***Internal Resistance*** - The inclusion of the internal resistance is to compensate for voltage drop across the resistance r, as shown in Figure 3.4 , during charging and discharging cycles. The output voltage of the battery system not only depends on the $V_{oc}$ but also on the current flowing through each battery. As the discharge current increases, the voltage drop also increases, and a result of which the output voltage decreases proportionately. Similar is the case for charging scenario, where it would create a negative voltage drop and hence the battery output voltage varies accordingly. The value of internal resistance of battery generally depends on SoC and temperature and it differs for charging/discharging cycles. However, due to low sensitivity to changes in battery terminal voltage, the internal resistance is considered constant (10 mΩ) for estimating the voltage drop [43].

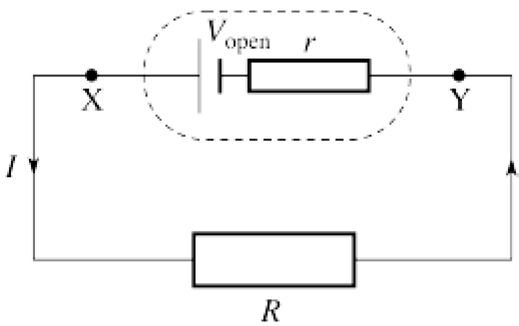


***Figure 3.4:*** *Equivalent circuit of battery* [34]

**<u>Voltage SoC dependency</u> -** The type of battery is yet another major aspect for consideration in the design of BESS. In comparison to alternative battery technologies, Li-ion batteries offer significant benefits – low energy density, minimal memory effect, least self-discharge, cyclic efficiency and long lifetime. In addition to these advantages, recent developments in Li-ion chemistry particularly in operating range establish Li-ion batteries as a promising technology for energy storage applications [44]. Due to above-mentioned reasons, Li-ion batteries was considered in the design of the battery model. The terminal voltage of the batteries varies with SoC, which implies that the input voltage to the DC to AC converter would also differ with SoC and hence, the modulation factor has to be altered in order to obtain same AC output voltage. The curve representing the dependency of SoC with terminal voltage, obtained from DNV-GL, is shown in Figure 3.5.

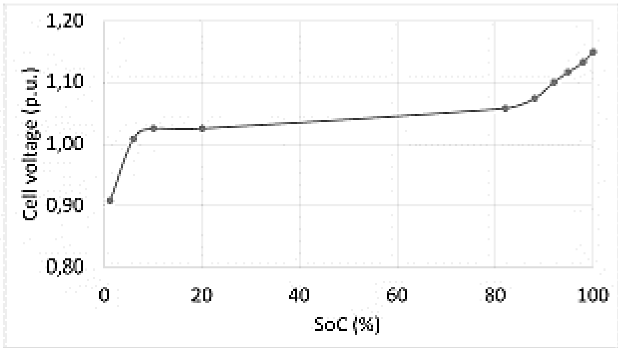


***Figure 3.5***: *Terminal voltage dependency on SoC* [45]

With reference to aforementioned factors – *SoC*, Internal resistance and $V_{oc}$– *SoC* curve, the layout of the battery model designed is depicted in Figure 3.6. The battery model accepts the measured power from the battery ($P_{bat}$) as an input. Dividing this $P_{bat}$ by the output terminal voltage of the battery bank ($V_{bat}$), the value of the DC current ($I_{bat}$ ) is calculated. The $I_{bat}$ value is subsequently integrated over a time constant of 3600 to compute SoC of the battery system. Knowing the value of SoC, the new $V_{oc}$ is computed using the curve in Figure 3.5. The voltage drop due to $I_{bat}$ flowing through internal resistance is subtracted from the previously calculated $V_{oc}$ to arrive at the battery terminal voltage ($V_{bat}$). As mentioned before, since the battery is modelled as a variable DC source, the calculated $V_{bat}$ is given as an input to this source.

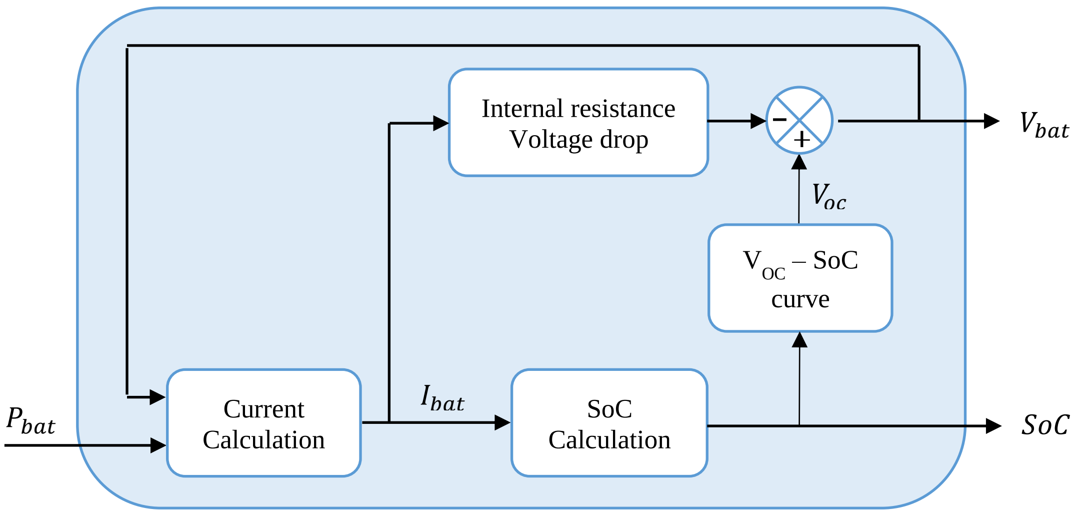


***Figure 3.6:*** *Battery model*

## 3.4 Voltage Source Converter

In order to interface the DC output voltage of the Battery model, as described in Section 3.4, to the AC network, a bidirectional Voltage Source Converter (VSC) is used. The converter is based on the standard Pulse Width Modulation (PWM) method, which is used to transfer power from DC to AC and vice versa. The direction of power flow to/ from the PWM converter determines whether the battery is being charged or discharged. The inbuilt PWM converter in PowerFactory is modelled as a self-commutated, voltage source converter as shown in Figure 3.7, with switches like GTO, IGBT that have turn-off capability. The two-level converter used in thesis employs a IGBT switches for conversion of AC to DC and vice versa.

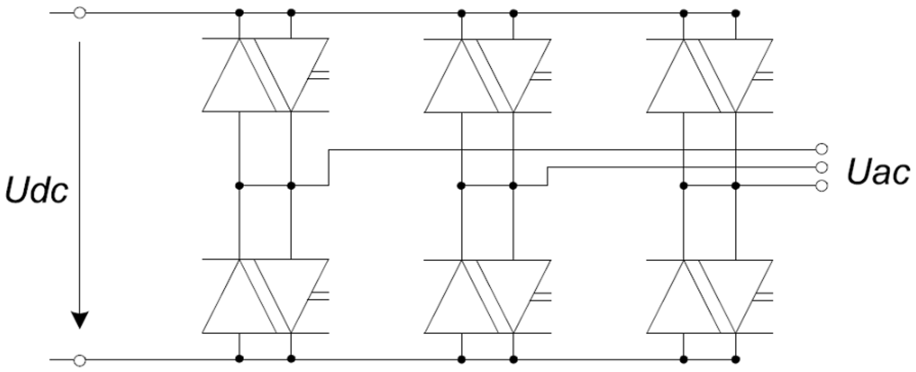


***Figure 3.7:*** *PWM Converter – Equivalent circuit* [46]

For the dynamic simulation of the converter, the model demands certain combination of inputs signals in PowerFactory software for calculation of the PWM. The combination of input signals is shown in Figure 3.8 and summarized below. The choice of combination of input signals depends whether the converter is modelled as a Voltage Source Inverter (VSI) or a Current Source Inverter (CSI).

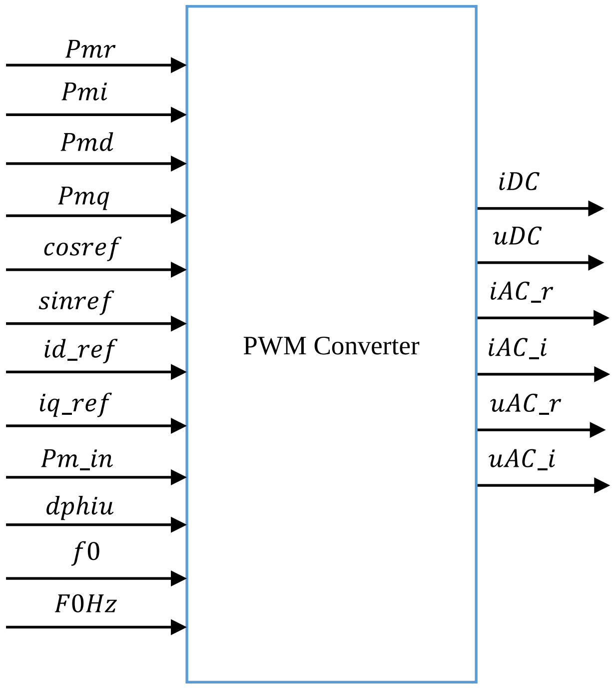


***Figure 3.8:*** *Input and Output signals of PWM Converter in PowerFactory* [46]

- *Pmr, Pmi*: Real and imaginary part of the pulse width modulation index have to be supplied to the inverter. A reference system e.g. a reference machine or an external network is required for providing the reference phase angles.
- *Pmd, Pmq, cosref, sinref*: The modulation index is provided as d-q components, defined by the reference frame signals – cosref and sinref. This means that an external network or a reference machine is needed, which is same as the first combination.
- *id_ref, iq_ref, cosref, sinref*: Reference values for the d and q-axis current are given with the internal current controller in the converter. Similar to the previous input, a reference machine is necessary for reference angle signals.
- *Pm_in, dphiu*: Magnitude and phase of the PWM modulation. This is exactly equivalent to Pmr, Pmi.
- *Pm_in, f0 (F0Hz):* Pm_in is the magnitude of the modulation index and f0 is the frequency in per unit (F0Hz is the frequency in Hertz). In this mode, the converter acts as a VSI.

In this thesis, the combination of *Pm_in, f0* inputs are utilized for ensuring that the converter of the BESS behave as the Grid-forming element in the MG network.

## 3.5 LCL Filter

As explained above, VSI are used for power conversion from DC to AC both in SA, IC or GC mode. The use of PWM based VSC introduces undesirable harmonics into the Cell, resulting in extra power loss [47]. So, passive filters are normally inserted between VSI and MG to attenuate voltage harmonics and current distortion to acceptable limits as defined by IEC 1000-3-4 regulation, thus improving the power quality [48]. The choice of type filter counts on a lot many factors – size, weight, voltage drop, harmonic attenuation etc. The basic filter topologies – L, LC and LCL types, are depicted in Figure 3.9.

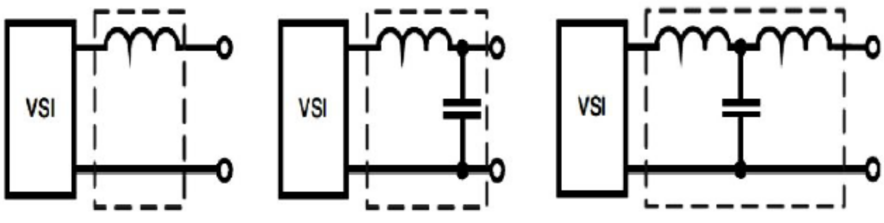


***Figure 3.9:*** *Basic filter topologies* [49]

The first type is an L filter (first-order), which demands a large inductor to achieve sufficient attenuation and thus greatly decreasing the dynamic response of the system. The other type is a second-order LC filter. In addition to large inductors, delayed time response and resonance frequency are other disadvantages of LC filters. In comparison to L and LC type, LCL filters (third-order) offers good current harmonics attenuation even with a small size of inductor [49], [50] . However, these filters can introduce resonance that could lead to unstable states into the MG. Active and passive techniques exist to suppress the resonances of LCL filter. However, passive techniques are preferred due to low-cost. A damped LCL filter with resistor in series with capacitor, as shown in Figure 3.10, is adopted for design of LCL filter in the thesis.

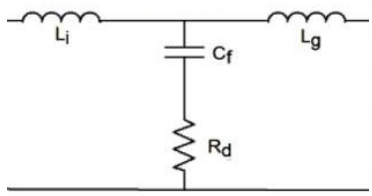


***Figure 3.10:*** *Damped LCL filter with series resistor* [49]

The design of LCL filter model is based on the per-phase equivalent model as shown in Figure 3.11, where $L_1$ and $R_1$ are inverter side inductor and resistor, $L_2$ and $R_2$ grid side inductor and resistor, $C_f$ filter capacitor in series with damping resistor $R_f$. Voltages $v_i$ , $v_g$ are input and output voltages and currents $i_i$ , $i_c$ and $i_g$ are input, capacitor and output currents respectively.

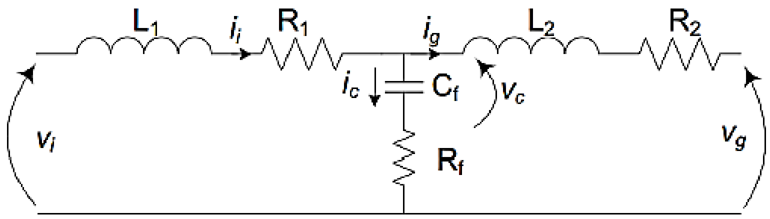


***Figure 3.11:*** *LCL filter per phase model* [51]

The knowledge of the base parameters is beneficial for the design of filter. The base impedance ( $Z_b$), inductance ($L_b$) and capacitance ($C_b$) are defined as per Eqn. (3.2) and all the filter values are referred as percentages of these base values.

$$Z_b = {U_n}^2/P_n \qquad\qquad L_b = Z_b/w_g \qquad\qquad C_b = 1/Z_b \cdot w_g \tag{3.2}$$

where $U_n$ - line to line rms voltage, $P_n$ - rated active power and $w_g$ $\left(2\pi f_g\right)$ - angular grid frequency. Knowing the base parameters, the methodology for design of LCL filter is described below [51], [52].

- The value of filter capacitance ($C_f$) influences the power factor and a higher capacitance value would result in higher reactive power consumption. The maximum power factor variation as seen by the grid is considered as 5% [53], which means that $C_f$ is given by Eqn. (3.3).

$$C_f = 0.05 \cdot C_b \tag{3.3}$$

- The value of inverter side filter inductor ( $L_1$) depends on the maximum allowable ripple current. A smaller ripple current indicates lower switching and conduction losses but requires a larger size of inductor, thus resulting in higher core and coil losses [54] . The maximum ripple current ($\Delta I_{Lmax}$) of a sinusoidal PWM inverter can be calculated with help of Eqn. (3.4).

$$\Delta I_{Lmax} = \frac{V_{dc}}{6\, f_{sw} L_1} \tag{3.4}$$

  where $V_{dc}$ - DC link voltage and $f_{sw}$- switching frequency. Typical values of ripple current vary between 10 -20% of rated current ( $I_{rated}$) [54]. Here, a 10% ripple of the rated current is assumed and the value of $L_1$ can be found by rewriting Eqn. (3.4) as

$$L_1 = \frac{V_{dc}}{6\, f_{sw} \Delta I_{Lmax}} \tag{3.5}$$

$$\text{where} \quad \Delta I_{Lmax} = 0.1 \cdot I_{rated}$$

- As per IEC 61000-4-7 standard, the grid current THD must be restricted to 5%. The ripple reduction of the LCL filter depends on the attenuation rate ($\delta$). The Eqn. (3.6) defines the attenuate rate, which correlates harmonics injected to grid by that generated by inverter.

$$\frac{i_g(h)}{i_i(h)} = \frac{1}{\left|1 + r\,[\,1 - L_1\, w_{sw}{}^2 C_f]\right|} = \delta \tag{3.6}$$

where $w_{sw} = 2\pi f_{sw}$. A lower value of attenuation rate means lower current harmonics. By choosing the desired attenuation rate, the value of r in Eqn. can be calculated to arrive at the value of grid side filter inductor ($L_2$ ) as per Eqn. (3.7).

$$L_2 = r \cdot L_1 \tag{3.7}$$

- The total value of LCL filter inductors, ($L_T = L_1 + L_2$), is preferable to be lower than 0.1 p.u. [53] (Eqn. (3.8)) to ensure that associated losses and voltage drops are negligible at normal frequency and enhance system dynamic response.

$$L_T = L_1 + L_2 = 0.1 \cdot L_b \tag{3.8}$$

- After selection of the filter parameters, the resonance frequency must be checked to satisfy the condition mentioned in Eqn. (3.9). This is basically to ensure that there is no resonance at low and high order frequencies [53].

$$\begin{gathered} w_{res} = \sqrt{\frac{L_1 + L_2}{L_1 L_2 C_f}} \\ 10\, f_g < f_{res} < 0.5\, f_{sw} \end{gathered} \tag{3.9}$$

where $f_{res}$ is resonance frequency.

- The damping resistor ($R_f$) in series with filter capacitance ($C_f$) attenuates the resonance by the LCL filter. The value of $R_f$ is computed at resonant frequency as per Eqn. (3.10).

$$R_f = \frac{1}{3\, w_{res}\, C_f} \tag{3.10}$$

## 3.6 DRES

DRES are the major sources of energy in the MG and as conventional methods these sources are interfaced with the MG as CSI as already explained in Section 2.3. Mainly two types of DRES – PV and Wind are considered here in this thesis. In case of PV, the DC power generated is inverted using the converter to match the MG parameters, voltage and frequency, and inject AC power to the MG. However, the wind turbines, which produce AC is passed to back-to-back converter before being fed to MG. So, with respect to MG, DRES behave as static device feeding in power. Additionally, more sources of energy could be also considered based on application.

In PowerFactory, Static generator is used to model any non-rotating generator, DRES and it basically supports 4 different modes: current, voltage, impedance and power source. However, since the DRES are grid feeding elements, the current source model of the static generator, as in Figure 3.12, is used for system design [55].

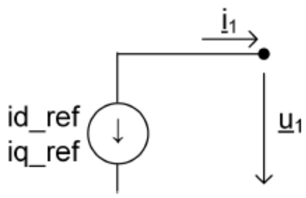


***Figure 3.12:*** *Static generator – Current source model* [55]

Since the data of the power produced from DRES was obtainable, the power is transformed into direct ($id$) and quadrature ($iq$) current per unit system. $id_{ref}$ is easily calculated by dividing the power by the nominal voltage of MG, and $iq_{ref}$ = 0 always as the reactive power contribution is considered zero. The calculated $id_{ref}$ & $iq_{ref}$ are given as input signals to the Static generator model [34].

### *DRES Control*

In a MG, there exist scenarios where the Cell has a high SEP, during which the frequency of the Cell ($f_C$) might cross the upper limit of 52Hz (EN50160 standard). For instance, consider the battery has a high SoC, say 80%, so the corresponding $f_{SOC}$ is 50.2Hz. At the same time, if the generation from DRES exceeds the load requirement, the surplus power is absorbed by the battery, since the battery convertor is operating as VSI. Following the droop curve (Eqn. (2.1)), the frequency of the cell would be higher than $f_{SOC}$ as the convertor absorbs power. As the battery absorbs power, the SoC increases and subsequently $f_{SOC}$ and $f_C$ increases, leading towards the crossover of the upper limit of 52 Hz. So, to avoid such situations, some curtailment or SSM schemes must be incorporated to ensure the operation of MG within the frequency interval of 47 - 52 Hz.

For the SSM scheme, the power output from DRES is curtailed by applying the German standard *VDE-AR-N4105*. The curve relating the power output and frequency is shown in Figure 3.13. When the frequency of Cell ($f_C$) crosses 50.2Hz, the DRES power is restrained at the rate of 40%/Hz. However, during this downward trend, if the MG frequency reduces due to larger load demand, the DRES output rises proportionately as per the defined slope. The moment the upper limit of 51.5Hz is crossed, the DRES output is cut directly from 48% to zero. The system regains its original power output only when the MG frequency drops below 50.05Hz for a minimum period of 60s [56].

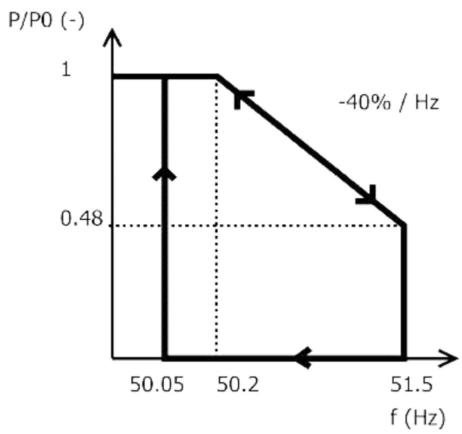


***Figure 3.13****: DRES curtailment profile* [34]

The DRES control, as depicted in Figure 3.14, comprises of three main blocks. The Power DRES profile block receives the power output from DRES as an input, further referred as $P_{DRES}$. The DRES curtailment standard (Figure 3.13) is implemented in the Over frequency power reduction block, which calculates the *Curtailment factor* (CF). As explained earlier, DRES act as grid feeding element and thus the direct and quadrature current references, $id_{ref}$ & $iq_{ref}$, are computed by current calculation block and fed as inputs to the static generator, employed for modelling DRES. The current references are determined using Eqn. (3.11).

$$id_{ref} = P_{DRES} \cdot CF/u \qquad iq_{ref} = 0 \tag{3.11}$$

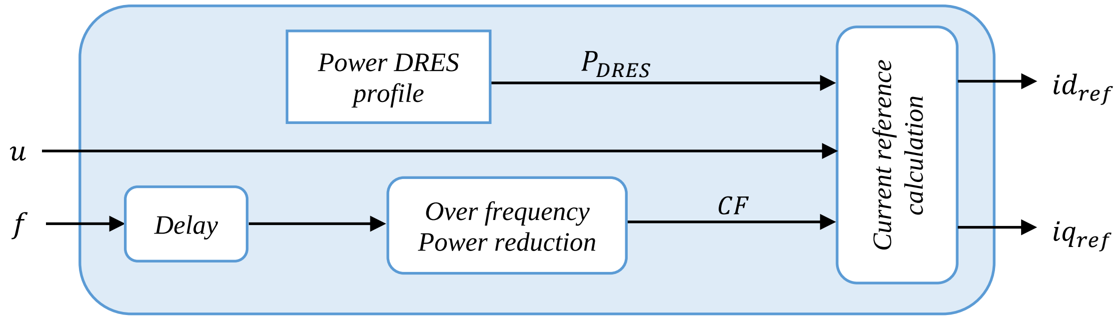


***Figure 3.14:*** *DRES over-frequency power control*

During the switching transitions when the connection and disconnection controllers are activated, the controllers create additional deviations preparing the Cell for a seamless transition. But during these periods, the MG frequency, $f_C$, may cross 50.2Hz for a short period (~ 10-20 s), before reaching its steady state value. This can mainly be attributed to PI or PID action of the associated connection and disconnection controllers. As a result of which, the $CF$, output of Over frequency power reduction block, attain a value very close to 1 as per DRES curtailment profile (Figure 3.13) and the DRES output marginally declines. This means that the DRES production is curtailed undesirably.

From EN50160 standard, it is clear that the Cell frequency $f_C$ is allowed to vary within a bandwidth 49.5 – 50.5 Hz, following grid requirements [56], even when the transitions occur. So, in a way, $CF$ would never be zero during transitions as the $f_C$ in no way reaches 51.5Hz. However, the value of $CF$ which deviates slightly from 1 for a brief interval regains its original value 1 as $f_C$ approaches its normal state. Subsequently, the output of DRES follows a similar behaviour and the maximum power from DRES is utilized in meeting the power demand of the MG.

Another way to encounter this undesired curtailment is by sending signals to respective DRES control for disabling the DRES over-frequency power control for a dead band time of approximately 20s. This demands a low bandwidth communication of the signal which may or may not be feasible based on application scenario. But, this would ensure that the output of DRES is not restricted during the switching periods as desired.

## 3.7 Load

In a power system, loads play a central role as they depict the energy consumption profile of the end consumers. Due to the presence of such a large variety of types of loads, modelling of these loads and their characteristics and behaviour is not a straightforward task. Each type of load would have a different impact on the operation state of MG. As defined in [57], there are two broad categories of loads These are

a) *Static loads*
b) *Dynamic loads*

Static loads respond to fast changes in grid frequency and voltage and they achieve their steady state condition within a short span of time. In contrast, dynamic loads, for example motors, have a slower response time with variations in grid frequency and voltage. A detailed modelling of dynamic loads and their effect on the system behaviour should be analysed to ensure stable operation under varying loading scenarios [57]. The loads can have three distinctive characteristics.

a) *Constant Power*
b) *Constant Current*
c) *Constant Impedance.*

The *exponential load model* is capable of simulating the characteristics of these loads [57]. In this model, the active and reactive power of the load is expressed as exponential functions of the voltage of the load terminal and are mathematically expressed as

$$P = P_0(\frac{V}{V_0})^a \tag{3.12}$$

$$Q = Q_0(\frac{V}{V_0})^b \tag{3.13}$$

where $P$ & $Q$ = Active and reactive power consumed by load at bus voltage $V$, $P_0$ & $Q_0$ = Active and reactive power of load at nominal bus voltage $V_0$, $a$ & $b$ are constants indicating the characteristics of the load as in Table 3.1.

***Table 3.1****: Exponents defining Load Type* [58]

| ***Value for a, b*** | ***Load Type*** |
|---|---|
| 0 | Constant Power |
| 1 | Constant Current |
| 2 | Constant Impedance |

The corresponding load model in PowerFactory is General Load [58]. These loads are modelled as constant power loads, which requires 2 inputs – active & reactive power set points $P_0$ & $Q_0$ as in Equations (3.12) & (3.13) to calculate the power consumed by the load.

### *Load Control*

Analogous to the previous scenario, there also exist scenarios where the Cell frequency $f_C$ goes below 49.5 Hz as the SEP of the MG is low. For example, consider the SoC of battery as 20% which correspond to $f_{SOC}$ of 49.2 Hz and the output of DRES is unable to satisfy the load requirement. In such situations, the battery would continue to supply power to maintain the power balance in the MG network and resulting in further decline in SoC from the previous unhealthy state of 20%. But if this proceeds, after certain moment the SoC approaches zero and the battery will no longer support the load requirement. This is completely undesirable as there may be some loads more critical than the other for example like hospital. This necessitates some control of the loads to ensure the stable of the critical loads in the MG.

For the load control, DSM schemes, as explained in Section 2.6, are applied for ensuring stable operation of MG, meeting the demand of emergency loads. The loads are classified on priorities – low medium and high, based on the application. Distinctive load shedding profiles may be utilized to control different variety of loads. Some loads like pump can modulate their power output based on the MG frequency while other loads can just switch between on and off states. Additionally, there may be some loads like the hospitals which always demand a certain power requirement. The different load shedding profiles as proposed in [34] are adopted here in this work and the same is depicted in Figure 3.15.

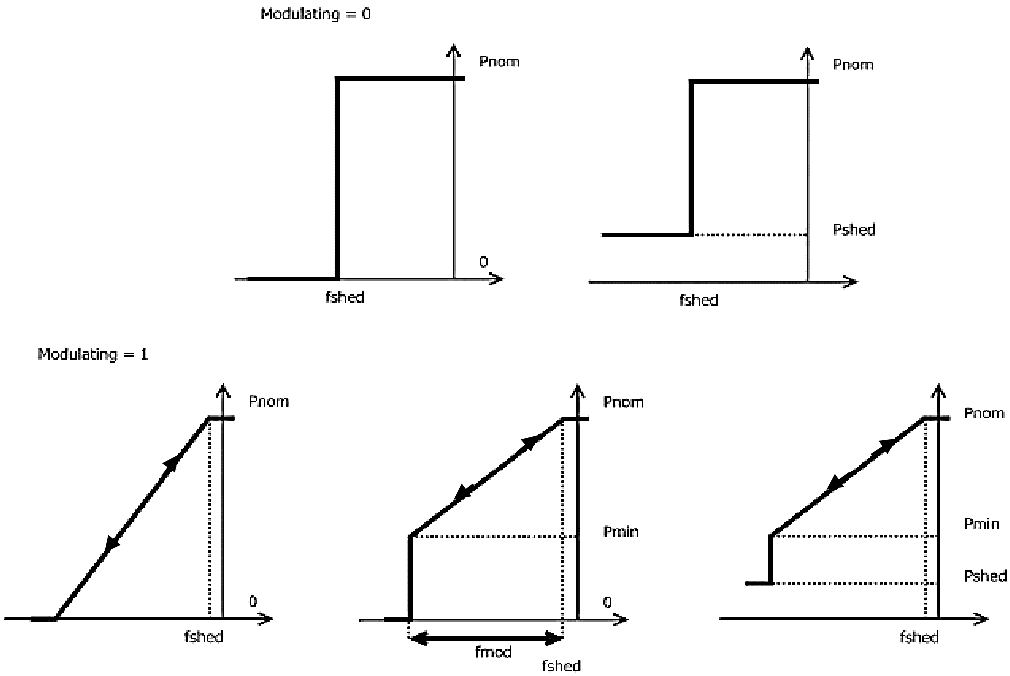


***Figure 3.15***: *Load shedding profiles*[34]

Restoration of loads is equally important as the shedding of loads as a cautious design is needed to avoid any oscillations in the behaviour of MG. For example, consider the case where a load is shed based on the shedding profile and the measured Cell frequency, $f_C$. As the load demand decreases, the value of $f_C$ increases. Due to this, the load is restored back and this might again trigger the load shedding scheme. Such oscillatory behaviour in MG can be avoided by devising two factors – Frequency restoration set points and Size of restoration [59]. So, a discrete load restoration, as proposed in [34], is adopted, meaning that loads are restored progressively as the MG regains a certain level of sustenance. For instance, the medium priority loads restore in the frequency band for low priority loads. Thus, a dead band is computed and integrated to guarantee non – trigger of load shedding following restoration.

The layout of the load control, comprising of 3 main blocks, is depicted in Figure 3.16. The Power Load profile receives the power pattern of the load and generates $P_L$. With frequency as an input to the Shedding/ Restoration block, the *Shedding factor* (ShF), is computed based on the load shedding profiles – whether its Modulating or Non-modulating and other parameters such as Dead band $(f_{mod}), P_{min}$, $P_{shed}$ and $f_{shed}$ (Figure 3.15). This factor is then used to calculate the new power consumed by the load, $P_{ext}$. The reactive power required by the load is computed by assuming a constant power factor (pf) and $P_{ext}$. Thus, the derived values $P_{ext}$ and $Q_{ext}$ are fed as inputs to the General Load.

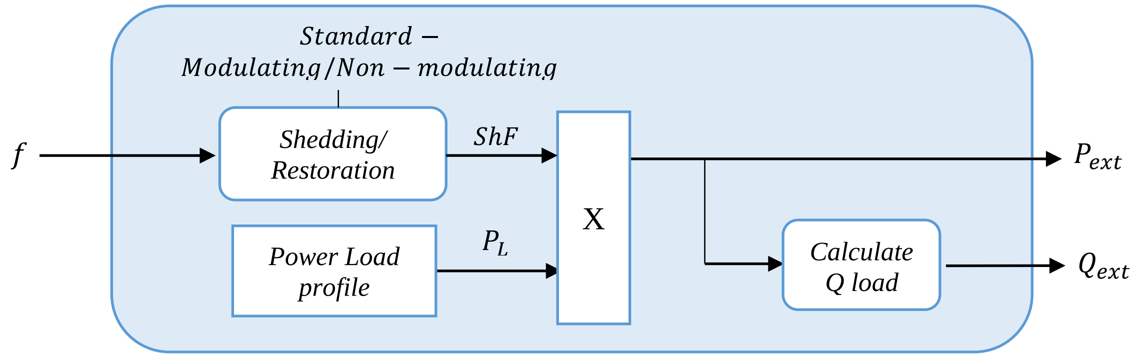


***Figure 3.16:*** *Load under-frequency power control*

Similar analysis as to how the load control responds for the additional deviations produced by the connection and disconnection controllers are performed. The deviations created by these controllers for a seamless transition last for a few cycles (approx. 20 s). During which, the Cell frequency $f_C$ may drop below 49.5 Hz due to PI/PID action of these controllers and thus resulting in undesirable trigger of load shedding. This is followed by an immediate restoration as the $f_C$ regains its steady state value within short period, thus injecting instability into the system.

To avoid such undesirable triggering, the way in which the shedding factor, $ShF$, calculated is modified. Based on the standard, the effect on the system response would vary. For a modulating scheme, these deviations would create a $ShF$ value almost close to 1 as per the slope defined for the load shedding schemes (Figure 3.15). However, as the $f_C$ approaches the steady state value, $ShF$ would gradually regain its previous value of 1 by moving up the slope and thus not creating sudden changes in the system. While for the Non-modulating scheme, $ShF$ value can attain either 1 or 0 based on the $f_{shed}$ parameter. So, this produces a sudden jump in the power consumed by the load during switching periods, creating oscillatory behaviour.

This system response can be prevented by calculating the value of $ShF$ based on the average value of $f_C$. For instance, consider a Cell having a low SoC, say 20%, and a certain load, following non-modulating scheme, for which the $f_{shed}$ frequency defined as 49.5 Hz. As the Cell frequency $f_C$ is below 49.5 Hz in SA mode, the load shedding is triggered, however $ShF$ would attain value of 0, only if Cell frequency $f_C$ is below $f_{shed}$ for a minimum of 10s. As soon as $ShF$ achieves the value of 0, the load demand becomes null. As the MG prepares for transition to GC mode, the Cell frequency $f_C$ goes above 50Hz as defined by the connection controller (Section 4.3.2). However, the $ShF$ is allowed to regain value of 1, only if the MG frequency $f_C$ is above $(f_{shed} + f_{mod}/2)$ for a minimum period of 10s [34]. So, this strategy aid in eliminating unwanted shedding and restoration process during transition stages.

As mentioned previously for the DRES control, another feasible way to avoid such undesirable behaviour is to disable these controls for a small dead band period of approximately 10s. This, would in a way support in eliminating such unwanted oscillatory behaviour but at the cost of low bandwidth communication signal to the load control.

## 3.8 Cables & lines

Cables and overhead lines are another major element in the power system, connecting different components within a MG and/or interconnecting multiple Cells and EG. They play a pivotal role in transmitting power between MG components and for sharing of power between MGs and External Grid in case of I or GC operation modes, thus influencing the overall dynamic performance of the system.

In the proposed MG architecture, AC-cables interconnect the loads, DRES and inverter to the Cell bus. However, depending on the physical location of the various components, the length of the cables might differ but relatively small due to proximity. Further there are AC-cables that connect each Cell bus to the BB bus and to the EG. The cable lengths may not be as small as the previous but depend on the distance between Cells.

Since all the cable lengths discussed in the project are comparatively small when compared to long transmission lines of conventional systems, detailed modelling of the cables can be neglected. The cables are modelled as lumped parameters based on π-model. The Figure 3.17 shows the π-model representation of a single-phase cable.

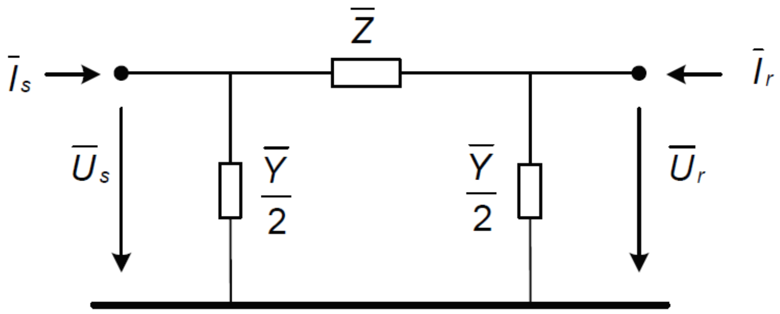


***Figure 3.17:*** *π-model representation of single phase cable* [60]

Where $U_s$ = Voltage at the sending end of the cable, $U_r$ = Voltage at the receiving end of the cable, $I_s$= Current at the sending end of the cable, $I_r$ = Current at the receiving end of the cable, $Z$ = Series impedance of the cable and $Y$ = Shunt admittance of the cable. The other parameters of cable like cross section area are depend on the current carrying capacity and the allowable voltage drop as per Ohms law.

## 3.9 Summary

This chapter discusses about the adopted MG architecture in the project and how each of the components of the Cell are modelled in PowerFactory software. In addition, it also deliberates on the DRES and Load control for implementing the SSM and DSM schemes.

# 4 Control for seamless (dis)connection

## 4.1 Introduction

In the previous chapter, a comprehensive discussion was presented on the diverse MG architectures and how each of the components of the MG are modelled in PowerFactory software. A stable operation of each of these MG components and their interaction with each other profoundly rely on the system control strategy. In other words, the control scheme plays a significant role in defining the dynamic and steady state behaviour of the MG following mode transitions.

A systematic approach on development of control scheme is the primary focus of this chapter. It mainly targets on the formulation of VSC control of the BESS. The BESS is the primary component in the Cell and the VSC of the battery acts as the master controller in the MG as the battery converter is responsible for defining the MG parameters: voltage and frequency. This section elaborates on the proposed control strategy for achieving a seamless transition between SA and GC modes.

The design of the controller of the Battery VSC is primarily dependant on the mode of operation. In SA mode, the battery VSC in the Cell should be a grid forming element. Multiple Cells with their respective VSC as grid forming element can interconnect with each other to build a stronger and robust network, known as IC mode. Or the Cell has the possibility of connection to the EG for operation, which is termed as GC mode. From literature, it is learned that in GC mode, the converter is switched from VSI to CSI mode and vice versa while switching back to SA mode [61], [62]A. As discussed in Section 1.2, one of the primary objective of the project is to avoid the use of ICT equipment, thus enhancing the reliability of operation of MG. This constraint restricts the operation philosophy, as each Cell cannot determine whether its IC or GC mode. Hence the converter is modelled as VSI in all these modes and the controller is devised accordingly to enable a stable operation in all the modes. From Section 3.4, to model the VSC as VSI, it demands the combination of the following inputs.

*a) Frequency of output voltage (f0)*
*b) Pulse Width Modulation index (Pm_in)*

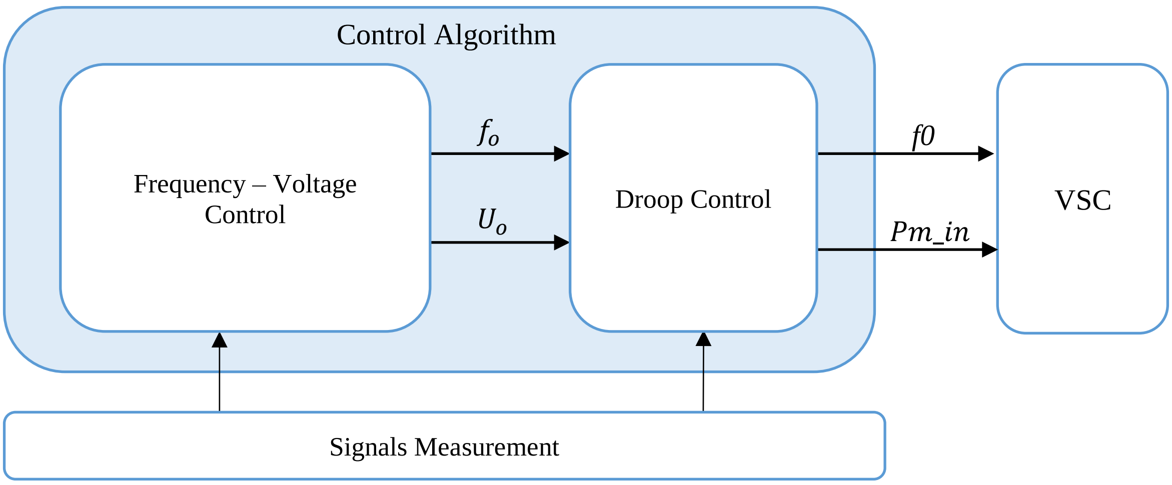


***Figure 4.1:*** *VSC Control Algorithm*

The proposed control algorithm for the VSC is depicted in Figure 4.1. It comprises of two main loops – Droop Control & Frequency – Voltage control. Based on the measured signals, these control loops calculate the desired operating parameters of MG and each of these loops would be discussed in detail in the subsequent sections.

## 4.2 Droop Control

In the MG, the converter being modelled as a VSI do not have any control over the Active power (*P*) and Reactive power (*Q*) delivered, however, the set points, *Pm_in* and *f0* decides the voltage and frequency of the bus through which *P* and *Q* are supplied by the battery VSC. The magnitude of *P* and *Q* depends on the net demand of power flow through the system, which is determined through load flow analysis of the MG. Further, it's worth reiterating that since the MG under consideration is low voltage, the conventional droop curve can be applied either by emulating the inductive behaviour of the grid inside the controller or by physically installing an inductor at inverter output terminal. In this project, it is proposed to install a LCL filter at the output of the inverter to filter out the high-frequency harmonics, thereby inducing the inductive character to the Low Voltage (LV) MG.

By employing the convention Active power – frequency (*P/f*) curve, the operating frequency $(f)$ of the MG is calculated using Eqn. (4.1).

$$f = f_o - k_P \cdot P \tag{4.1}$$

Where $f_o$ is zero-power frequency set-point, $k_p$ active power droop coefficient and *P* power delivered by the inverter. The operating frequency $(f)$ is the same as the input $f0$ to VSC. The (*P/f*) curve is graphically represented in the Figure 4.2. The point of intersection of the curve with the y-axis represents $f_o$, zero-power frequency. The *P* supplied by the VSC is considered positive when the battery is in discharging state and considered negative while it is in charging state. The instantaneous operating frequency $(f)$ would move along the droop curve based on active power output of VSC and the $f_o$ set point input to droop control. This is the case when the VSC operates in SA or IC mode. However, when it is operating in the GC mode, the operating frequency is governed by the conventional grid and remains steady at 50 / 60 Hz.

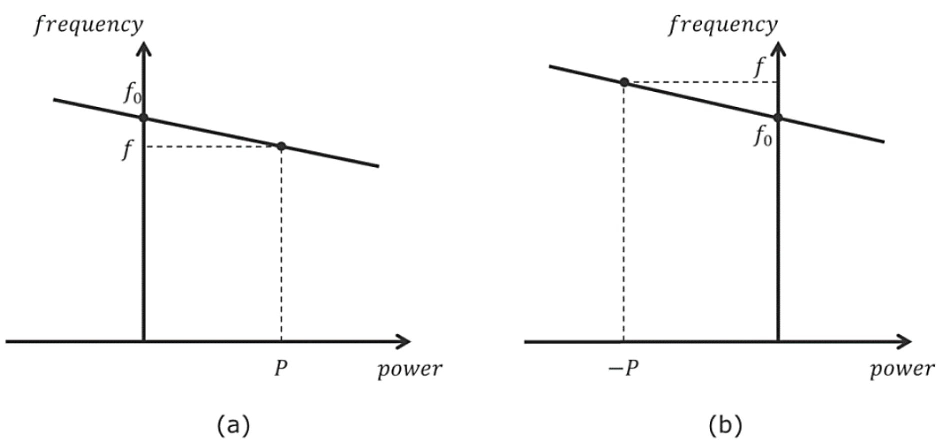


***Figure 4.2:** Active power – frequency droop curve* [63]

It is desired to maintain voltage of a MG as close to its nominal value, but based on the reactive power required by the system, the voltage varies. In order to maintain the voltage deviations within ±10 % of the nominal value as per EN 50160 [56] and to ensure $Q$ sharing in IC and GC modes, the reactive power – voltage (*Q/V*) droop curve is applied. Similar to *P/f* droop, the operating voltage ($U$), is computed using Eqn. (4.2).

$$U = U_0 - k_Q \cdot Q \tag{4.2}$$

where $U_0$ is the set point, $k_Q$ reactive power droop coefficient and $Q$ the reactive power delivered /absorbed by VSC. The graphical representation of *Q/V* droop curve is depicted in Figure 4.3. The point of intersection of the curve with the y-axis represents $U_o$, zero-power voltage. The $Q$ supplied by the VSC is considered positive and absorbed negative. In I or IC mode, the instantaneous operating voltage ($U$) would move along the droop curve based on reactive power output of VSC and the $U_o$ set point input to droop control. But when connected to External Grid, the operating voltage ($U$) is fixed at nominal grid voltage.

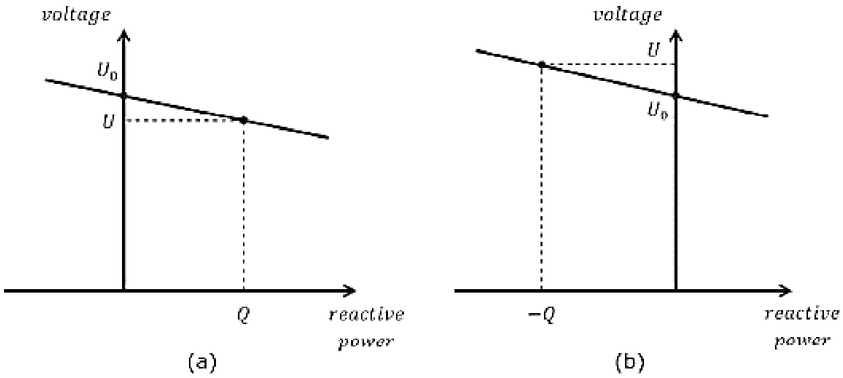


***Figure 4.3:*** *Reactive power – Voltage droop curve* [63]

Once, the desired AC voltage $U_{AC}$ (same as $U$) is tabulated, the magnitude of PWM needs to be calculated for providing as an input to VSC. The magnitude of the PWM depends on the type of modulation technique. In the model, a sinusoidal type of modulation is adopted due to inherent low harmonics and the magnitude of PWM is calculated by Eqn. (4.3).

$$Pm\_in = \frac{U_{AC}}{(k_0 \cdot U_{DC})} \quad \text{with} \quad k_0 = \frac{\sqrt{3}}{2\sqrt{2}} \tag{4.3}$$

where $U_{AC}$ is the desired AC voltage and $U_{DC}$ is the terminal DC voltage of the battery, which is dependent on SoC of battery.

## 4.3 Frequency – Voltage Control

As discussed in Section 4.2 , Droop control, based on conventional P/f & Q/V curve, works on two basic control inputs $f_o$ and $U_o$ (Figure 4.1). As the frequency and voltage set points are varied, the Droop curves shifts vertically upwards or downwards, to arrive at the desired voltage and frequency operating point. The dynamic calculation of these set points, $f_o$ and $U_o$, is performed using Frequency – Voltage control. The proposed control layout of the Frequency – Voltage control is depicted in Figure 4.4. The primary control of the Frequency – Voltage control is determined by the Normal Controller, which defines the normal operating frequency ($f_{norm}$) and voltage, ($U_{norm}$) of the MG, either in SA mode or GC mode. However, to enable a smooth transition between SA and GC modes and vice versa, two secondary control schemes - Disconnection and Connection, are devised. The secondary controllers become active only when respective Enable signals are triggered and produces necessary frequency and voltage deviations - $f_{dis}$ & $U_{dis}$ in case of disconnection and $f_{con}$ & $U_{con}$ in case of connection. All these controllers are comprehensively elaborated in the subsequent sections. But, it's worth mentioning that in all the modes - SA & GC modes and transition state, the converter is still operated as a VSI.

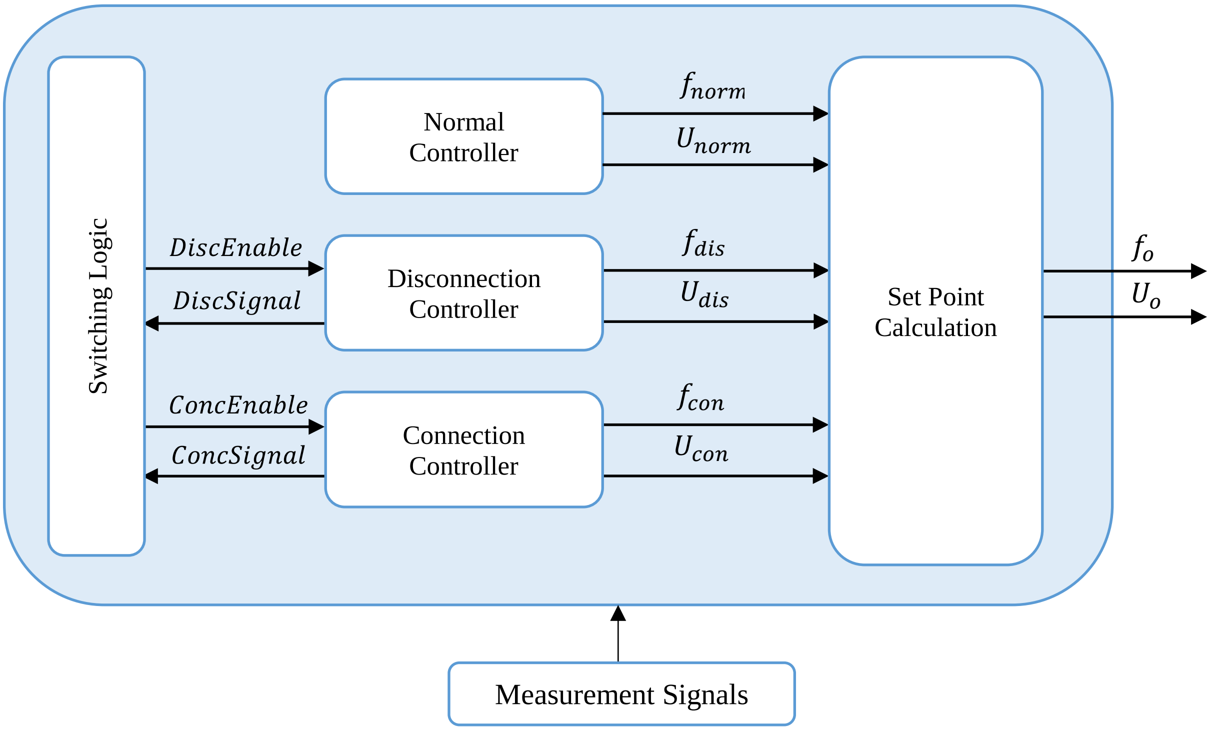


***Figure 4.4:*** *Frequency – Voltage Control*

### 4.3.1 Normal Controller

The Normal controller is the dominant controller in the Frequency – Voltage control, both in IC & GC modes. The Normal Controller generates two output signals – Normal frequency ($f_{norm}$) and voltage, ($U_{norm}$), which contributes largely to the set point calculation $f_o$ and $U_o$.

#### Frequency Control

The control strategy for calculation of normal frequency is presented in Figure 4.5. The Normal frequency of MG represent the State of Energy & Power (SEP) of the cell, in other words, it is based on the SoC of the batteries ($f_{SOC}$).

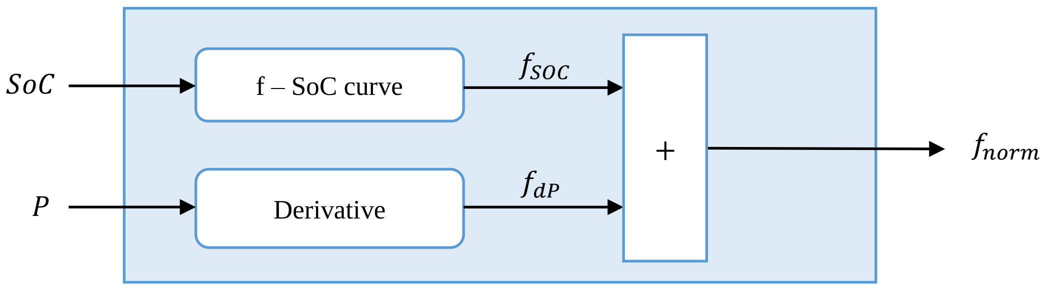


***Figure 4.5:*** *Normal Controller - Frequency*

But to achieve desirable behaviour in all circumstances, more factors are necessary. The frequency deviation due to derivative of power ($f_{dP}$) is added to the main factor $f_{SOC}$ , to formulate the final set point ($f_{norm}$) as per Eqn. (4.4).

$$f_{norm} = f_{soc} + f_{dP} \tag{4.4}$$

*State of charge (**$f_{soc}$**)*

The absence of any ICT equipment restricts the system functionality that it should rely only on local measurement for control and operation of MG. The frequency of the MG is used to assess the healthiness of MG and that is heavily dependent on SoC of battery. So, based on the SoC of BESS, the frequency of the MG is set. A BESS with high SoC will meet the load requirement even in case of reduction in DRES production. Such a system is fully charged, translating to a higher frequency. However, when the SoC of the BESS is low, it may not meet the load demand and thus, the batteries may be discharged more than what is desired. Hence, a lower frequency is preferred for such scenarios Finally, when the SoC is healthy, it is desired to operate the MG close to 50 Hz.

The Figure 4.6 shows the Frequency dependency on SoC ($f_{SOC}$ curve) of batteries. EN 50160 [56] specifies grid parameters with allowable frequency interval of 47 to 52 Hz. Similar to what have been proposed in [34], for the $f_{SOC}$ curve, the frequency band of 48 to 51.5 Hz is chosen corresponding to $SoC_{min}$ and $SoC_{max}$ respectively.

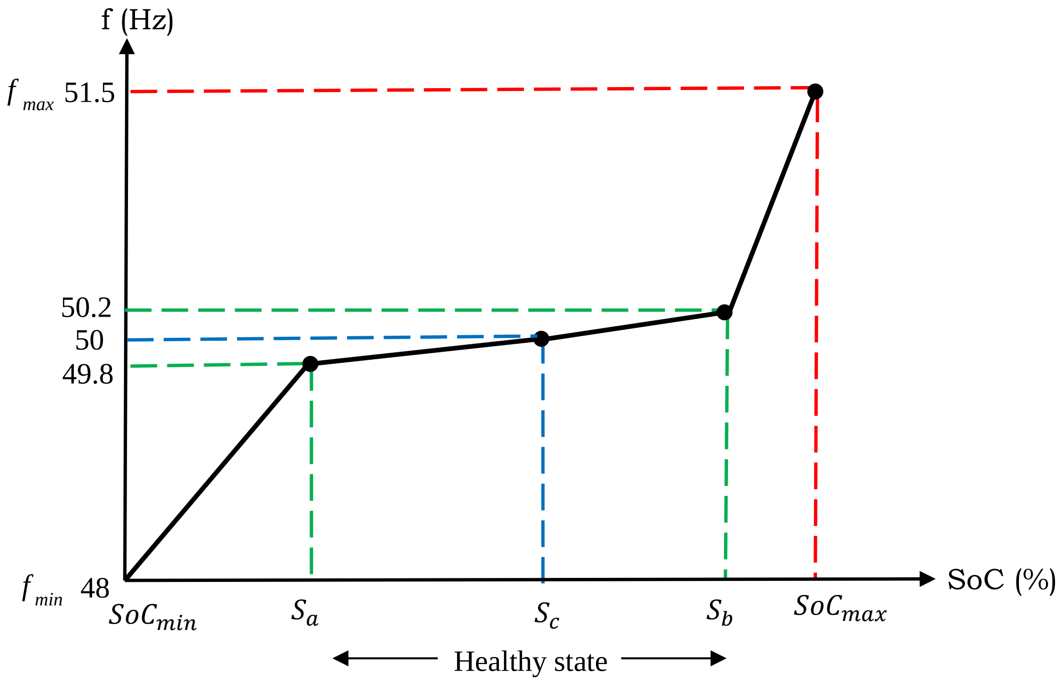


**Figure 4.6:** *f - SoC curve*

To operate the MG as close to 50 Hz, when the BESS is healthy, two limits – lower limit ($S_a$) and upper limit ($S_b$) are defined on the $f_{SOC}$ curve. The healthy SoC state limits - $S_a$ and $S_b$, corresponds to frequencies of 49.8 and 50.2 Hz respectively, so that changes in SoC of BESS in the healthy state leads to minor deviations in frequency, $f_{SOC}$. However, when the battery is out of the healthy limits, a slight change in SoC results in significant frequency deviations. The operating frequency of the MG in GC mode would generally remain fixed at 50 Hz. So, a Cell with high SoC, for instance 80%, connecting to the EG would discharge the battery power till the point, where the SoC of the battery corresponds to the EG frequency ($f_g$). Similar is the case, when the MG with lower SoC, say 30%, when grid connected, absorbs power from the EG and charge the battery to a limit which corresponds to 50 Hz. This is however a limitation while working the converter as VSI in GC mode. To solve this issue, a central State of Charge ($S_c$) is defined on the $f_{SOC}$ curve which corresponds to 50 Hz, normally same as $f_g$. In most cases, the $S_c$ is fixed at 50%, meaning that a frequency of 50 Hz matches a SoC of 50%. This limit could either be increased or decreased based on the objective of operation of each Cell. For instance, if a MG has critical loads like hospitals, it is always preferred to maintain a higher SoC, to ensure a safe and stable operation in I mode. In such cases, the $S_c$ can be raised, say 70%, and hence when in GC mode, the battery would try to maintain this SoC equivalent to $S_c$.

This scheme is implemented in PowerFactory in DIgSILENT Simulation Language (DSL) using the help of the Eqn. (4.5), taking the SoC of the batteries as an input signal.

$$\begin{aligned}
f_1 &= 48 + (1.8 \cdot SoC/(S_a - SoC_{min}) && \forall\, SoC \in [SoC_{min}, S_a] \\
f_2 &= 49.8 + (0.2 \cdot (SoC - S_a)/(S_c - S_a) && \forall\, SoC \in [S_a, S_c] \\
f_3 &= 50 + (0.2 \cdot (SoC - S_c)/(S_b - S_c) && \forall\, SoC \in [S_c, S_b] \\
f_4 &= 50.2 + (1.3 \cdot (SoC - S_c)/(SoC_{max} - S_b) && \forall\, SoC \in [S_b, SoC_{max}]
\end{aligned} \tag{4.5}$$

*Derivative of power ($\boldsymbol{f_{dP}}$)*

A Cell in operation can experience a sudden jump in the power supplied by the inverter, which then leads to sudden discharge of battery. This might be due to variety of reasons - increase in load demand or a sudden decline in DRES production or an unprecedented disconnection from the External Grid. The resulting power imbalance in the MG is offset by the Battery VSC and hence SoC & consequently $f_{SOC}$ drops. For improving the stability of the system, it is preferred to add damping, thereby ensuring that no sudden frequency jump arises. The power of the inverter is passed through a derivative block to create a frequency deviation ($f_{dP}$), as shown in Figure 4.5. The impact of $f_{dP}$ is negative in case of a positive jump and positive in case of a negative jump in power supplied by the battery VSC. So, the frequency of the MG would remain stable in case of sudden power imbalances [34], [63].

To sum up, the formulation of the frequency set point of the Normal frequency controller ($f_{norm}$) depends on the above-mentioned terms - State of charge and Derivative of power.

### *Voltage Control*

The philosophy of calculation of voltage set point, $U_{norm}$, is rather straightforward. It is always desired to maintain the voltage of the MG as close to the nominal value of 400 V ($U_{nom}$). But deviations from the nominal value due to losses needs to be addressed. The proposed layout for the Normal voltage controller with loss compensation is shown in Figure 4.7.

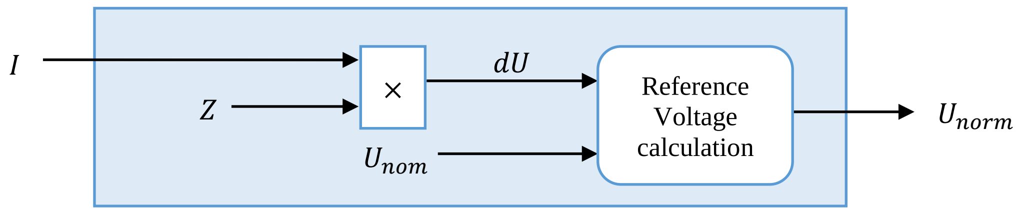


***Figure 4.7:*** *Normal Controller - Voltage*

*Voltage Compensation ($\Delta \boldsymbol{U}$)*

The resistive nature of LV grid contributes significant voltage drop across lines when compared to that of HV. This voltage drop is compensated by increasing the reference voltage using the Ohms law. Measuring the current ($I$) of VSI, the related voltage drop (d$U$) is calculated by using Eqn. (4.6) knowing the value of impedance ($Z$).

$$dU = Z \cdot I \tag{4.6}$$

This voltage drop, $dU$, is used along with the nominal reference voltage $U_{nom}$ to derive the new reference point $U_{norm}$ of the normal controller.

### 4.3.2 Connection Controller

The grid parameters – Voltage and frequency, when the MG is in SA mode is governed by the Normal Controller, as described in Section 4.3.1. For the connection of MG with the EG, the MG parameters must be adapted to match with those values for the EG, before actual close of the contactor. The foremost function of connection controller is to allow a smooth transition from SA to GC mode, still maintaining the operating philosophy of the converter as VSI. Direct connection of the MG to the External Grid results in high transient currents, consequently leading to large power flow in the network. Such abnormalities accelerate component failure rate and degrades the overall stability of the system [64]. To eliminate such transient behaviour in transition, the principle of synchronization is applied. This means that difference in the magnitude, frequency and phase of voltage of the two systems should reduce to a certain limit, before the system changes its mode. The magnitude of error values of voltage, frequency and phase vary with the system configuration. Convention generating units has higher error limits for connection to EG due to its inherent capability and high inertia. A Cell mainly comprising of DRES, BESS is rather weak and has very low or zero inertia when compared to that of the main grid.

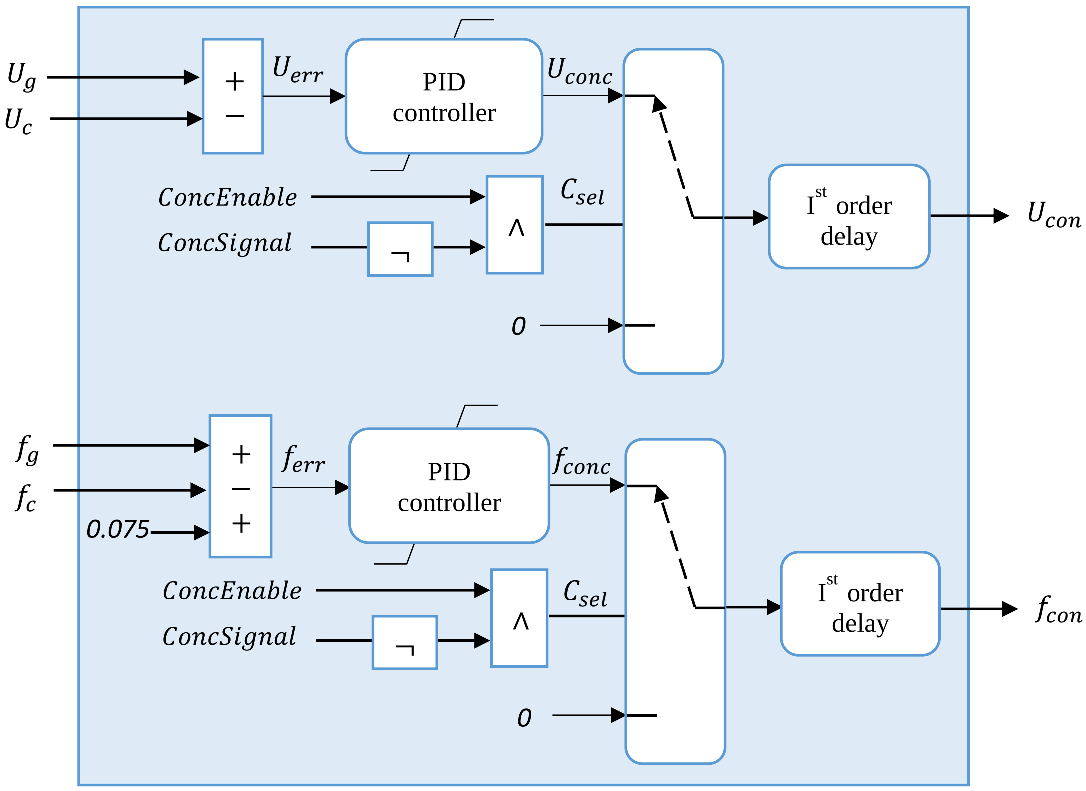


***Figure 4.8:*** *Connection controller*

The algorithm for the connection controller is designed to minimize these errors, creating additional frequency ($f_{con}$) and voltage deviations ($U_{con}$) thus allowing a smooth transition of MG from SA to GC mode. The layout of the algorithm is presented in Figure 4.8.

It comprises of voltage error & frequency error controllers, which are described in the following sections. Both the controllers are activated when it receives enable signal with the state of MG is in I mode, meaning that

$$C_{sel} = 1 \implies ConcEnable = 1 \,\&\, ConcSignal = 0 \text{ (Figure 4.8).}$$

*Voltage error*

Synchronization of two systems with a considerable difference in voltage magnitude would result in a voltage drop, leading to a large current flow. This sudden surge of power flow through the connecting line can destabilize the system. So, to match the voltages of the two systems, the difference between the measured values of voltage of MG ($U_c$) and voltage of External Grid ($U_g$) is fed to the PI controller as an error signal ($U_{err}$). The PI controller tries to minimize this error and bring voltages of the two systems as close as possible. The output of the PI controller is passed through a switching block, which switches between $U_{conc}$ and 0 based on the selection criteria signal ($C_{sel}$). The selected signal is passed through a first order filter to generate the final voltage deviation, $U_{con}$, as shown in Figure 4.8.

*Frequency error*

As in conventional systems comprising of synchronous generators, the interconnection between systems with high-frequency differences results in transient spikes in current, leading to unstable condition. So, before switching from SA state to GC state, the frequency of the both MG and External Grid should be matched. A PID controller is implemented for the frequency error ($f_{err}$). The $f_{err}$ signal is generated taking the difference of frequency of MG ($f_c$) and frequency of External Grid ($f_g$) and then adding a small deviation of 0.075 Hz. Addition of the small deviation would enable faster phase matching between the signals. The PI controller, minimizes the $f_{err}$ signal produces required frequency deviation ($f_{conc}$). The switching block, selects the appropriate signal based on $C_{sel}$ and passes through a first order filter to create the final frequency deviation, $f_{con}$ (refer Figure 4.8).

*Phase error*

The third criteria for synchronization is the phase angle difference, which is a measure of phase shift between the voltage waveforms. A larger phase difference would lead to huge power flow at moment of connection to External Grid, leading to system instability. It is known that integral of frequency difference over time gives the relative phase angle. Due to practical constraint of phase angle measurement, no additional controller is considered. The phase error ($\delta_{error}$) is minimized because of the output of frequency error controller, $f_{con}$. This frequency deviation reduces slowly due to the application of first order delay, indirectly contributing to phase angle error correction.

*Connection criteria*

A cell is rather a weak and very low inertia system when compared to that of the main grid. Therefore, the value of the error magnitudes is chosen to be much more stringent, also keeping in mind the resolution of the sensing elements. Once the errors are within limits, as in Figure 4.9 for a minimum period of 10 cycle (~ 0.2 s), the Cell and the EG connect with generation of $ConcSignal$, which enables closing of the breaker and enable a smooth transition to GC state.

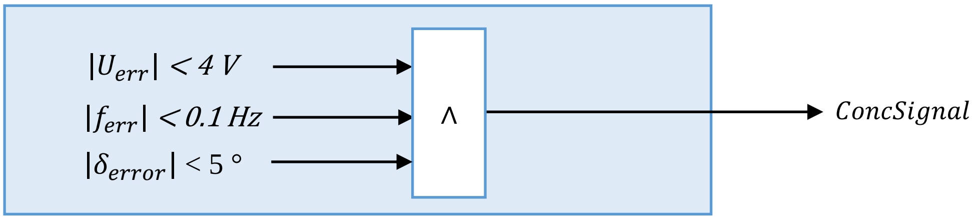


***Figure 4.9:*** *Connection criteria*

### 4.3.3 Disconnection Controller

The main function of the disconnection controller is to ensure a smooth and seamless transition from GC to SA state. When connected to the External Grid, the grid parameters, voltage and frequency, are no longer defined by the converter of the battery, rather, the stiff grid influences these parameters. The External grid tries to maintain the MG voltage and frequency at the operational values of the grid. It is desired in this thesis that the converter still operates as VSI even in GC mode. The reason behind this is to avoid the use of ICT equipment. Hence the converter can rely on local measurements and is unable to distinguish whether the Cell is connected to another cell or the Main Grid.

In GC mode, the battery converter still operating as VSI, has no direct control over the flow of active and reactive power. It is indirectly controlled by the $f_o$ & $U_o$ parameter. This is governed by the Eqn. (4.7) & (4.8) keeping droop coefficients constant.

$$P = (f_0 - f_g)/k_p \tag{4.7}$$

$$Q = (U_0 - U_g)/k_Q \tag{4.8}$$

For instance, consider a Cell which has low state of charge, say 30%, connects to the External Grid. The $f_0$ parameter, is mainly influenced by the $f_{SOC}$ corresponding to SoC of 30% and the operating point of the converter remains fixed as $f_g$. Thus, the battery inverter would absorb power or charge till the battery attains a SoC which corresponds to $f_g$, referred to as $S_c$ in $f_{SOC}$ curve (Figure 4.6). It is worth reiterating that the term $S_c$ could be set at 50 % or higher, to ensure stable operating situation in event of disconnection. When a sudden disconnection occurs, the active and reactive power flow from the EG is interrupted, which is compensated by the VSI of the Cell. Due to the sudden rise of power flow in the Cell, disturbances, particularly in cell frequency and voltage are engendered in the system.

The disconnection controller not only enables a smooth disconnection of Cell from GC mode but also ensures that associated disturbances in the disconnected system are minimal. The control strategy for disconnection is accomplished through a PI controller with anti-wind up limits. The layout of the algorithm is presented in Figure 4.10. The active power and reactive power from the EG are measured and compared with zero to create error signals $P_{err}$ & $Q_{err}$. The error signals are passed through a PI controller generating the frequency and voltage deviations, $f_{disc}$ & $U_{disc}$ . These values are passed through a switching block, which passes the required signal based on the selection criteria signal $D_{sel}$ . The disconnection controller is activated when it receives enable signal in the GC state. In other words, it means that

$$D_{sel} = 1 \implies DiscEnable = 1 \;\&\; DiscSignal = 0.$$

The output of the switching block is passed through a first order delay to avoid the abrupt changes in the signals $f_{disc}$ & $U_{disc}$ . After the filters, the final deviations - $f_{dis}$ & $U_{dis}$ are generated which are used in the formulation of final set points - $f_o$ & $U_o$.

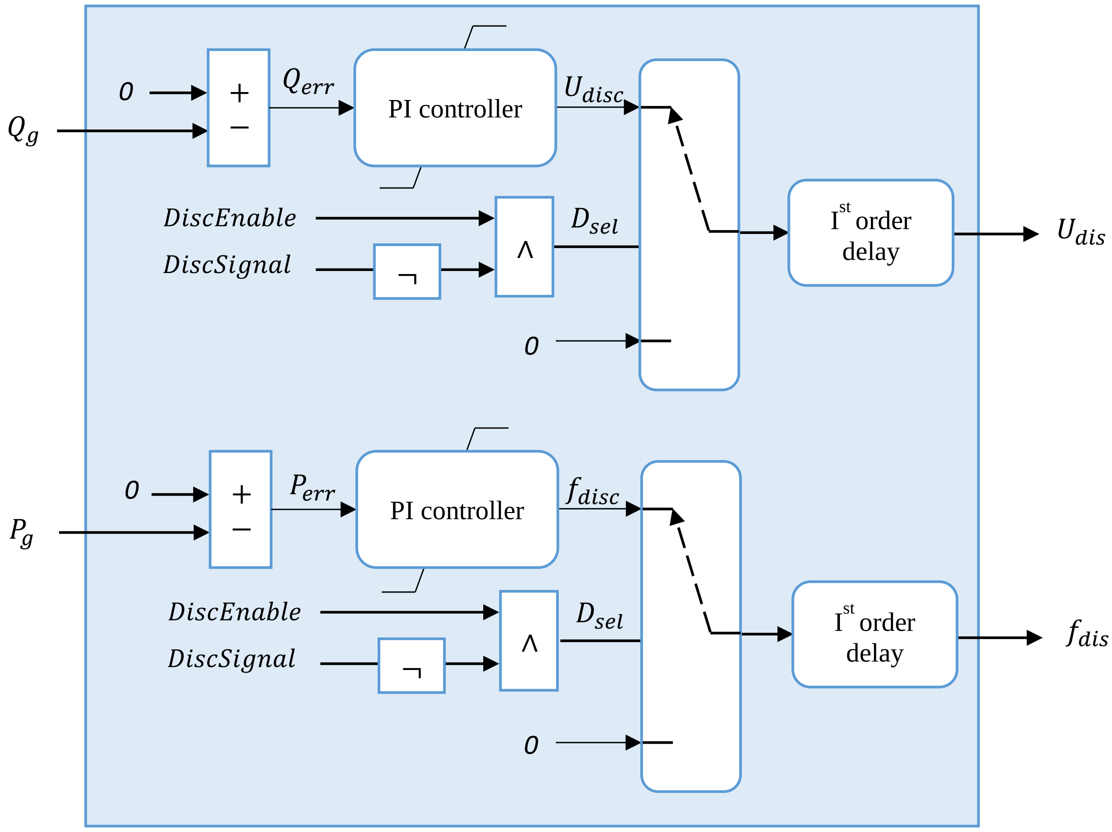


***Figure 4.10:*** *Disconnection controller*

*Disconnection criteria*

The controller prepares the system for disconnection and is permitted to disconnect when $P_{error}$ and $Q_{error}$ falls below 0.001 pu. for at least 1s, ensuring a smooth transition from GC to SA mode.

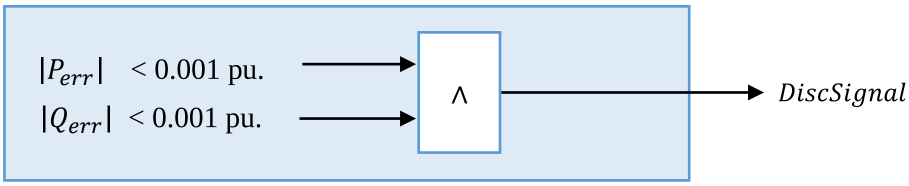


***Figure 4.11:*** *Disconnection criteria*

### 4.3.4 Set point calculation

In this block, the final set points to the Droop control - $f_o$ & $U_o$ are based on the input signals of the normal, connection and disconnection controllers. The graphical representation of the block is depicted in Figure 4.12. As evident from the figure, final $U_o$ set point is calculated by the direct summation of all the input signals - $U_{norm}, U_{conc}$ and $U_{disc}$, whereas final $f_o$ set point is not the consequence of a direct summation.

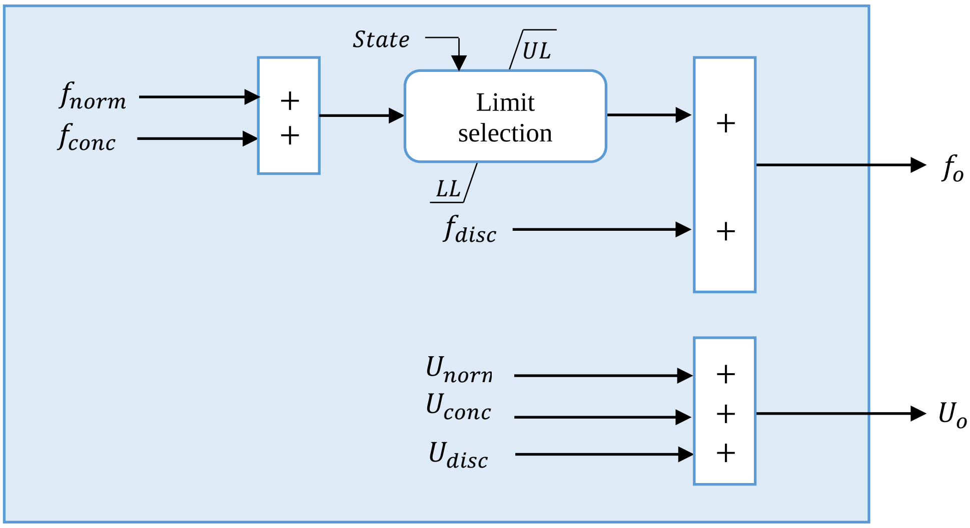


***Figure 4.12:*** *Set point Calculation*

In the GC mode, since the converter of the battery is still a VSI and if a low value of droop coefficient is selected, it is more likely that the inverters are overloaded [34]. To assure that the inverters are not overloaded beyond limits of $\pm$ 1 pu., a limiting signal is applied to $f_o$ value when its GC mode. The variable $State$ represent the Status of the breaker at PCC or BB bus. In other words, its indicates whether the MG is in SA or GC mode. As long as the $State$ = 0, there are no limits applied to ensure that final $f_o$ set point correctly signifies the SEP of the Cell and also to prepare the MG for additional deviations in the event of connection to EG, i.e. change of $State$ from 0 to 1, indicating GC mode. When the $State$ signal turns high, dynamic upper and lower limits, $UL$ and $LL$, are applied to summation of frequencies of normal and connection controllers. The resultant is then added to the frequency deviation created by the disconnection controller to arrive at the final set point $f_o$ to the droop control. The dynamic limits, $UL$ and $LL$, are calculated based on Eqns. (4.9) and (4.10).

$$UL = f_{bb} + k_P \tag{4.9}$$

$$LL = f_{bb} - k_P \tag{4.10}$$

where $f_{bb}$= frequency of BB bus and $k_P$ = *P/f* droop coefficient. The application of these dynamic limits ensures that the operation of the inverter within the limits of $\pm$ 1 pu. and hence avoiding the overloading behaviour in less than a minute, which is acceptable to inverter of any manufacturer.

### 4.3.5 Switching Logic

For simulation of seamless transition of MG from SA to GC mode and vice versa, a simple switching logic was conceived. The use of Manual commands as in existing power system switchgear logic was considered and analogous to this operation, manual trigger signals - $ConcEnable$ and $DiscEnable$, are formulated at different timing instants for change of modes. Once these enable signals are produced, the corresponding controllers are activated and the process of preparation of seamless transfer proceeds. The respective controllers produce ready signals - $ConcSignal$ and $DiscSignal$, after error minimization, which are fed as inputs to the Switching Logic block as seen in Figure 4.4. As these signals turn high, the desired transition is performed by opening or closing the breaker at PCC and the $State$ from 0 to 1 or from 1 to 0. To facilitate multiple switching or transitions between modes, the enable signals, $ConcEnable$ and $DiscEnable$, are reset to low status, based on the $State$ of operation of MG preparing for the next switching.

## 4.4 Summary

This chapter mainly discusses about the voltage source control of the converter of the BESS, which is the primary component in the Cell defining the grid parameters, voltage and frequency. The Normal controller defines the operating set points of voltage and frequency in SA mode of operation. Additionally, two controllers: Connection and Disconnection controllers are developed to create extra deviations when switching between different operating modes: SA, IC and GC modes. Finally, a combined control scheme is formulated for enable a smooth and seamless transfer of modes.

# 5 Automated Decision Algorithm

## 5.1 Introduction

The previous chapter was primarily focussed on developing a control strategy for achieving a seamless transition between SA and GC modes of operation of a cell and analysing the system dynamics. The timescale for simulation for evaluating the system behaviour involved in the process is in the order of seconds. Even in the transition phase and subsequent operation modes, the VSC of the BESS is still operated as a VSI unlike the conventional control scheme. This feature aided in extending the same control strategy for multiple cell operation i.e. transition between SA and IC modes. However, in all the simulations performed, the instants for switching between different modes viz. SA, IC and GC modes, were realized through manual commands at specific time instants, analogous to manual operation of a switchgear in power system. But in reality, an autonomous operation of multiple cells is preferred, where transferring of modes of the various cells in the MG occur based on a philosophy. An extensive analysis is essential for exploring into diverse methods of how to achieve this transition operation in an autonomous manner. This chapter centers around the formulation of this philosophy for enabling the automated operation of the MG and thus the development of an automated decision-making algorithm applicable to each of the cells in the MG.

## 5.2 Decision-making algorithm

The proposition for formulation of any type of algorithm depends on several dependent and independent factors, forming the integral part of the system. Likewise, the decision-making algorithm is also governed by a variety of aspects, namely, the structure of the MG and the components comprising the cell, type of control and objective of the algorithm. As explained before in Section 3.1, each cell encompasses DRES, BESS and controllable and uncontrollable loads and the operation of each cell is evolved around the converter of the BESS. Further, it's worth reiterating that the VSC of BESS is the grid-forming element in the network and defines the magnitude and frequency of voltage of the Cell AC bus.

Once, these basic features of the MG are known, for developing the algorithm, certain limits shall be defined for evaluating the SEP of each cell, in this case particularly for the BESS. Based on these limits, it is proposed to develop three different states, namely, Need Help state (NH), Ready Help state (RH) and Disconnect state (DISC) for each cell for defining the mode transition of the MG. The details of which would be dealt extensively in the following sections.

### 5.2.1 MG Structure, Control & Objective

*Layout of MG*

The layout of the MG considered for the development of the decision-making algorithm is depicted in Figure 5.1. As seen the MG comprises of various cells, interconnected through a BB bus through the respective breakers (B1, B2, B3 & B4) in absence of EG. Such a structural layout of the MG is applicable particularly in developing nations, where a major portion of area is devoid of reliable main grid.

Each Cell on its own is a MG by itself, however the capacity of the MG would be rather limited in SA mode. However, with multiple cells in parallel operation, the capacity of the system is enhanced and consequently, forming a stronger and robust MG. Moreover, parallel operation of cells in a MG augments the stability of the system. For instance, consider a case where all Cells are in SA mode of operation and SEP of Cell 1 to be low and that of Cell 2 to be high. If SA mode of operation is prolonged for a long duration, the Cell 1 activates the DSM schemes i.e. load shedding process, while Cell 2 activates the SSM schemes i.e. curtailment process. But, if Cell 1 & 2 were interconnected through the BB bus, then the healthier Cell 2 would aid the weaker Cell 1 by diverting the excess power into the Cell 1. So, in a way, the curtailment of DRES is inhibited in Cell 2 and as the BESS regains the healthy state due to charging of the battery through the interconnected operation, the load shedding is also averted. Thus, an IC mode of operation of MG in such a case aids in maximizing the use of renewable energy and boosting customer satisfaction.

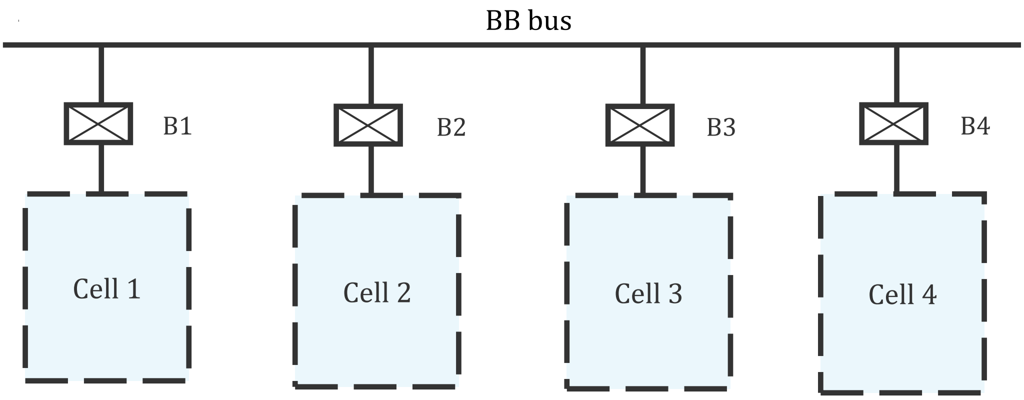


***Figure 5.1:*** *Multiple Cells interconnected through Backbone bus*

To realize such a behaviour, an algorithm has to be formulated for switching between SA and IC modes of operation. This could further be expanded to third mode i.e. GC if an EG connection is envisioned in the future in the MG architecture as in Figure 3.3 in Section 3.2.

*Type of control*

The type of control is another major aspect which is relevant in the formulation of decision-making algorithm. As elaborated in Section 2.4.2, a MG may be controlled in two different ways, viz. the centralized and decentralized approach. A detailed comparison of both approaches has been analysed and it was realized that the decentralized approach has benefits with respect to scalability and modularity.

In the centralized approach, a MGCC receives signals from each of the cells, based on the obtained data, the MGCC makes the decision to fulfill its objective and maintain the overall stability of the system. This kind of approach is also known as Agent control strategy; however, this demands a dedicated communication network for transfer for data between the MGCC and its agents. Absence of use of any type of ICT equipment in the MG is the prominent feature of the CSGriP project, making the project viable in remote locations without the requirement of investment for installation of communication infrastructure. Hence, in the thesis, it is proposed to follow a decentralized approach in the formulation of the algorithm, meaning that each of the cells in the MG would independently decide on its mode of operation. As a result of which, for each cell, there are challenges pertaining to how to interpret the state of other cells in the MG. But it’s worth mentioning that the decentralized approach would allow simple and easy expansion of the power system.

*Objective*

Referring to the MG layout in Figure 5.1, the primary objective is to develop a decentralized algorithm for stable operation of each cell and MG. In other words, each cell in the MG would attempt to meet its own energy requirement and if not urge for interconnected mode of operation. This indirectly, facilities in nearly full utilization of the renewable potential and prevention of shedding of loads. Only in extreme scenarios, where no cell in the MG is in a healthy state and ready to support the other cells, it is unavoidable to apply the load shedding schemes. On the contrary, when there is excess of renewable generation in the MG and the frequency of the MG raises above 50.2 Hz, there is none other option than renewable curtailment. The devised algorithm would inhibit such cases of load shedding and curtailment at a cell level and to a great extent, at the MG system level.

In addition to the above, there are certain assumptions which shall be considered while formulating the algorithm. The BB bus in the MG layout is in deenergised state i.e. the bus is dead. This means that the initial condition of each cell in the MG is in SA mode and based on the limits and NH, RH and DISC states, which are explained below, each cell independently decide on its mode of operation and switch between SA and IC modes.

### 5.2.2 Defining Limits

The previous chapter distinctly defined the rationale of a Battery VSC as grid-forming element in each cell, which is central in regulating the frequency and voltage of the Cell AC bus. As explained in the Section 4.3.1, the chief contributing factor to the frequency of the Cell Bus is the $f_{SOC}$ term. This term is dependent on the SoC of the BESS in each cell as defined by the curve in Figure 5.2.

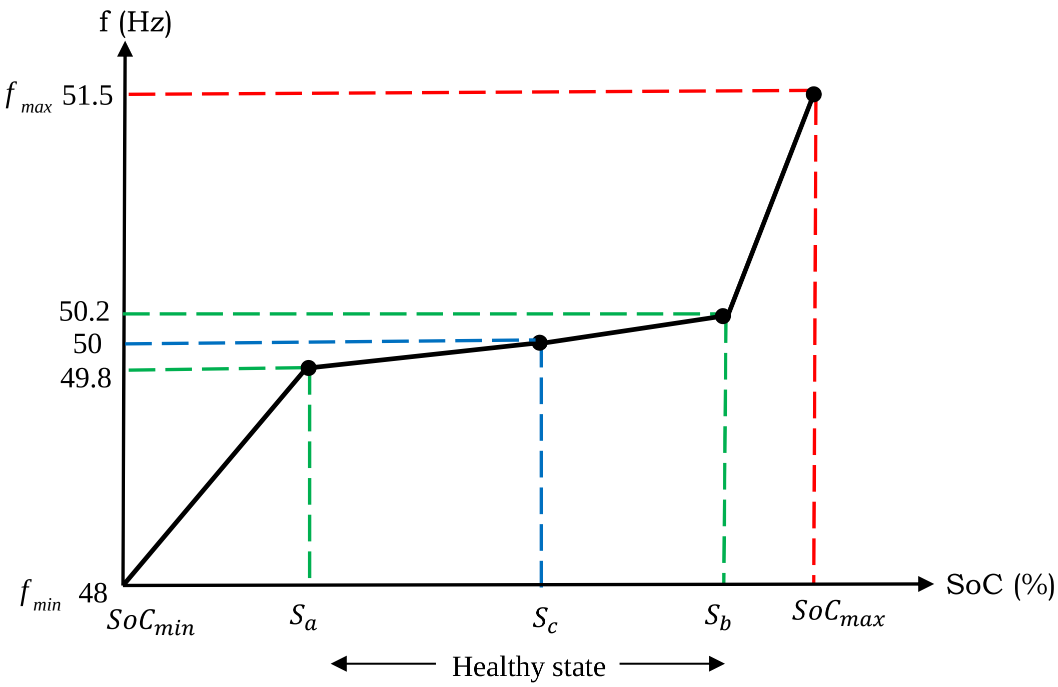


***Figure 5.2:*** *$f_{soc}$ curve*

It is now crucial to define certain limits to characterize various states, NH, RH and DISC, which plays a significant role in the formulation of the decision-making algorithm. The diverse limits employed for the algorithm are stated in Eqn. (5.1) .

$$
\begin{array}{ll}
\mathit{SoC\ Lower\ Limit} & SoCLL = S_a \\
\mathit{SoC\ Need\ Help\ Limit} & SoCNH = (S_c + S_a)\,/2 \\
\mathit{SoC\ Critical\ Limit} & SoCC = S_c \\
\mathit{SoC\ Ready\ Help\ Limit} & SoCRH = (S_c + S_b)\,/2 \\
\mathit{SoC\ Upper\ Limit} & SoCUL = S_b
\end{array}
\tag{5.1}
$$

The chosen limits based on $f_{SOC}$ curve of BESS is explained below

- $\underline{SoC\ Lower\ Limit, SoCLL}$ : This corresponds to the Lower limit of the healthy state of the BESS as in $f_{SOC}$ curve ($S_a$). From the curve, it's evident that $S_a$ refers to a frequency of 49.8 Hz. If a cell with SoC as $S_a$ was delivering power at 1p.u., the $f_{SOC}$ decreases further and subsequently the load shedding is triggered at 49.5 Hz. So, the value of $SoCLL$ was chosen as $S_a$.

- $\underline{SoC\ Need\ Help\ Limit, SoCNH}$ : This refers to the Need Help state of the BESS, the value of which is the mean of lower limit and the central frequency corresponding to 50 Hz. This limit is defined as a precautionary step for ensuring that the SoC does not stretch towards the lower limit if other cells in MG are in ready state to help.

- $\underline{SoC\ Critical\ Limit, SoCC}$ : The $SoCC$ denotes the Critical state of the BESS, referring to the value of $S_c$ in the $f_{SOC}$ curve. This indicates the state of the BESS which the cell shall sustain for stable operation of cell in SA mode.

- $\underline{SoC\ Ready\ Help\ Limit, SoCRH}$ : This indicates the ready help state of the BESS. The value is set to be the mean of upper limit and the central frequency. Once the limit is surpassed, the cell is in healthy state to aid the cell in the need state.

- $\underline{SoC\ Upper\ Limit, SoCUL}$ : This links to the Upper limit of healthy state of BESS ($S_b$). As a cell attains this limit, it. Rather than curtailing the generation, the limit implies that there is excess of renewable generation in the network and advances towards the curtailment process employed as a signal for supporting other cells in the MG.

These limits are utilized in determining the different states for development of a logic for making a conclusive decision to switch between SA and IC modes.

### 5.2.3 Need Help State

The Need Help State of a cell, known as NH State, signifies that the cell in a MG has comparatively a low SoC and requires support from other healthy, ready cells in the MG for a stable operation fulfilling the customer necessities. A declining trend of SoC of BESS owing to higher demand than generation results in lowering of frequency of Cell AC bus. In this state, the BESS is in healthy state of SoC as in $f_{SOC}$ curve, but approaching towards the limit where the load shedding is initiated, say SoC corresponding to frequency of 49.5 Hz. Further, NH state may be forced to be high (value of 1) to deal with scenarios where there exists a higher frequency of BB bus.

The block in Figure 5.3 shows the register of input signals required for arriving at the NH state. The major output of this block is the NH variable which is utilized for creating the enable signal for mode change. Additionally, there are some intermediate outputs which are used for arriving at DISC state. The functions devised for generating these outputs are dealt later in this section. With the input signals, the output signals are generated following a set of rules, which are explained below.

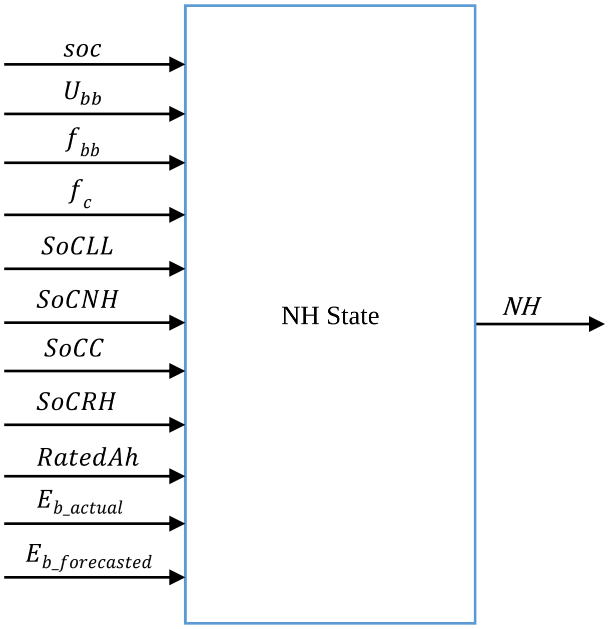


***Figure 5.3:** Need Help State*

*Rule 1*: The BB bus is deemed *Live* only when $U_{bb}$ is above 0.6 pu. for minimum of 0.5 s, in all other cases, the BB is regarded as *Dead* Bus.

*Rule 2*: If the $soc$ of BESS in the cell becomes less than $SoCLL$ with *Dead* BB bus, the *NH* state of the cell is set high.

*Rule 3*: For a *Live* BB Bus, 2 or more *NH* cells are restrained from connecting with each other, if no ready cells are supporting the interconnected network.

*Rule 4*: To differentiate multiple cells in the MG with $soc$ lower than $SoCLL$, a graph of *SoC vs time (increasing)* is incorporated before generating the final NH signal. A cell with lower SoC would have a lower time delay (order of 10 s) than cell with higher SoC.

*Rule 5*: If BB bus is *Live* due to forced energisation of cell with high renewable generation, the *NH* state is forced high for absorbing the excess power, this is referred to as Need Help Forced condition.

*Rule 6*: Following the past energy profile of the BESS for 15 minutes, $E_{b\_actual}$ , a *HECN* signal is generated based on the evaluation of the expression in Eqn. (5.2).

$$E_{b\_actual} > ((SoCNH - SoCLL))/4 * RatedAh \tag{5.2}$$

*Rule 7*: Expecting a similar energy profile in the future, a cell with a high *HECN* signal would set the *NH* signal to 1 to proactively avoid the lower SoC of BSES.

*Rule 6*: Based on the forecasted energy profile for 15 minutes, $E_{b\_forecasted}$, and assessing the term in Eqn. (5.3) , a *LECN* signal is created, which is utilized for resetting the *NH* variable.

$$E_{b\_forecasted} > ((SoCLL - SoCNH))/4 * RatedAh \tag{5.3}$$

*Rule 8*: The final *NH* signal comprises of Need Help Actual (*NHA*) and Need Help Forced (*NHF*) signals. The cells are connected to the BB bus till these signals are reset back to 0, denoting that the cells are not more in Need state.

### 5.2.4 RH State

As a cell in a MG becomes healthy with a higher SoC than the critical level, the cell has the ability to support other needy cells in the MG. Such a state is recognized as Ready Help state, further referred to as RH state. Additionally, there may occur a forced RH state when the frequency of Cell bus crosses 50.2 Hz, denoting a surplus renewable potential with no needy cells in the network. A rising trend of SoC because of lower demand than generation leads to rising frequency of Cell AC bus. It's imperative to generate the RH state, which otherwise would force restricting generation output in the cell and thus impacting the stability of the MG.

The list of input variables needed for generating the RH state is shown in Figure 5.4. Like the NH block, the major output of RH block is the *RH* variable, which is used for mode transition. Additional intermediate outputs are devised to perform the disconnection operation.

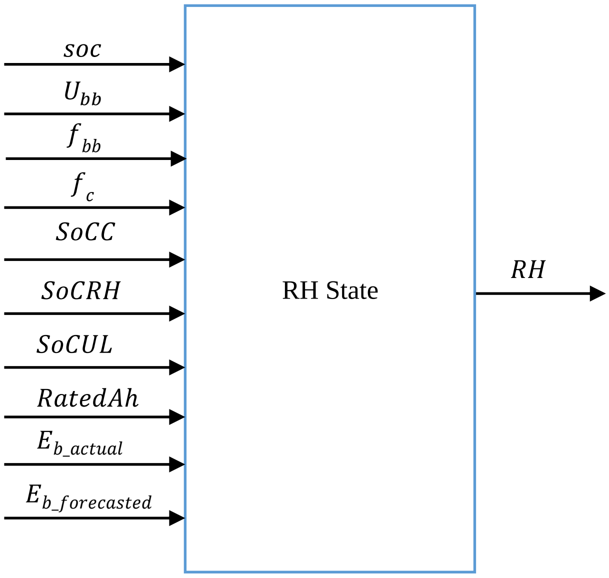


***Figure 5.4:*** *Ready Help State*

The set of rules and conditions followed by the RH block are described as follows

*Rule 1*: The BB bus is deemed *Live* only when $U_{bb}$ is above 0.6 pu. for minimum of 0.5 s, in all other cases, the BB is regarded as *Dead* Bus.

*Rule 2*: If the $soc$ of BESS in the cell is higher than $SoCRH$ with *Live* BB bus, the *RH* state of the cell is set high.

*Rule 3*: In a *Dead* BB bus condition, the *RH* signal is set high if $soc$ becomes higher than $SoCUL$ indicating excess renewable generation in the cell. This refers to the forced *RH* state.

*Rule 4*: When multiple cells in a MG arrive at high RH signal, a graph of *SoC vs time (decreasing)* is combined to create the final *RH* signal. A cell with lower SoC would have a higher time delay (order of 100 s) than cell with lower SoC.

*Rule 5*: Analogous to *HECN* signal, tracking the past energy profile of the BESS for 15 minutes, $E_{b\_actual}$, a *LECR* signal is generated evaluating the expression in Eqn. (5.4). This *LECR* signal is used to set the *RH* state high.

$$E_{b\_actual} < ((SoCC - SoCRH))/4 * RatedAh \tag{5.4}$$

*Rule 6*: Following the forecasted energy profile for 15 minutes, $E_{b\_forecasted}$, and assessing the term in Eqn. (5.5) , a *HECR* signal is created, which is employed for resetting the *RH* variable.

$$E_{b\_forecasted} > ((SoCRH - SoCC))/4 * RatedAh \tag{5.5}$$

*Rule 7*: The Ready Help Forced (*RHF*) signal is a subset of the final *RH* state. The cells would no longer support the needy cells in the BB network as *RH* variable is reset to low value (0).

### 5.2.5 DISC State

The Disconnection (DISC) state can be described as a condition where the cell in the MG is no longer willing to aid other cells in the network. The DISC block accepts a list of inputs as shown in Figure 5.5 and simultaneously generate a few internal signals. Based on these input signals and the derived signals, the final DISC signal is created following the rules stated below.

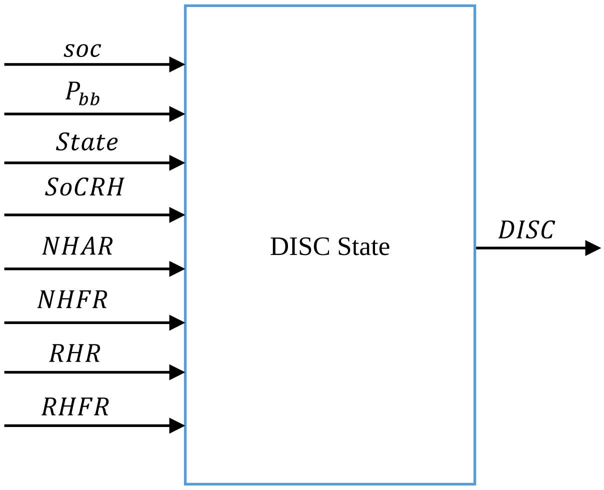


***Figure 5.5:*** *Disconnect State*

*Rule 1*: The *NH* cells are disconnected from the BB network, as the reset variables, *NHAR* and *NHFR* are reset to 0, indicating that these cells no longer require support. Hence the disconnect signal (*DISC*) is made high.

*Rule 2*: When only multiple NH cells are connected to the network, the cell with higher SoC is forcibly disconnected from the BB bus to ensure that SoC of this NH cell do not deteriorate even more.

*Rule 3*: Based on the signals, *RHR* and *RHFR*, the *RH* state of the cells are reset and parallelly the *DISC* variable is made high, initiating the enabling condition for disconnection from the network. This situation implies that the cells are not ready to support other needy cells in the network.

*Rule 4*: If only *RH* cells are present in the BB interconnected network, the cells are persuasively disconnected from the BB bus though the *RH* state is not reset.

*Rule 5*: Multiple cells trying to disconnect are differentiated by employing a *SoC vs time (decreasing)* graph. The cell with higher SoC will be disconnected before the one with the lower SoC.

## 5.3 Modelling & Control flow

The previous section elaborated on the philosophy of the decision-making algorithm with detailed focus on the limits and the states used for switching modes. With all these inputs, the control algorithm is modelled in PowerFactory and the layout of the decision-making module is depicted in Figure 5.6.

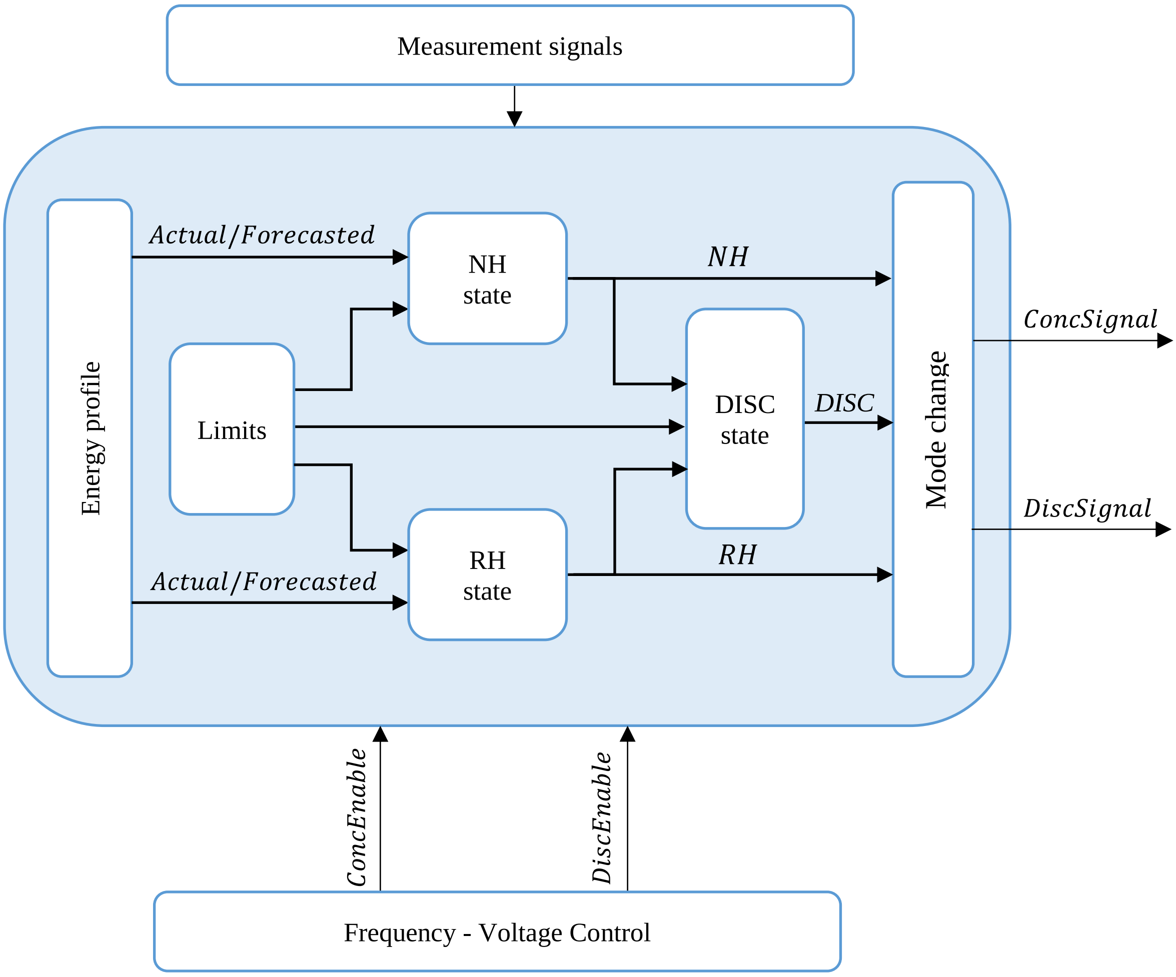


***Figure 5.6:*** *Decision-making module*

As seen in the Figure 5.6, the decision-making module accepts measured signals and two additional signals from the Frequency - Voltage Control block, $ConcEnable$ and $DiscEnable$, as inputs for further evaluation of the algorithm. The module comprised of 5 different blocks viz. Energy profile, Limits, NH State, RH State, Disc State and Mode Change.

The Energy profile block calculates a moving average of the net energy absorbed/received from the BESS for 15 minutes. This can also be referred as the difference of the power flow between generation and load, which is compensated by the BESS to maintain the power balance. The average value is taken for 15 minutes and Actual Energy delivered or absorbed, $E_{b\_actual}$, is tabulated using Eqn. (5.6) .

$$E_{b\_actual} = (P_G - P_L) * 0.25 \tag{5.6}$$

Similarly, the Forecasted Energy delivered or absorbed, $E_{b\_forecated}$, is formulated using Eqn. (5.7).

$$E_{b\_forecated} = \left(P_{G\_forecasted} - P_{L\_forecasted}\right) * 0.25 \tag{5.7}$$

The limits block tabulates all the required limits for defining the states, *NH, RH* and *DISC,* as per Eqn. (5.1) explained in Section 5.2.2 . The flowchart for each of these states are explained in the following sections. Several intermediate functions are essential for arriving at these states. One of the functions, which is common to all the *NH*, *RH* and *DISC* block is *Live* function.

As explained earlier, all the cells are in SA mode initially. The *Live* function is used to detect whether the BB bus is energised through any of the cells by closing the respective breakers. The function is realized by checking the voltage of the BB bus, $U_{bb}$, and if the value is more than 0.6 pu. for a minimum of 5 s, then *Live* is assigned as 1, meaning that the BB is a Live Bus. In other cases, the *Live* is set a value of 0, which indicates that the BB is a dead bus. The flowchart of the Live function is depicted in Figure 5.7.

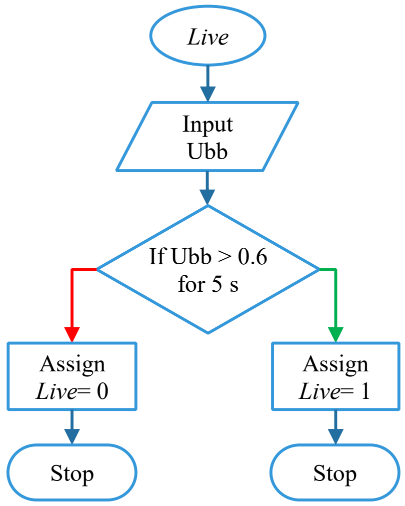


***Figure 5.7:*** *Live bus function*

### 5.3.1 NH flow diagram

The Need Help State of a cell represents that the cell is in unhealthy state and requires support from other cells to avoid load shedding schemes in its own cell to maintain a stable operation. To evaluate whether a cell is in Need Help State, the variable *NH* is used. When *NH* is allotted the value of 1, it implies the need state of the cell and this value is passed on to *Mode Change* block for performing the transition from SA to IC mode. However, to assess the value of *NH*, certain functions are formulated which are explained below.

***NH Set Conditions:*** Primarily, it's imperative to determine the set conditions for the NH state of each cell. Each cell based on its SoC decides whether the cell is in need state or not. Once the *SoC* of the cell falls below *SoCLL* limit as defined in Section 5.2.2 , a variable, Need Help Set1 (*NHS1*) is set high after passing through the *SoC vs increasing time* delay function. The delay function enables distinction between multiples cells with SoC below SoCLL. A second Need Help Set (*NHS2*) is conceived based on the past & forecasted energy profile. If the SoC of the cell falls below *SoCNH* limit and the cell observes a High Energy Consumption in Need (*HECN*), the *NHS2* is set to 1 otherwise 0 in all other scenarios. The *HECN* signal implies that the SoC of the cell would decrease and reach its lower limit, *SoCLL*, on high consumption of energy from BESS. So, to avoid such scenario of need, the *NHS2* is set high as soon as the SoC of the cell crosses the *SoCNH* limit. The flow diagram for the *NHS* signals are shown in Figure 5.8.

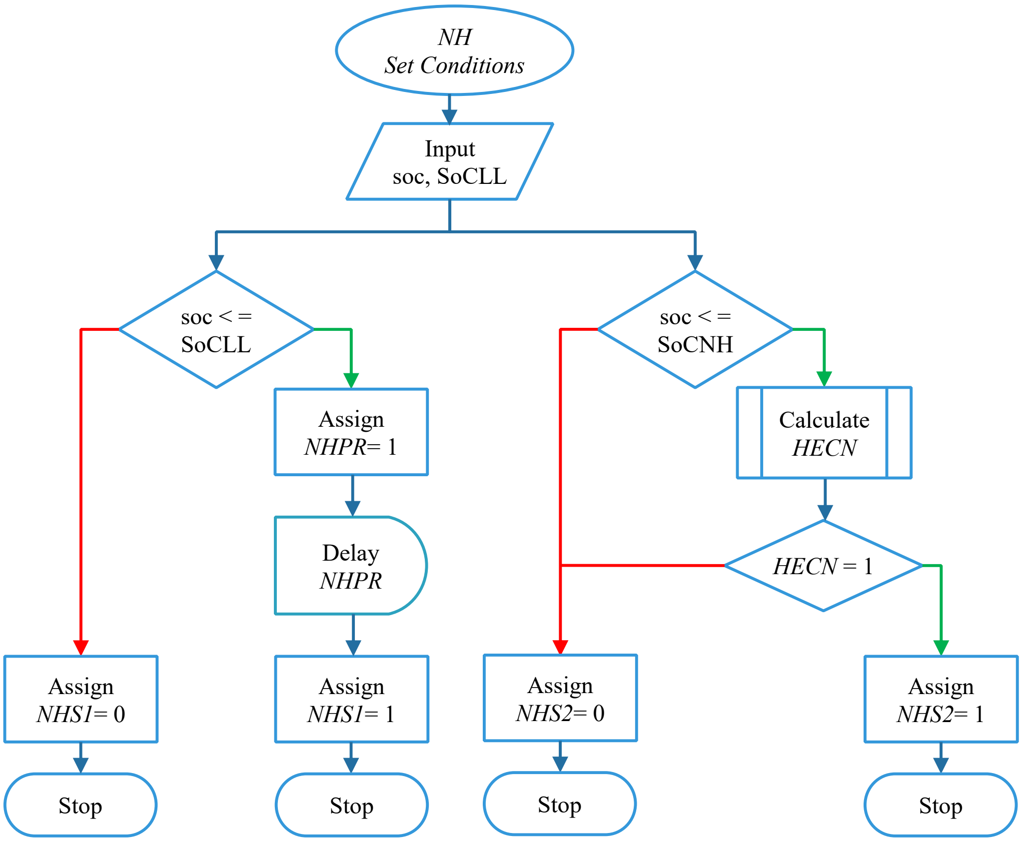


***Figure 5.8****: Need Help Set conditions*

***NH Doconnect:*** The *NH Set conditions* demands the requirement of additional functions in the event of disconnection of a NH cell from the BB bus. The *NH Doconnect* function is used to recreate the *NH* condition if the BB bus is Live. However, this function ensures that the BB frequency, $f_{bb}$, is higher than the cell frequency, $f_c$ , (in SA mode) by a value of 0.0005 pu. (.025 Hz) and passes through a delay function of *SoC vs increasing time* before assigning *NH Doconnect* variable, the value of 1. The delay function ensures that *NH Doconnect* of the cell with lowest SoC becomes high earlier than the one with the higher SoC. In other words, this helps in distinguishing cells in *NH* state. In all other cases, *NH Doconnect* is set 0, thus not allowing the cell to connect to BB bus, though the cell is in *NH* state. The flow diagram of *NH Doconnect* function is shown in Figure 5.9.

***NH Connect:*** To cater for the cases when the BB bus is *Live* and the cell is not in *NH* state, *NH Connect* function is employed. Such a scenario would exist when a cell in the network has surplus of renewable generation and is forced to energise the BB bus with no *NH* cells to divert the excess power rather than curtailing the renewable generation. When SoC becomes lower than mean of *SoCC* and *SoCRH*, the function checks whether the frequency of BB bus is higher than 1.004 p.u. (50.2 Hz) for 60 s and holds the result for 60 s, as seen in Figure 5.10. If the result of this value is true, then the *NH Connect* signal is assigned 1, while in all other cases, it is set a value of 0. Thus, it corresponds to case of Need Help forced situation as explained previously.

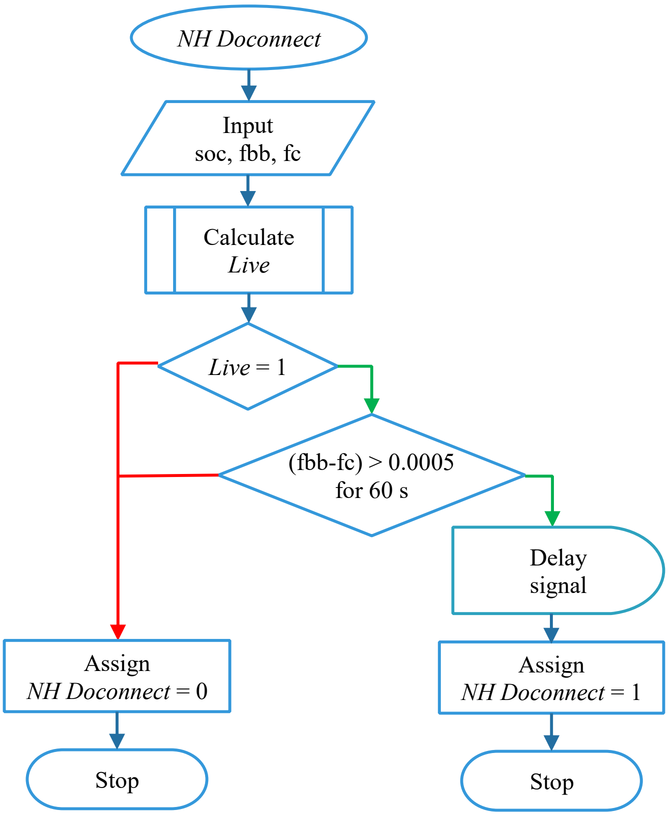


***Figure 5.9:*** *Need Help Doconnect function*

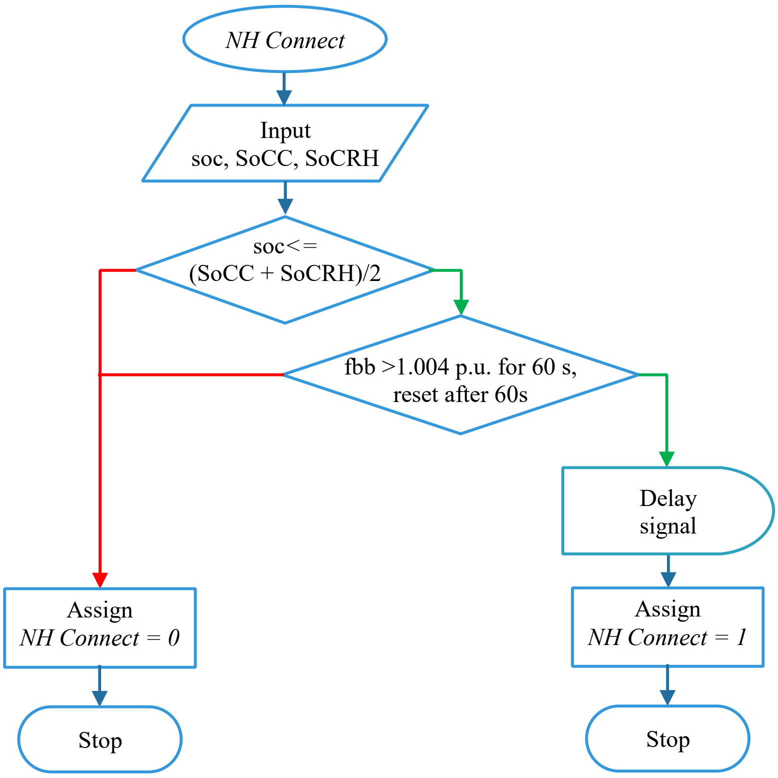


***Figure 5.10:*** *Need Help Connect function*

***NH Reset conditions:*** When the *NH* cell remains connected to BB bus, it receives support from the ready cells and the battery is charged. But as the cell reaches a SoC of *SoCRH – 5*, the value of *NH* can be reset as the SoC has surpassed the critical limit of *SoCC*, which is the prime purpose of the decision-making algorithm. The layout of the flowchart of the *NH Reset conditions* is depicted in Figure 5.11. So, when the value of SoC crosses the value of *SoCRH* – 5, a new variable, *NHR1* is set 1 and if less, then is assigned a value of 0. This value was chosen as the cell reaches *SoCRH* limit, it moves into the ready help state. So, to distinguish between the two states, it is desired to reset the *NH* at this value.

A second reset condition (*NHR2*) is created when the Cell foresees a Lower Energy Consumption in Need (*LECN*) with SoC less than *SoCC*. This means that the *NH* cell does not need more support from other Cells due to higher net power inside its own Cell.

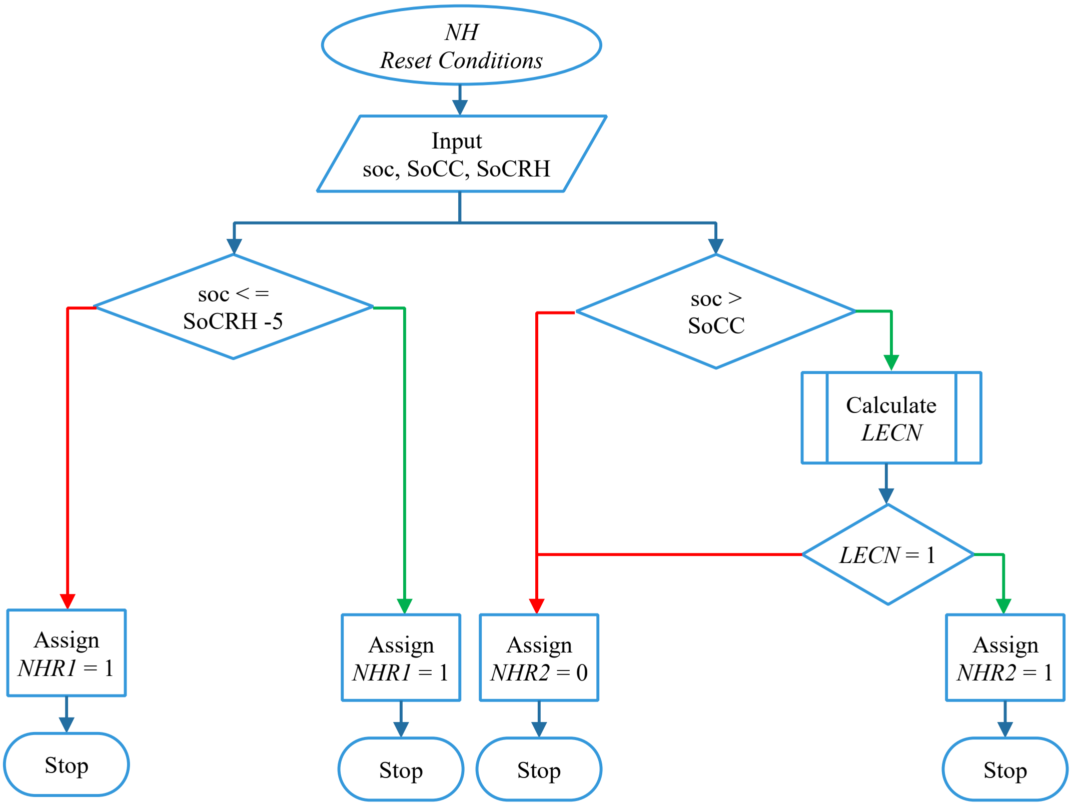


***Figure 5.11:*** *Need Help Reset conditions*

***NH Flowchart:*** Combining the NH functions, *NH Doconnect* and *NH Connect*, and the *NH Set Conditions*, the final *NH* variable is evaluated based on the flowchart as in Figure 5.12.

In the flow diagram, initially the *NH Set Conditions* is called and a new variable, *Need Help Actual* (NHA) is coined to characterize the actual need state requirements of each cell. This *NHA* variable is employed in evaluating Need help forced condition, which are elaborated later in this section. From the *NH Reset conditions*, a new *Need Help Reset Combined* signal (NHRC) is formulated through *or* function of reset conditions, NHR1 and NHR2. To hold the value of *NHA*, additional variable, *Need Help Actual Set* (NHAS) variable is formulated using the flip function, where the reset variable is *NHRC*.

If the value of *NHAS* is one, the flow in the right part of the figure is followed. It later checks for the condition of BB bus, whether it's *Live* or *Dead*. Hence the *Live* function is called upon and evaluated.

If the *Live* is 0, then final *NH* variable is set high directly, however if *Live* is 1, the *NH* variable is assigned a value of 1, only if *NH Doconnect* is high. In all other scenarios, the *NH* variable is set to 0. For the case when the value of *NHAS* is zero, it follows the left part of the Figure 5.12. Even in this path, the *Live* function is assessed and if *Live* is 1 and *NH Connect* is 1, then *NH* variable is set the value of 1. In all other cases, where *Live* is 0 or *NH Connect* is 0, the *NH* variable is allocated 0.

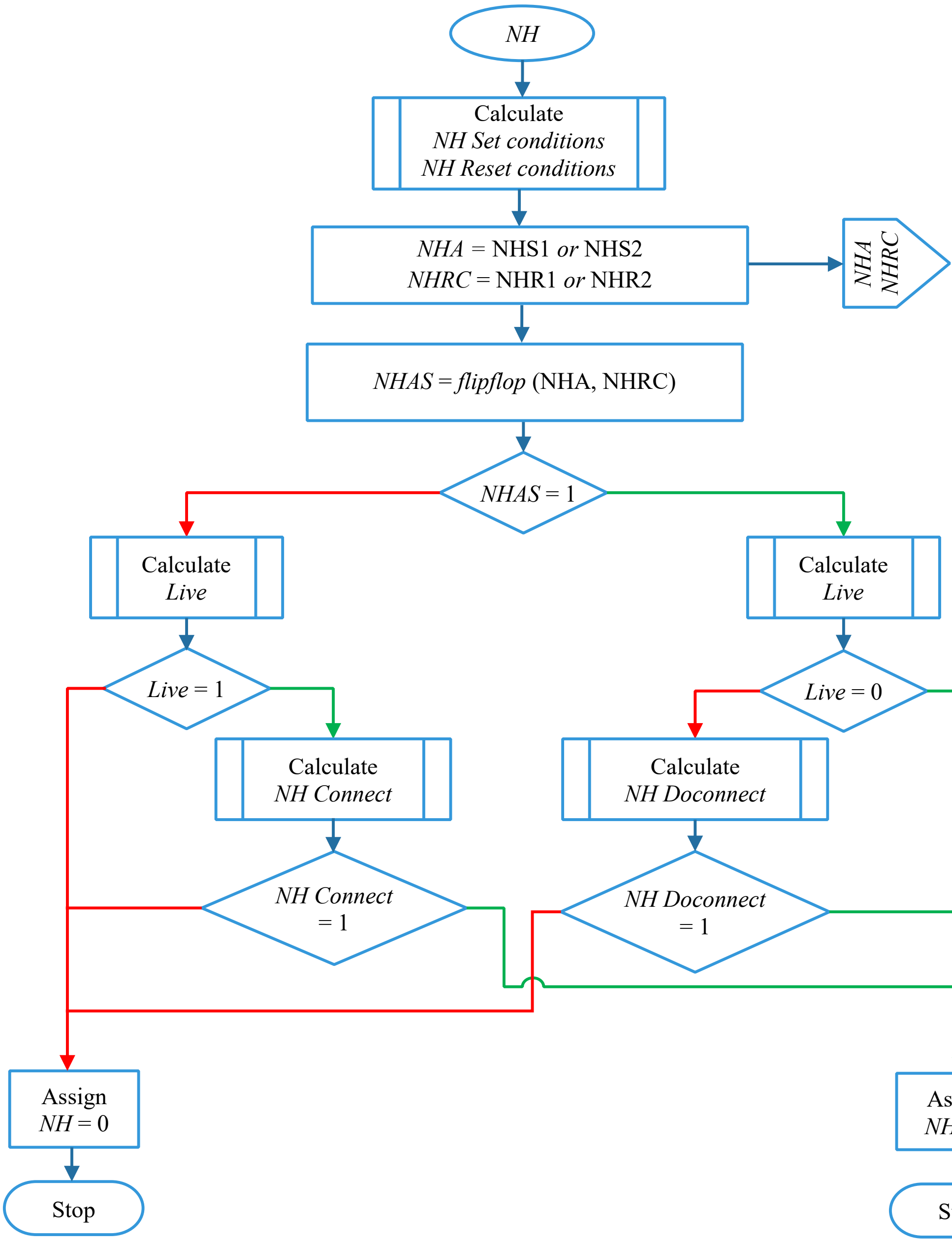


***Figure 5.12:*** *Need Help state flow diagram*

***NHR & NHAR:*** The *NH* value so calculated using the *NH flow diagram* is passed on to the mode change block which subsequently performs the mode change. But to reset the *NH* variable as it fulfils the reset conditions, the function *NH Reset conditions* calculates the NHR1 and NHR2 value. Using the value of *NHRC* value from the *NH flow diagram* (Figure 5.12), the value of *NH* is reset using a flipflop function. A similar approach is followed to reset *NHA* signal. The flow diagram of the reset conditions is depicted in Figure 5.13 and the respective signals *NHR* and *NHAR* are tabulated.

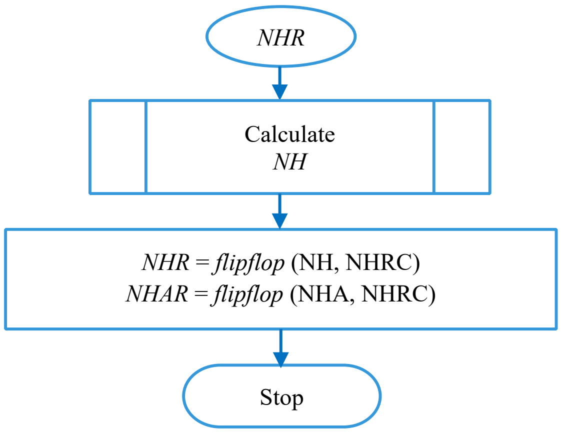


***Figure 5.13:*** *Need Help Reset & Need Help Actual Reset*

***NHF signals:*** There may be situations where cell has surplus renewable potential, thus crossing the upper limit of frequency of 50.2 Hz with no other cells in Need help state. Due to which, the renewable curtailment is triggered as explained in the SSM schemes. To avoid such curtailment, the cell with high renewable potential is forced to energise the BB bus and the other cells, though not in Need state i.e. *NHA* is 0, connect to BB bus to absorb the excess power. To distinguish this state from *NHA*, a *Need Help Forced* (NHF) signal is created. The flow diagram for evaluating this *NHF* signal is shown in Figure 5.14(a). Initially the value of *NHR* signal is estimated through *NHR* function. If the value of *NHR* is 1, further it is checked whether this is due to *NHAR* signal. But if the *NHAR* is 0, then the *NHF* variable is ascribed a value of 1 and *NHF* signal is 0 in all other scenarios.

Based on this *NHF* signal, a reset signal is also formed to disconnect the cell from the BB bus. The reset signal, *NHFR*, is calculated by utilizing a flipflop function as displayed in Figure 5.14(b). So as the SoC reaches *SoCRH-5*, the value of *NHFR* is forced to 0. The reset value is lower than that of *NHAR* signal to ensure that the cell with high renewable potential discharges marginally to avert curtailment. This *NHFR* signal is further utilized in *DISC* block to arrive at the disconnect state.

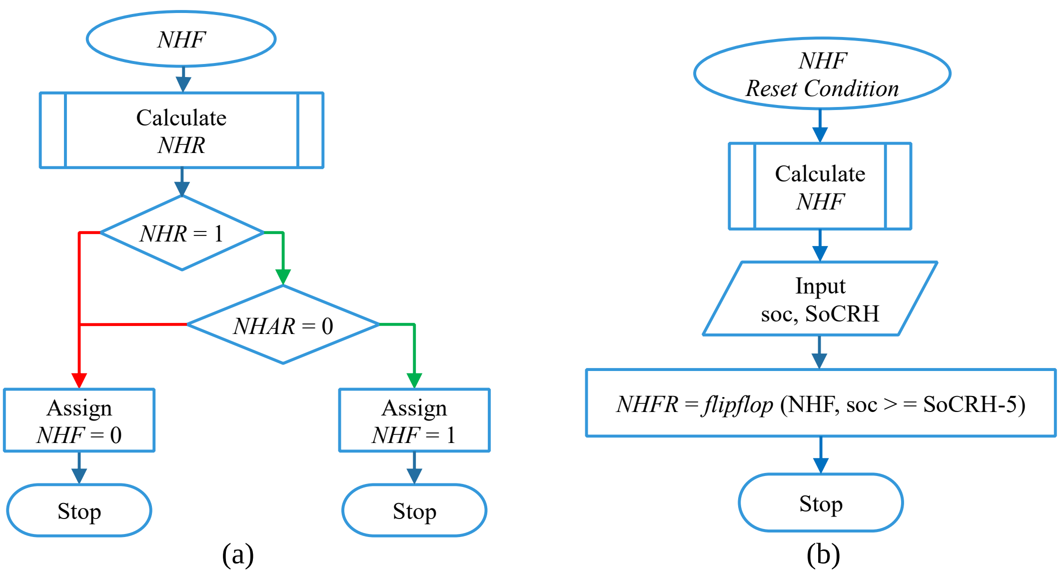


***Figure 5.14:*** *Need Help Forced & Need Help Forced Reset values*

### 5.3.2 RH flow diagram

The Ready Help state of a cell signifies that the cell is in a healthy condition with SoC above its critical limit and can support other needy cells in the MG network. The variable *RH* is used to indicate whether the cell is in Ready help, which is subsequently passed to the *Mode Change* block. If the value of *RH* is 1, the *Mode Change* block changes its mode from SA to IC by closing the breaker connecting to the BB bus. Similarly, to the NH evaluation, an intermediate function, RH Connect, as shown in Figure 5.15, is devised for estimation of RH signal.

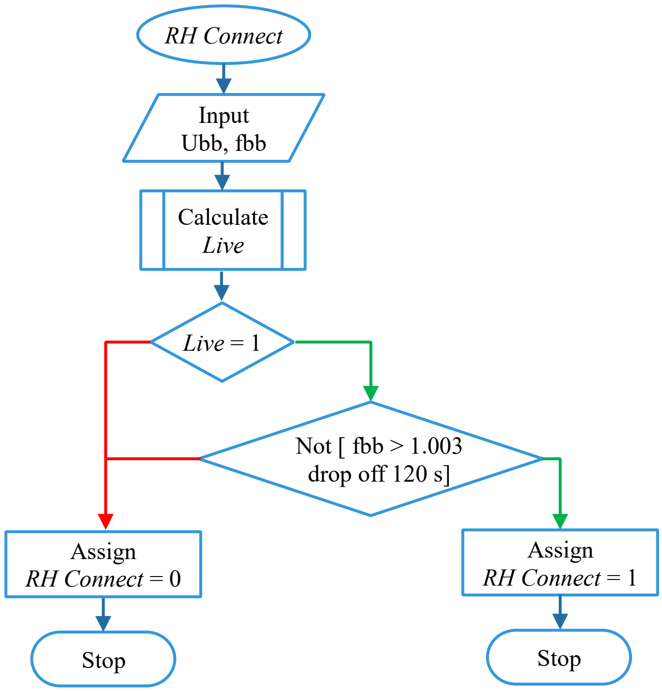


***Figure 5.15:*** *Ready Help Connect function*

***<u>RH Connect:</u>*** The primary function of *RH Connect* is to inhibit the connection of RH cell to BB bus if the BB bus is *Live* and the BB frequency, $f_{bb}$, is higher than 1.004 pu (50.2 Hz). Once the high signal is generated, it remains hold for 120s and then drops off if $f_{bb}$ becomes lower than 1.003 pu. Thus, if there exists a high signal, then *RH Connect* is assigned 0 and 1 if the it becomes low. If the cell is allowed to connect the BB bus without the *RH Connect* function, due to higher frequency of BB bus, the RH cell would receive support and again disconnect signal is initiated. So, there occurs multiple mode transitions between a short span of time. To avoid such fast switchings, *RH Connect* signal is used.

***<u>RH Set conditions:</u>*** With the definition of *RH Connect,* each cell based on its SoC determine whether it is in a ready state to support other needy cells. The flow diagram of RH Set conditions is shown below in Figure 5.16.

Determining whether a cell is in ready state can be split into 2 different sections. The first is the case when the BB is energised, which is assessed by *Live* function. This is the natural path which is followed because the BB bus, which is initially in deenergised state, is charged through a *NH* cell in the network. So, when BB bus is *Live*, a RH Set signal (*RHS2*) is set as high if SoC becomes greater than equal to *SoCRH* and *RH Connect* is true. In all other scenarios, where SoC is less than *SoCRH* or if *RH connect* signal is false, *RHS2* is allotted a value of 0 and hence, not allowed to support the needy cell which is already connected to the BB bus. Another ready help state (*RHS3*) is created if the cell detects a Low Energy Consumption in Ready (*LECR*). That means if the SoC of the cell is above the mean of *SoCC* and *SoCRH* and the *LECR* signal is high, then *RHS3* is deemed high and synchronizes with the BB bus for aiding the needy cell. It's worth iterating that this *RHS3* signal is also devised if BB bus is energised.

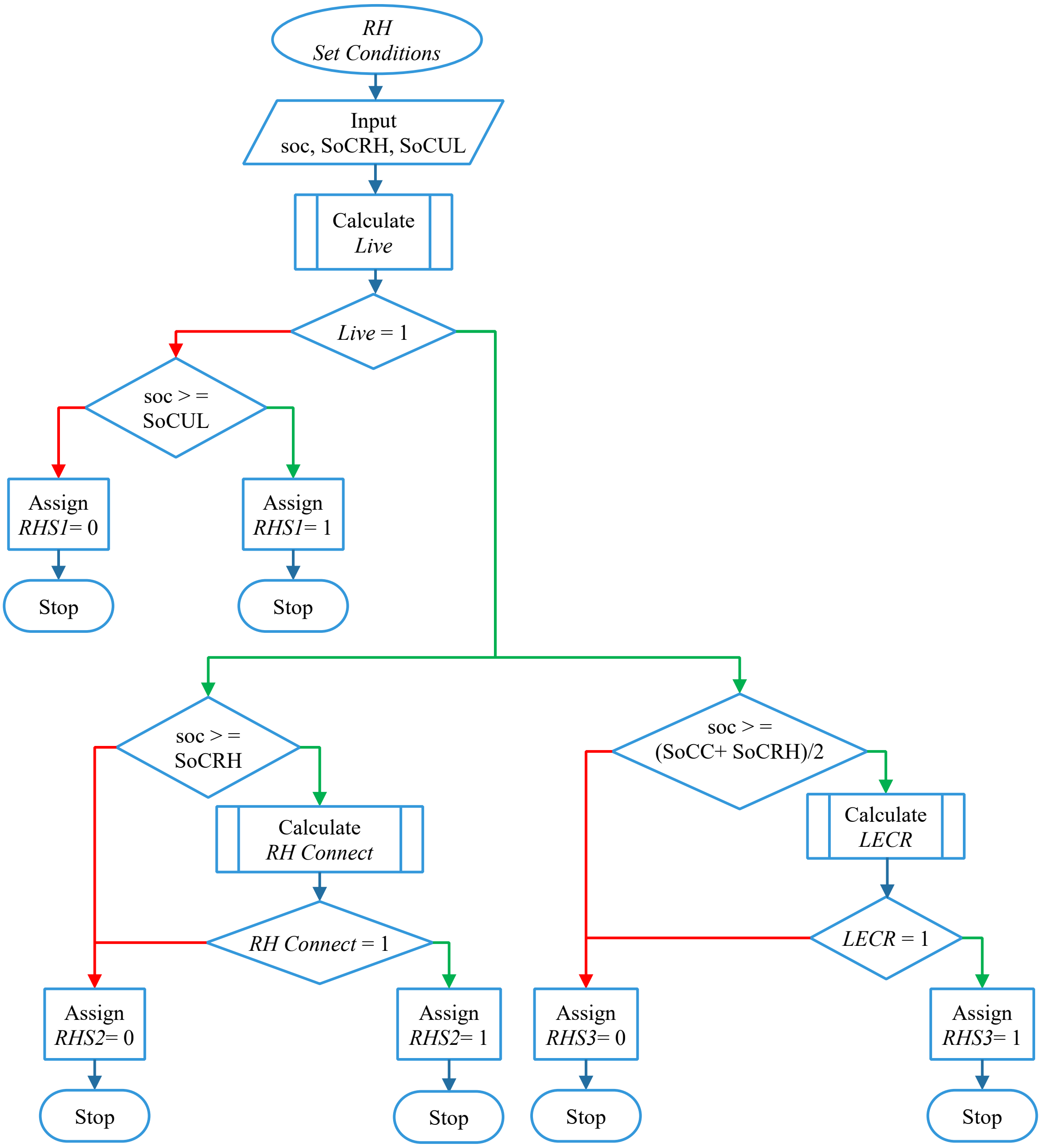


***Figure 5.16:*** *Ready Help Set conditions*

The second is the case where the BB bus is not energised, meaning that there are no needy cells in the network. If in this situation, if any the cells have a very high renewable potential and the SoC is above the upper limit of the healthy state of the BESS i.e. *SoCUL*, another ready help set signal (*RHS1*) is initiated to energise the BB and the divert the excess power to the other cells if connected to the BB bus. In other words, when *RHS1* is high, it connects to BB bus and thus averting the renewable curtailment in the process.

***RH Reset conditions:*** Once the *RH* cell is synchronised to the BB bus, it supports the needy cell, resulting in decrease of its own SoC. But, the main objective of the decision-making algorithm outlines that each cell shall always maintain the critical SoC i.e. *SoCC*, to meet its own energy requirement. So, to avoid such unstable conditions, the *RH* signal has to be reset based on certain conditions. The first reset condition (*RHR1*) is made high if the SoC falls below *SoCC* and a second reset condition (*RHR2*) is generated if the cell identifies a High Energy Consumption in Ready (*HECR*) when the SoC falls below the mean value of *SoCC* and *SoCRH*. This means that the *RH* cell supporting the other needy cells in the network is soon approaching its critical limit of SoC, tracking high energy requirement in the cell. So, these reset conditions as in Figure 5.17 are formulated to disconnect the cells from the network.

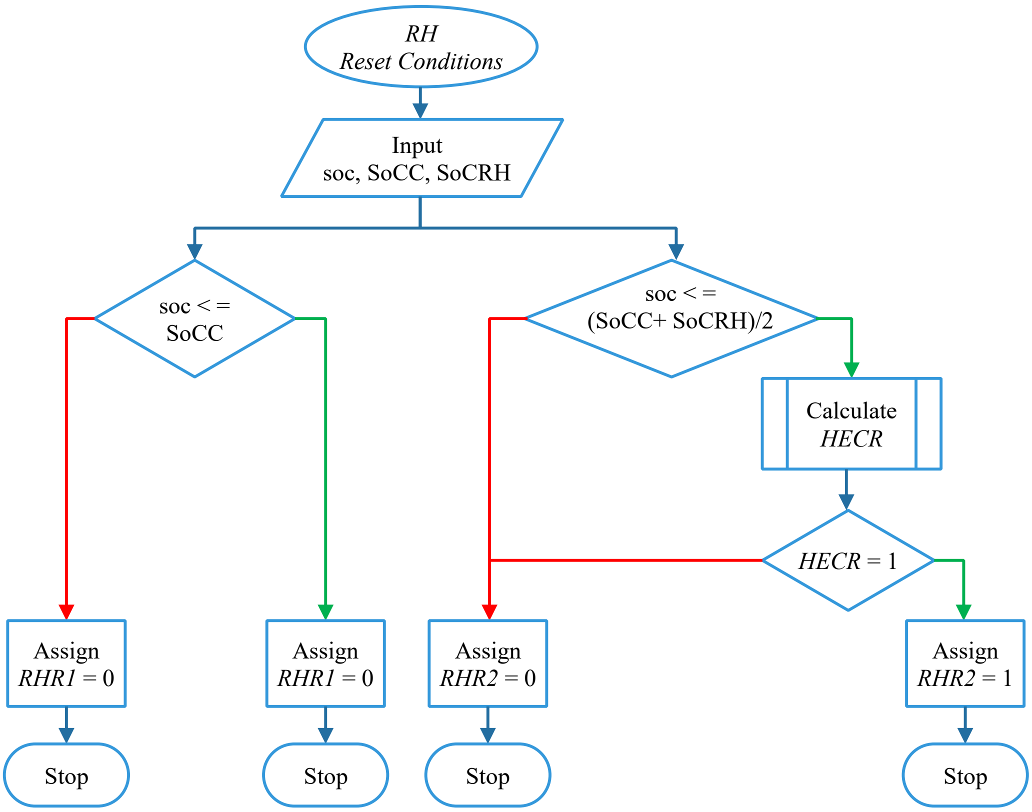


***Figure 5.17:*** *Ready Help Reset conditions*

***RH Flowchart:*** Based on the defined functions, *RH Connect* and *RH Set conditions*, the final *RH* variable is estimated as in Figure 5.18. From the *RH Set conditions*, a new *RHS* signal is formed and set high if any of *RHS1* or *RHS2* or RHS3 is true. However, the final *RH* signal is generated after passing the *RHS* signal through a delay block defined by *SoC vs decreasing time*. This *SoC vs decreasing time* delay function is incorporated to differentiate between different cells, so the cells with higher SoC connect earlier than the cells with lower SoC. This *RH* signal is subsequently passed on to the *Mode Change* block, which creates the enabling signal for triggering connection controller in the Frequency-Voltage control as explained in Section  and once the connection criteria is met, based on the *ConcSignal*, the switching operation takes place from SA to IC mode.

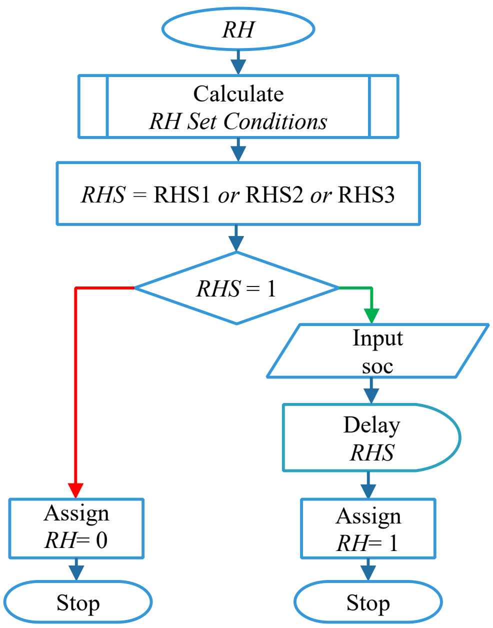


***Figure 5.18:*** *Ready Help state flow diagram*

***RHR signal:*** The *RH* signal so formed by the *RH flow diagram* is utilized for mode transition and if the cell remains connected to the BB bus, the RH cell supports the needy cell, thus resulting in decline of its SoC. From the *RH Reset conditions*, a new *Ready Help Reset Combined* signal (*RHRC*) is generated through *or* function of reset conditions, RHR1 and RHR2. The *RH* value is reset to 0 using this *RHRC* signal through a flipflop function as shown in Figure 5.19(a) and is stored in Ready Help Reset (*RHR*).

***RHF signals:*** In the *RH Set conditions*, RHS1 signal is generated when the SoC goes above the upper limit *SoCUL*, owing to high renewable generation in the cell. Based on this RHS1 signal, the RH cell is forced to energise the BB bus thus forming the *Ready Help Forced* (RHF) signal. Additionally, a separate reset signal, RHFR, is tabulated using a flipflop function when SoC becomes less than equal to *SoCUL - 4*. The reset value was chosen in a way to ensure that the cell does not continuously cross the *SoCUL* and to avoid dissipation of energy to other cells which are not in need state. The layout of the signals is depicted in Figure 5.19(b).

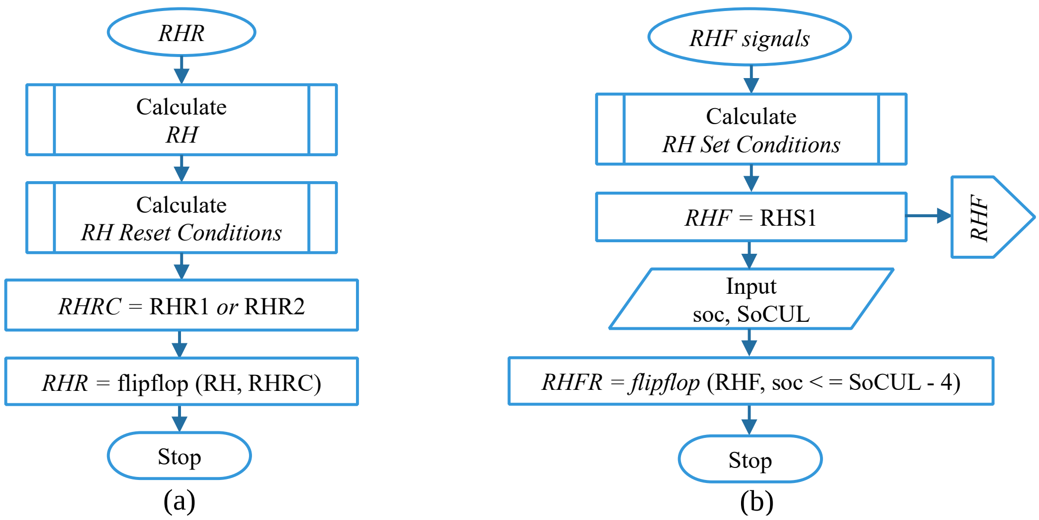


***Figure 5.19:*** *Ready Help Reset & Ready Help Forced signals*

### *5.3.3 DISC flow diagram*

As the NH and RH variables from NH and RH flow diagram respectively remain high, the cells remain connected to BB bus. This implies that the cells are in IC mode and based on the SoC of each cell, the cell either receive or support each other to ensure that the cell has a SoC over the crucial limit. But as soon as the NH and RH variables are reset, the cells are disconnected from the BB bus. Further, two additional functions are also devised to ascertain that cells are not connected to BB bus when either no NH cells or RH cells exist in the network.

***PbbND function:*** The primary application of this function is when multiple *NH* cells are in IC mode with no *RH* cells in BB network. In other words, this means that the *NH* cell with comparatively higher SoC would assist the other *NH* cells with lower SoC. This results in the deterioration of stability of the supporting *NH* cell because of the reduction of its SoC. To avoid such behaviour, the power flowing from the cell to the BB Bus, $P_{bb}$, is measured as seen in Figure 5.20(a). If this value is greater than 0.001 pu. for 120 s, it indicates that the cell is supporting the other NH cells. Hence a new variable, Power Backbone Need Disconnect (*PbbND*) is created and assigned a value of 1, while in other cases, *PbbND* is set to 0. This variable is later utilized for arriving at the Disconnect (*DISC*) variable.

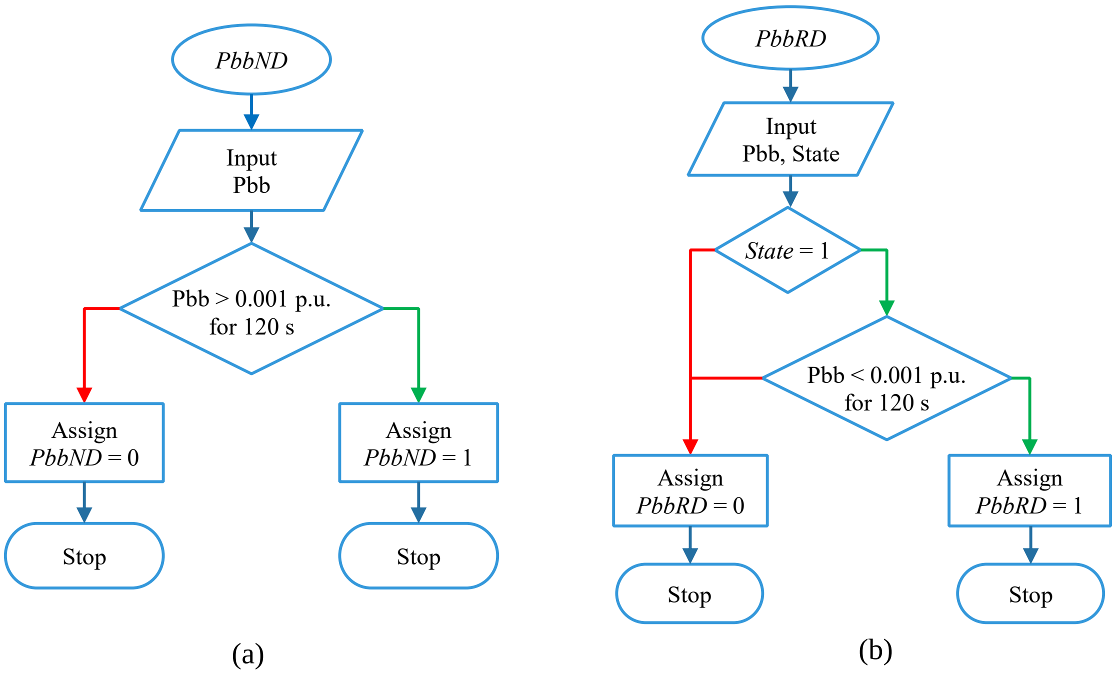


***Figure 5.20:*** *Disconnect functions*

***PbbRD function:*** Analogous to *PbbND* function, *PbbRD* function is employed when the BB network comprises of only *RH* cells with no *NH* cells. This indicates that the *RH* cell with higher SoC would support the other *RH* cells, which is not a desired property. To evaluate the condition, another variable Power Backbone Ready Disconnect (*PbbRD*) is formulated. If the cell is connected to the BB bus and the value of $P_{bb}$ is less than 0.001 pu. for a minimum of 120 s, then *PbbRD* is set high, otherwise it is set low. Like *PbbND*, the variable *PbbRD* is further used for assessing the *DISC* variable. The flow diagram of the function is shown in Figure 5.20(b).

***DISC flow diagram:*** With the defined *DISC functions*, *PbbND* and *PbbRD*, and the reset conditions of the *NH* and *RH* states of the cells, its evaluated whether the cell needs to be disconnected or not. The flow diagram for estimating the Disconnect variable, *DISC*, is depicted in Figure 5.21.

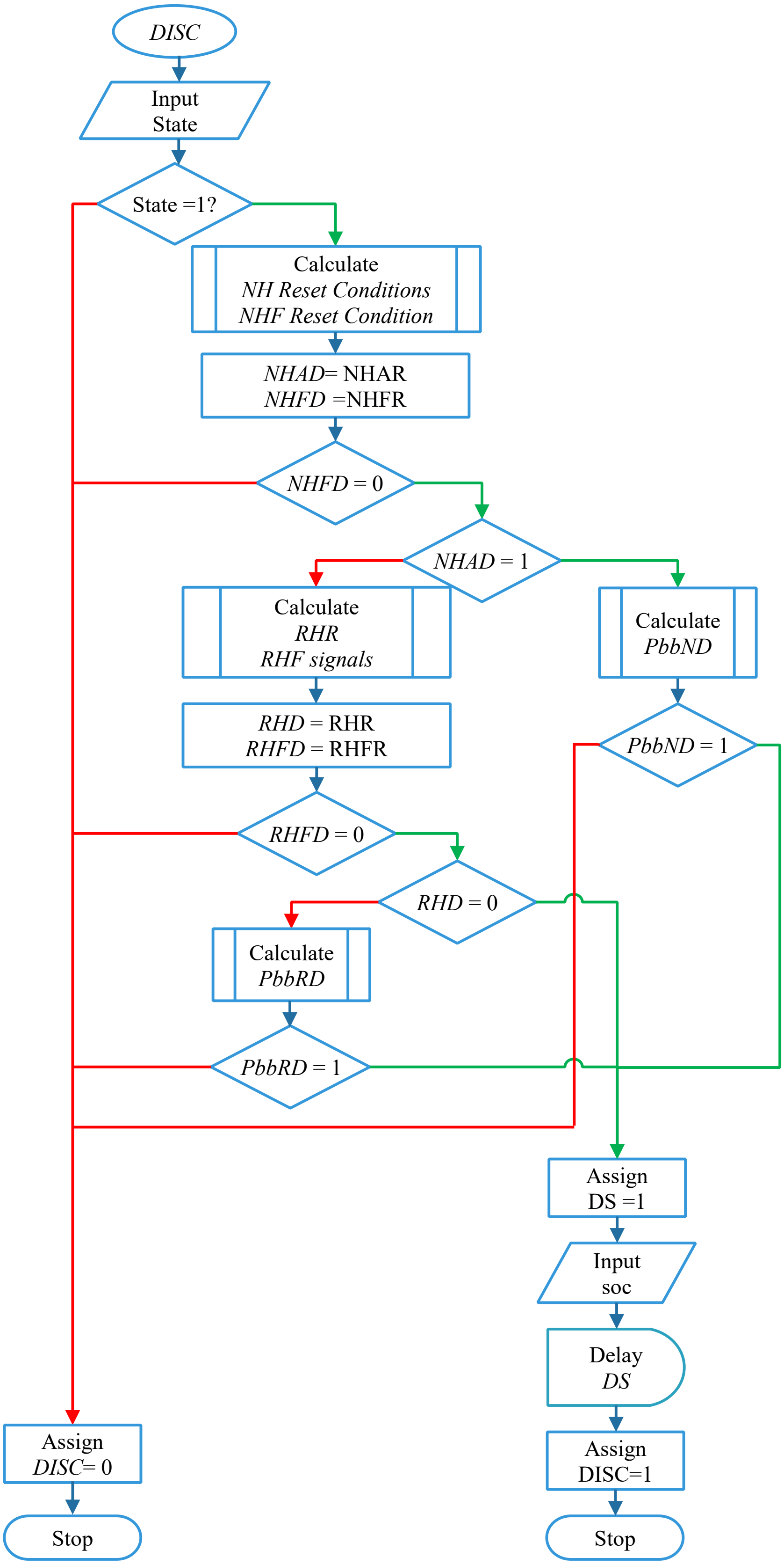


***Figure 5.21:*** *Disconnect state flow diagram*

As seen in the above figure, initially the state of the cell is checked to ensure whether it's in SA or IC mode. If the cell is in SA mode, no action has to be performed, but if in IC mode, subsequently *NHF* and *NH Reset conditions* are evaluated to estimate the variables *NHAR* and *NHFR* respectively. These values are assigned to the variables Need Help Actual Disconnect (*NHAD*) and Need Help Forced Disconnect (*NHFD*).

Now the value of *NFHD* is checked, if the value is 1, the current mode is presumed i.e. *DISC* is assigned value of 0. However, if the value of *NHFD* is 0, then the value of *NHFD* is compared with 1. If evaluated to be true, meaning there is *NH* cells in the network, the function *PbbND* is evaluated to ensure that *RH* cells exist in the network to support the *NH* cells. For zero value of *PbbND* variable, the previous mode of operation is continued. But, if the *PbbND* is true, then a new variable *DS* is assigned the value of 1.

However, if the comparison of *NHFD* with 1 turns out be false, indicates that the cell is not in *NH* state. With this, the *RH* state of the cell is further analysed by valuating *RHR* and *RHF signals*. From these functions, the value of *RHR* and *RHFR* are assigned to Ready Help Disconnect (*RHD*) and Ready Help Forced Disconnect (*RHFD*) respectively. Following this, the condition of *RHFD* is compared and if the value is 1, then current mode is sustained. If the value of *RHFD* is 0, then *RHD* is assessed to decide on the *DISC* variable. A zero value of *RHD* indicates that the cell is no longer ready to support, hence the *DS* is assigned 1. But if *RHD* is 1, then *PbbRD* is evaluated to verify that only *RH* cells are in the network. If so, then again *DS* is set high with the value of *PbbRD* as 1, else *DISC* is set low, meaning that IC mode is still prolonged.

Once the value of *DS* is set high, the value is delayed by a *SoC vs increasing time* function to distinguish between multiple cells trying to disconnect at the same instant. After the corresponding delay time, the variable *DISC* is set high (1), which is then passed on the *Mode change* block.

### 5.3.4 Mode Change

As seen in Figure 5.6, the *Mode change* block accepts 3 inputs – *NH*, *RH* and DISC, from within *Automated Decision-making* module. Once the block receives a true signal for *NH* and *RH*, an enabling signal, *ConcEnable*, is generated, which is fed as an input to the *Control Algorithm* module. In the control algorithm module, the *ConcEnable* triggers the *Connection controller* and as the connection criteria is met, *ConcSignal* is produced. This *ConcSignal* comes back as an external input to the block, indicating that the cell is ready for seamless transfer from SA to IC mode. As the block receives this signal, it performs the desired transition.

Analogous to mode transition from SA to IC, the *Mode change* block creates another enabling signal, *DiscEnable*, as an output to the *Control Algorithm* module. The *DiscEnable* signal activates the *Disconnection controller* and as the disconnection criteria is satisfied, the *DiscSignal* is produced, fed as the second external input to the *Mode change* block. Upon receipt of this signal, signalling that cell can be seamlessly transferred from IC to SA mode, the *Mode change* block opens the breaker connecting to BB bus and switches its mode.

Both the signals, *ConcEnable* and *DiscEnable* signals, are reset upon State change to ensure that they are prepared for the next transition operation, if required.

## 5.4 Summary

Combining the *Control Algorithm*, as defined in Section 4, and *Automated Decision Algorithm* in Section 5, the layout of the *Overall system control* is transformed as seen in Figure 5.22 . Both *Control Algorithm* and *Automated Decision Algorithm* module accepts a register of input signals, as explained in the previous sections. The *Automated Decision Algorithm* determines the instants for changing its operation mode i.e. from SA to IC or vice-versa. While the *Control Algorithm* decides the frequency and modulation index of the VSC, thus regulating the frequency and voltage of the AC bus.

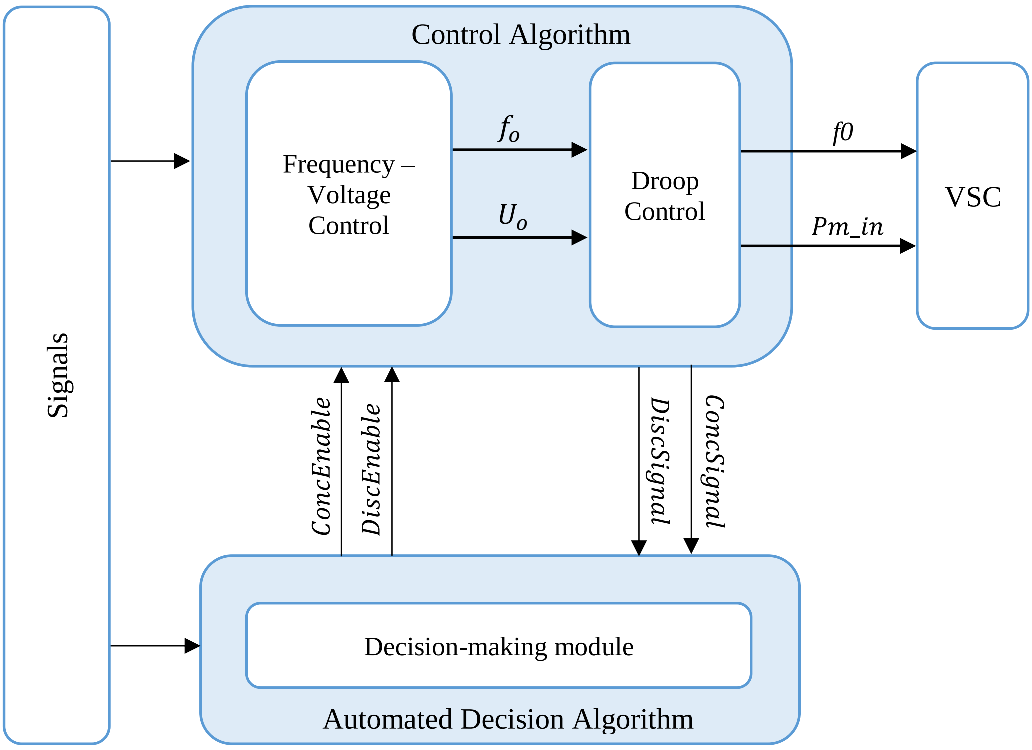


***Figure 5.22:*** *System Control*

# 6 Simulations & Results

## 6.1 Introduction

The proposed control strategy for seamless transfer of modes and automated decision-making algorithm, as explained in Section 4 and 5, are assessed and evaluated for varied simulation scenarios to prove its functionality. The chapter may be subdivided into 2 main sections. The first section emphases on analysing the dynamics associated with seamless (dis)connection of a single cell to main EG and of multiple cells to each other. The second part focusses on the different cases to examine the algorithm devised for automated transition of cells to switch between different modes of operation.

## 6.2 Sizing and Selection of parameters

As explained in Section 3.2, each cell, as shown in Figure 3.1, consists of BESS with converter as the master component, PV and Wind generation sources and controllable loads. The sizing of the components in the cell is based on the initial test site parameters at ACRRES test site [65].

The Table 6.1 shows the chosen parameters for modelling the Cell in Figure 3.1. The major source of power in Cell is 15 kWp Solar system integrated into the distribution network through a 3 phase, 15 kVA SMA inverter. Also, it is also intended to install a 10kW wind turbine to further supply to the distribution network. To apprehend the average load requirement of the distribution network, the energy consumption data was obtained. Analysing the data for the months of July and August, the average demand of 10 kW is observed.

***Table 6.1:*** *Sizing of components in Cell*

| *Load Demand [kW]* | *PV system Capacity [kW]* | *Wind Capacity [kW]* | *Battery Bank Capacity [kWh]* | *Inverter Rated Power [kVA]* |
|---|---|---|---|---|
| 10 | 15 | 10 | 120 | 120 |

Once the sizing of the components is fixed, the next step is to select the parameters of the controller. As previously described, the battery inverter is modelled as a VSI for the grid forming capabilities. The VSI works based on the droop curves – Active power/frequency and Reactive power/voltage. In 'Frequency Based Microgrid Control – DSM & SSM' [34], a study on the Small-signal stability Vs Steady-state stability for the Cell was performed and arrived at allowable value for active power droop coefficient ($k_P$) and reactive power droop coefficient ($k_Q$). The value for $k_P$ of 0.3 % and $k_Q$ of 2 % is adopted for the thesis.

The frequency dependency on SoC, $f_{SOC}$ curve as depicted in Figure 4.6 is the most significant with respect to the control and operation of the Cell. The various limits and ranges defining the $f_{SOC}$ curve is crucial for determining the grid parameters and also the applicability of DSM and SSM schemes. The $f_{max}$, coinciding with $SoC_{max}$ is chosen as 51.5 Hz, because this value corresponds to the limit beyond which DRES production is reduced to zero, as explained in Section 3.6. The $f_{min}$ value coinciding with $SoC_{min}$ is selected at 48 Hz which allows a range of 1.8 Hz for the DSM schemes to be applied. Hence a frequency band of 48 to 51.5 Hz is selected for the project.

The range of SoC is chosen from 0 to 90% with $SoC_{min}$= 0 % and $SoC_{max}$ = 90 %, for avoiding over charging of the battery. If a fully charged cell with $SoC_{max}$ as 100 %, with corresponding frequency of 51.5 Hz, wants to connect to another cell or EG with backbone frequency of 50 Hz, then the frequency of the former cell has to be reduced to 50 Hz. During the process, the DRES starts injecting more power into the cell as per SSM scheme (Section 3.6), which might result in overcharging of the battery, degrading the life of the battery drastically.

The system is healthy when the SoC of batteries is between 30 and 80 %. The lower limit of SoC 30 % corresponds to frequency of 49.8 Hz. The DSM schemes are triggered at 49.5 Hz, corresponding to a SoC of 25%. The upper limit of 80 % corresponding to a frequency of 50.2 Hz is the start point for the SSM schemes. So, this means that the SSM/ DRES curtailment is active in the SoC band of 80 – 90 % and the DSM scheme is active in the SoC band of 0 % - 25 %. A higher band for DSM allows to have different load shedding profiles in steps based on load priorities.

The SSM schemes are applied when frequency of the MG crosses 50.2 Hz and decreased at the rate of -40 % / Hz till 51.5 Hz, as already discussed in Section 3.6. The DSM schemes are activated when frequency falls below 49.8 Hz based on different load shedding curves, as deliberated in Section 3.7.

## 6.3 Simulation results – Seamless (dis)connection

For enabling a smooth and seamless transition between different operating modes: SA, GC and IC, a control strategy was developed which prepares the cell for the desired switching operation. Due to absence of any communication infrastructure, the converter of the BESS, the master component in each cell, is still maintained in voltage source mode. Once triggered, the corresponding connection and disconnection controller is activated, which then generates additional deviations, contributing to the final frequency and voltage set points to the converter. On achieving the required connection and disconnection criteria, the desired operation is performed by opening or closing the breaker connecting to the network.

### 6.3.1 Case I: Single Cell transition between SA & GC mode

The primary focus of this case to understand the grid behaviour when a cell is being connected or disconnected from the main EG. The layout of the MG architecture utilized for simulations is depicted in Figure 6.1.

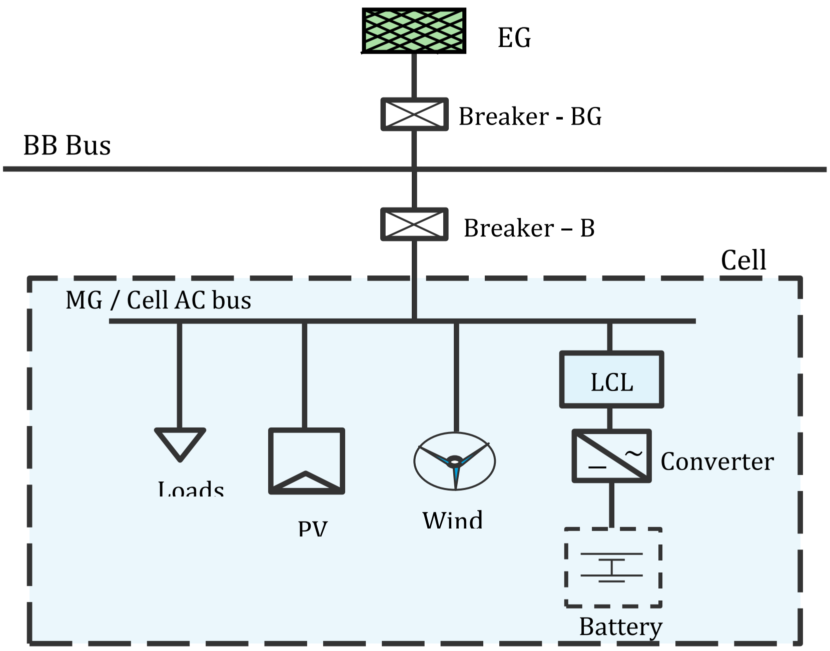


***Figure 6.1:*** *Single Cell architecture*

For simulating the case, as in the Figure 6.1, the BB bus is already coupled with the EG by closing the breaker BG. This means that the BB bus is live with nominal voltage of 400V and frequency of 50 Hz. However, the condition of the Breaker B is in open condition, indicating the Cell operates in SA mode.

## Case I.A: Connection

*(i)* *Battery with SoC of 40 %*

The connection of Cell with the EG is studied here. It is assumed that the Cell is initially operating in SA mode with *SoC* of BESS as 40 %. To simulate the connection of this Cell to the EG, a manual trigger signal is initiated for connection of Cell. The connection controller becomes active and tries to reduce the frequency, voltage and phase angle error. When the connection criteria are met, the Cell is connected to the EG by closing the *Breaker B*. The Cell then operate in GC mode.

At time t = 10s, the connection command is triggered. Figure 6.2 and Figure 6.3 show the frequency and voltage graphs of the Cell and EG. After the initiation of the command, the connection controller tries to bridge the initial voltage difference of 1.08 V and frequency deviation of 0.08 Hz. Also, simultaneously the phase error is also reduced within limits of 5°.

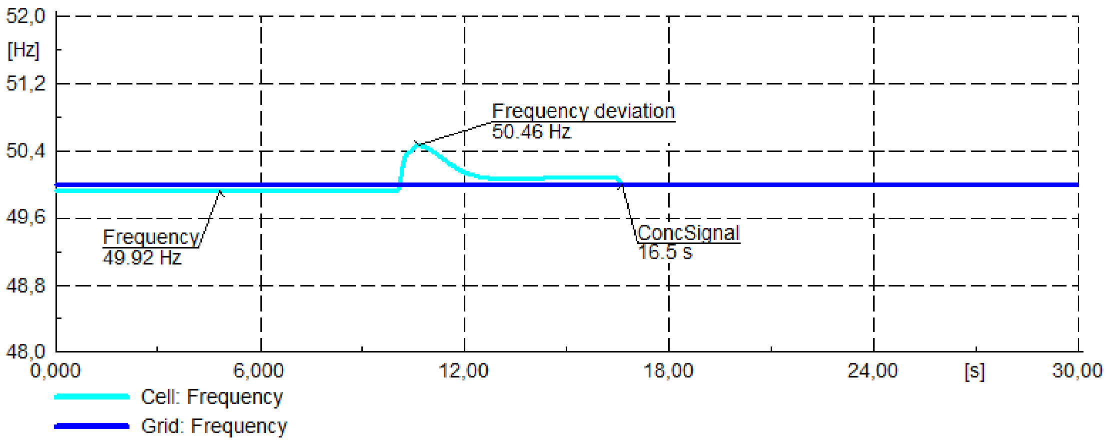


***Figure 6.2:*** *Frequency of Cell and External Grid - Connection*

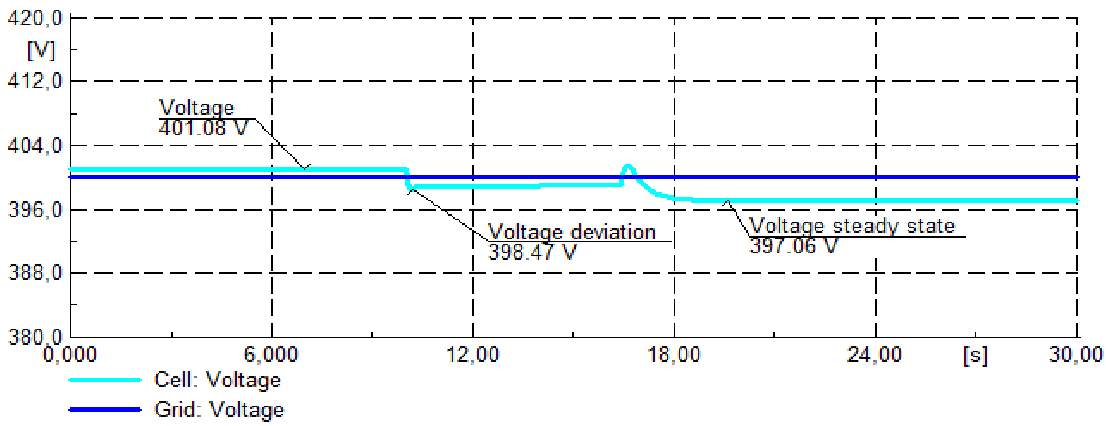


***Figure 6.3:*** *Voltage of Cell and External Grid - Connection*

The voltage and frequency graphs represents a smooth transfer from SA to GC mode. Once the cell is in GC mode, the operating frequency of the cell is 50 Hz, as determined by the EG and the voltage of the cell attains a steady state value of 397.06 V.

When all the errors according to the Connection criteria, as mentioned in Section 4.3.2, are within the required limits, a signal is generated for the closure of the circuit breaker. In this case, the closing command is given at 16.5 s, as indicated in Figure 6.2 (*ConcSignal)*. The Figure 6.4 shows the Triggering command, *MConcT*, at 10s and the closing command, *ConcSignal* at 16.5 s, which clearly defines the switching of modes.

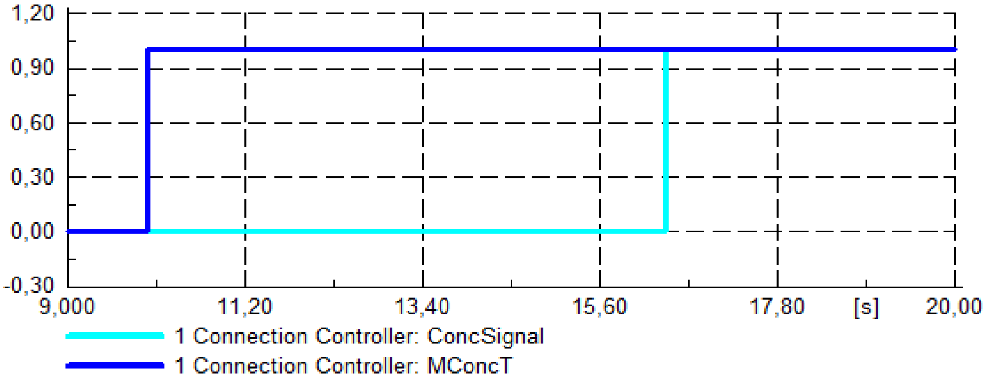


***Figure 6.4:*** *Triggering and mode switching command for Connection*

Further, if we zoom into voltage waveforms as shown in Figure 6.5, it is observed that the frequency, amplitude and phase of the voltage are in sync, implying a smooth and seamless transition.

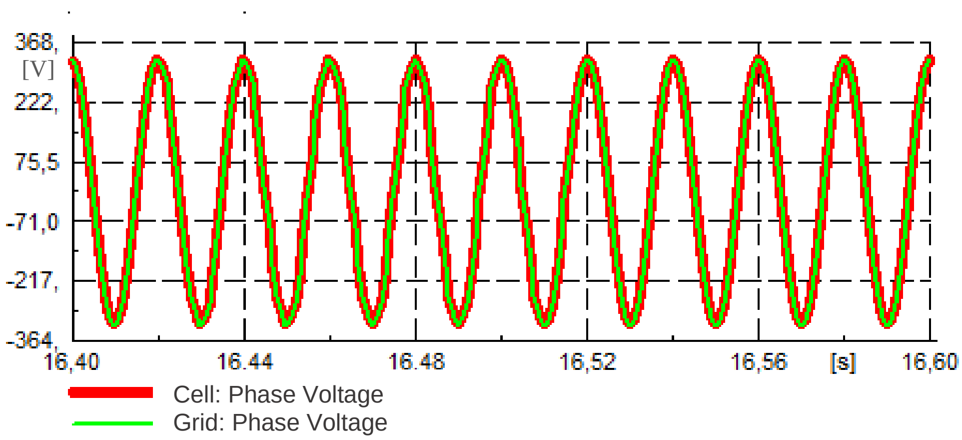


***Figure 6.5:*** *Voltage waveforms of Cell and External Grid at instant of connection*

To minimize the frequency, voltage and phase angle errors, the connection controller, as explained in Section 4.3.2 , receives EG frequency $f_g$ and voltage $U_g$. The frequency controller tries to reduce the frequency error through a PID controller and generates the additional deviation, $f_{conc}$. This signal is then added to the normal frequency of the Cell generated by the Normal Controller, $f_{norm}$, to arrive at the final frequency set point, $f_o$. All the signals, $f_{conc}$ and $f_{norm}$, contributing to value of $f_o$ is depicted in Figure 6.6. Analogous to the frequency controller, the voltage controller generates the necessary deviation, $U_{conc}$, to minimize the voltage error. The signal is further combined with the normal voltage signal, $U_{norm}$, to tabulate the final voltage set point, $U_o$, as shown in Figure 6.7. Because of this controller action, the Cell observes a maximum frequency deviation of 50.46 Hz and voltage deviation of 398.47 V during the connection period. These values are indicated in Figure 6.2 and Figure 6.3, which are in the bandwidth of allowable grid code variations as per EN50160 [56].

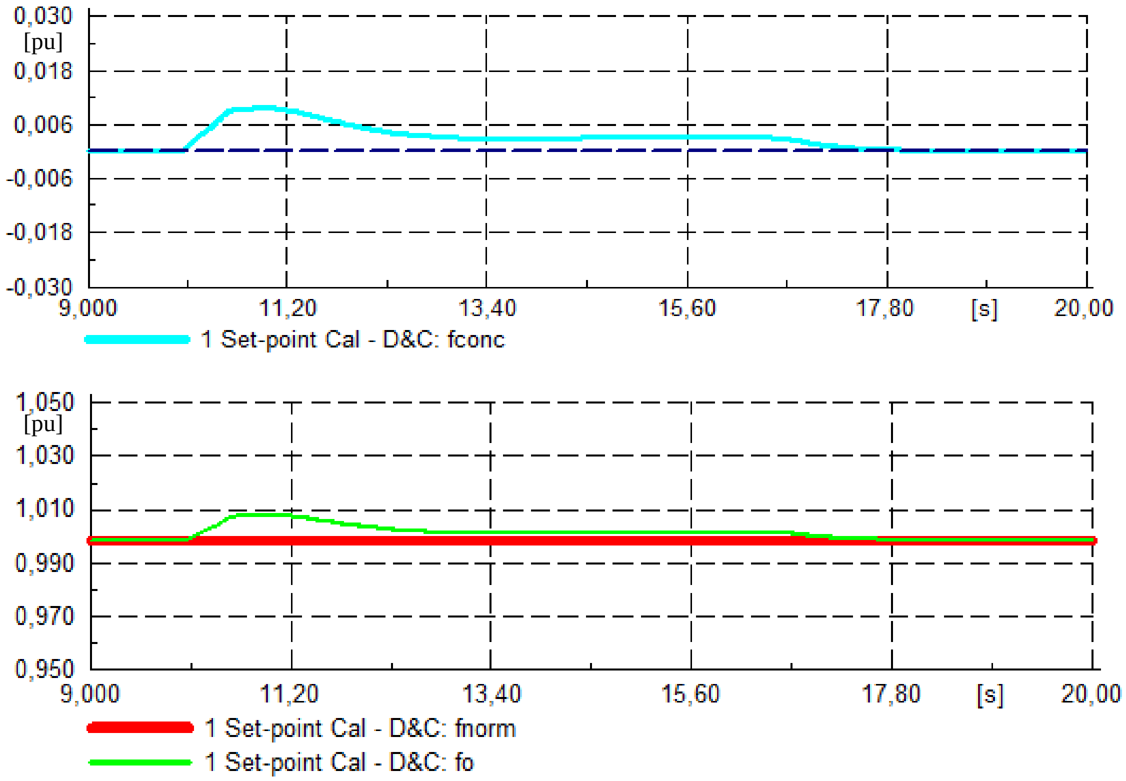


***Figure 6.6:*** *Frequency setpoint signals for connection*

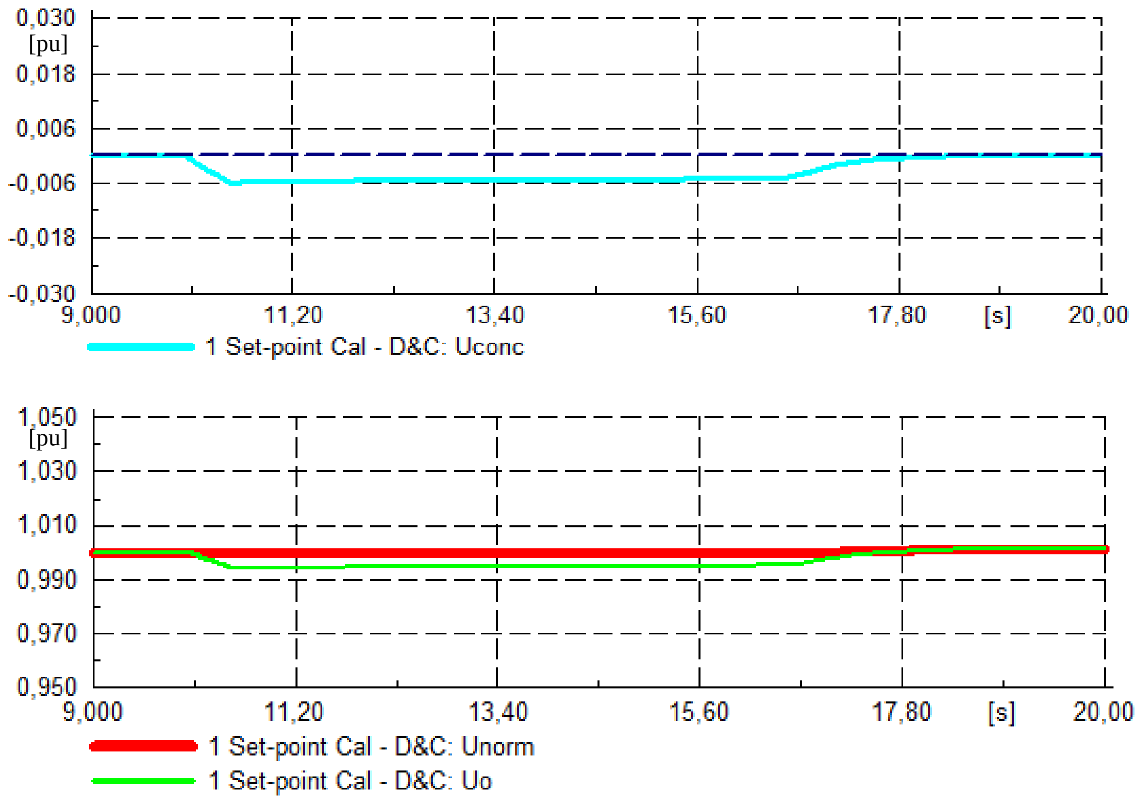


***Figure 6.7:*** *Voltage setpoint signals for connection*

The power absorbed by the converter of battery is shown in Figure 6.8. At 16.5 s, when the Cell is synchronized with EG, the frequency of the Cell is always maintained at 50 Hz as evident in Figure 6.2. As per the droop Eqn. (4.7), the power is absorbed by the converter. The initial change in power is due to the contribution of $f_{conc}$ to the ultimate set point $f_o$ and as the value of $f_{conc}$ slowly degrades to zero at 18.5 s, the power absorbed by the converter also stabilizes at 0.5 p.u.

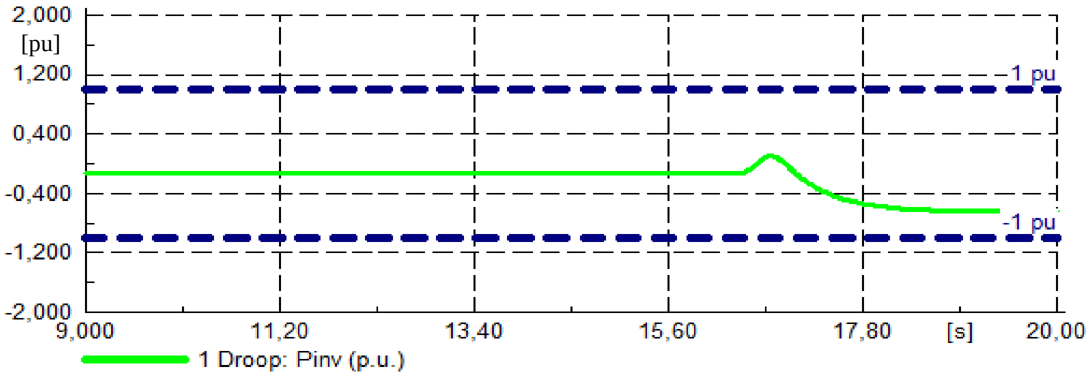


***Figure 6.8:*** *Power delivered/absorbed by the converter of battery*

*(ii)* <u>*Inverter Overloading - Battery with SoC of 20 %*</u>

The power absorbed by the converter once synchronised with the EG is determined by the Eqn. (4.7). As per this Eqn. due to the value of $f_o$, there are possibilities for the converter to be overloaded. In this case, as similar to the previous scenario, the Cell is initially operating in SA mode, but with a SoC of 20 %. As per the Frequency – SoC Dependency curve, the operating frequency of the Cell is tabulated to be 49.22 Hz, as shown in Figure 6.9.

The manual triggering command for connection of Cell to the EG is given at 10 s and as analogous to the previous case, the connection controller minimizes all the errors to the respective limits. The controller calculates the necessary deviations to match with the parameters of the EG and finally the closing command to the breaker is initiated at 16.0 s, when the voltage of the Cell and EG are in sync. The frequency and voltage graphs of the Cell and EG are depicted in Figure 6.9 and Figure 6.10. As clear from the figures the maximum frequency deviation is 50.34 Hz and the voltage deviation is 398.43 V due to the connection controller. The voltage attains a steady state value of 395.04 V after connection of Cell to EG.

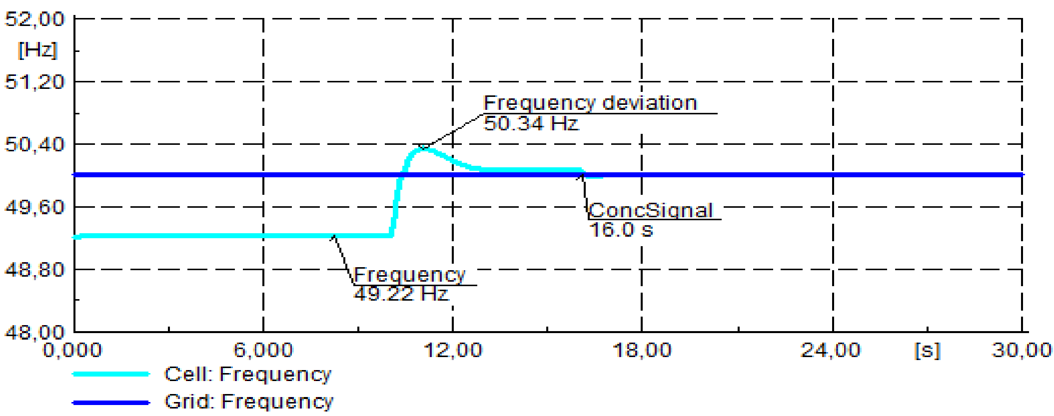


***Figure 6.9:*** *Frequency of Cell and External Grid – Connection: Inverter overloading*

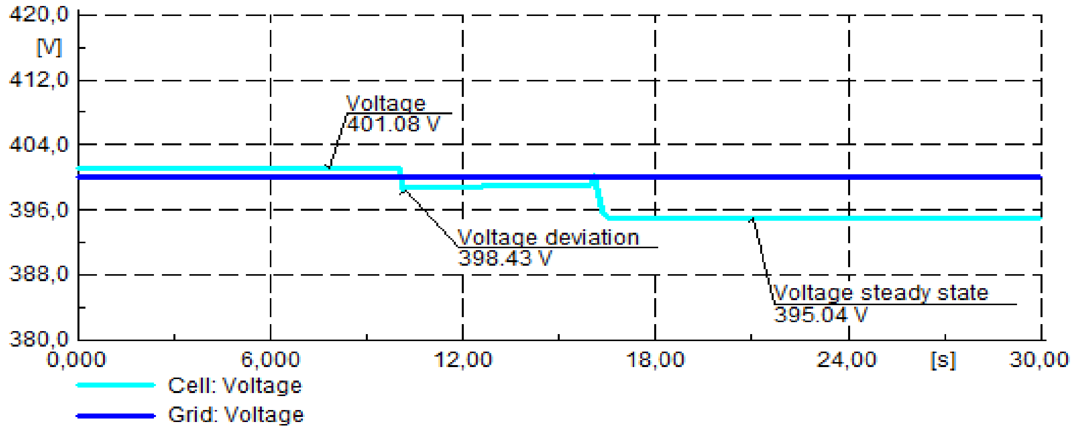


***Figure 6.10:*** *Voltage of Cell and External Grid – Connection: Inverter overloading*

Now focussing on the power consumed by the converter of the battery. Since the Cell has a low SoC of 20 %, the corresponding operating frequency is 49.22 Hz as shown in Figure 6.9. When synchronized with the EG, due to its low $f_o$ set point, the converter of the battery approaches the limit of - 1 p.u. As soon as the power crosses these limits, the dynamic limiters, as defined by Eqn. (4.9) and (4.10) in Section 4.3.4, plays its role of limiting the $f_o$ set point. Due to this, the converter power is limited to +/- 1p.u. as desired and this is evident in Figure 6.11. However, in the absence of the dynamic limiters, the converter absorbs high power, which drastically affects the life of the battery.

As power is absorbed by the battery, its SoC keeps on increasing and at 420 s, the power absorbed by the converter starts decreasing due to fixed grid frequency and rising $f_{soc}$, thus the value of $f_o$. When the situation is prolonged for a long time, as seen in the Figure 6.11, the SoC approaches the limit of the point $S_c$ corresponding to 50 Hz and the power gradually reaches the value of 0, following the droop curve.

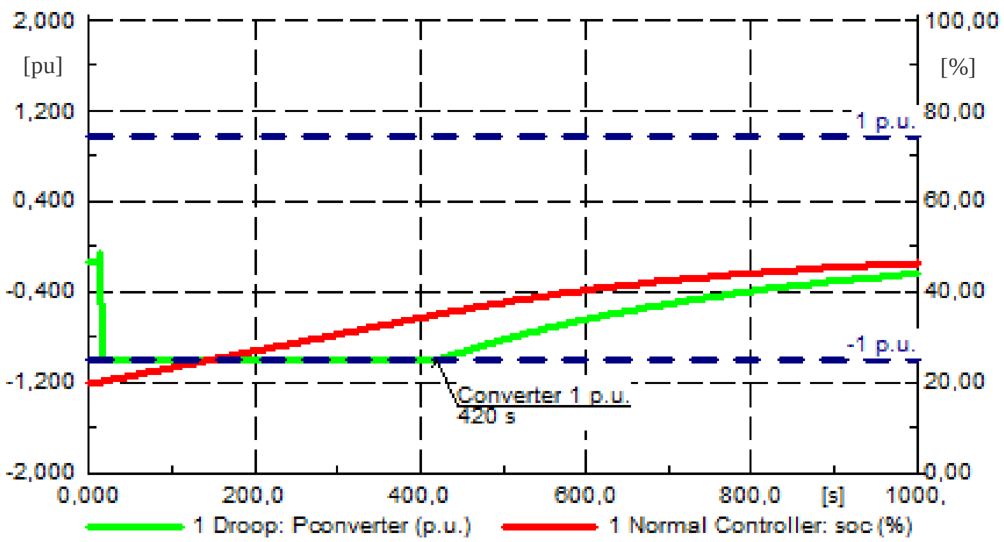


***Figure 6.11:*** *Converter power and SoC of battery – Overloading*

*(iii) <u>Comparison of PI vs PID controller</u>*

To evaluate the effect of using a PID controller to a PI controller, the case of connection of a Cell having Battery with SoC of 40 % is assessed for both scenarios.

First, the Cell in SA mode is given a triggering command for connection at 10 s employing a PI controller. The PI controller reduces the error upon initiation and generates the additional deviation, $f_{conc}$, for synchronizing with the grid voltage. As a result of which, the frequency of the Cell observes a maximum deviation of 51.1 Hz as shown in Figure 6.12. This rise of frequency during the connecting period forces the DRES to curtail its power as explained in Section 3.6. This curtailment of power from DRES is undesired, and it results in creating disturbances in the system.

In other scenarios, a Cell with higher SoC (70 %) trying for synchronizing with EG encounter a frequency deviation on the lower side, 49.0 Hz, due to the controller action. As a result of which, the DSM schemes are activated. The various schemes of load shedding schemes, as seen in Figure 3.15 becomes operative as the frequency becomes less than 49.5 Hz. The Cell frequency of 49.0 Hz results in unnecessary shedding of loads, thus restricting the consumer demand. But in the process of synchronization with EG, the Cell reaches its steady state value of 50 Hz and the Shedding factor, as explained in Section 3.7, regains the value of 1 and the respective loads are restored. This sudden shedding and restoration of loads due to the controller behaviour instils instability to the system.

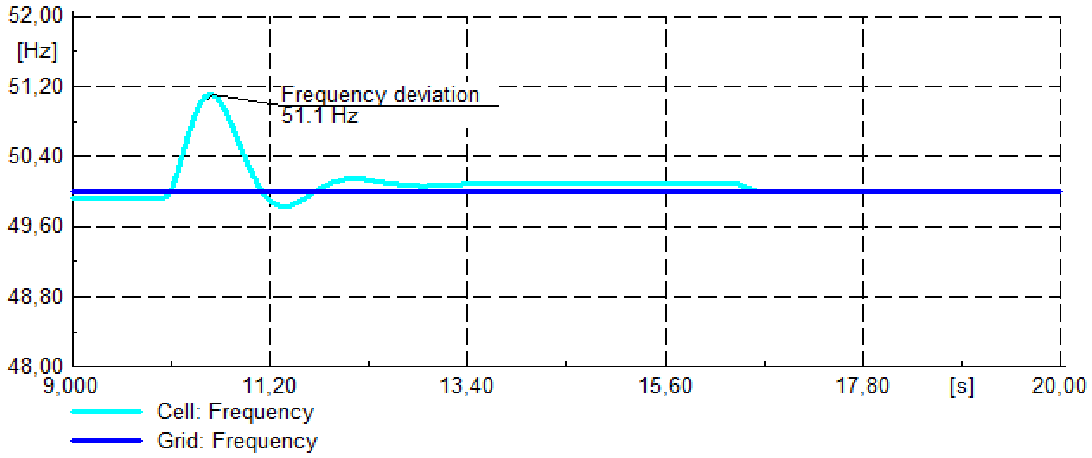


***Figure 6.12:*** *Frequency profile of Cell with PI connection controller*

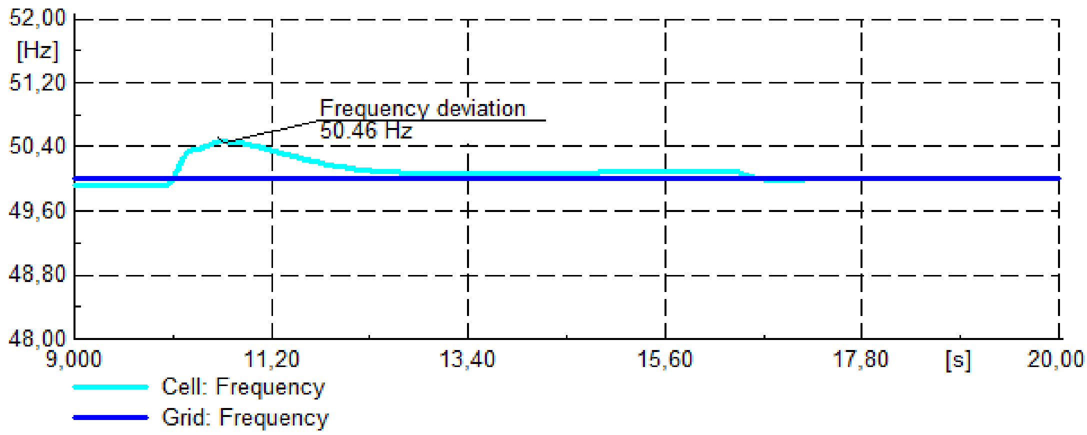


***Figure 6.13:*** *Frequency profile of Cell with PID connection controller*

To avoid such undesired behaviour during connection period, the PID controller is utilized instead of a PI controller. This aids in reducing the overshoot in the frequency created due to connection controller behaviour. The Figure 6.13 shows a maximum frequency overshoot of 50.46 Hz in the event of a connection with the EG, for the same case of Cell with battery of SoC of 40 %. Hence, while utilizing a PID controller, the frequency changes are restricted within a bandwidth 49.5 – 50.5 Hz, which complies with EN50160 standard, [56], even when the transitions occur. Moreover, this improves the transient response, thus increasing the stability of the system.

The discussions above were focussed on connection of Cell with EG for 2 cases: one with Battery of SoC of 40% and other with SoC of 20% for evaluating the overloading scenario. Similarly, to these cases, the connection algorithm was tested for different SoC, starting from very low value 10% to a high value of 90%. Analysing the waveforms, the deviations were observed to be within the limits, with a smooth and seamless transfer from SA to GC mode. The results of all the simulated cases with different SoC are tabulated in Table A.1 in Appendix A.

### Case I.B: Intentional Disconnection

In this section, the Intentional Disconnection of Cell from EG is being examined. It is assumed that the Cell is connected to the EG. In the process of disconnection, a manual trigger signal is initiated for disconnection of Cell and the disconnection controller becomes active. The disconnection controller tries to reduce the active and reactive power flowing through the line connecting to the EG to zero and when the criteria is met, the Cell is disconnected from EG by opening the *Breaker B*. The Cell then operates in SA mode.

The Cell comprising of the Battery with a SoC of 40 % is connected to the EG using the connection control as described above. Upon reaching a steady state at around 18.5 s (Figure 6.8), the Cell absorbs power from the EG for charging the battery. At time t = 30s, a manual disconnection command is initiated. As explained in Section 4.3.3, the disconnection controller tries to reduce the active and reactive power flow to/from the EG. The frequency and voltage of the Cell and EG associated with the disconnection is depicted in Figure 6.14 and Figure 6.15.

Examining these graphs, after the DiscSignal at 33.15 s, a smooth transfer of voltage and frequency is observed, indicating a seamless transfer of modes from GC to SA. After disconnection, the Cell is in SA mode, during which the frequency and voltage is largely based on their normal controllers, as described in Section 4.3.1.

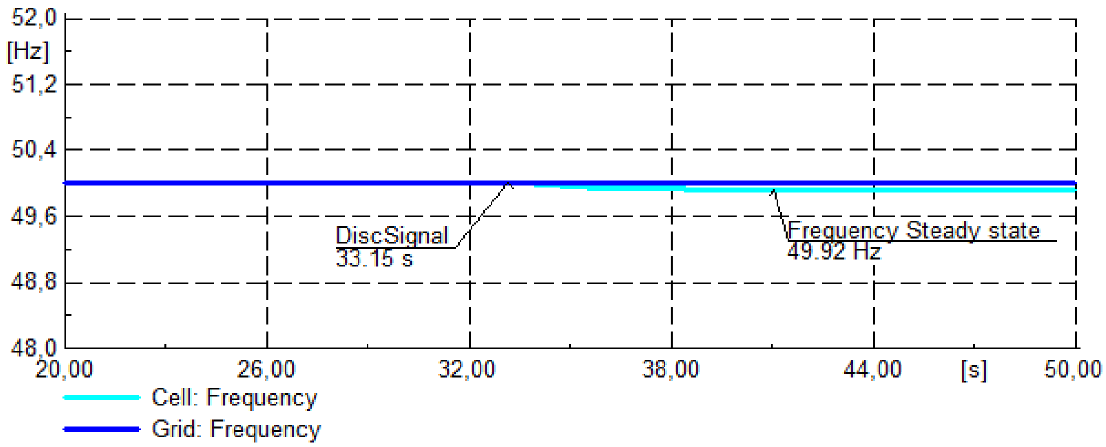


***Figure 6.14:*** *Frequency of Cell and External Grid – Intentional Disconnection*

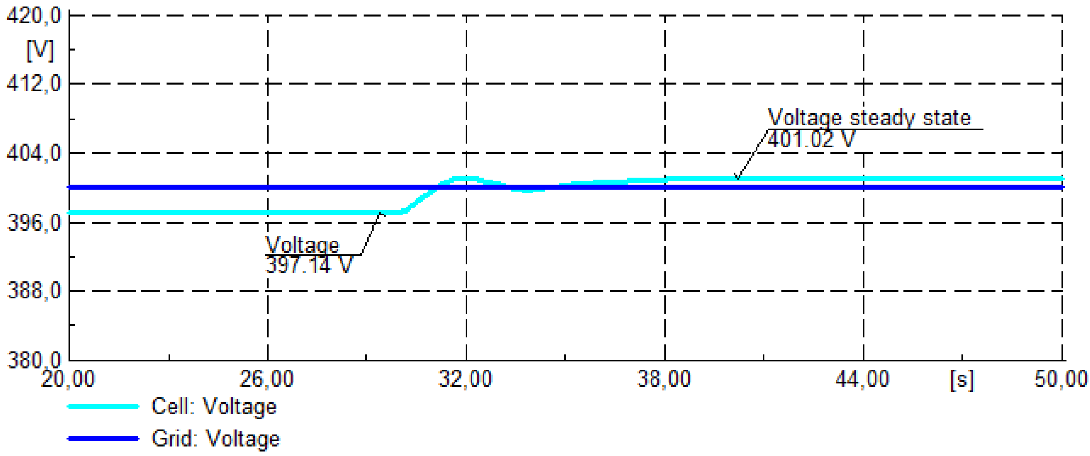


***Figure 6.15:*** *Voltage of Cell and External Grid – Intentional Disconnection*

Upon initiation of the disconnection algorithm, the PI controller minimizes the power flowing to / from the EG to the Cell. The Figure 6.16 shows that the active and reactive power errors are gradually reduced to zero. In other words, the Cell is being prepared for a safe disconnection and when the errors are within limits as per the disconnection criteria as detailed in Section 4.3.3, a signal, *DiscSignal* is produced for opening of the circuit breaker. The trigger command, *MDiscT*, at 30s and the opening command, *DiscSignal*, at 33.15 s are clearly depicted in Figure 6.17. This signal is utilized for switching of modes from GC to SA.

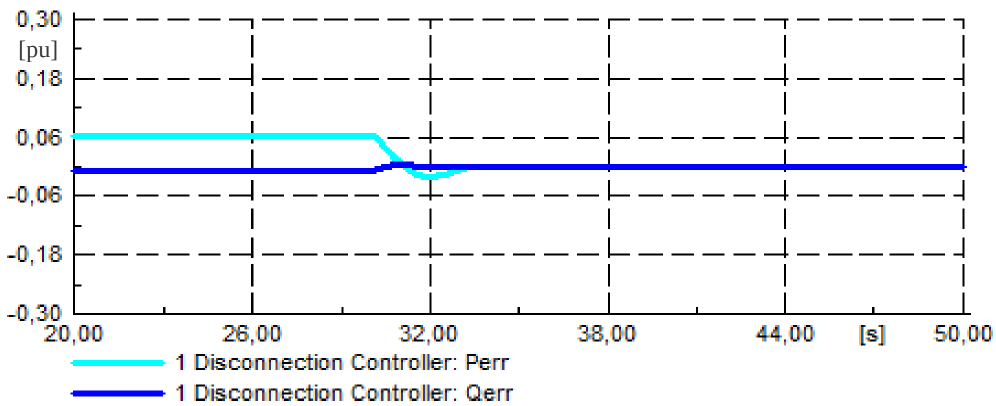


***Figure 6.16:*** *Active and reactive power flow – External grid*

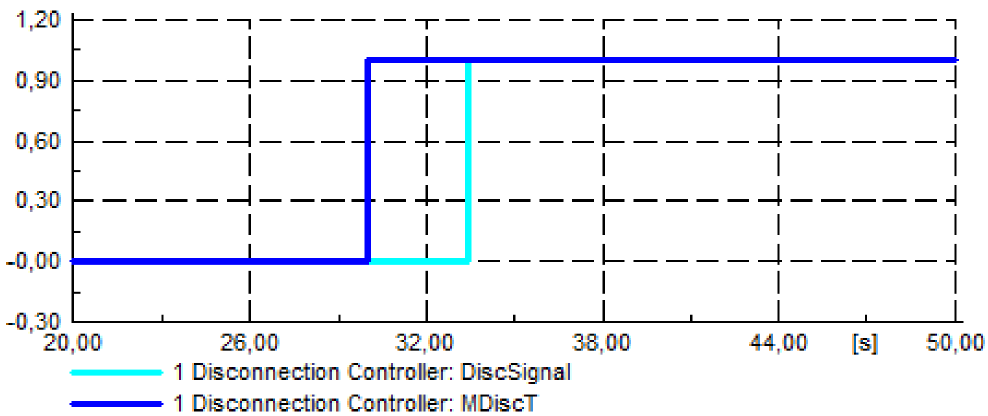


***Figure 6.17:*** *Triggering and mode switching command for Disconnection*

During the process of disconnection, the controller receives active and reactive power flow of EG, $P_g$ and $Q_g$. To reduce the power flow to zero, a PI controller is utilized, as described in Section 4.3.3. This results in generation of additional deviations, $f_{disc}$ and $U_{disc}$, as shown in Figure 6.18 and Figure 6.19.

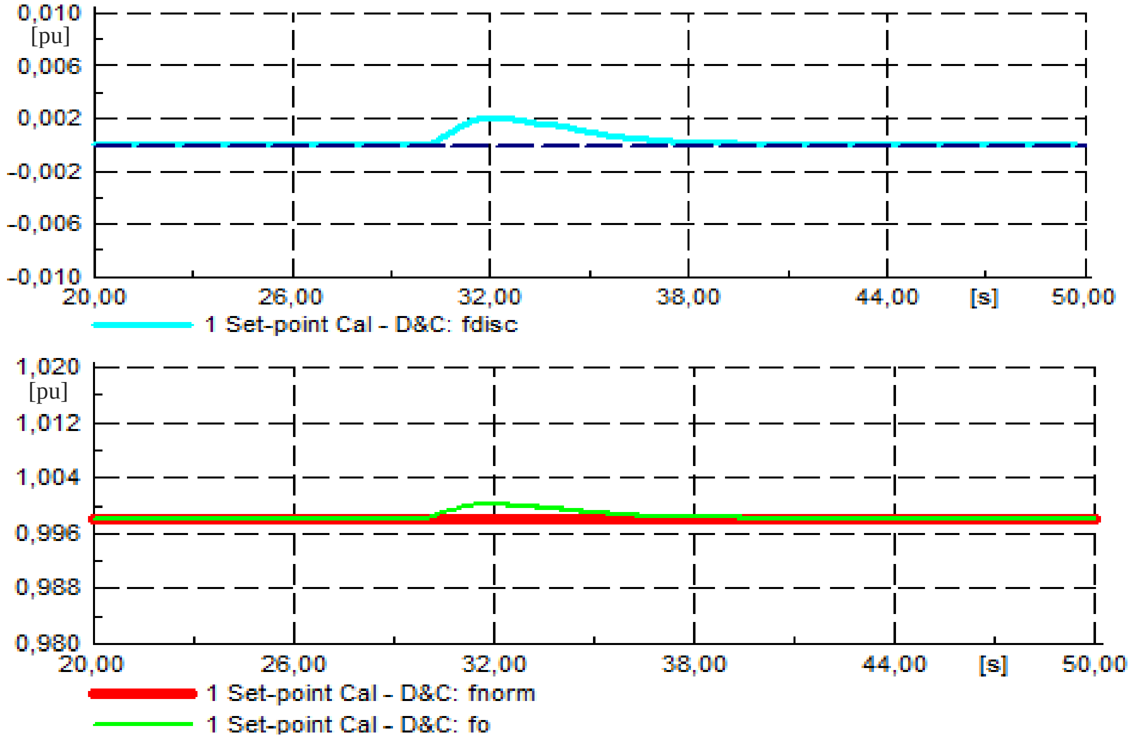


***Figure 6.18:*** *Frequency setpoint signals for disconnection*

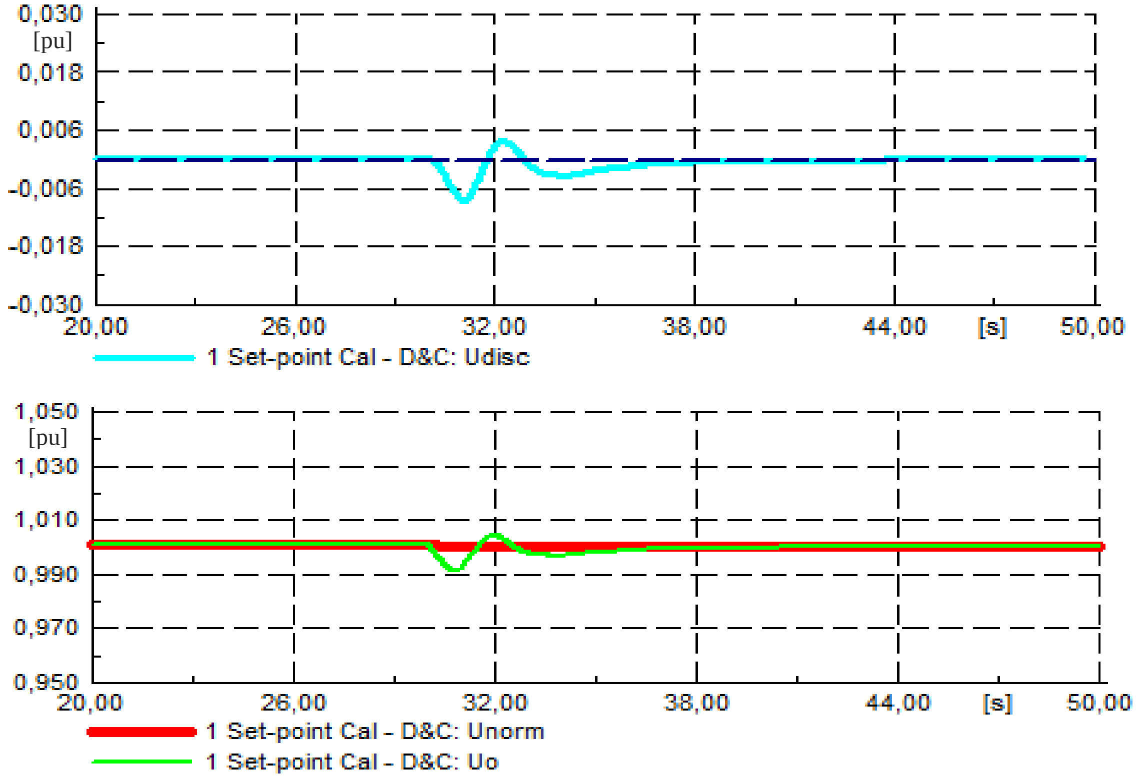


***Figure 6.19:*** *Voltage setpoint signals for disconnection*

The $f_{disc}$ and $U_{disc}$ signals are utilized to compensate for the power absorbed / received from EG and prepare the Cell for operation in SA mode. These deviation signals are summed with the normal frequency and voltage set points, $f_{norm}$ and $U_{norm}$, to calculate the final set points, $f_o$ and $U_o$, as evident in Figure 6.18 and Figure 6.19. The frequency and voltage deviations are gradually reduced to zero to avoid abrupt changes in the system, causing instability. It is observed from the graphs that the $f_{disc}$ and $U_{disc}$ drop to zero at 39.6 s, beyond which the frequency and voltage of the Cell is regulated by the normal controller. Hence, once these signal dies out, the Cell achieves a steady state value of 49.92 Hz and 401.02 V as depicted in Figure 6.14 and Figure 6.15.

A detailed analysis on the impact on the dynamics of the system was performed for a Cell containing Battery of SoC of 40 %. However, to test the efficacy of the disconnection controller, a similar analysis was carried out for varied SoC, from 10 % to 90 % in steps of 10. The results of all these simulated cases are presented in Table A.2 in Appendix A. For a SoC of 10% or 90 %, the battery absorbs/ delivers the maximum power from/to EG. But, the disconnection controller effectively reduces the power flow and was successful in attaining a seamless transition.

### Case I.C: Unintentional Disconnection

In this section, the behaviour of the Cell is simulated for an abrupt disconnection of EG. This occurs when the *Breaker B* connecting to EG is opened instantly. There might be several reasons for instant opening of the breaker. For instance, a fault in the line might result in the operation of protection relay, as desired, and this in turn leads to unintentional disconnection. In such a case, the disconnection controller is not activated and because of which the power flow to the Cell is cut-off instantly. The result of which is that, the battery inverter would have to compensate for the difference to maintain the power balance in the Cell, resulting in a sudden variation in frequency and voltage.

Two extreme cases are assessed for evaluating the response of the Cell upon sudden disconnection. The first case is when the Cell is connected to EG with SoC of 10% and the second with SoC of 90 %.

*(i) <u>Battery with SoC of 10 %</u>*

In this scenario, a Cell with SoC of battery as 10 % is initially connected to the EG utilizing the connection controller. Once synchronized with the EG, the $f_o$ set point of the converter is limited to a value of 0.997 p.u. by the dynamic limiters, as described in Section 4.3.4. As a result, the battery converter absorbs the maximum power of +1 p.u., similar to Figure 6.11 . To maintain the power balance of the system, the EG supplies a power amounting to 104.3 kW, as shown in Figure 6.20.

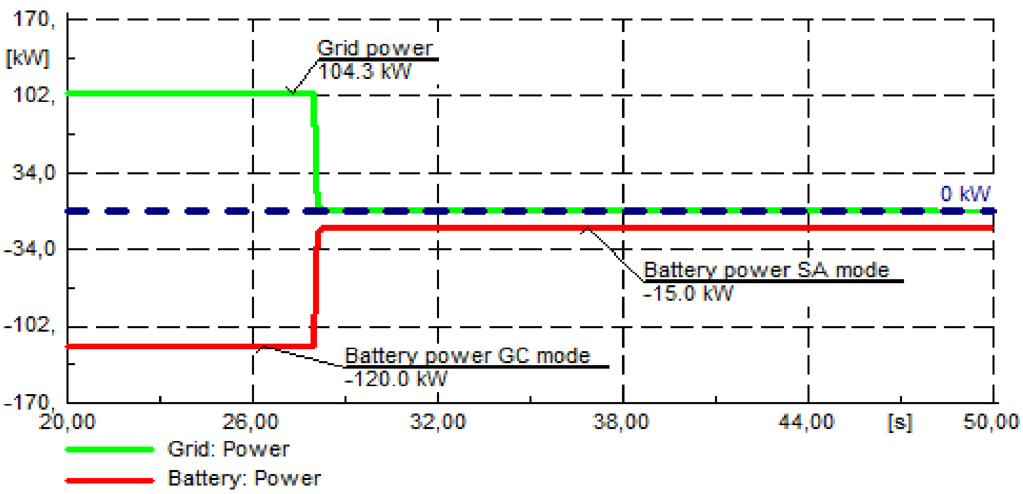


**Figure 6.20:** *Power flow – Unintentional Disconnection: SoC 10 %*

To simulate the case of Unintentional disconnection, the *Breaker B* is abruptly opened at t = 28 s. The result of which is that, the power flow from the Grid becomes zero immediately. Associated with this change, the power flow to the battery changes instantly from -120 kW to -15 kW as per the Cell power balance, which is clearly shown in Figure 6.20.

This creates a sudden disturbance in the Cell, which is evident in Figure 6.21 and Figure 6.22. The frequency of the Cell suddenly dips to a minimum of 48.42 Hz, but suddenly before stabilizing at a steady state value of 48.46 Hz. This drastic variation can be attributed to sudden change of power consumed by the battery and $f_o$ set point, which defines the frequency of the Cell in SA mode. Analogous, to the frequency variation, the voltage of the Cell confronts a sudden variation from 395 V to 401.08 V.

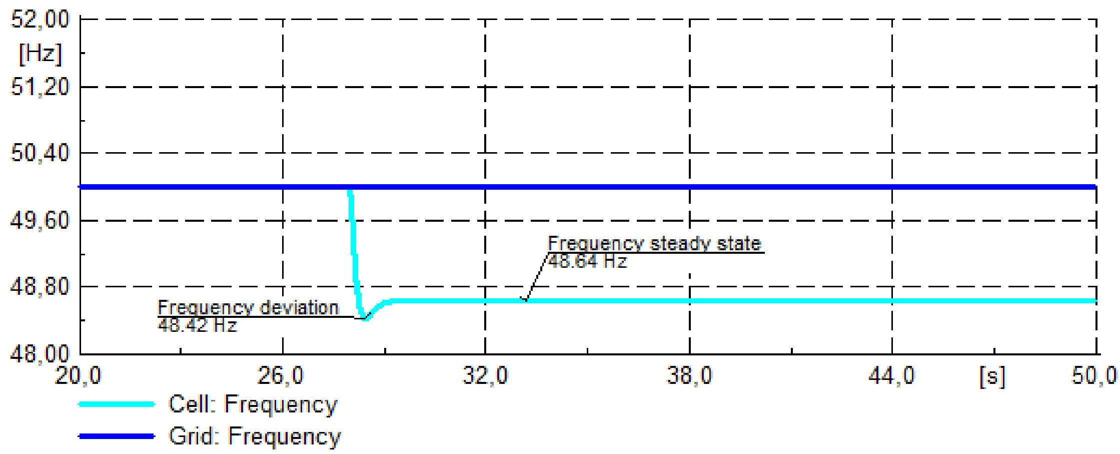


***Figure 6.21:*** *Frequency of Cell and External Grid – Unintentional Disconnection: SoC 10 %*

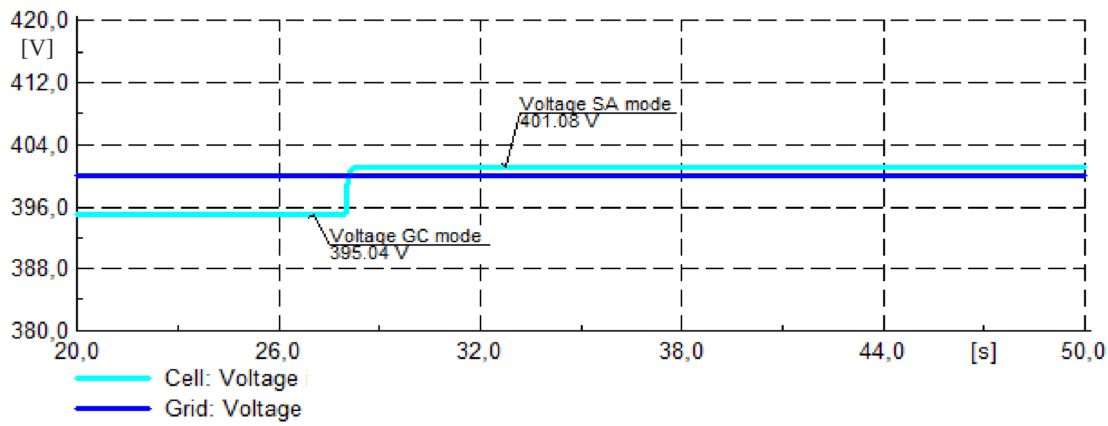


***Figure 6.22:*** *Voltage of Cell and External Grid – Unintentional Disconnection: SoC 10 %*

*(ii) Battery with SoC of 90 %*

The second scenario is simulated for the case when the SoC of the battery is 90 %. Analogous to the case of SoC of 10 %, upon connection to the EG, the dynamic limiters fix the $f_o$ set point of the to a value of 1.003 p.u. The result of which is that the battery converter delivers a power of +1 p.u. and the Grid absorbs a power of 135.7 kW, as depicted in Figure 6.23. Similar to the previous scenario, the Breaker B is abruptly opened at t = 28 s. Hence the Grid power reduces to zero and the battery converter observes a sudden change of power from 120 kW to -15 kW.

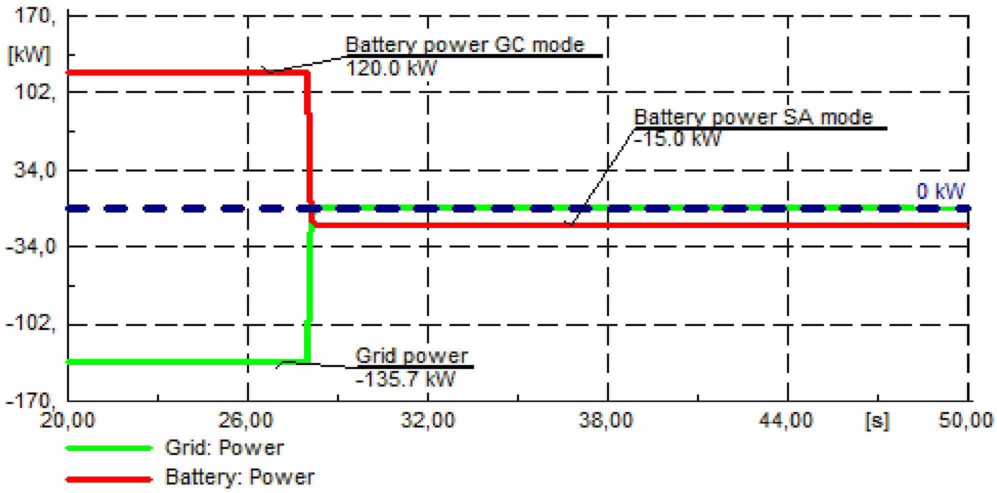


***Figure 6.23:*** *Power flow – Unintentional Disconnection: SoC 90 %*

Due to this sudden change of power, the Cell observes a sudden disturbance. From Figure 6.24, it is witnessed that the frequency of the Cell suddenly rises to a maximum of 51.73 Hz and stabilizes at 51.5 Hz, which is set by the $f_o$ set point due to change of mode from GC to SA. The voltage of the Cell experiences a sudden jump from 406.5 V to 401.08 V, as shown in Figure 6.25.

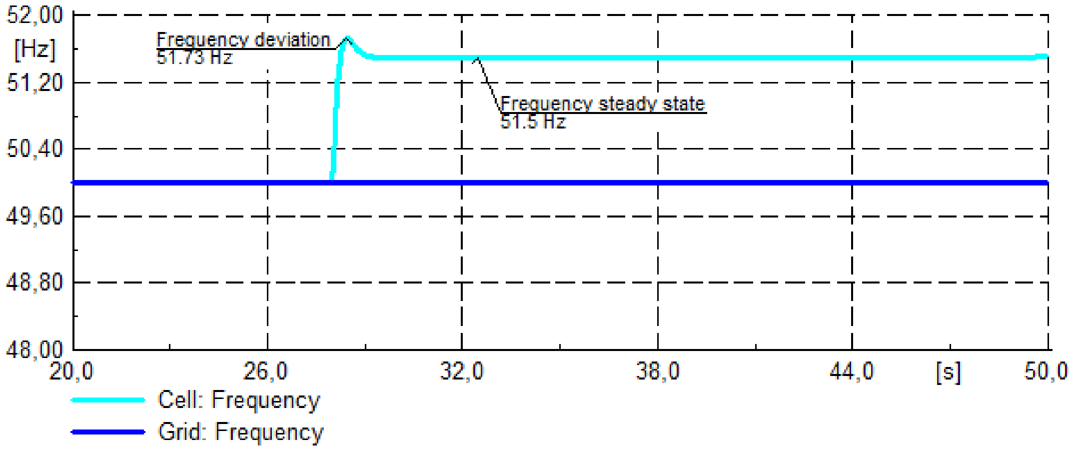


***Figure 6.24:*** *Frequency of Cell and External Grid – Unintentional Disconnection: SoC 90 %*

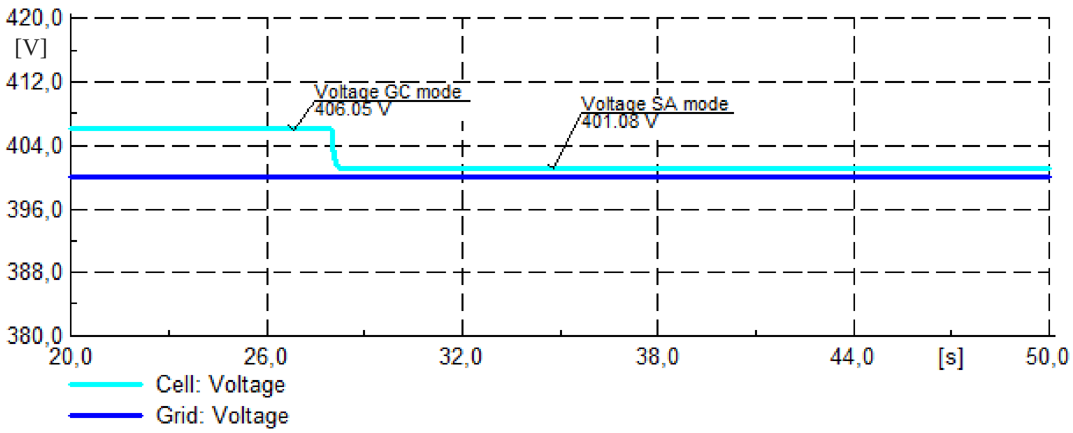


***Figure 6.25:*** *Voltage of Cell and External Grid – Unintentional Disconnection: SoC 90 %*

From the above simulated scenarios with SoC of 10 % and 90 %, it can be inferred that the Cell experiences sudden jump in frequency and voltage in case of Unintentional disconnection. These jumps are proportional to the magnitude of change of power flow in the battery converter. When compared to that of Intentional disconnection, a smooth change of frequency and voltage is observed. Hence, it is preferred to have an intentional disconnection, due to stresses, which in turn hamper the life of the power electronic components inside the converter and other loads. But, it's worth mentioning that the magnitude of the voltage and frequency variations are within limits even in case of worst SoC cases. Further, the Cell attains a stable operating point within a short span of 1 s, demonstrating that the Cell is capable of handling such sudden and abrupt disturbances in the system.

### 6.3.2 Case II: Multiple cells transition between SA & IC mode

All the previous simulations were focussed on analysing the dynamics involved in connection and disconnection of a single Cell to EG. But, the major characteristic of the proposed system is that it is devoid of any communication equipment, it has knowledge of the parameters within the Cell. Meaning that the Cell is not able to distinguish whether it is being connected to EG or to another Cell.

To prove that universal application of the proposed control strategy, simulations are performed for multiple Cells. The simulations primary focus is on the connection and disconnection of multiple Cells through a BB bus. The layout of the MG architecture utilized for the following simulations is represented in Figure 6.26. Each Cell comprises of components as depicted in Figure 6.1 and the sizing of these components as in Table 6.1.

The individual breakers, *B1*, *B2*, *B3* and *B4*, of each Cell are initially considered to be in open condition, meaning that each Cell is in SA mode. By closing of the breakers, the Cell changes from SA to IC mode. To accomplish a seamless transfer between modes, the proposed connection and disconnection algorithm, similar to that applied for Single Cell (dis)connection to EG, is utilized.

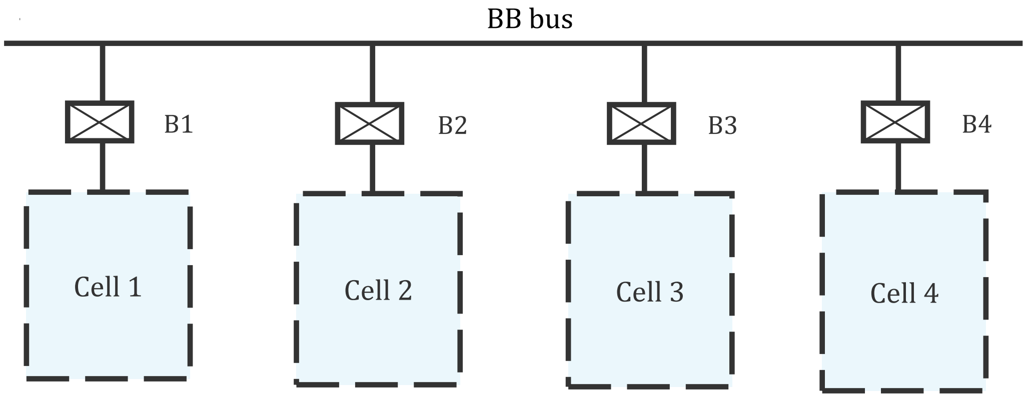


***Figure 6.26:*** *Layout of Interconnection of multiple Cells through BB bus*

#### Case II.A: Multiple Cells Connection at different time instants

In this case, the connection controller is evaluated for multiple cells, with varied *SoC*, trying to synchronize with the BB bus at different time instants, as mentioned in Table 6.2. The Cell 2 is assumed to be connected initially, meaning that the BB bus is energised through Cell 2.

***Table 6.2:*** *Case II.A Parameters – SoC & Connection trigger command*

| *Cell* | *1* | *2* | *3* | *4* |
|---|---|---|---|---|
| *SoC (%)* | 10 | 80 | 50 | 30 |
| *Connection trigger (s)* | 20 | - | 30 | 40 |

The Figure 6.27 and Figure 6.28 represent the frequency and voltage of each Cell synchronizing with the BB bus. After the triggering command for connection for each Cell, as specified in the Table 6.2, the voltage, frequency and phase errors are minimized using a PID controller. From these graphs, it can be interpreted that there is a smooth and seamless transfer from SA to IC mode and finally the system attains a steady state frequency of 49.94 Hz.

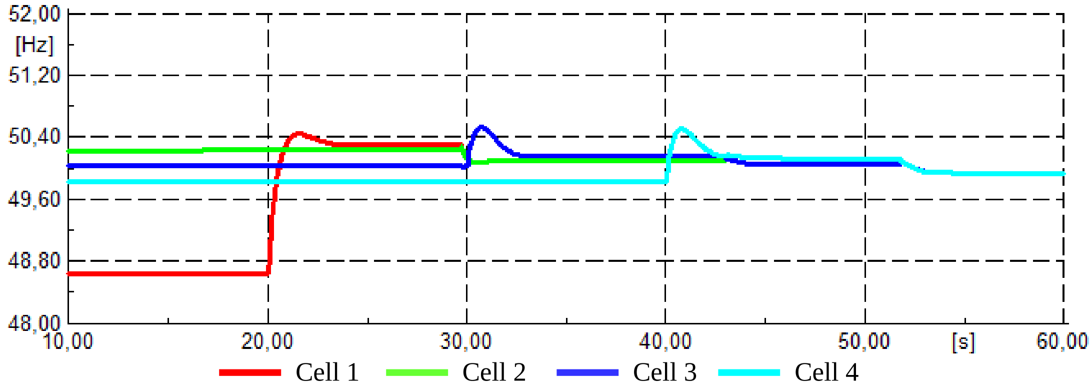


***Figure 6.27:*** *Frequency of multiple Cells – Connection at different time instants*

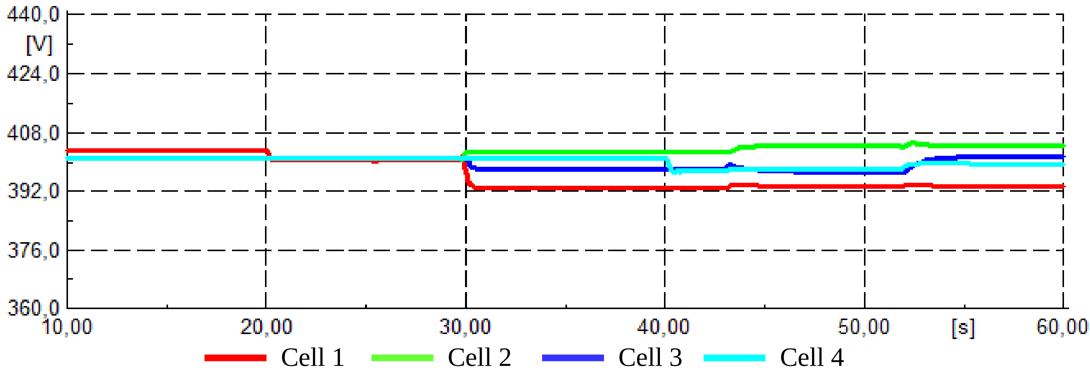


***Figure 6.28:*** *Voltage of multiple Cells – Connection at different time instants*

When the connection criteria are met, as described in the Section 4.3.2, the *ConcSignal* is generated for switching of modes. The *State* indicates the condition of each Cell, whether it's in stand-alone or interconnected. When the value of *State* is 0, the Cell is in SA mode and if it is 1, it implies IC mode. The Figure 6.29 shows the *State* of each of the Cell. Cell 2 is already connected to BB bus, so State of Cell2 2 is 1. The State of Cell 1, Cell 3 and Cell 4 changes at 29.71 s, 43.0 s and 51.91 s respectively.

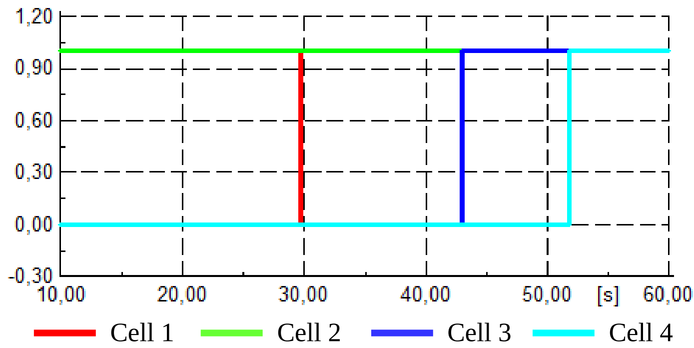


***Figure 6.29:*** *State of multiple Cells – Connection at different time instants*

The power absorbed / consumed by each of Cell during and after connection to the BB bus is depicted in Figure 6.30. It can be inferred from the graph that the converter is restricted to power limits of +/- 1 p.u., as desired, and the power is shared according to the SoC of each Cell. The Cells with higher SoC deliver power through the BB bus to the Cells with lower SoC.

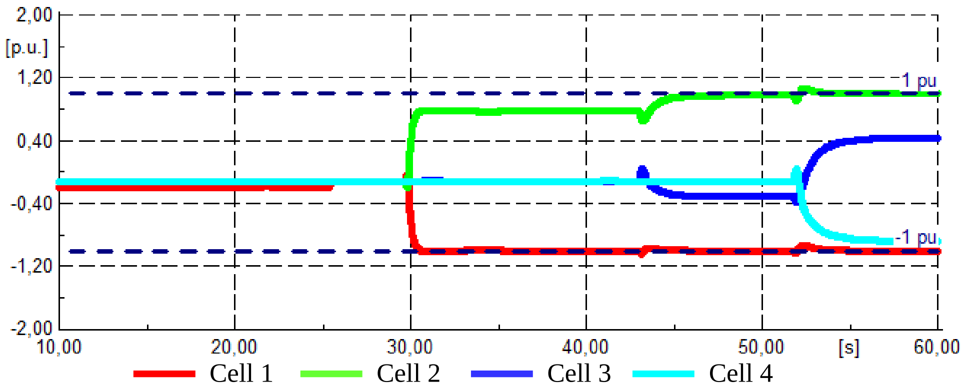


***Figure 6.30:*** *Power of multiple Cells – Connection at different time instants*

### Case II.B: Multiple Cells Disconnection at different time instants

Similar analysis is performed for disconnection of multiple Cells at different time instants. The disconnection controller is activated for each of the Cell as indicated in Table 6.3. Based on the power flow through the line connecting to the BB bus, additional frequency and voltage deviations are generated, as explained in Section 4.3.3, for preparing each Cell for disconnection.

***Table 6.3:*** *Case II.B Parameters – SoC & Disconnection trigger command*

| *Cell* | *1* | *2* | *3* | *4* |
|---|---|---|---|---|
| *SoC (%)* | 10 | 80 | 50 | 30 |
| *Disconnection trigger (s)* | 70 | - | 80 | 90 |

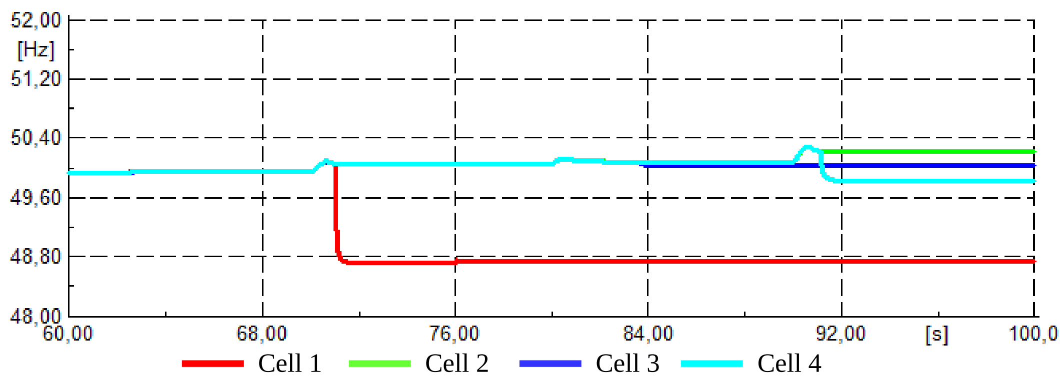


***Figure 6.31:*** *Frequency of multiple Cells – Disconnection at different time instants*

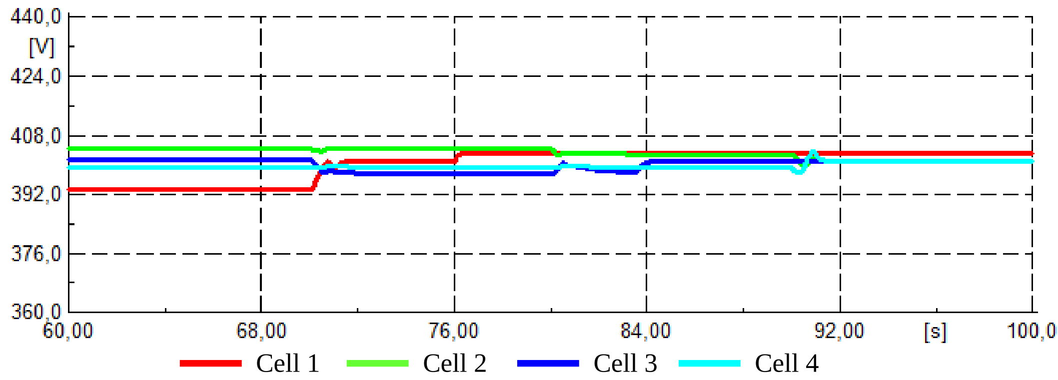


***Figure 6.32:*** *Voltage of multiple Cells – Disconnection at different time instants*

The frequency and voltage waveforms associated with the disconnection of Cells are shown in Figure 6.31 and Figure 6.32. The graphs indicate a smooth transfer of frequency and voltage while switching from IC to SA mode. The disconnection controller tries to minimize the power flow through the BB bus and as the disconnection criteria is satisfied, a DiscSignal is generated, which is subsequently utilized for change of *State* of each Cell, as depicted in Figure 6.33. The *State* changes for Cell 1, Cell 3 and Cell 4 are observed at 71.07 s, 83.53 s and 91.06 s respectively. After disconnection of each Cell, the frequency of each Cell is regulated within using the *Normal controller,* as explained in Section 4.3.1. It is found that each Cell attains a steady state value as: Cell 1 – 48.74 Hz, Cell 2 – 50.21 Hz, Cell 3 – 50.02 Hz and Cell 4 – 49.83 Hz.

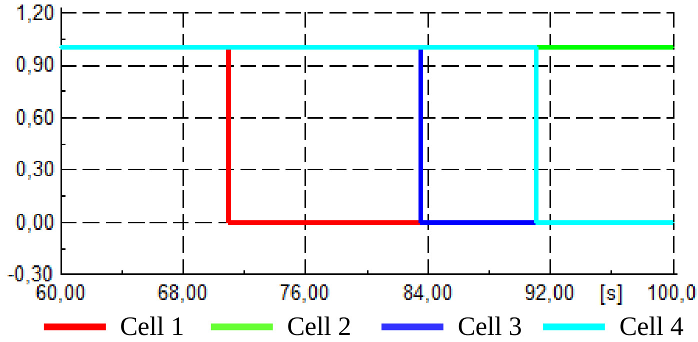


***Figure 6.33:*** *State of multiple Cells – Disconnection at different time instants*

The Figure 6.34 shows the power absorbed / consumed by battery of each Cell during before and after disconnection. Before disconnection, the converter power of each Cell is regulated by the droop curve to establishing a common operating point for the entire system. Preparing the Cells for mode change from IC to SA, the battery converter either absorbs or delivers power to maintain the power balance in each Cell.

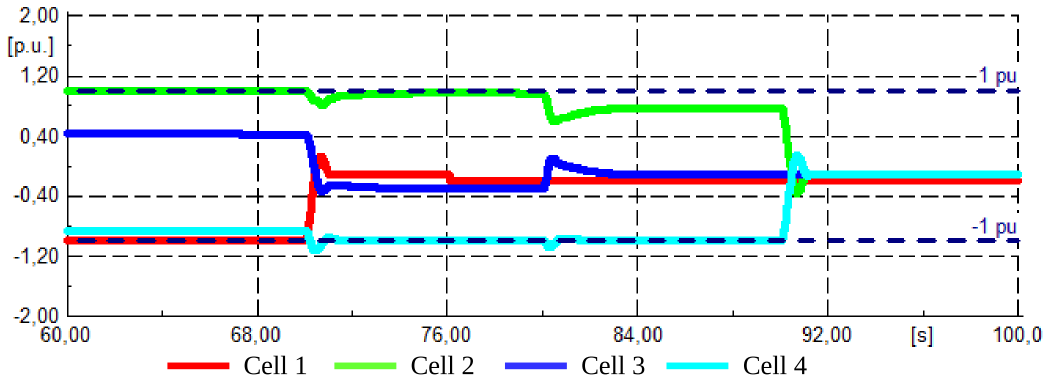


***Figure 6.34:*** *Power of multiple Cells – Disconnection at different time instants*

### Case II.C: Multiple Cells Connection at same time instant

In this case, one Cell, for instance Cell 2 is connected to the BB bus, energising the bus and the system is evaluated when multiple Cells receive a connection trigger command at the same instant. The Table 6.4 details about the SoC of battery of each Cell and their connection trigger instant.

***Table 6.4:*** *Case II.C Parameters – SoC & Connection trigger command*

| *Cell* | *1* | *2* | *3* | *4* |
|---|---|---|---|---|
| *SoC (%)* | 10 | 80 | 50 | 30 |
| *Connection trigger (s)* | 20 | - | 20 | 20 |

The Figure 6.35 and Figure 6.36 shows the frequency and voltage of each Cell linked with connection to BB bus. From the waveforms, it can be inferred each Cell tries to synchronize with BB bus, by creating its own frequency and voltage deviations. Since the all the Cells are modular in nature, each controller would behave individually on the recycled input signals.

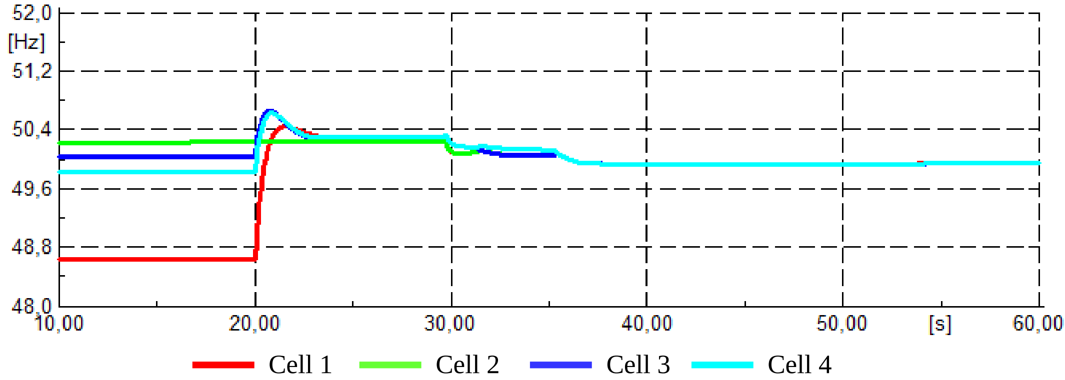


***Figure 6.35:*** *Frequency of multiple Cells – Connection at same time instant*

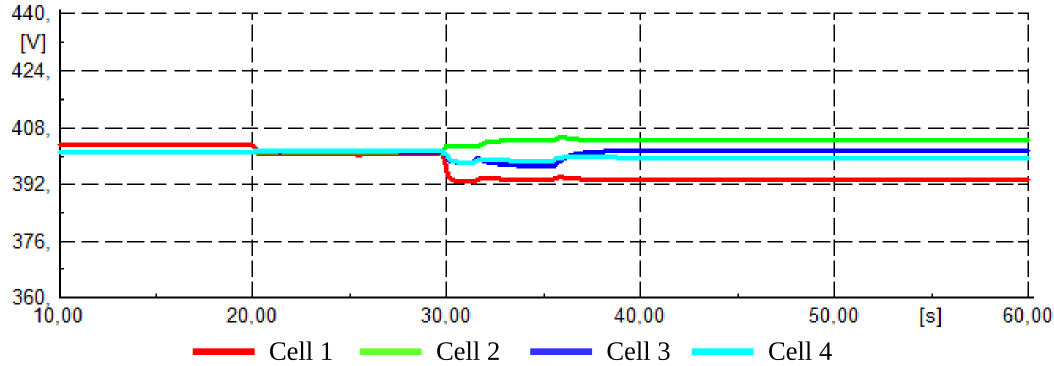


***Figure 6.36:*** *Voltage of multiple Cells – Connection at same time instant*

As the additional frequency and voltage deviation signals along with its normal frequency and voltage signals are successful in reducing the errors in magnitude, frequency and phase of voltage signals, *ConcSignal* is produced for initiating the mode change. The figure  shows the change of State of each Cell and it is observed that each Cell connect at a different time instant, though receiving the command at the same time. Upon synchronization with the BB bus, the power is shared among the interconnected Cells based on the SEP and droop coefficient. The Figure 6.29 shows that Cell 2 and Cell 3, having SoC of 80 % and 50 % are indeed delivering power to the Cell 1 and Cell 3, which have lower SoC. The power is shared between the interconnected network so that the system arrives at a common operating point. And as time proceeds, the SEP of the interconnected system improves.

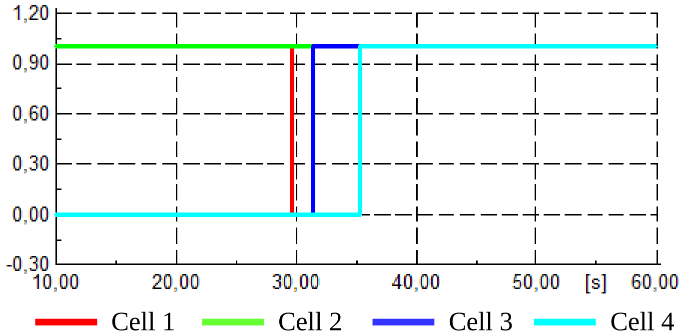


***Figure 6.37:*** *State of multiple Cells – Connection at same time instant*

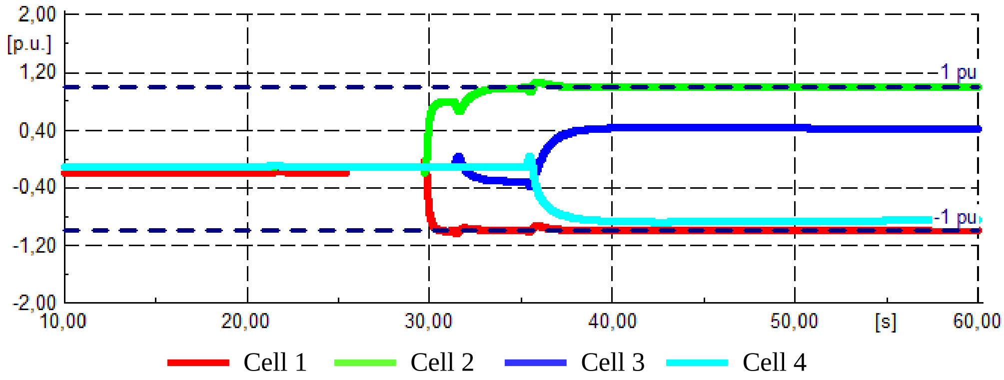


***Figure 6.38:*** *Power of multiple Cells – Connection at same time instant*

### Case II.D: Multiple Cells Disconnection at same time instant

Analogous to the case III.C, a simulation is performed for testing the disconnection controller, when multiple Cells are trying to shift its mode at the same time. The SoC of battery and disconnection trigger signals are mentioned in Table 6.5 and its worth mentioning that Cell 2 remains connected to BB bus.

***Table 6.5:*** *Case II.D Parameters – SoC & Disconnection trigger command*

| *Cell* | *1* | *2* | *3* | *4* |
|---|---|---|---|---|
| *SoC (%)* | 10 | 80 | 50 | 30 |
| *Disconnection trigger (s)* | 70 | - | 70 | 70 |

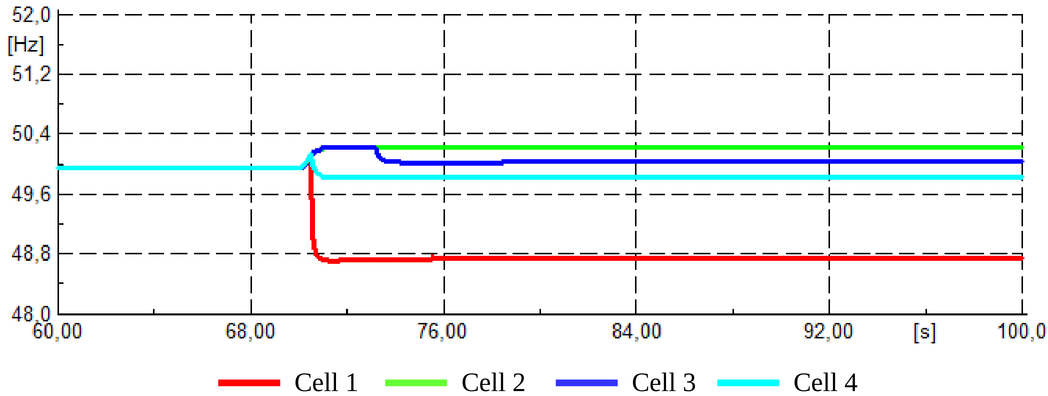


***Figure 6.39:*** *Frequency of multiple Cells – Disconnection at same time instant*

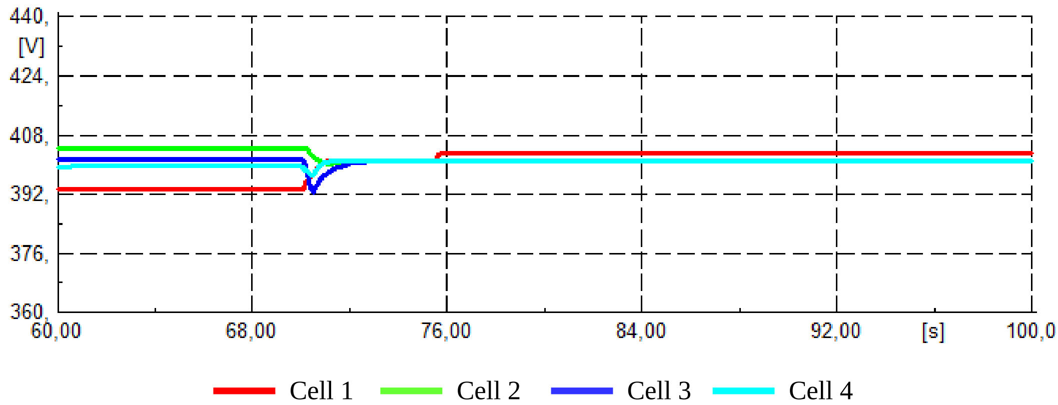


***Figure 6.40:*** *Voltage of multiple Cells – Disconnection at same time instant*

When all the Cells are connected to BB bus, i.e., all the Cells are in IC mode, the Cells exchange power through the interconnected BB bus, but maintain the common system frequency of 49.94 Hz. When the disconnection controller is enabled, each Cell would try to minimize the power exchange between the connected Cells at the same time. The controller for each Cell would create additional deviations, which contribute to the final set points of converter, and thus preparing the respective cell for safe disconnection. The Figure 6.41 and Figure 6.42 shows the frequency and voltage graphs of each Cell for the process of disconnection. From the figures, it can be deduced that after disconnection of Cell, the frequency and voltage of each individual Cell are regulated by its normal controller, as described in Section 4.3.1.

As the disconnection controller tries to minimize the exchange power to zero, the Cell in turn prepares itself for meeting its own power requirement either by supplying the deficient power or absorbing the excess power. The same can be observed in Figure 6.42 , where the converter of the battery of each Cell maintains the power balance within the Cell. Also, as the exchanged power are reduced to limits as described in Disconnection criteria, the *DiscSignal* are produced and the *State* changes from IC to SA mode. The Figure 6.41 shows the associated *State* change and it can be found that both Cell 1 and Cell 4 gets disconnected from the BB bus at 70.6 s and Cell 3 at 73.09 s.

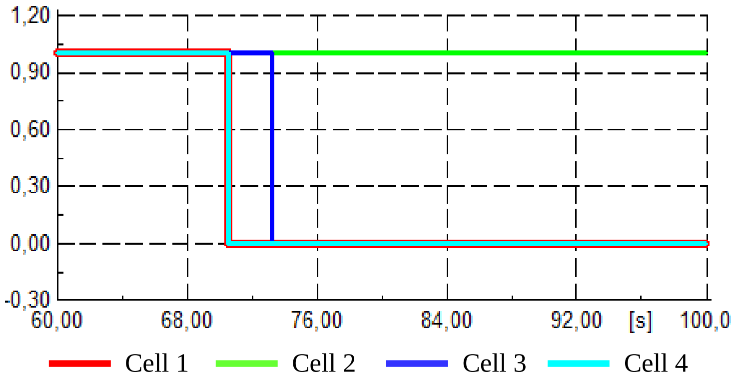


***Figure 6.41:*** *State of multiple Cells – Disconnection at same time instant*

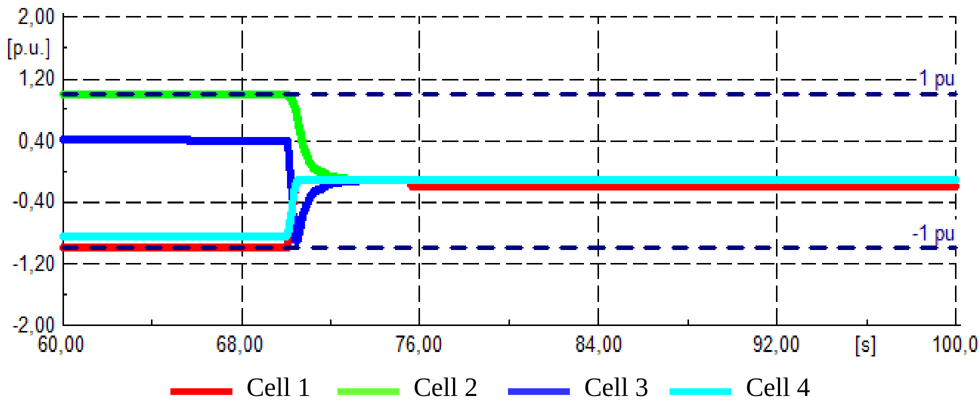


***Figure 6.42:*** *Power of multiple Cells – Disconnection at same time instant*

From all these simulations, it can be summarized that the developed control strategy for connection and disconnection controller is able to accomplish a seamless transfer between various modes, in every scenario. The algorithm is universally applicable whether the Cell is being (dis)connected to EG or to any other Cell. Further, the modular nature of the algorithm makes it easily scalable and expandable, in case of future demand, to build a strong and robust MG network.

## 6.4 Simulation results – Automated Decision algorithm

In the previous simulations, the connection and disconnection of Cells to EG or other Cells were initiated through manual triggering commands. The developed decision-making algorithm, as described in Section 5, is focussed on automated control of switching between modes based on the SEP of each Cell. A decentralized approach is followed in formulation of the algorithm, with the fact that there is no ICT equipment involved. The primary objective of the algorithm is to maintain the critical SoC for ensuring a stable operation of Cell in stand-alone condition.

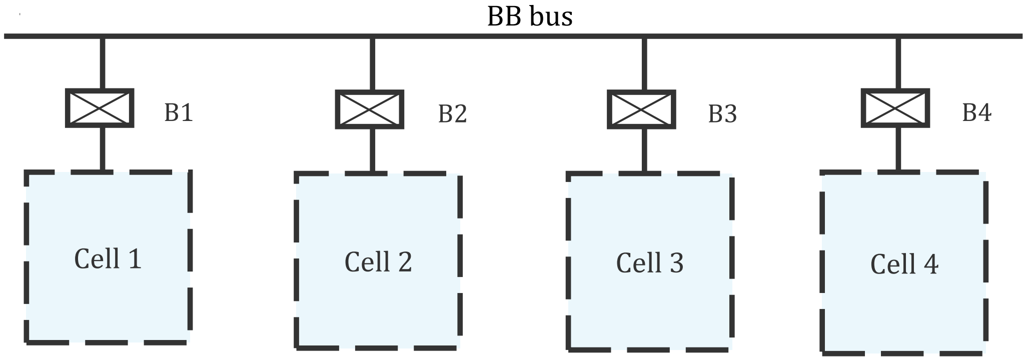


***Figure 6.43:*** *Microgrid layout for automated decision-making algorithm*

The layout of the MG architecture followed for the simulations is shown in Figure 6.43. Each Cell contains the components as described in Figure 6.1. The sizing of each of components are shown in Table 6.6. For evaluating the developed algorithm, various cases are simulated and the results are analysed in the following sections. In the cases being simulated, a constant load, PV and Wind power is assumed throughout the simulation period, unless specified. Due to the constant net power supply or demand, the rate of change of SoC is faster than the actual, practical conditions. Moreover, the smaller size of the battery also aids in the process. So due to faster change of SoC and with the help of defined states, the efficacy of the algorithm could be evaluated within a short simulation period.

***Table 6.6:*** *Sizing of components in Cell for automated decision-making algorithm*

| *Load power [kW]* | *PV power [kW]* | *Wind power [kW]* | *Battery Capacity [kWh]* | *Inverter rated Power [kVA]* |
|---|---|---|---|---|
| 10 | 15 | 10 | 120 | 120 |

In each of the following simulated cases, initially the Breakers: *B1*, *B2*, *B3* and *B4*, are assumed to be in open condition, meaning that each of the Cells are in SA mode. In other words, the BB bus is in deenergised condition. Each Cell based on the algorithm decides to either connect or disconnect from the BB bus, thus creating triggering signals. These signals are subsequently utilized by the control algorithm for enabling a seamless transfer. Hence, in the process, the Cells switches between SA and IC mode.

The frequency dependency on SoC plays a significant role in control and operation of the Cell. Each Cell adopts the curve as shown in Figure 5.2. Referring the figure, it is observed that the assumed limits defining the curve are as follows:

$$SoC_{min} = 0\ \%,\ S_a = 30\ \%, S_c = 50\ \%, S_b = 80\ \% \text{ and } SoC_{max} = 90\ \%$$

Using the above curve, the various defined limits for the automated decision-making algorithm are calculated using Eqn. (5.1), as explained in Section 5.2.2. The tabulated values are shown in

***Table 6.7:*** *Limits definition for automated decision-making algorithm*

| $SoCLL$ | $SoCNH$ | $SoCC$ | $SoCRH$ | $SoCUL$ |
|---|---|---|---|---|
| 30 % | 40 % | 50 % | 65 % | 80 % |

It is now significant to define certain notations, which would be utilized often in the simulated cases. These are *Low SoC*, *High SoC* and *Very High SoC*. The SoC of battery of each Cell would be defined for each of the simulated cases. The terms are better explained in the Table 6.8, which are linked with the defined limits.

***Table 6.8:*** *Definition of terms for simulated cases*

| *Term* | *SoC of battery* |
|---|---|
| *Low SoC* | < = SoCLL |
| *High SoC* | > = SoCRH |
| *Very High SoC* | < = SoCUL |

The term *State* is associated with condition of the Breaker connecting each Cell to the BB bus, as depicted in Figure 6.43. When the breaker is in *Open*, the *State* is set low, while when it's *Closed*, the *State* is set high. In other words, *State = 0* implies that Cell is in SA mode and *State = 1* indicates IC mode of operation.

### 6.4.1 Case I: 2 Cells Low SoC, No Cells High SoC

As explained before, each Cell in the MG layout in Figure 6.43, is assumed to be in SA mode of operation. The algorithm is simulated for automatic definition of states with the initial SoC of battery, in percentage, for each Cell as follows

***Table 6.9:*** *SoC for Case I*

| *Cell* | 1 | 2 | 3 | 4 |
|---|---|---|---|---|
| *SoC (%)* | 10 | 55 | 60 | 25 |

The simulation was performed for a small-time frame of 200 s and the results are plotted in Figure 6.44.

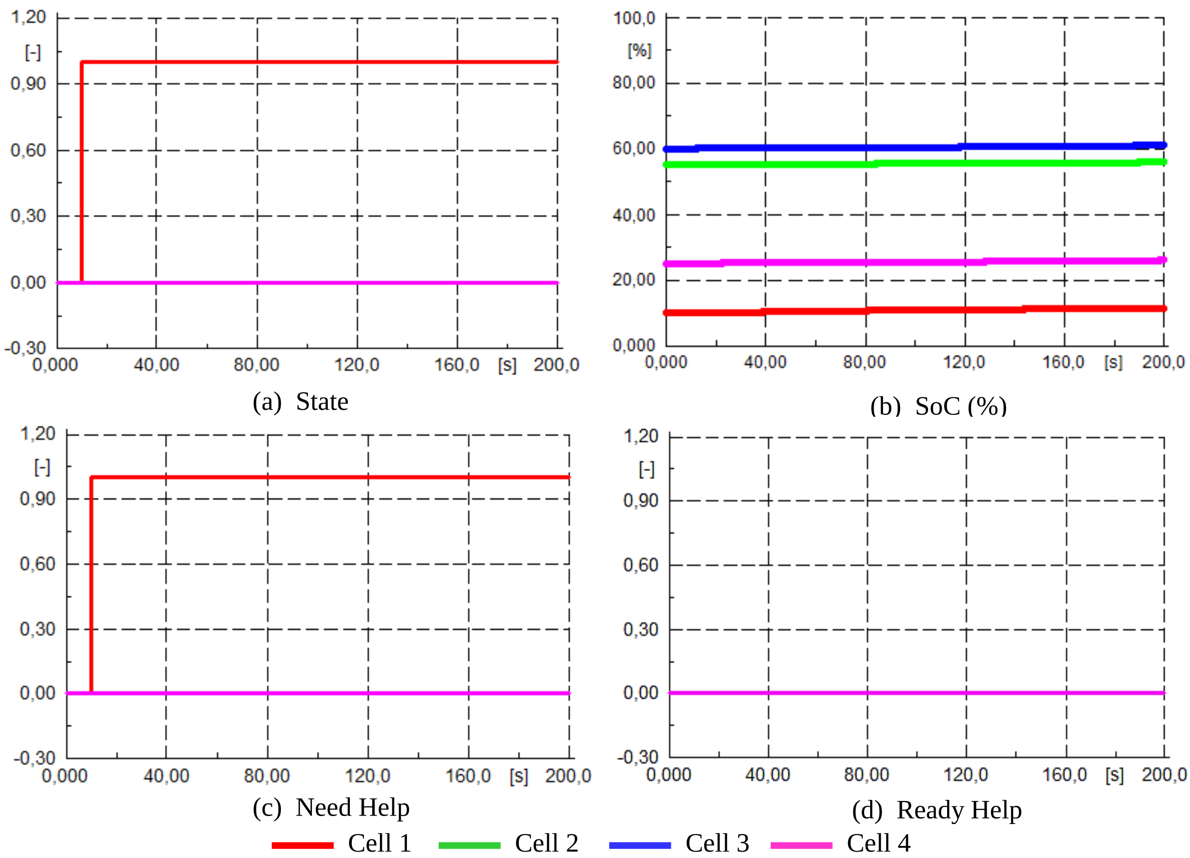


***Figure 6.44:*** *Graphs for Case I*

From Figure 6.44(b), it is observed that the Cell 1 with the lowest SoC among all, creates a Need Help State (1NH = 1) at 10.56 s, as SoC is lower than *SoCLL*. As 1NH becomes high, the Cell 1 closes its breaker and energises the BB bus. Hence the Cell 1 changes its State from SA to IC mode, as seen in Figure 6.44(a), indicating that there is a Cell in the MG that is in need.

As no Cells in the MG have a SoC higher than *SoCRH*, the Ready Help (*RH*) state of each Cell is low, which can be seen in Figure 6.44(d): 1RH = 2RH = 3RH = 4RH =0

There exists another Cell in MG, Cell 4 which has a SoC lower than *SoCLL* (refer Figure 6.44(b)). As per the defined *NH set conditions*, as explained in Section 5.3.1, 4NHS1 = 1 meaning that the Cell 4 is also in Need help state. But this is inhibited by the *NH Doconnect* function as shown in *NH flow diagram* in Figure 5.12. The *NH Doconnect* function checks whether the frequency of the BB bus is higher than that of the Cell by 0.0005 p.u. for at least 60 s. If the function is true it means that there is a Ready Help Cell in the MG, which can aid the Cell 4 in needy state. In the absence of the function, the Cell 4 synchronises with the BB bus and the 4State becomes high. This results in a scenario where the NH Cell 4 supports the NH Cell 1and the SoC of Cell 4 deteriorates even further.

So, to summarize, if BB bus is *Dead*, *NH* state =1, as soon as the need arises and if BB bus is *Live*, *NH* state =1, only if *NH Doconnect function* is true.

### 6.4.2 Case II: No Cells Low SoC, 2 Cells High SoC

In this case, the simulation is performed for a MG compromising a deenergised BB bus and 4 Cells with Battery of SoC as mentioned below.

***Table 6.10:*** *SoC for Case II*

| *Cell* | 1 | 2 | 3 | 4 |
|---|---|---|---|---|
| *SoC (%)* | 40 | 65 | 70 | 50 |

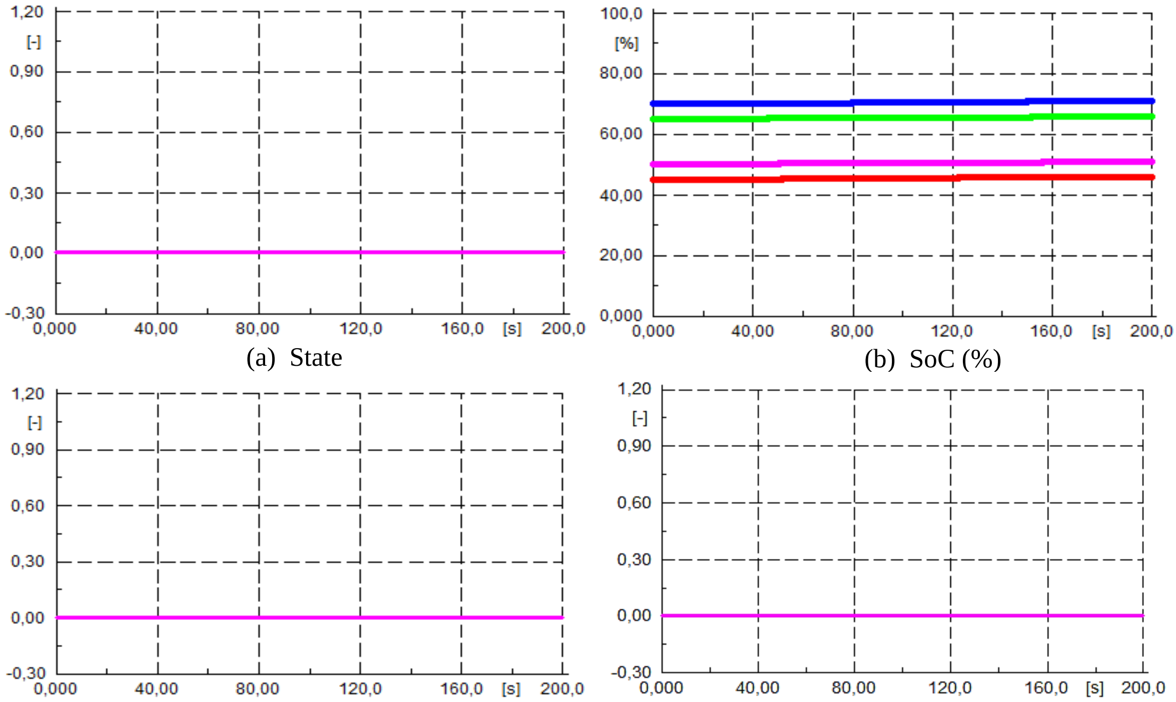


(a) State (b) SoC (%) (c) Need Help (d) Ready Help

Cell 1 Cell 2 Cell 3 Cell 4

***Figure 6.45:*** *Graphs for Case II*

The case was simulated for a period of 200s and the Figure 6.45 displays the plots of State, SoC, NH and RH state of each Cell. It is observed that since the MG does not have any Cell with SoC less than *SoCLL*, the *NH* state of each Cell is in false condition or has a zero value as visible in Figure 6.45(c).

While there exits 2 Cells in the MG with SoC higher than *SoCRH*, which signals a condition of ready help to support other Cells. But since there is no *NH* Cells in the MG, the *RH* Cells are not allowed to energise the BB bus, based on the *RH Set conditions* (Figure 5.16). Hence the *RH* state of Cell 2 and Cell 3 remains low as shown in Figure 6.45(d).

As the *NH* and *RH* stays low for each Cell, the *State* does not change for any of the Cells in the MG and they continue to operate in SA mode and the SoC varies according to the SEP in each Cell. Figure 6.45(a) and Figure 6.45(b) represent the state and SoC of each Cell as explained before.

From the simulated case, it can be inferred that the *RH* state =1 only when BB bus is *Live* and *Ready help set condition* (RHS) is true.

### 6.4.3 Case III: 2 Cells Low SoC, 2 Cells High SoC

Here, simulation is performed for the MG (Figure 6.43), where 2 Cells contain Battery of Low SoC and the other 2 cells with Battery of High SoC. The initial battery SoC of each Cell are as follows

***Table 6.11:*** *SoC for Case III*

| *Cell* | 1 | 2 | 3 | 4 |
|---|---|---|---|---|
| *SoC (%)* | 10 | 65 | 70 | 25 |

*(i)* *Simulation time – 200s*

First, the algorithm is evaluated for a small-time frame of 200 s and the results of the decision-making module are plotted in Figure 6.44.

The Cells, 1 and 4, have batteries with SoC less than *SoCLL*, hence the Cells are in need state according to defined *NH* conditions. But, as seen in Figure 6.46(c), the Cell 1 which has the lowest SoC of 10% becomes high at 10.48 s, followed by the Cell 4 with the second lowest SoC of 25% at 126.6 s. This distinction between 2 Cells in need state has been achieved with the Delay block in *NH Set conditions* (Figure 5.8). The block implements *SoC vs increasing time* delay. In other words, the signal is delayed by a time which increases with the SoC of the battery. Hence, the *NH* state of Cell1 becomes high before Cell 4.

Similarly, the Cells 2 and 3 have a SoC higher than *SoCRH*, implying that the Cells can support the needy Cells in the MG. Analogous to the delay function in defining the *NH* state, there exists a Delay block in *RH Set conditions* (Figure 5.16). But the block implements *SoC vs decreasing time*, the inverse of what has been implemented in *NH Set conditions*. So, the *RH* state of Cell 3, with highest SoC, becomes high at 35.53 s, as in Figure 6.46(d), and later followed by Cell 2, with second highest SoC, at 40.95 s.

The *State* of the Cells in MG shifts from SA to IC mode, as the *NH* and *RH* states changes, as shown in Figure 6.46(a). Here, the 1State = 1 at 10.48 s due to 1NH signal. Later because of 3RH signal becoming high at 35.53 s, Cell 3 synchronises with BB bus at 39.86 s. This is followed by the Cell 2 synchronising at 50.42 s because of 2RH signal. Finally, the 4State = 1 at 138.8 s upon receipt of high value of 4NH signal. The extra delay of 60 s is due to the *NH Doconnect function*, the implication of which was explained in Case I.

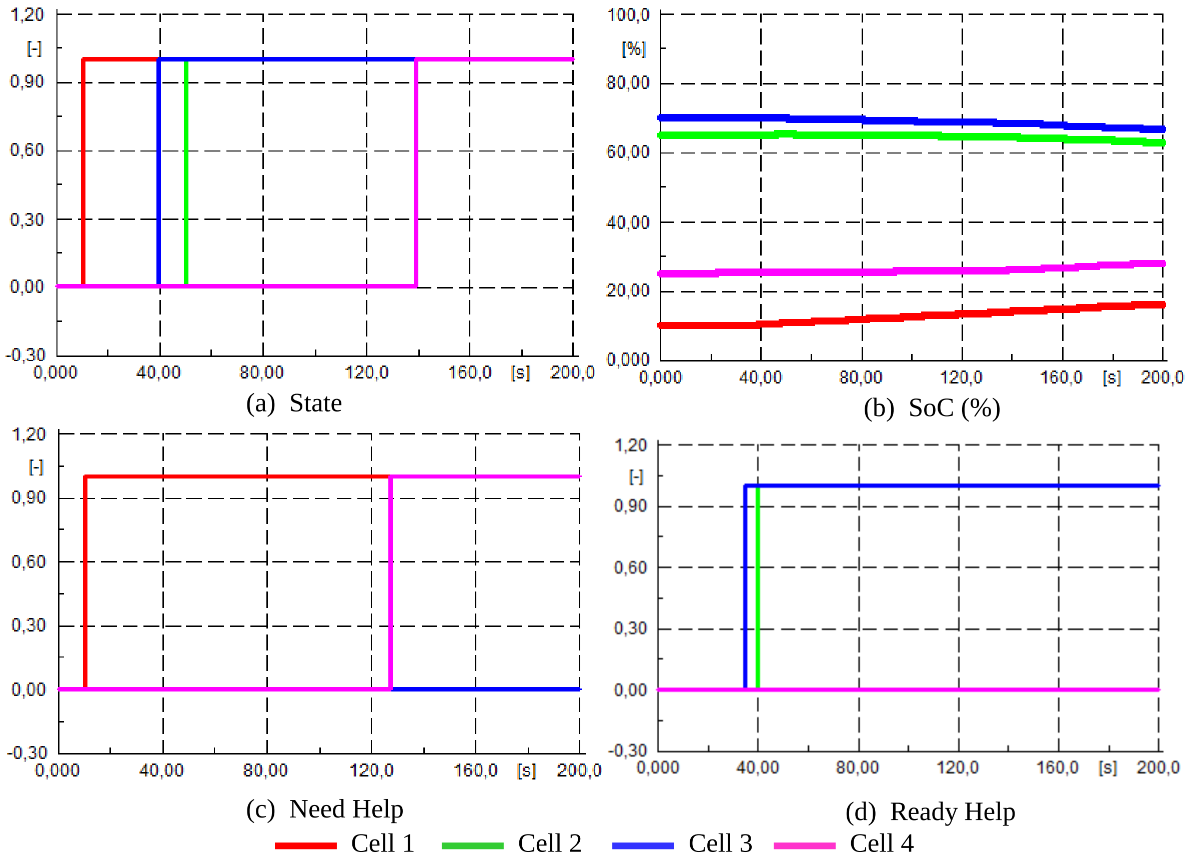


***Figure 6.46:*** *Graphs for Case III: Simulation time – 200s*

So, from these results, it can be deduced that the *NH* and *RH* states of Cells are differentiated with each other with time delay function varying with SoC.

*(ii)* *<u>Simulation time – 1500s</u>*

The simulation was prolongated for 1500 s and the results are examined for comprehending the developed algorithm. As the Cells are in the IC mode, the SoC of Cells 3 and 2 are declining as seen in Figure 6.47(b), as they are supporting Cells 1 and 4. Subsequently, a SoC increase is observed for these Cells.

But as time proceeds, SoC of battery of Cell keeps on decreasing. The *RH* signal is reset as the SoC becomes less than *SoCC*, as deliberated in Figure 5.17. In Figure 6.47(d), it is observed that for Cell 2 the *RH* signal is reset at 1082 s (2RHR) and Cell 3 at 1319 s (3RHR). Using this signal, the *RHD* signal is used to set the *DISC* signal high as detailed in *Disconnect flow diagram* (Figure 5.21). Subsequently, this signal is employed for triggering the disconnection controller. As the criteria is met, the *State* changes from IC to SA mode, as seen in Figure 6.47(a).

Now a situation arises, where there are no *RH* Cells in the MG and the remaining 2 *NH* Cells, Cell 1 and Cell 4 are connected to BB bus in IC mode. This means that there is a power flow from the comparatively healthier Cell 4 towards Cell 1, which is undesired. The *PbbND function*, shown in

Figure ***5.20***, is employed to inhibit such an operation. As the *NH* state of Cell 2 and 4 are high and no reset, the *4PbbND* signal is utilized to set the *4DISC* signal high (refer Figure 5.21). As a result, the *State* of Cell 4 switches to SA mode at 1409 s.

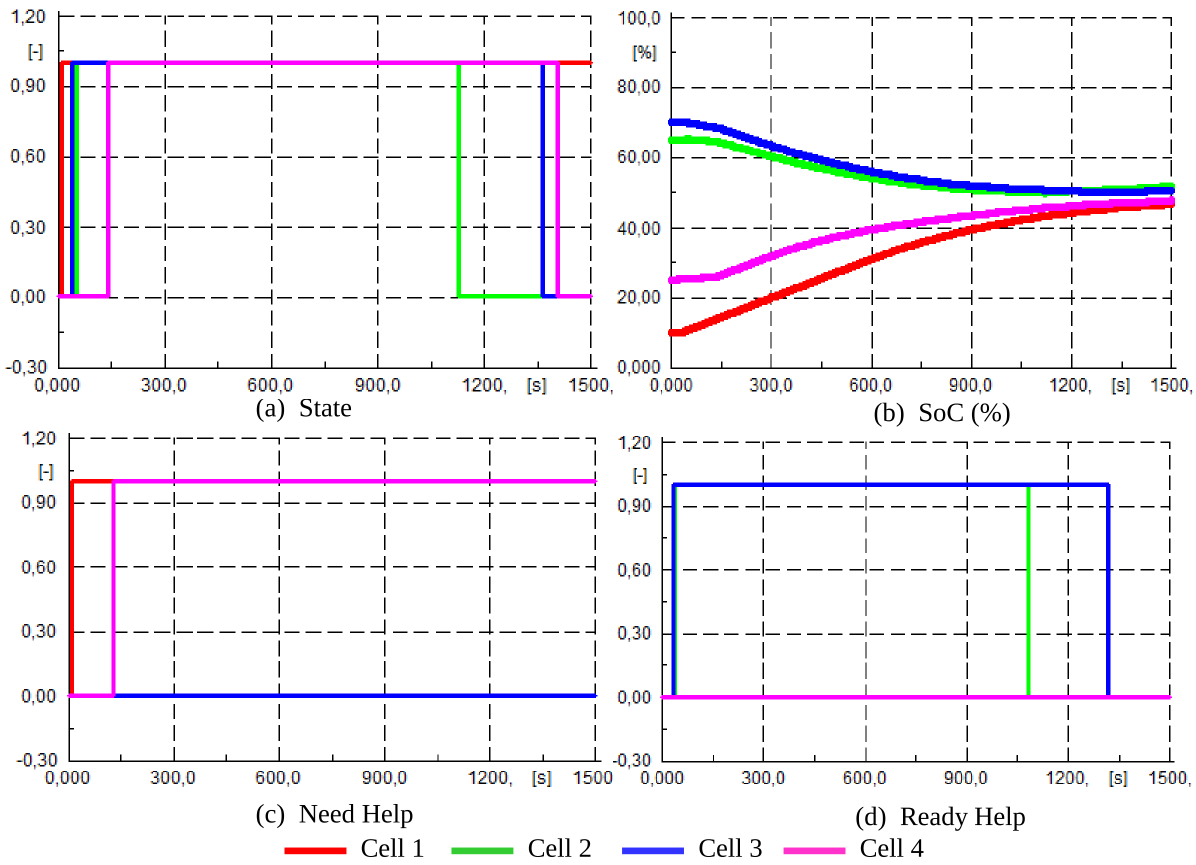


***Figure 6.47:*** *Graphs for Case III: Simulation time – 1500s*

It can be summarized that as SoC becomes less than *SoCC*, the Cell is no longer ready to help, i.e. *RH* signal is reset, enabling *DISC* signal and disconnecting from the BB bus. Further, the *NH* Cell with higher SoC in the MG disconnect (DISC =1) and change its operation to SA mode, as the *PbbND* signal becomes high.

### 6.4.4 Case IV: 1 Cell Very High SoC

In this case, a Cell in the MG is considered to have a surplus of renewable potential and the remaining Cells are not in need state. As per the simulated cases above, the BB bus is energised by a NH Cell. As there are no NH Cells in the network, the BB bus is deenergised and the Cell with high renewable potential starts to curtail its power to ensure a stable operation. This is avoided by modifying the developed algorithm and creating a forced situation. The following cases clearly explain the benefits of the modified algorithm.

#### Case IV.A: Remaining Cells – Low SoC < SoC < High SoC

The SoC of battery of each Cell in the MG (Figure 6.43) is mentioned below. One of the Cells is approaching to a *Very High SoC* due to surplus renewable power and the remaining Cells are within *Low SoC* and *High SoC*.

***Table 6.12:*** *SoC for Case IV.A*

| *Cell* | 1 | 2 | 3 | 4 |
|---|---|---|---|---|
| *SoC (%)* | 45 | 79 | 60 | 55 |

*(i)* *Simulation time – 600s*

Initially, the simulation is performed for a small-time frame of 600 s. From Figure 6.48(b), it is observed that the SoC of Cell 2 crosses the *SoCUL*, which initiates a *Ready Help forced* (RHF) state, as depicted in Figure 5.16. Hence, 2RH =1 at 235.3 s (Figure 6.48(d)) and subsequently, 2State becomes high, energising the BB bus.

As the BB bus becomes live, though the remaining cells are not in need state, following the *NH flow diagram* (Figure 5.12), a *Need Help forced* (NHF) state is created if SoC is less than mean of *SoCC* and *SoCRH*. In Figure 6.48(c), due to the forced states 1NH becomes high at 338 s and 4NH at 350.2 s. However, the Cell 3 which has a higher SoC of 60 % does not connect to the BB bus. If connected this would result in sudden mode change due to *NH Reset conditions*, which would be explained in the following parts. As the *NH* state changes, the Cell 1 and 4 are synchronised to the BB bus, as seen in Figure 6.48(a). Thus, the excess power in Cell 2 is diverted to Cell 1 and Cell 2 and the SoC of Cell 2 decreases marginally and that of Cell 1 and 4 improves mildly, Figure 6.48(b).

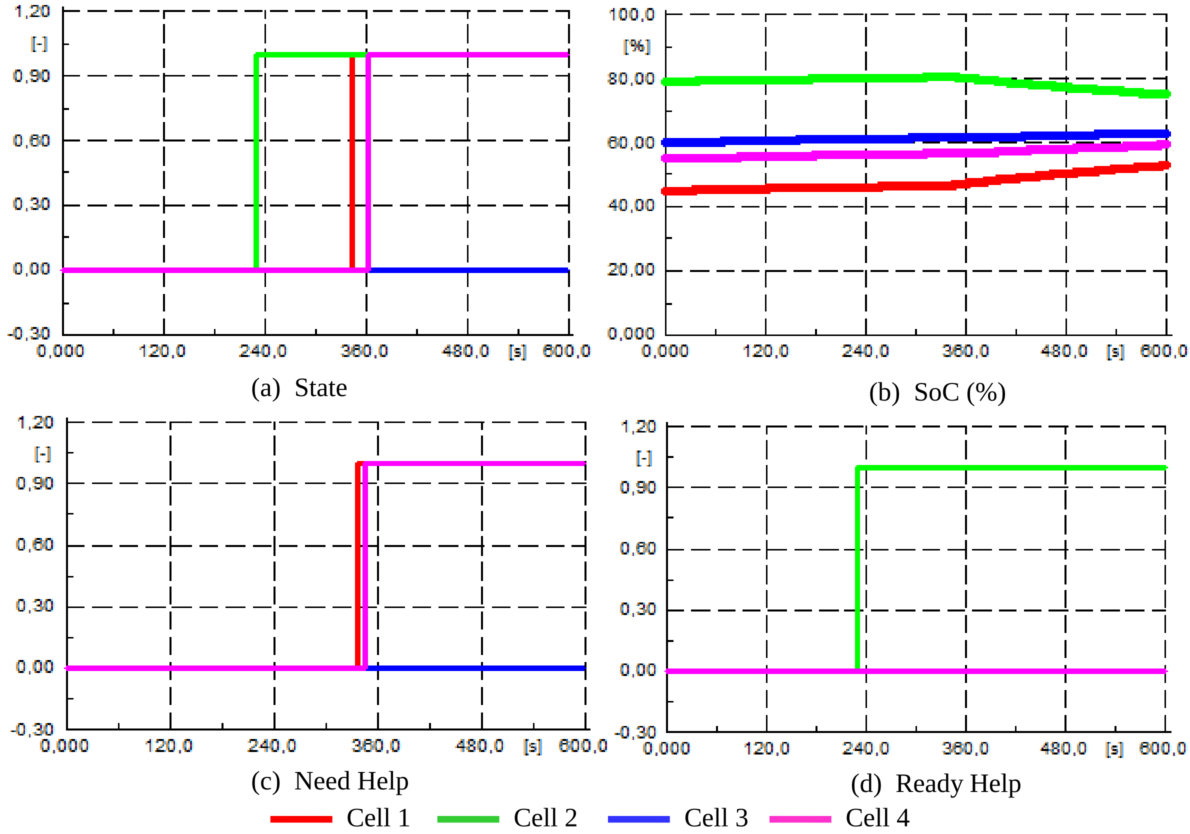


***Figure 6.48:*** *Graphs for Case IV.A: Simulation time – 600s*

From the above simulation, it can be concluded that a *RHF* state = 1 arises, as the SoC crosses the *SoCUL*, which makes the BB bus *Live* and following this, the excess power is redirected to other Cells employing their *NHF* states.

*(ii)* *<u>Simulation time – 1500s</u>*

The simulation is further advanced to 1500 s and the results are analysed here. The *NHF* states are reset (NHFR), as the SoC becomes higher than *SoCRH-5*, as explained in Section 5.3.1. Accordingly, the 4NHF is reset at 681.6 s and 2NHF at 1030 s, as seen in Figure 6.49(c). This *NHFR* signal is further utilized to set *DISC* signal high, as evident in *DISC flow diagram* (Figure 5.21). As 4DISC =1and 2DISC = 1, the disconnection controller is enabled. Following the controller action, both 4State and 2State changes its mode from IC to SA, which is shown in Figure 6.49(a).

Beyond this, there are no *NHF* Cells in the MG. The *RH* state is reset when SoC becomes lower than SoCC, as laid out in Figure 5.17, *RH Reset conditions*. However, in this case, due to absence of communication network, it’s impossible to distinguish between an actual or forced *RH* condition. This is rather a limitation of distributed approach, which can be resolved in a centralized control. However, the Cell 2 is disconnected from the BB bus by utilizing the *PbbRD function*, as in Figure 5.20. When 2PbbRD = 1, because of the power flow through the interconnected line, then 2DISC signal is set high (Figure 5.21). This signal is further used for triggering disconnection controller and the 2State becomes low at 1186 s, as seen in Figure 6.49(a), meaning that it switches to SA mode.

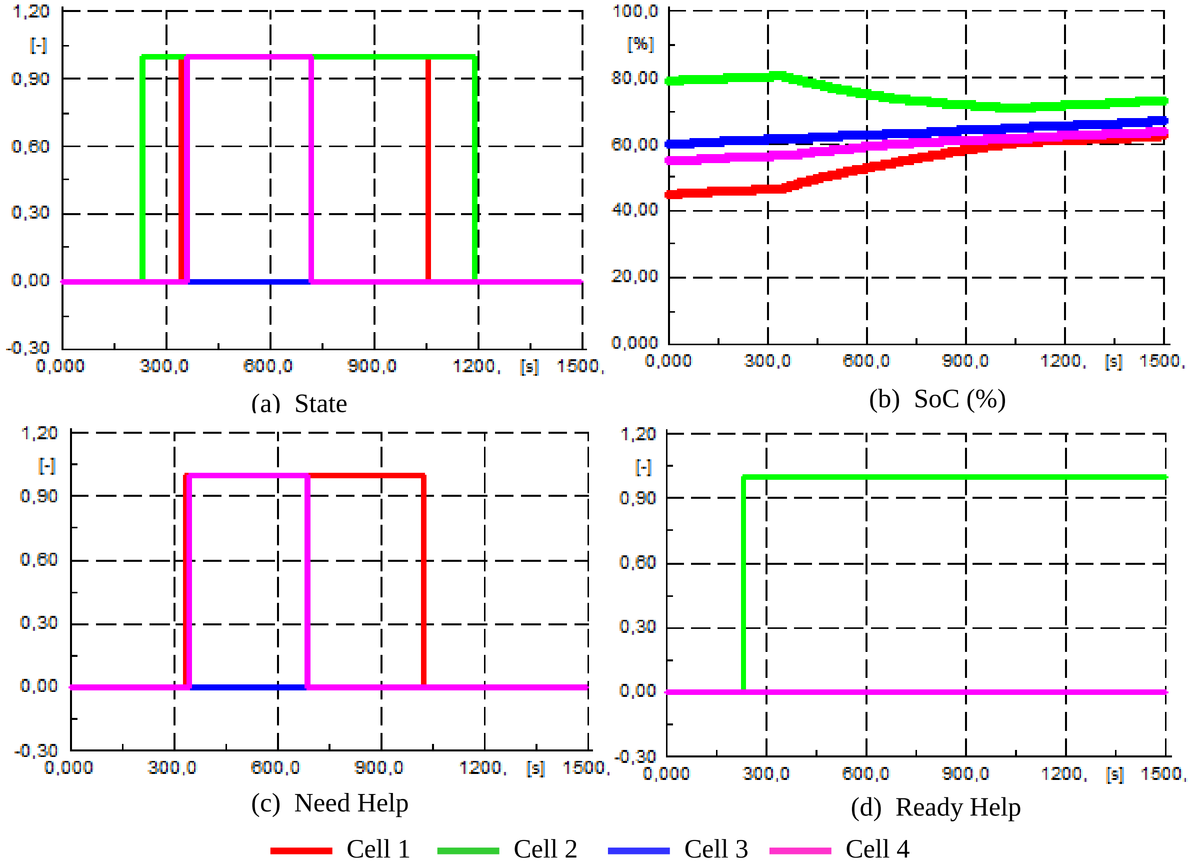


(a) State (b) SoC (%) (c) Need Help (d) Ready Help

***Figure 6.49:*** *Graphs for Case IV.A: Simulation time – 1500s*

### Case IV.B: Remaining Cells - High SoC

Analogous to the case IV.A, one of the Cells is approaching a *Very High SoC* and the remaining Cells have a state of *High SoC*. The MG is simulated with SoC of the battery for each Cell, as mentioned below.

***Table 6.13:*** *SoC for Case IV.B*

| *Cell* | 1 | 2 | 3 | 4 |
|---|---|---|---|---|
| *SoC (%)* | 70 | 79 | 65 | 75 |

The Figure 6.50(b) shows that the SoC of Cell 2 crosses the *SoCUL*, resulting in *RHF* set condition. Because of this 2RHF, the *RH* state of Cell 2 becomes high and Cell 2 connects to the BB bus by changing its State from 0 to 1. Associated changes of *RH* and *State* are depicted in Figure 6.50(a) and Figure 6.50(d).

However, the remaining Cells have SoC higher than *SoCRH*, implying a ready help condition. But the Cells are inhibited from making the corresponding *RH* state as high by utilizing the *RH Connect function*. The *RH Connect function*, as shown in Figure 5.15, ensures that the frequency is lower than 1.003 p.u. for a minimum of 120 s, for allowing the Cell to connect to BB bus. So, this averts the condition of *Ready Help Set condition*, as depicted in the Figure 5.16. Since the RH states of Cell 1, 3 and 4 are no high, these Cells continue to operate in SA mode. The result of which is that there is curtailment of power in Cell 2.

It can be summarized from the above simulations that the curtailment of surplus power in any Cell in MG can be avoided as long as the *NHF* states exists in the network. For the remaining scenarios, where the Cells in the network has a *High SoC*, curtailment is inevitable for maintain the stability of each Cell. This is basically a limitation of the decentralized approach, where the status of the interconnected Cells is not known too each other. However, if a centralized approach is followed, the state can be optimized suitably to further restrict the renewable curtailment. But the constraint of using any ICT equipment in the thesis, confines the management of the deciding the *State* changes in a decentralized manner.

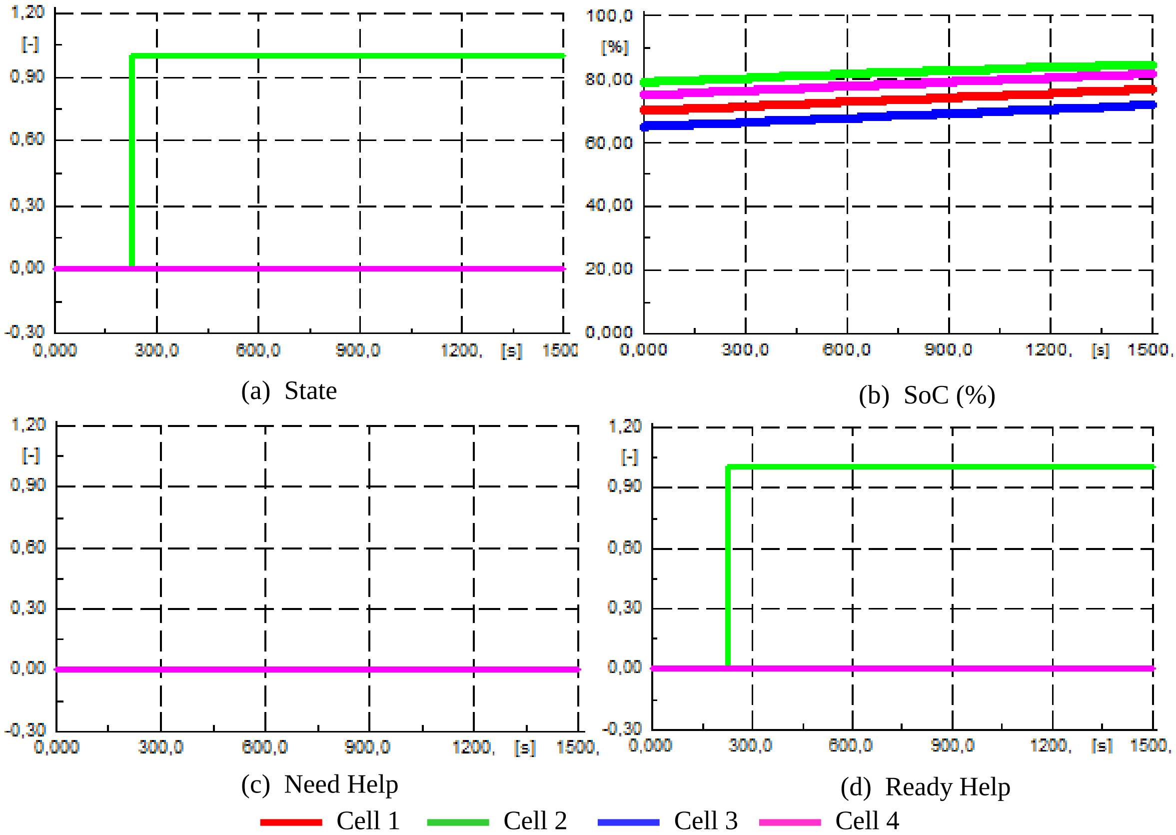


***Figure 6.50:*** *Graphs for Case IV.B*

### 6.4.5 Case V: Past/forecasted energy profile

Based on the past and forecasted energy profiles for each Cell, the algorithm can proactively decide to switch between SA and IC modes. So, in a way, the Cell can prepare itself to maximally avoid any undesirable future occurrences in the MG.

The same layout of the MG architecture, as in Figure 6.43, is followed for the simulations. The SoC of the battery of each Cell at the start of simulation is specified below. From the previous simulations, the profile of load and generation is slightly modified to simulate the situation. The difference of net power, generation and load, is specified for each Cell with simulation time for each Cell in Table 6.14.

***Table 6.14:*** *SoC and Net power profile for Case V*

| *Cell* | 1 | | 2 | | 3 | 4 |
|---|---|---|---|---|---|---|
| *SoC (%)* | 35 | | 50 | | 50 | 50 |
| *Simulation time (t)* | t ≤ 1800 s | t > 1800 s | t ≤ 1800 s | t > 1800 s | t ≤ 3600 s | t ≤ 3600 s |
| $P_g$ - $P_l$ | - 10 kW | 15 kW | 15 kW | - 20 kW | 15 kW | 15 kW |

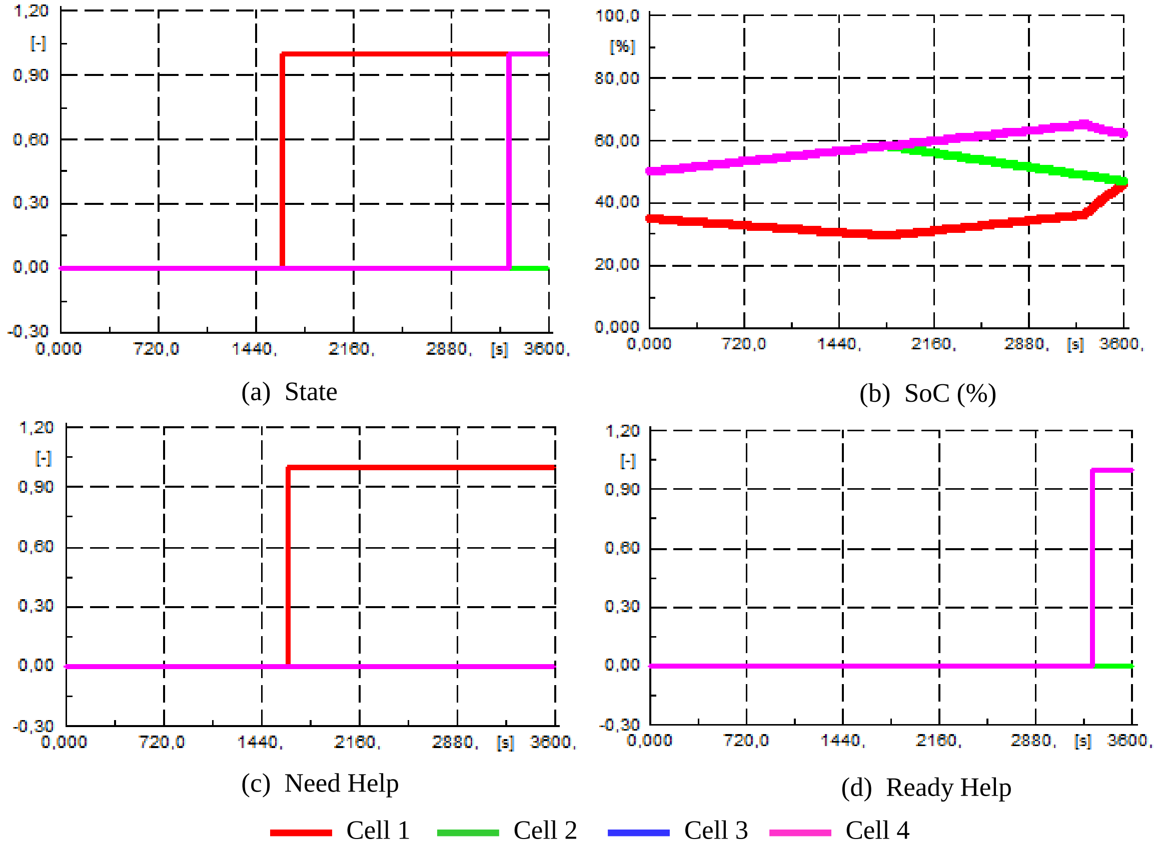


***Figure 6.51:*** *Graphs for Case V: No inclusion of past/forecasted energy profile*

Initially, the MG is simulated for a time frame of 3600 s without inclusion of past/forecasted profile logic modification and the graphs of the various parameters, State, SoC, Need Help and Ready Help states, are plotted in Figure 6.51.

It is seen that the NH state of Cell 1 becomes high at 901.1 s, as depicted in Figure 6.51(c). This occurs because SoC becomes less than SoCLL of 30 %, as explained in *NH Set conditions*. As result, the 1State = 1 and energises the BB bus. The SoC of battery of Cell 4, which has initial SoC of 50%, increases gradually because of positive net power. When the SoC crosses the SoCRH limit of 65 %, the 4RH =1 at 1684 s, as shown in Figure 6.51(d). Correspondingly, the Cell 4 synchronizes with BB bus and 4State becomes high at 3294 s. This change of mode from SA to IC can be seen in Figure 6.51(a). Thus, the SoC of Cell 1 increases more rapidly as it receives support from Cell 4, only after 3294 s and from Figure 6.51(b), the SoC of Cell 1 and Cell 4 reaches a value of 45.3 % and 62.4 % respectively at end of simulation.

In the second phase, the case was simulated for the same profile as in Table 6.14 with adaptation of logic for past/forecasted energy for each Cell. As the SoC of Cell 1 becomes lower than *SoCNH*, the *HECN* signal becomes high, as defined in Eqn.(5.2). As a result, the 1NH becomes high at 901.1 s (Figure 6.52(c)), as per the defined *NH Set conditions* in Figure 5.8. This signal is further utilized to change the *State* of Cell 1 from SA to IC mode, which energises the BB bus.

Parallel to this, the *LECR* signal in *RH Set conditions* attains a value of 1, as it satisfies Eqn. (5.4). However, the *RH* signal is set high, only when the SoC becomes higher than mean of *SoCC* and *SoCRH*. In Figure 6.52(d), it can be observed that 2RH and 3RH is set high at 1684 s and subsequently, both the Cells are synchronised with the BB bus at 1699 s. Due to which, the SoC of Cell 1 improves and reaches a higher value of 45 % at 2160 s, as in Figure 6.52(b), when compared to that without including past/forecasted profile ( 32 % at 2106 s – Figure 6.51(b)).

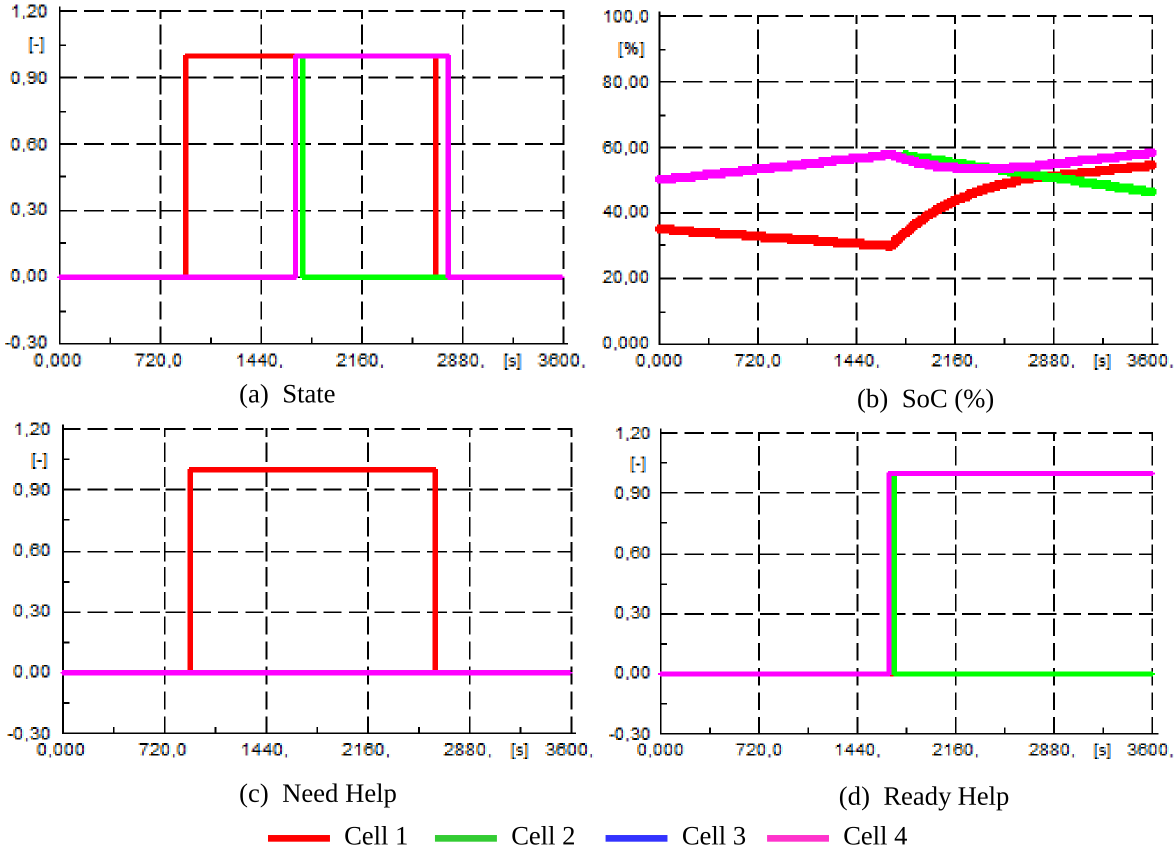


***Figure 6.52:*** *Graphs for Case V: Inclusion of past/forecasted energy profile*

Further as the simulation proceeds, the *HECR* signal, defined as per Eqn.(5.5) is evaluated as shown in Figure 5.17. When the SoC of Cell 2 becomes less than the mean of *SoCC* and *SoCRH*, according to the *RH Reset conditions*, the *RHR* signal is set high. Based on this signal, 2RH is reset at 1732 s, as seen in Figure 6.52(d), which sets the *DISC* signal high. Following this the *State* of Cell 2 switches from IC to SA mode at 1745 s.

Parallelly, *NH Reset conditions* also calculates the *LECN* signal as described in Eqn. (5.3). This signal is used to set *NHR* signal high as shown in Figure 5.11. As the *NHR* signal, the 1NH state is reset at 2628 s and corresponding *DISC* signal is set high as per the *DISC flow diagram* in Figure 5.21. This results in change of State of Cell 1 at 2691 s and linked with this, the PbbRD function sets the 4DISC = 1. Finally, the 4State = 0 at 2779 s, after disconnection criteria is met. All the associated *State* changes can be observed in Figure 6.52(a). From Figure 6.52(b), it is found that the final SoC of Cell 1 and Cell 4 are 54.5 % and 58.1 % respectively at the end.

So, in comparison with the simulation without inclusion, the *NH* and *RH* states achieves a true state well before the Cell reaches *SoCLL* and *SoCRH* limits and *RH* Cell proactively supports the *NH* Cell, examining the past/forecasted profile. Moreover, the *NH* and *RH* states are reset before defined reset limits if the Cell foresees a low energy consumption in case of *NH* signal and high energy consumption in case of *RH* signal. With the modified *NH / RH Set conditions* and *Reset conditions*, the SoC value is also enhanced, ensuring an improved stability of each Cell in SA condition.

### 6.4.6 Case VI: 2 Cells Low SoC, 1 Cell High SoC

In this case, a detailed analysis is performed to evaluate the effectiveness of all the rules used in formulating the decision-making algorithm by simulating the MG layout, as in Figure 6.43, for a longer time frame of 3 hrs. Regarding the sizing of the components in each Cell, it is desired to follow the constant load and generation profile as mentioned in Table 6.6, to observe the State changes in that time frame. However, with usage of actual load and generation data, the State changes may be reflected in the MG system over span of days or weeks. So, it would be like an extrapolation for the former case with time frame of 3 hrs. As previously mentioned, that each of the Cells in the MG initially operate in SA mode with SoC of battery for each Cell as mentioned in Table 6.15.

***Table 6.15:*** *SoC for Case VI*

| *Cell* | 1 | 2 | 3 | 4 |
|---|---|---|---|---|
| *SoC (%)* | 10 | 65 | 60 | 25 |

*(i) Simulation time – 360s*

The MG for the case is primarily simulated for a period of 360s to observe the changes associated with the decision-making algorithm and mode changes between SA and IC.

At the start of the simulation, the Cell 1 with lowest SoC, less than *SoCLL* limit, creates a *NH* signal, ensuing the *NH flow diagram* (Figure 5.8 and Figure 5.12). The signal is generated at 10.87 s, which also energises the BB bus. This results in *State* change of Cell 1 from 0 to 1, indicating IC mode of operation. With the BB bus as *Live*, the Cell 2 which has a SoC of 65 %, higher than *SoCRH* limit, forms the *RH* signal, following the *RH flow diagram* (Figure 5.16 and Figure 5.18), at 40.0 s and the Cell 2 synchronises with BB bus at 44.5 s. With the IC operation of Cell 1and Cell 2, the SoC of Cell 1 increases and that of Cell 2 decreases.

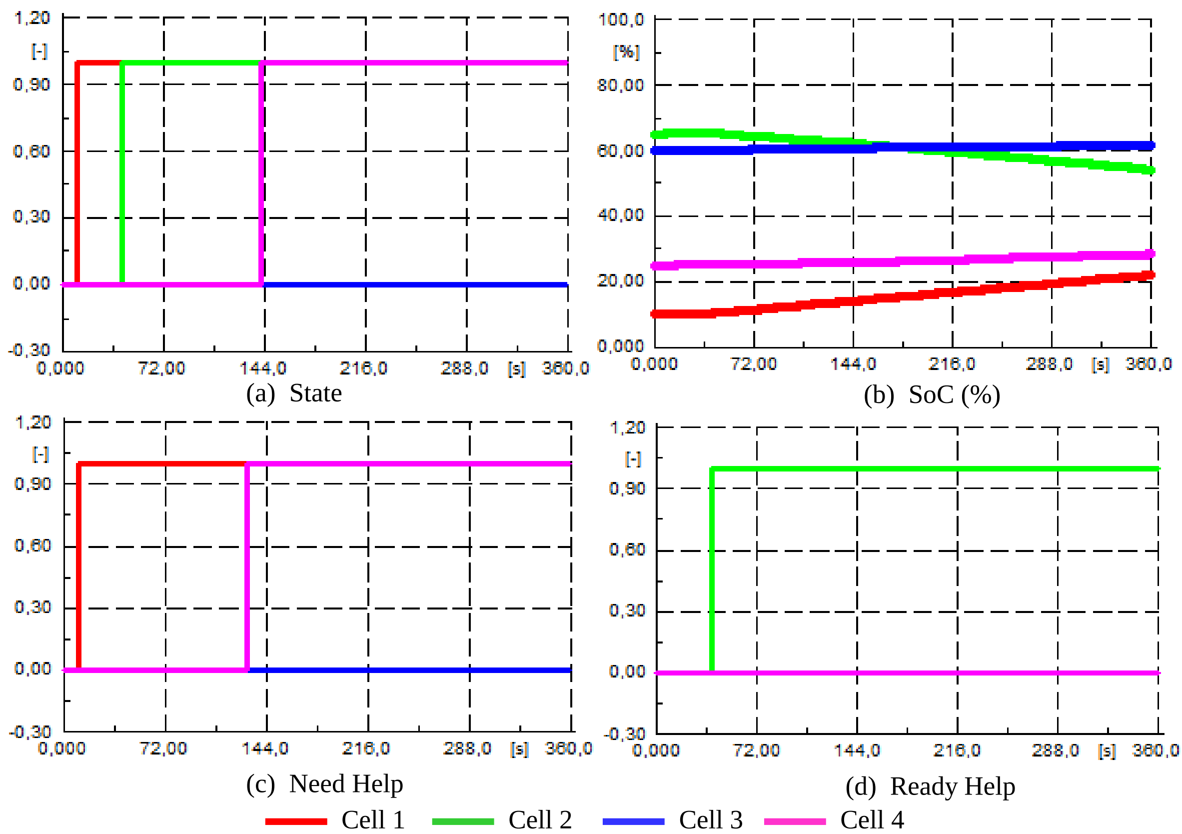


***Figure 6.53:*** *Graphs for Case VI: Simulation time – 360 s*

Further, the *NH Doconnect function*, as in Figure 5.9, forms the enabling signal, which subsequently allows the Cell 4 with SoC of 25 % to create a *NH* signal at 131.7 s. Thus, the Cell 4 also synchronizes with the BB bus and the power is shared among Cell 1, 2 and 4 based on droop curve. All the related *NH* and *RH* signal variations and *State* change of each Cell can be observed in Figure 6.53(c), (d) and Figure 6.53(b) respectively.

*(ii) Simulation time – 1500 s (25 min)*

As the simulation further advances, the SoC of Cell 2 declines as the Cell is supporting Cell 1 and 4. With time the SoC of battery of Cell 2 reaches the critical limit of *SoCC*, as shown in Figure 6.54(b). The defined *RH Reset conditions* forms the signal for resetting *RH* signal of Cell 2. As a result, 2RH = 0 at 471 s, as visible in Figure 6.54(d). With this, the *RHD* signal, as shown in *DISC flow diagram* (Figure 5.21) sets 2DISC signal high after delay function. Hence, the *State* of Cell 2 switches from IC to SA mode at 515 s. Now in the MG, only Cell 1 and 4 are connected to BB bus in IC modes. Due to higher SoC of Cell 2 (30.2 %), the Cell starts aiding the Cell 1. To avoid this operation, the *PbbND* function generates a high signal, which then forces 4DISC signal =1, though the Cell 4 is in need state. With the 4DISC signal, Cell 4 disconnects from the BB bus at 576 s, as seen in Figure 6.54(a).

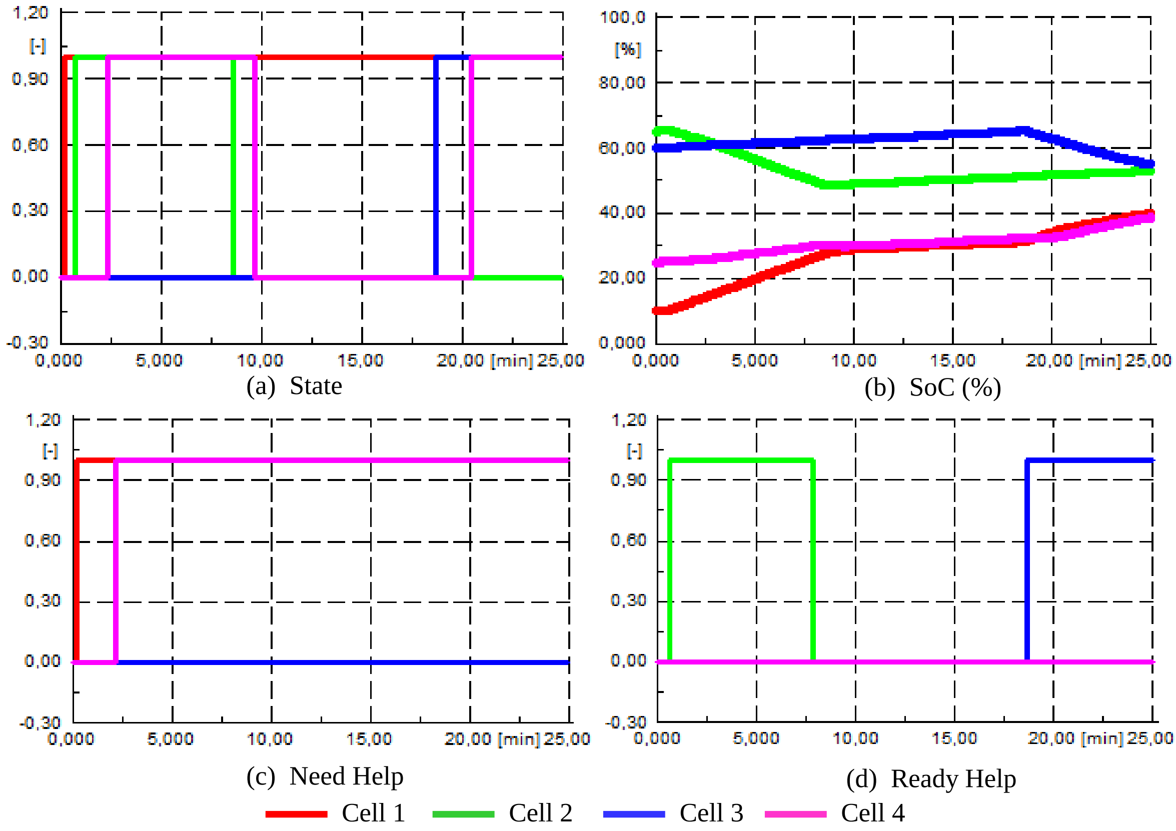


***Figure 6.54:*** *Graphs for Case VI: Simulation time – 1500 s (25 min)*

With the surplus net power in Cell 3, the SoC of battery increases and crosses the *SoCRH* limit, as depicted in Figure 6.54(b). As per the *RH Set conditions*, 3RH = 1 at 18.58 min, as seen in Figure 6.54(d). This high *RH* signal initiates command for connection controller for synchronizing and the Cell 3 changes its State to 1 at 18.69 min. Detecting a higher frequency on the BB bus, Cell 4, which is still in need state, creates an enabling signal for mode switching with the help of *NH Doconnect* function. The result of which is that the Cell 4 prepares for synchronising with the BB bus and the Cell 4 switches to IC mode at 20.38 min (Figure 6.54(a)).

*(iii) <u>Simulation time – 2700 s (45 min)</u>*

With Cell 3 supporting both Cell 1 and 4, the SoC of battery of Cell 3 declines, which is evident from Figure 6.55(b). As explained before, the 3RH signal resets at 32.96 min (Figure 6.55(d)), based on *RH Reset conditions*. Following this the 3DISC signal is set high and the state of Cell 3 shifts to SA mode at 33.64 min. Consequently, the Cell which has comparatively higher SoC among the needy cells disconnect as there are no *RH* cells in the MG. Here, the Cell 1 which has the higher SoC disconnects from the BB bus using the 1PbbND signal at 34.43 min. The State changes of Cell 3 and 4 are depicted in Figure 6.55(a).

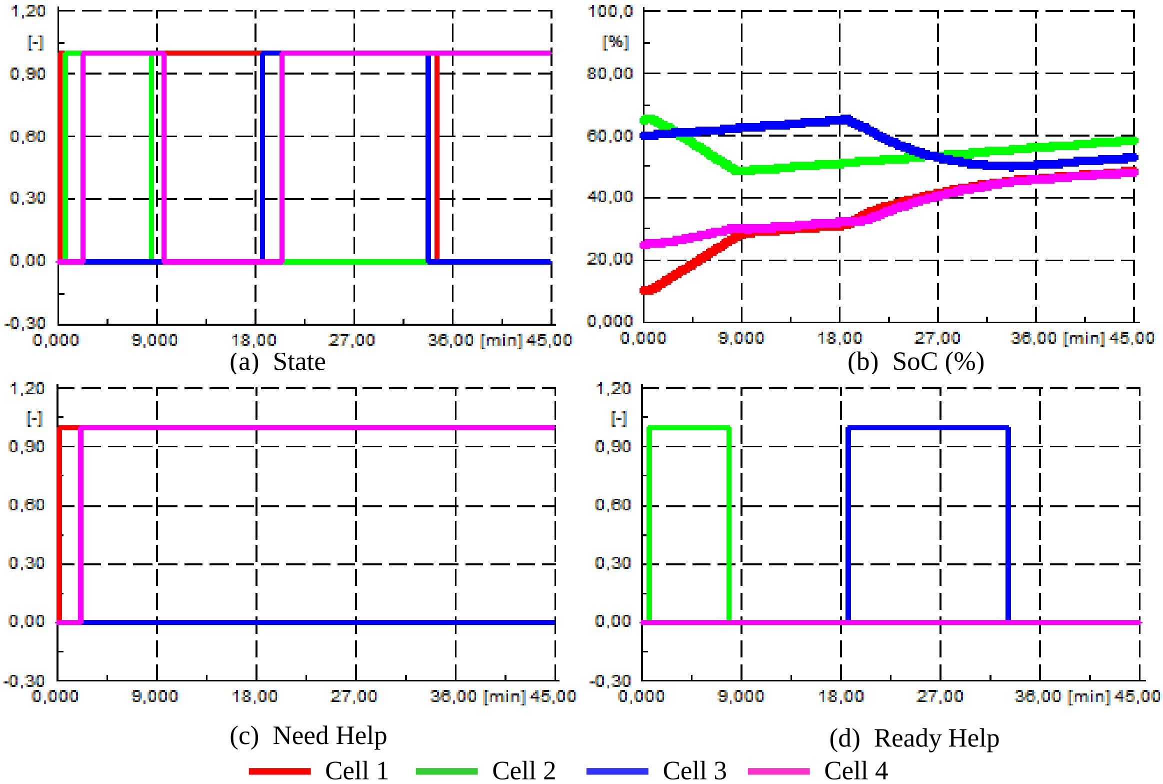


***Figure 6.55:*** *Graphs for Case VI: Simulation time – 2700 s (45 min)*

*(iv) <u>Simulation time – 5400 s (1.5 hrs)</u>*

The SoC of Cell 2, which is in SA mode, gradually increases and crosses the *SoCRH* limit owing to the surplus power. As a result, the 2RH signal becomes high, as seen in Figure 6.56(d) and the *State* of Cell 2 changes from SA to IC mode at 69.23 min. Following this, *NH Doconnect* function enables the connection command of Cell 1, since still in need, and the Cell 1 connects to BB bus at 71.8 min (Figure 6.56(a)).

The Cell 1, 2 and 4 are connected to BB bus in IC mode and the SoC of each Cell gradually improves. As the SoC crosses the limit of *SoCRH – 5*, as defined in *NH Reset conditions*, the *NH* signal of Cell 1 and Cell 4 are reset at 79.39 and 81.0 min respectively (Figure 6.56(c)). As 1NH and 4NH signals become low, *DISC* signals are made high as per the *DISC flow diagram*. The 1DISC and 4DISC signals successively triggers the disconnection controller and the Cell 1 and Cell 4 changes its State to SA mode at 79.95 min and 81.7 min respectively, as seen in Figure 6.56(a).

As all there are no needy cells in the MG, the Cell 2 which is in ready help condition disconnects from the BB bus using the *PbbRD* function (Figure 5.20). The *PbbRD* signal sets 2DISC signal as high and consequently the *State* of Cell 2 switches to SA mode at 83 min (Figure 6.56(a)).

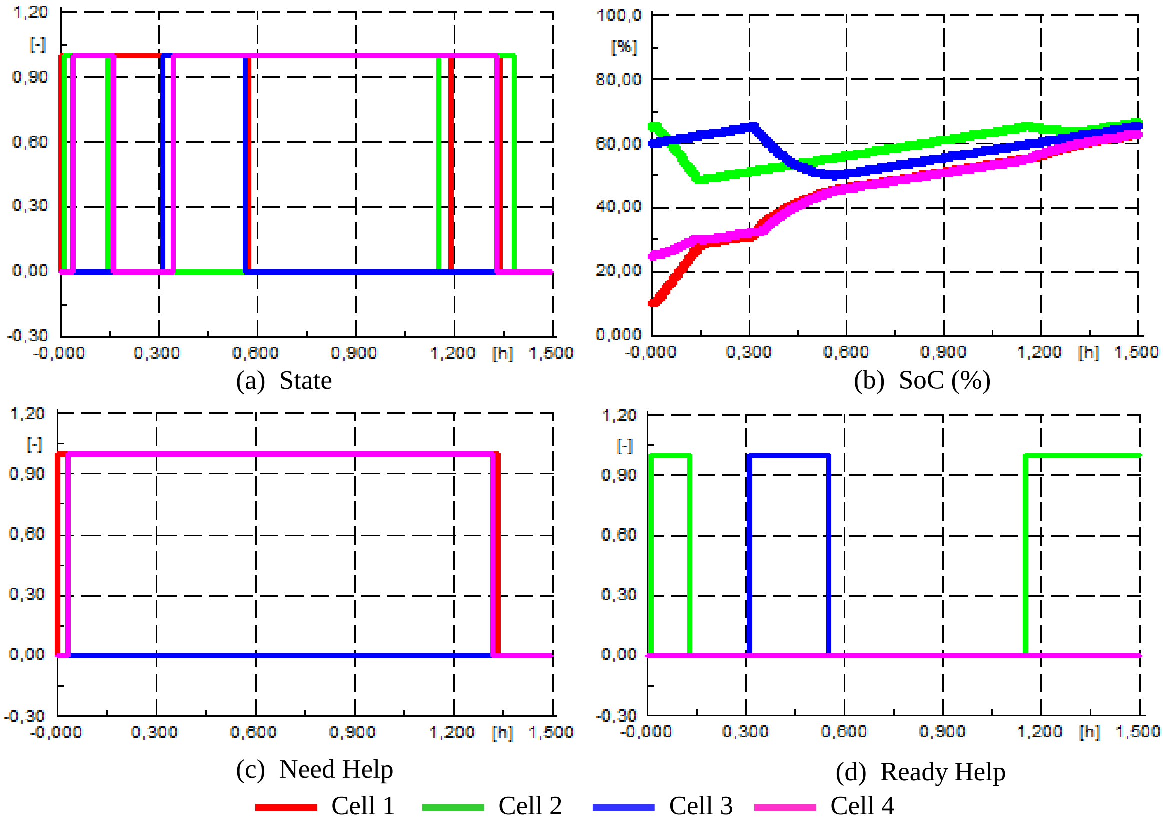


***Figure 6.56:*** *Graphs for Case VI: Simulation time – 5400 s (1.5 hrs)*

*(v)* *Simulation time – 10800 s (3 hrs)*

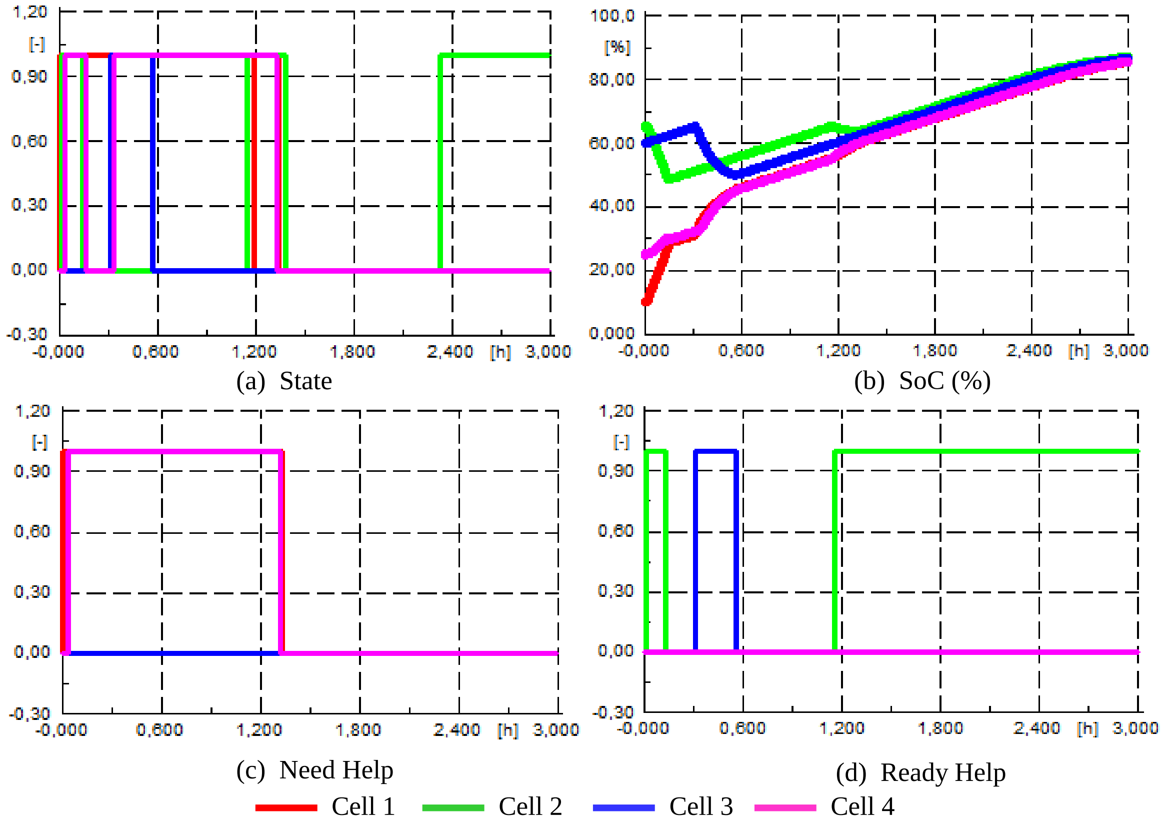


***Figure 6.57:*** *Graphs for Case VI: Simulation time – 10800 s (3 hrs)*

All the Cells are now in SA mode, maintaining its own power balance and stability. It is observed that when the simulation is prolonged, the SoC of the battery of all Cells increases, as seen in Figure 6.57(b). Among the four Cells in the MG, firstly, Cell 2 crosses the *SoCUL* limit of 80 %, indicating a surplus of renewable potential in the Cell. Thus, Cell 2 forces its connection to BB bus using the *RHF* signal in *RH Set conditions*, expecting other cells to connect and divert its excess power. But, since all the other Cells have a SoC of above *SoCRH* limit, none of the Cells connect to the BB bus, which is evident in Figure 6.57(a). Thus, the Cell 2 has no other option than curtailing its renewable potential.

The logic behind defining the different states and the flow diagrams of NH, RH and DISC states are exhaustively evaluated and analysed in the above simulations. Hence, it can be inferred that the devised decision-making algorithm can certainly be applied and expanded in real life applications to a MG comprising of multiple Cells.

### 6.4.7 Case VII: MG Case in Netherlands

As a final case, the decision-making algorithm is evaluated for a MG in the Netherlands for a week with actual load and generation profile. The layout of the MG is same as in Figure 6.43 with 4 Cells comprising of DRES, BESS and controllable loads.

The sizing of the components in the MG is based on the energy consumption and generation data obtained from DNV-GL[45]. The energy consumption data for 60 households in the Netherlands were used calculated to find the annual energy consumption. From this, the average daily energy consumption for each household was found out to be 10 kWh. The 60 households were divided into four groups, i.e. each Cell would comprise of 15 households with the daily load consumption profile.

As the main grid is not present for the case, 3 Days of Autonomy was considered to handle the worst-case scenarios of lower generation profile. So, the size of the battery in each Cell is tabulated to approximately 450kWh. For sizing of the DRES component in each Cell, a factor of 60 % is chosen for the annual energy produced [45]. In other words, 60 % of the annual energy consumption needs to be satisfied with renewable energy generation in each Cell. So, the average daily renewable generation is calculated to approximately 90 kWh.

The average generation of 1kWp Solar system is estimated using a capacity factor as 10.3% [66]. Similarly, the a capacity factor 21.5 % is used for calculation of generated energy from on-shore Wind turbine in the Netherlands [67].

To have a clear distinction between each Cell, the percentage of energy generation is selected differently for each Cell. It is assumed that Cell 1 comprises of only Solar, while Cell 2 only of Wind, meaning that 100 % of energy generation in Cell 1 and 2 is met by only Solar and Wind respectively. For Cell 3, an ideal renewable energy ratio of 20:80 is chosen for solar to wind energy in the Netherlands, based on previous investigation in SOPRA project [68]. A combination of Solar and Wind is chosen for Cell 4, but with a ratio of 50:50. Based on the above factors, the sizing of DRES component is calculated as in Table 6.16.

***Table 6.16:*** *Sizing of DRES components for Case VII in the Netherlands*

| *Cell* | 1 | 2 | 3 | 4 |
|---|---|---|---|---|
| Solar (kWp) | 35 | - | 10 | 15 |
| Wind (kW) | - | 20 | 15 | 10 |

For the purpose of simulation, the first week of May was chosen and the associated load and generation profiles of each Cell are plotted in Figure 6.58. While observing the generation of profile of Cell 1, it is observed that the Solar profile is high for the first two days and followed by a day with very lower production. Similarly, the wind generation is spotted to be very low for the initial two days, later followed by a day of very high and remaining days with average production. So, the chosen week would be perfectly apt to evaluate the devised decision-making algorithm.

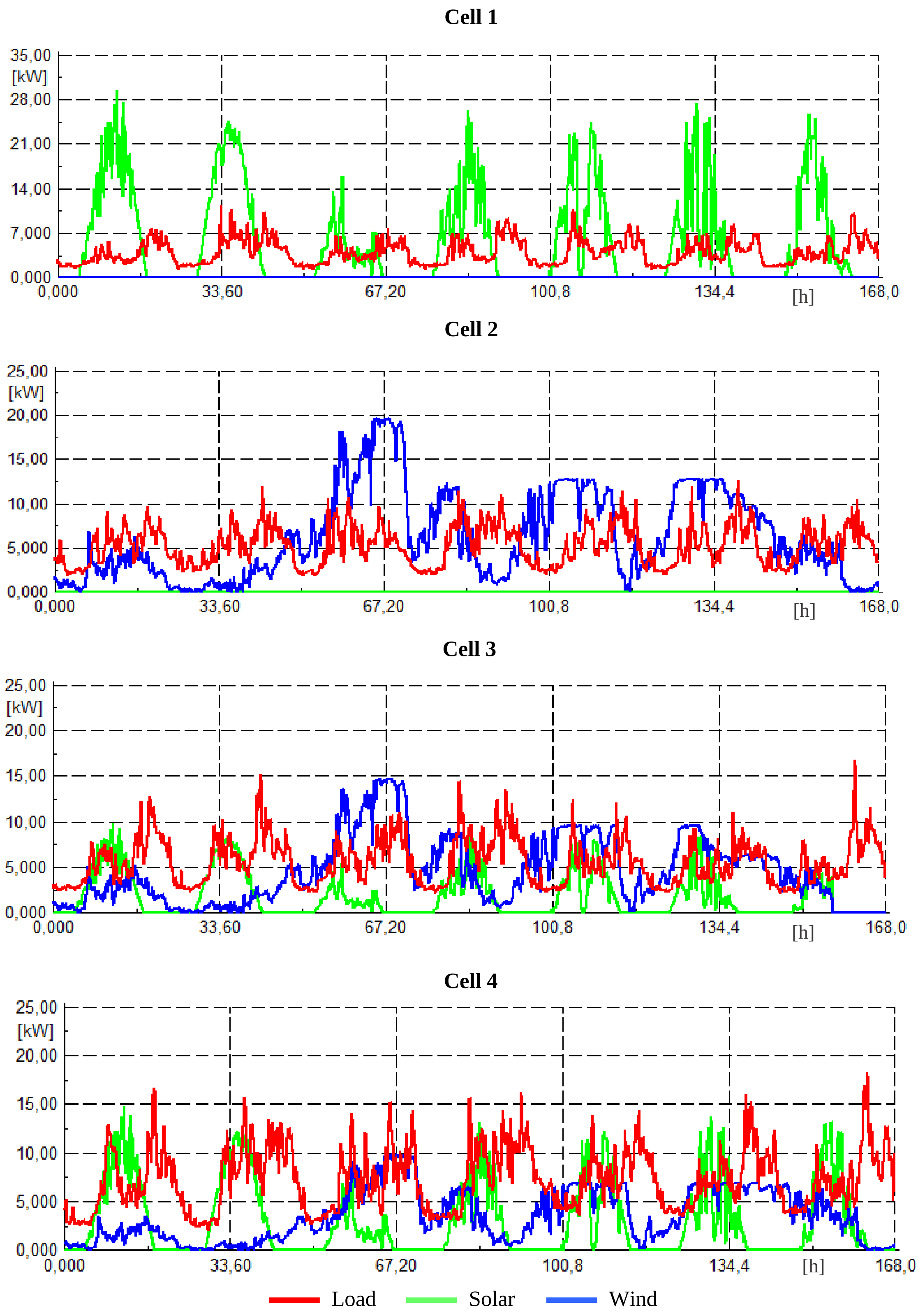


***Figure 6.58:*** *Load and Generation profile for a week*

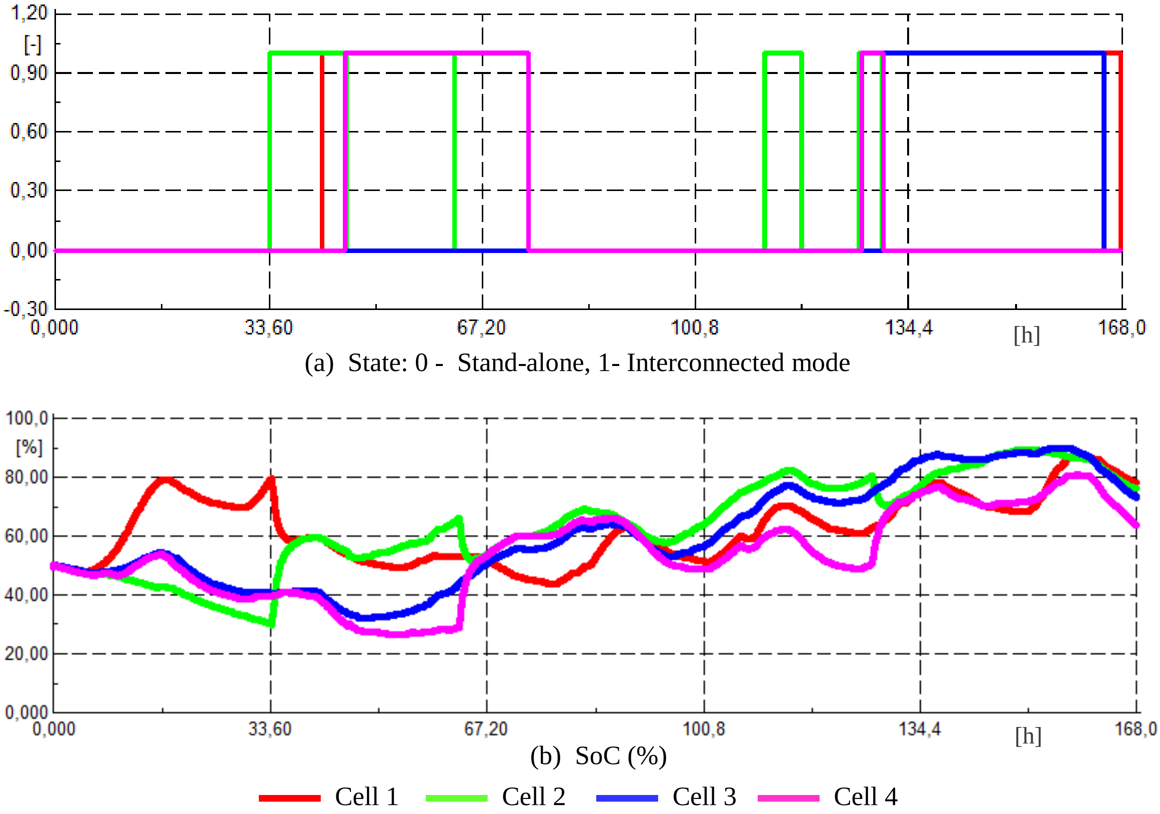


***Figure 6.59:*** *Graphs for Case VII: State and SoC (with decision-making algorithm)*

The initial SoC of battery in each Cell is assumed to be 50 % and the simulation was performed for the entire week. As seen in Figure 6.59(a), there are less *State* changes in each Cell as excepted, with respect to that of previous simulations.

The initial NH state of Cell 2 is formed at 33.6 hrs and simultaneously, the State of Cell 2 changes to 1, indicating that a Cell is in need state in the MG. Since the Cell 1 is in ready help condition, the Cell 2 synchronizes and support Cell 2. Similarly, based on the developed decision-making algorithm, the *NH*, *RH* and *DISC* variables change their values throughout the simulation period following the *NH, RH and DISC flow diagrams* respectively. The associated changes in *State* and *SoC* of battery of each Cell are depicted in Figure 6.59(a) and Figure 6.59(b).

From Figure 6.59(b), it is observed that the SoC of each Cell has not dropped below 25 %, which is the triggering point of load shedding as explained in Section 3.7. The load shedding factor was tabulated for each Cell and was found to be 0 %. Similarly, the SoC of Cell 1, 2 and 3 goes above 80 % on the last day, indicating a high renewable potential in the Cell but other Cells do not connect to the BB bus due to higher SoC of its own cell. The percentage of renewable curtailment for Cell 1 and 4 was close to 0 %, while that of Cell 2 and Cell 3 is 5.2 % and 8.47 %. The average SoC of battery in each Cell was found be above 50 % for the week.

Another simulation was performed for the same MG layout and the load and generation profile, but, without the incorporation of decision-making module. In other words, the Cells would always remain in SA mode and meet its own energy demand. The corresponding State and SoC of each Cell are plotted in Figure 6.60(a) and Figure 6.60(b) respectively.

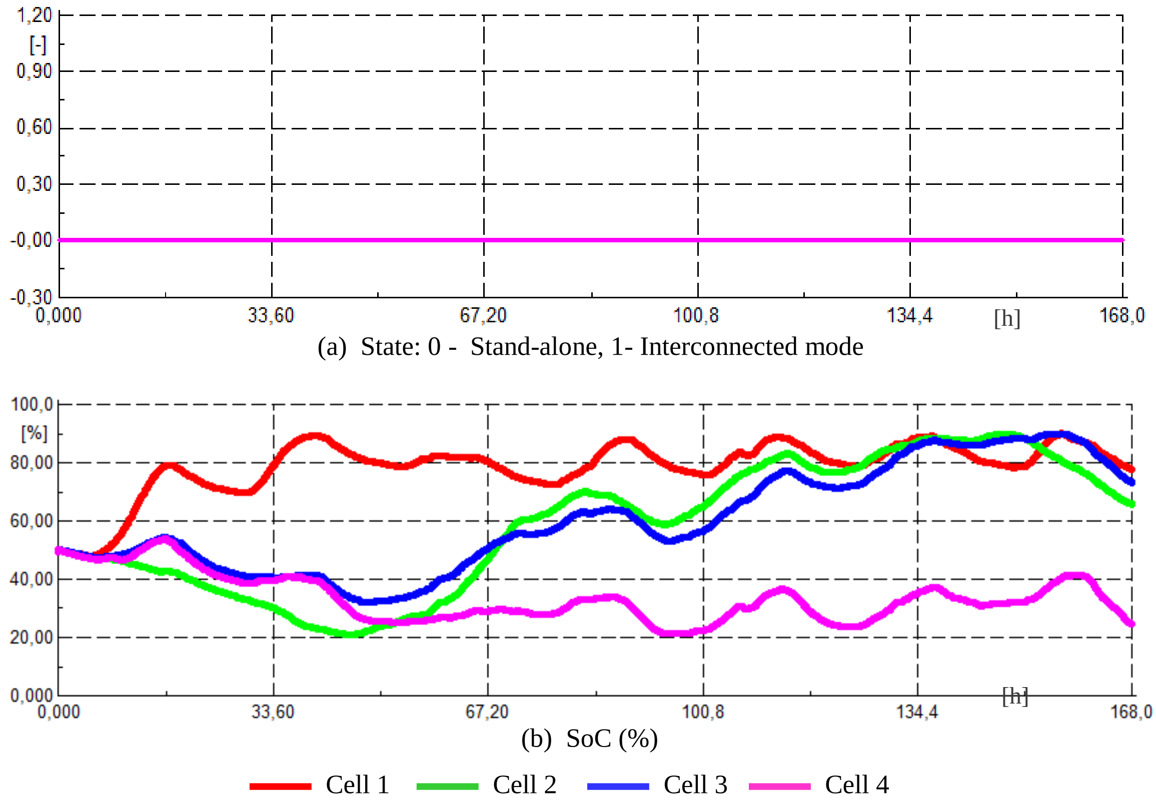

(a) State: 0 - Stand-alone, 1- Interconnected mode

(b) SoC (%)

***Figure 6.60:*** *Graphs for Case VII: State and SoC (w/o decision-making algorithm)*

Analogous to the previous simulation, the percentage of load shedding was calculated and found to be 0 % for Cell 1and 3, while it was 2.64 % and 2.81 % for Cell 2 and Cell 4 respectively. The renewable curtailment percentage was calculated to be high for Cells 1, 2 and 3: approximately 15 %. The Table 6.17 gives an overview of the results for both scenarios with and without Decision-making algorithm.

***Table 6.17:*** *Comparison of results with and without Decision-making algorithm*

| *Simulation* | *With Decision-making algorithm* | | | | *W/o Decision-making algorithm* | | | |
|---|---|---|---|---|---|---|---|---|
| *Cell* | 1 | 2 | 3 | 4 | 1 | 2 | 3 | 4 |
| SoC at start of week (%) | 50 | 50 | 50 | 50 | 50 | 50 | 50 | 50 |
| Curtailment (%) | 1.5 | 5.2 | 8.47 | 0 | 17.36 | 16.64 | 12.13 | 0 |
| Load Shedding (%) | 0 | 0 | 0 | 0 | 0 | 2.64 | 0 | 3.81 |
| Average SoC (%) | 62.46 | 63.86 | 60.31 | 53.85 | 78.72 | 58.54 | 60.3 | 33.54 |

From Table 6.17, it can be inferred that with the application of the devised decision-making algorithm, the average value of SoC of batteries in MG is improved, with only Cell 1 with lower value. This is because Cell 1 supports other Cells, but maintains an average SoC value of above 50 %. Furthermore, the percentage of load shedding and the curtailment has been lowered, ensuring more reliable supply to end consumers, maximizing the usage of renewables. A similar analysis was performed for another week in winter: first week of November and the results were found comparable to that of the above case. The related graphs and comparison are presented in Appendix B.

## 6.5 Summary

In this chapter, initially the MG architecture and the selection of parameters for each Cell was presented for both simulations: Seamless (dis)connection and Automated decision algorithm. Later, the different case scenarios for each kind of simulations are elaborated upon and simulations were performed in

PowerFactory for each section. From the results of Section 6.3 (Seamless dis/connection), it can be inferred that the formulated control scheme was successful in achieving a seamless transition between modes, even though the Cell is being (dis)connected to EG or to another Cell. The results of Section 6.4, focussed on the automated decision-making algorithm, shows that the defined states of *NH*, *RH* and *DISC* were effective in creating decision for autonomous mode transition to maintain the overall stability of the system. However, some limitations were observed when the Cells in the MG has a higher SoC due to surplus renewable potential.

# 7 Validation

## 7.1 Introduction

The Voltage Source Converter (VSC) of the Battery Energy Storage System (BESS) is the master controller that defines the MG parameters – Frequency and Voltage, as explained in Section 3.4. The control strategy for operation of VSC of BESS for seamless transition of MG between Isolated (I) and Grid Connected (GC) modes and its steady state behaviour has been discussed in detail in the Section 4.3. The intriguing question that arises is how such a control strategy could be implemented in a Voltage Source Converter/ Inverter.

There are two possible ways for resolving this. One solution is to design and build the complete circuit for a VSC with the devised controls from its individual circuit components. The complete circuit design comprises of, but not limited to, control circuit, drive circuit, filter circuit, selection of system components and thermal management [69] . The second solution is to develop a control interface with possible outputs that can adapt to the existing VSC.

The development of such a universal interface may be applied to inverter of any manufacturer with slight adaptations, but with certain constraints in influencing the internal control parameters. Additionally, the technicalities involved in complete design and the cost involved in building such an inverter logically favoured the adoption of the second solution [70], [71]. However, the implementation of this proposed control strategy in a VSC for a pilot demonstration profoundly depends on the type of Inverter and its operational behaviour. A detailed analysis is essential for evaluating the applicability of the devised control loops in the VSC/ Inverter.

This chapter mainly focusses on understanding the behaviour of the Inverter, performing experiments to comprehend the internal operating modes, testing the formulated control loops and adapting of the control strategy for possible interfacing with the Inverter for a pilot demonstration.

## 7.2 Experimental Set-up

In the technology demonstration of the CSGriP project, a 250 kW VSC of VACON make is envisaged to be utilized for interfacing the BESS with AC MG. To evaluate the behaviour of the VSC, a test set up, with a smaller rating 10kW VACON converter, at HAN University was utilized for performing tests. The motive behind these tests involves the application of these converters in Isolated / Stand – Alone and Grid Connected states, identifying the parameters required for possible interface for developed control strategy and evaluating the influence of these parameters in the operation of the converter.

The Figure 7.1 shows the snapshot of the experimental set up with the power measurement unit at HAN University for evaluating the applicability of the proposed control strategy to the inverter and prove its functionality as VSI in SA and GC mode with the conventional *P/f* and *Q/V* droop curves.

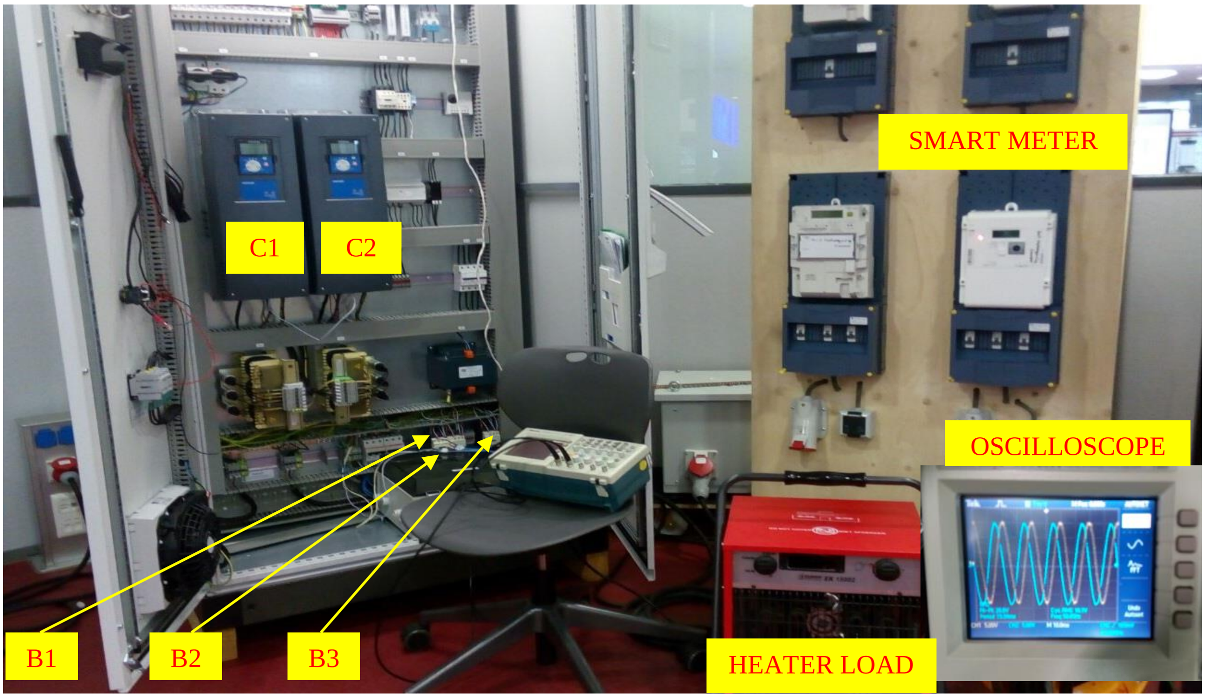


***Figure 7.1***: *Experimental set-up at HAN University*

### 7.2.1 Single Line Diagram

The Single Line Diagram (SLD) of the test set up at the HAN University is depicted in Figure 7.2.

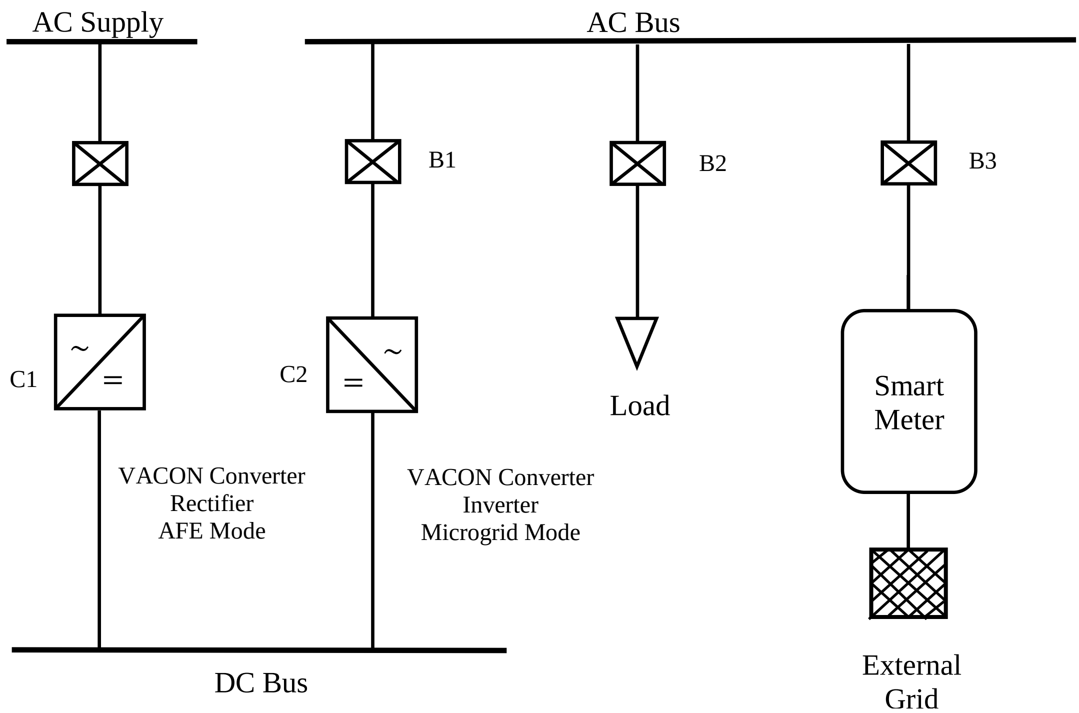


***Figure 7.2:*** *Single Line Diagram*

The test setup encompasses of 2 VACON make inverters with LCL filters, DC and AC Bus, Contactors – B1, B2 and B3 for connection to AC Bus, Load and External Grid respectively, Heater load of 5 kW, Smart meter for power measurement to External Grid, Oscilloscope for analysing the voltage waveforms and Programmable Logic Control (PLC) for setting the parameters of VACON converter and defining the control operation.

### *7.2.2 Limitations*

Due to absence of a BESS at the test site, one of the VACON converters (*C1*) is used as a rectifier to create a DC Bus and the other VACON converter (*C2*) inverts this DC Bus voltage to desired AC voltage based on the parameter setting. The working modes and operating principles of the converter would be dealt in detail in the following Section 7.2.3.

The generated DC Bus emulates the battery behaviour, but with a constant DC voltage. Such a system has apparent limitations. The voltage of the BESS would never remain same; it varies with State of Charge (SoC) based on whether the converter is absorbing / receiving power. Hence in the test set up, the converter *C2* always delivers constant power to the AC network regardless of the DC voltage, in other words in discharging mode. Further, the system setup does not permit absorption of power to charge the battery when there is excess of generation or when connected to external grid. This means that tests can be performed only in delivering mode, which limits comprehensive analysis of the proposed control strategy.

### *7.2.3 VACON converter*

The VACON Grid Converter can be used to make AC grids with possibility of parallel operation with other power sources.

*Operating modes*

The converter has three different operation modes [72], which are described below

a) Active Front End (AFE) – The main functionality of this mode is to keep a constant DC voltage and transfer power between DC and AC. AFE cannot create grid by itself, but needs to be connected to existing grid.

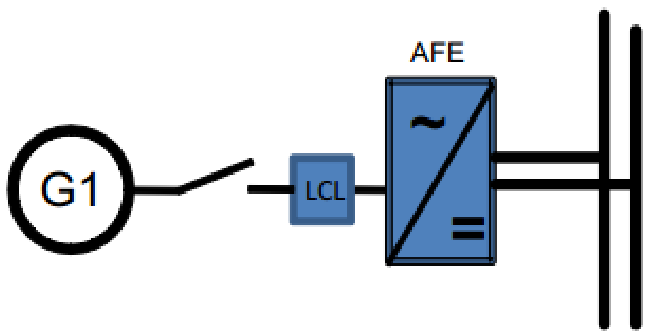


***Figure 7.3:*** *AFE mode*

b) Island (Static Power Supply) – In this mode, DC voltage is not controlled, but used to generate constant voltage and frequency. Island mode cannot operate with other power sources as it cannot balance active and reactive power with other sources. A certain DC voltage level has to be mainlined to have a correct voltage on AC side in different loading conditions, considering losses in LCL filter and transformer.

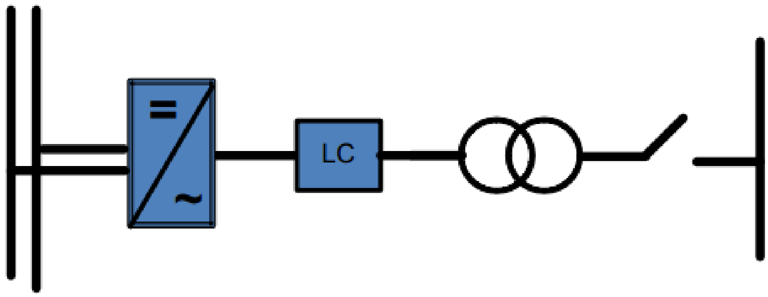


***Figure 7.4:*** *Island mode*

c) Microgrid – This mode is used to control grid voltage and frequency. As in normal generators, Microgrid mode does not control DC voltage. More than one Microgrid and/or Generators can work together with the help of voltage and frequency droop.

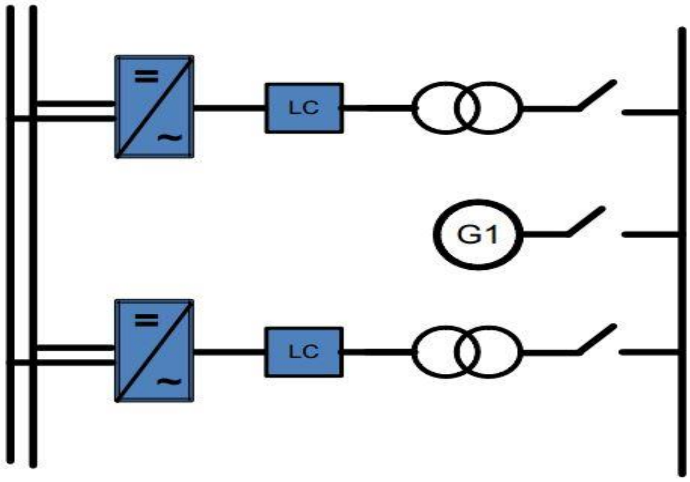


***Figure 7.5:*** *Microgrid mode*

<u>*Operating principles*</u>

In the Microgrid mode, the operating principles of the converter can be categorized into Droop Speed Control Mode and Isochronous Speed Control Mode [72].

a) Droop Speed Control mode – As the power demand increases, all generators on the grid allows frequency to droop and based on the droop value, load or active power is shared between all generators on grid. Then the Power Management System (PMS) will give a command to increase frequency so that grid frequency is maintained at its nominal value. Similarly, as the load decreases, generators frequency will increase and subsequently, PMS will give command to decrease frequency.

b) Isochronous Speed Control mode – The Microgrid frequency is same as the grid frequency which is measured with the help of OPT-D7 card. This will ensure that the power output is zero regardless of the grid frequency. If the drive operates in drooping mode, the power output is controlled by Base Current Reference. This reference is controlled by power management system (PMS), that regulates the power sharing between different machines on the grid.

*OPTD7 card*

The OPTD7 card is an AC sinusoidal voltage measurement unit which measures the line voltage, frequency and voltage angle information. The drive compares this measured values with its output voltage angle when it's running [72].

In the Microgrid mode, the card can be used in two different configurations, depending on which the application varies.

a) OPTD7 card for measurement of voltage parameters of the External Grid as shown in the Figure 7.6. In this configuration, this can be used to synchronize to External Grid while the drive is running to enable a bump less transition and a zero-power connection.

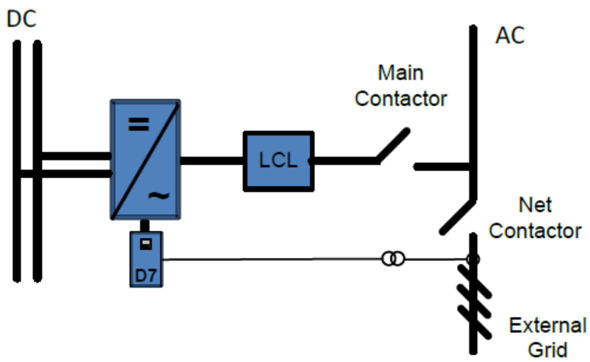


***Figure 7.6:*** *D7 card measurement – External Grid* [72]

b) OPTD7 card for measurement of voltage parameters of internal grid after the LC filter and Transformer as in Figure 7.7. The converter system has voltage losses and depending upon the system losses, the voltage loss needs to be compensated so that the grid voltage stays at nominal value. Uncompensated system may lead to unnecessary reactive power circulation in a grid with multiple power sources along with resulting wrong grid voltage.

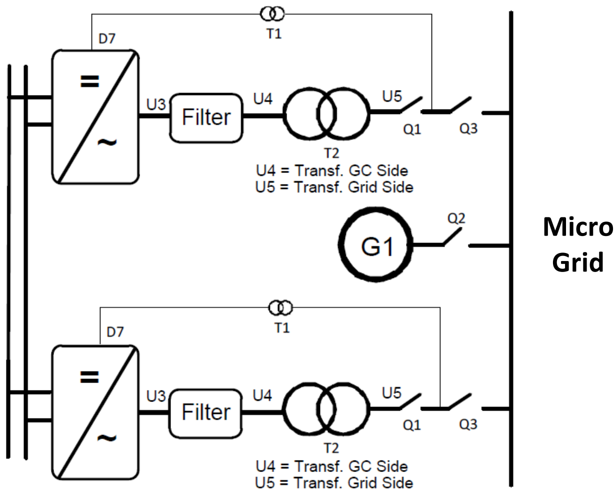


***Figure 7.7:*** *D7 card measurement - Microgrid* [72]

It’s worth knowing that the former configuration of the OPT D7 card is used in the test set-up at HAN University.

## 7.3 Testing

Knowing about the various operating modes and principles of the converter, tests are being performed to evaluate the applicability of the proposed control strategy. Referring to Figure 7.2, Converter C1 is in AFE mode creating a DC bus and Converter C2 is in Microgrid mode generating AC bus. Prior to description of each test, first a quick glance through the influencing parameters and their significance is worth exploring to comprehend the results in a more beneficial way.

### 7.3.1 Parameters

The parameters utilized for performing the tests are described below

Nominal Frequency –Base frequency set point of the converter. In Microgrid mode, it is used as a reference point for the Base Current reference and drooping.

Frequency Droop – Defines the frequency deviation in Hz with the percentage of loading of the inverter.

Frequency Offset – This parameter is used to adjust the base frequency for drooping purposes. For example, if frequency droop (Figure 7.8) is set to 2 Hz, this parameter can be set to 1 Hz so that when the load is 50%, the frequency will be at the nominal point. The offset can also be set by the supply frequency parameters.

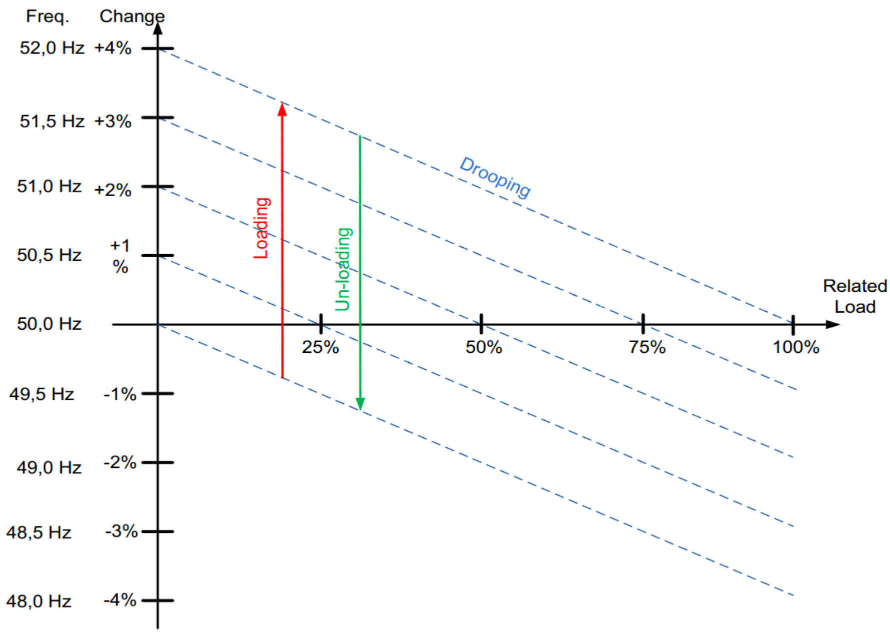


***Figure 7.8:*** *Frequency Droop curve* [72]

Base Current Reference – The Base Current Reference determines offset for frequency reference within Frequency Drooping. For example, if frequency droop (Figure 7.8) is set to 2.0 Hz and grid frequency is constant 50Hz with very small or non-existent changes (isochronous or strong grid), and if 100% of Base Current Reference is given, the drive will feed 100% power to the grid. The situation is the same with the frequency reference set to 52 Hz and with 2.000 Hz drooping.

Supply Frequency – This parameter defines the frequency output of the converter with frequency drooping.

*Power Inverter* – Power delivered / absorbed by the converter. The power delivered is considered positive and power absorbed by the inverter is considered negative. Similar convention is followed for Power Load and Power Grid.

### 7.3.2 Test A – Stand-alone mode

In this test, the converter is in Microgrid mode and B1 is closed, generating the AC Bus. This means that the converter is in Isolated / Stand-alone condition capable of delivering power to loads in its own MG. However, in the initial phase, no load is connected to the network, i.e. the contactor B2 is open state (Refer Figure 7.2). The parameters – Nominal frequency, Frequency droop and Base current reference are varied and the Supply frequency and Power supplied by the converter is presented in Table 7.1.

***Table 7.1:*** *Stand-alone mode w/o Load*

| Nominal Frequency (Hz) | Frequency Offset (Hz) | Frequency Droop (Hz) | Base Current Reference (%) | Supply Frequency (Hz) | Power Inverter (kW) |
|---|---|---|---|---|---|
| 50 | -1 | 1 | 0 | 49 | 0 |
| 51 | -1 | 1 | 0 | 50 | 0 |
| 50 | -1 | 2 | 0 | 49 | 0 |
| 50 | -1 | 2 | 100 | 51 | 0 |
| 50 | -1 | 1 | 100 | 50 | 0 |

From the above table, it can be inferred that

- Frequency Reference = Nominal frequency – Frequency offset, if Base current reference is zero.
- Frequency Reference = Nominal frequency – Frequency offset + Frequency droop, if Base Current Reference is 100%.
- Supply frequency = Frequency reference, in absence of load.

To evaluate the droop behaviour, a heater load of rated 5 kW is connected by closing B2 (Refer Figure 7.2). The Table 7.2 describes the influence of Nominal frequency, Frequency droop and Base current reference on Supply frequency, irrespective of the load demand.

***Table 7.2:*** *Stand-alone Mode with Load*

| Nominal Frequency (Hz) | Frequency Offset (Hz) | Frequency Droop (Hz) | Base Current Reference (%) | Supply Frequency (Hz) | Power Inverter (kW) | Power Load (kW) |
|---|---|---|---|---|---|---|
| 50 | -1 | 1 | 0 | 49 | 0 | 0 |
| 50 | -1 | 1 | 0 | 48.53 | 4.7 | -4.7 |
| 51 | -1 | 1 | 0 | 49.53 | 4.6 | -4.6 |
| 50 | -1 | 2 | 0 | 48.06 | 4.7 | -4.7 |
| 50 | -1 | 2 | 100 | 50.06 | 4.7 | -4.7 |
| 50 | -1 | 1 | 100 | 49.53 | 4.7 | -4.7 |

As the Frequency Droop is increased, the supply frequency is reduced from its reference frequency, which is defined by Nominal frequency, Frequency offset and Base current reference. It is evident that

- Supply frequency of the convertor follows the droop behaviour as per Eqn. (7.1) the $f0$ is reference frequency, $k_P$ frequency droop and $P$ power supplied by Inverter.

$$f = f0 - k_P \cdot P \tag{7.1}$$

### 7.3.3 Test B – Grid connected mode - Internal Sync

This test is focused on the converters capability of synchronizing with the External Grid. Here the synchronization process is done using the internal sync command with the help of D7 card measurement. In the process, at first Breakers B1 & B2 are closed and subsequently when the converter output voltage is in sync, B3 is closed (Figure 7.2). Once it is synchronized, the parameters - Nominal frequency, Frequency offset, Frequency droop and Base current reference are varied to evaluate their influence on the operating behaviour. The measured values are noted in Table 7.3.

***Table 7.3:*** *Grid Connected Mode - Internal Sync command*

| Nominal Frequency (Hz) | Frequency Offset (Hz) | Frequency Droop (Hz) | Base Current Reference (%) | Supply Frequency (Hz) | Power Inverter (kW) | Power Grid (kW) | Power Load (kW) |
|---|---|---|---|---|---|---|---|
| 51.75 | -1 | 1 | 0 | 50 | 0 | 4.6 | -4.5 |
| 51.75 | -1 | 1 | 20 | 50 | 1.8 | 2.8 | -4.5 |
| 51.75 | -1 | 2 | 20 | 50 | 1.8 | 2.8 | -4.5 |
| 51.25 | -1 | 2 | 20 | 50 | 1.8 | 2.8 | -4.5 |
| 51.25 | -1 | 2 | 50 | 50 | 4.7 | -0.25 | -4.5 |
| 51.25 | -1 | 2 | 50 | 50 | 4.5 | -4.4 | 0 |

It can be summarized that

- When internal sync command is used for synchronization with External grid, the parameters - Nominal frequency, Frequency offset and Frequency droop would have no effect on operation, in other words no drooping behaviour.
- The power output from the converter can be controlled by modifying the Base current reference value, which means that converter is set to a Power set-point.
- The supply frequency is always 50 Hz.

### 7.3.4 Test C – Grid connected mode – Manual Sync

In this test, the primary concern is to check the applicability of the drooping behaviour even when connected to External Grid. This means that converter operates in Voltage Source mode rather than shifting its mode to Current Source mode. Initially, in the setup, only B1 & B2 are closed to operate in Islanded (I) / Stand-alone (SA) mode (Figure 7.2). To synchronize with the External Grid, a manual procedure is followed. The frequency and voltage set points are changed on the converter Human Machine Interface (HMI). Another way to change these values is to send commands from PLC for the required frequency and voltage values. As the voltage and frequency were matched, the command is send to close Breaker B3, when both Inverter and External Grid voltages are in phase, while observing on the oscilloscope. In practical scenarios, this command could be generated by a Check Synchronizing relay. Once synchronized, parameters - Nominal frequency, Frequency offset, Frequency droop and Base current reference are differed and the recorded values are presented in Table 7.4.

*Table 7.4: Grid Connected Mode – Manual Sync*

| Nominal Frequency (Hz) | Frequency Offset (Hz) | Frequency Droop (Hz) | Base Current Reference (%) | Supply Frequency (Hz) | Power Inverter (kW) | Power Grid (kW) | Power Load (kW) |
|---|---|---|---|---|---|---|---|
| 51 | -1 | 1 | 0 | 50 | 0 | 0 | 0 |
| 51.15 | -1 | 1 | 0 | 49.99 | 1.5 | -1.5 | 0 |
| 51.25 | -1 | 1 | 0 | 50 | 2.3 | -2.25 | 0 |
| 51.25 | -1 | 2 | 0 | 50.01 | 1.3 | -1.3 | 0 |
| 51.55 | -1 | 2 | 0 | 50 | 2.6 | -2.58 | 0 |
| 51.55 | -1 | 1 | 0 | 50 | 5.2 | -5.15 | 0 |
| 51.75 | -1 | 1 | 0 | 50 | 7.4 | -7.2 | 0 |
| 51.75 | -1 | 1 | 0 | 50 | 7.4 | -2.1 | -4.5 |
| 51.75 | -1 | 2 | 0 | 49.99 | 3.8 | 0.95 | -4.5 |
| 51.25 | -1 | 2 | 0 | 49.99 | 1.3 | 3.3 | -4.5 |
| 51.05 | -1 | 2 | 0 | 50 | 0.3 | 4.2 | -4.5 |
| 51 | -1 | 2 | 0 | 50 | 0 | 4.5 | -4.5 |
| 51 | -1 | 1 | 0 | 49.99 | 0 | 4.5 | -4.5 |

From the above results, it can be interpreted that

- When synchronization with External grid is done without using the internal sync command, the parameters - Nominal frequency, Frequency offset and Frequency droop influence the operation of the converter.
- The power output from the converter is regulated by the drooping behaviour - Nominal frequency and Frequency droop, as per Eqn. (7.1).
- Power balance is always maintained within the network. If excess power is generated by the converter than required by the load, the External Grid absorbs the difference and if there is shortage of power from the converter, the External Grid supplies the remaining power required by the load.
- The supply frequency is always 50 Hz.

## 7.4 Summary

To sum up, various tests were performed to comprehend the operating behaviour of the Inverter in Islanded and Grid Connected states and to evaluate the applicability of the proposed control strategy in both modes. The tests proved beneficial in knowing the operating mode and principles of the converter and the influence of parameters on the output voltage, current and power characteristics of the inverter. From the analysis, it is concluded that the VACON converter can operate as a VSI in Islanded and Grid Connected modes with the formulated control strategy, comprising of Frequency- Voltage and Droop control. This is a vital input for the practical realization of the CSGriP project.

# 8 Conclusions and Future work

After the various simulations and discussion of results supported by validation, general conclusions are drawn. Finally, some recommendations are proposed, which could be implemented for further improvement of the designed algorithms.

## 8.1 Conclusions

The CSGriP Cell is a MG comprising of DRES, BESS and controllable loads. Each of these components are modelled in PowerFactory software with associated controllers. The battery is modelled as a voltage source varying with SoC. The major component of each Cell is the converter of the BESS, which is essentially modelled as Voltage source, forming the grid parameters, frequency and voltage. So, this converter, following the droop control is naturally the grid forming element in SA mode. The DRES component, Solar and Wind, are defined as current sources feeding the grid. The loads are varying power elements in the Cell.

The prominent feature of the thesis is that no communication is involved for transfer of signals. Hence each Cell has to rely on measurement of local variables for operation of the Cell. The DRES control employs the SSM schemes for curtailing the excess renewable power, while the Load control utilizes the DSM schemes for shedding and restoration of loads. All these controls respond to the frequency signal, which is the only communicating signal in the system.

The initial part of the thesis was focussed on evaluating the grid performance and dynamics involved in connection and disconnection of a Cell to an External Grid (EG). Control schemes for connection and disconnection were formulated for enabling a smooth and seamless transition between SA and GC modes. However, in the proposed control strategy, the operation of the converter of the BESS is maintained in voltage source mode, though connected to EG. Simulations were performed for various scenarios and it is realized that the developed control schemes were successful in accomplishing a seamless transition.  It is observed that the associated frequency and voltage deviations are within grid code limits and overloading of the converter was avoided, even for extreme cases. Later, the same control scheme was expanded for connection and disconnection of multiple Cells, as a Cell cannot distinguish whether its connected/ disconnected to another Cell (IC mode) or an EG (GC mode). The simulations for multiple Cells prove the functionality of the developed control strategy for both mode transitions, SA to GC or IC and vice versa.

For technology demonstration, the developed control scheme is envisaged to be implemented as an interface to a converter of standard manufacturer. Experiments were performed on the proposed VACON converter for understanding its operating behaviour and to test the applicability of the control philosophy. From the tests performed, the converter follows the droop curve in SA condition in Microgrid mode, Using the internal sync command for connection to EG, forces the converter to change to current source mode, which is not desired in our case. However, the converter follows the droop curve, behave as voltage source converter, only when using an external sync command.

Finally, the thesis was focussed on development of decision-making algorithm for autonomous operation of the Cell and transfer between SA and IC modes. A decentralized approach is followed for the formulation of the algorithm due to absence of any kind of communication infrastructure. In the process, different rules are defined for the constructed Need Help (NH), Ready Help (RH) and Disconnect (DISC) states. The NH and RH states indicates that a Cell is in need help state and ready help condition respectively, which initiates the command for transfer of mode from SA to IC, connecting to Backbone (BB) bus. While the DISC state is utilized for disconnecting the Cell from the BB bus, which triggers the disconnection controller in the developed control scheme. The flow diagrams of NH, RH and DISC states are tested by simulating for autonomous operation of multiple Cells with different case scenarios. The simulation results illustrate that the decision-making algorithm was effective in maintaining the over stability of the system by sustaining a critical SoC for each Cell and minimizing the need for curtailment and load shedding.

However, there are limitations in developed decision-making algorithm when multiple Cells in the MG are achieving a higher SoC due to excess renewable power in each Cell. This is rather due to constraint of no communication between Cell regarding the State of Energy and Power (SEP). A better optimized solution could be formulated if a MGCC is employed. The modular and decentralized approach of the formulated control scheme and decision-making algorithm enables the system to be easily expandable by adding more Cells in desire to build a strong and robust MG network.

## 8.2 Future work

An area which would be worth exploring is the optimal tuning of the controllers. A steady state representation of the MG system may be derived and root locus analysis of the transfer functions would be helpful in establishing the value of gains of controllers. Similar analysis could be performed for evaluating the effect of droop constants on the system. A proper selection of the droop values would result in best operating point for the system, even during switching modes.

Furthermore, the developed decision-making algorithm was confined to Stand-alone and Interconnected operation of Cells. The algorithm could be further expanded for connection to main EG or even initiate the command for start-up of a Diesel Generator in case of emergency. So, in a way, the percentage of load shedding could be further decreased, thus increasing the reliability of power to the end consumers. Additionally, it is interesting to incorporate cost factors to the traded energy, so that each Cell could operate relentlessly at the least cost.

Finally, the pilot demonstration of the CSGriP control philosophy is planned in the month of November at ACRRES. It would be good to analyse the results obtained from the test site and compare with that of the simulated ones. Adaption or modification may be required in the control and system modelling to replicate the real-life implementation of CSGriP project.

# Bibliography


[1] International Energy Agency and World Bank, *Energy for All 2015-Progress Toward Sustainable Energy*. 2015.

[2] S. Parhizi, H. Lotfi, A. Khodaei, and S. Bahramirad, “State of the Art in Research on Microgrids: A Review,” *IEEE Access*, vol. 3, pp. 890–925, 2015.

[3] M. S. Mahmoud, S. Azher Hussain, and M. A. Abido, “Modeling and control of microgrid: An overview,” *J. Franklin Inst.*, vol. 351, no. 5, pp. 2822–2859, 2014.

[4] Z. Chen, W. Zhang, J. Cai, T. Cai, Z. Xu, and N. Yan, “A Synchronization Control Method for Micro-Grid with Droop Control,” pp. 519–524, 2015.

[5] J. Rocabert, A. Luna, F. Blaabjerg, and P. Rodríguez, “Control of power converters in AC microgrids,” *IEEE Trans. Power Electron.*, vol. 27, no. 11, pp. 4734–4749, 2012.

[6] E. Raaijen, “Sustainable Off-grid Powerstation for Rural Applications Sustainable Smart Micro Grids,” *Sustain. Smart Micro Grids Energy Storage, Alfen*, 2014.

[7] P. Fraser, “Distributed Generation in Liberalised Electricity Markets,” *Fr. Int. Energy Agency*, 2002.

[8] U. S. Irvin J. Balaguer-Álvarez, “Seamless Transitions between Grid-Connected and Stand-Alone Operations of Distributed Generation in Microgrids,” *Int. J. Eng. Res. Dev.*, vol. 10, no. 11, pp. 06–16, 2014.

[9] K. O. Oureilidis, E. A. Bakirtzis, and C. S. Demoulias, “Frequency-based control of islanded microgrid with renewable energy sources and energy storage,” *J. Mod. Power Syst. Clean Energy*, vol. 4, no. 1, pp. 54–62, 2016.

[10] R. Majumder, “Some Aspects of Stability in Microgrids,” *IEEE Trans. Power Syst.*, vol. 28, no. 3, pp. 3243–3252, Aug. 2013.

[11] M. Ahmed, Y. Kang, and Y.-C. Kim, “Communication Network Architectures for Smart-House with Renewable Energy Resources,” *Energies*, vol. 8, no. 8, pp. 8716–8735, Aug. 2015.

[12] C. N. Papadimitriou, V. A. Kleftakis, and N. D. Hatziargyriou, “Control strategy for seamless transition from islanded to interconnected operation mode of microgrids,” *J. Mod. Power Syst. Clean Energy*, vol. 5, no. 2, pp. 169–176, Mar. 2016.

[13] In-Su Bae and Jin-O Kim, “Reliability Evaluation of Customers in a Microgrid,” *IEEE Trans. Power Syst.*, vol. 23, no. 3, pp. 1416–1422, Aug. 2008.

[14] A. Llaria, O. Curea, J. Jiménez, and H. Camblong, “Survey on microgrids: Unplanned islanding and related inverter control techniques,” *Renew. Energy*, vol. 36, no. 8, pp. 2052–2061, Aug. 2011.

[15] R. Lasseter *et al.*, “Integration of distributed energy resources. The CERTS Microgrid Concept,” Berkeley, CA, Apr. 2002.

[16] P. Gaur and S. Singh, “Investigations on Issues in Microgrids,” *J. Clean Energy Technol.*, vol. 5, no. 1, pp. 47–51, 2017.

[17] A. Arulampalam, M. Barnes, A. Engler, A. Goodwin, and N. Jenkins, “Control of power electronic interfaces in distributed generation microgrids,” *Int. J. Electron.*, vol. 91, no. 9, pp. 503–523, Sep. 2004.

[18] H. Zareipour, K. Bhattacharya, and C. Canizares, “Distributed generation: Current status and challenges,” *Naps’04*, no. August, pp. 1–8, 2004.

[19] D. Bakken and K. Iniewski, "Smart grids : clouds, communications, open source, and

automation."

[20] P. Dondi, D. Bayoumi, C. Haederli, D. Julian, and M. Suter, “Network integration of distributed power generation,” *J. Power Sources*, vol. 106, no. 1–2, pp. 1–9, Apr. 2002.

[21] M. Bollen, J. Zhong, O. Samuelsson, and J. Bjornstedt, “Performance indicators for microgrids during grid-connected and island operation,” in *2009 IEEE Bucharest PowerTech*, 2009, pp. 1–6.

[22] B. Lasseter, “Microgrids - Distributed power generation,” in *2001 IEEE Power Engineering Society Winter Meeting. Conference Proceedings (Cat. No.01CH37194)*, vol. 1, pp. 146–149.

[23] G. Pepermans, J. Driesen, D. Haeseldonckx, R. Belmans, and W. D’haeseleer, “Distributed generation: Definition, benefits and issues,” *Energy Policy*, vol. 33, no. 6, pp. 787–798, 2005.

[24] S. Morozumi, “Micro-grid Demonstration Projects in Japan,” in *2007 Power Conversion Conference - Nagoya*, 2007, pp. 635–642.

[25] S. Koohi-Kamali, V. V. Tyagi, N. A. Rahim, N. L. Panwar, and H. Mokhlis, “Emergence of energy storage technologies as the solution for reliable operation of smart power systems: A review,” *Renew. Sustain. Energy Rev.*, vol. 25, pp. 135–165, 2013.

[26] L. J. Ricalde, E. Ordonez, M. Gamez, and E. N. Sanchez, “Design of a smart grid management system with renewable energy generation,” in *2011 IEEE Symposium on Computational Intelligence Applications In Smart Grid (CIASG)*, 2011, pp. 1–4.

[27] L. Xu, “Modeling, Analysis and Control of Voltage-Source Converter in Microgrids and HVDC,” *Grad. Theses Diss.*, 2013.

[28] Institute of Electrical and Electronics Engineers, *ICSTCC : 2012 16th International Conference on System Theory, Control and Computing : joint conference SINTES 16, SACCS 12, SIMSIS 16, proceedings : October 12-14, 2012, Sinaia, Romania.* [IEEE], 2012.

[29] J. M. Guerrero, M. Chandorkar, T.-L. Lee, and P. C. Loh, “Advanced Control Architectures for Intelligent Microgrids—Part I: Decentralized and Hierarchical Control,” *IEEE Trans. Ind. Electron.*, vol. 60, no. 4, pp. 1254–1262, Apr. 2013.

[30] T. Dragicevic, J. M. Guerrero, and J. C. Vasquez, “A Distributed Control Strategy for Coordination of an Autonomous LVDC Microgrid Based on Power-Line Signaling,” *IEEE Trans. Ind. Electron.*, vol. 61, no. 7, pp. 3313–3326, Jul. 2014.

[31] J. Schiffer, R. Ortega, A. Astolfi, J. Raisch, and T. Sezi, “Conditions for stability of droop-controlled inverter-based microgrids,” *Automatica*, vol. 50, no. 10, pp. 2457–2469, 2014.

[32] J. M. Guerrero, L. Hang, and J. Uceda, “Control of Distributed Uninterruptible Power Supply Systems,” *IEEE Trans. Ind. Electron.*, vol. 55, no. 8, pp. 2845–2859, 2008.

[33] A. Engler, “Applicability of droops in low voltage grids,” *Int. J. Distrib. Energy Resour. Smart Grids*, no. 1, pp. 1–5, 2005.

[34] T. Vral, “Frequency Based Microgrid Control - Demand Side Management & Supply Side Management using Grid Frequency in a Cellular Grid,” Delft University of Technology, 2016.

[35] A. Engler and N. Soultanis, “Droop control in LV-grids,” *2005 Int. Conf. Futur. Power Syst.*, p. 6 pp.-pp.6, 2005.

[36] K. De Brabandere *et al.*, “A voltage and frequency droop control method for parallel inverters,” *Power Electron. Spec. Conf. 2004. PESC 04. 2004 IEEE 35th Annu.*, vol. 4, no. 4, p. 2501–2507 Vol.4, 2004.

[37] J. Schiffer, T. Seel, J. Raisch, and T. Sezi, “Voltage Stability and Reactive Power Sharing in Inverter-Based Microgrids With Consensus-Based Distributed Voltage Control,” *IEEE Trans. Control Syst. Technol.*, vol. 24, no. 1, pp. 96–109, Jan. 2016.

[38] UNIDO, “Demand-side management in Sustainable Energy Regulation and Policymarking for Africa,” *REEP*, p. Chap. 14, 14.1–14.48., 2008.

[39] T. Zhang, D. Yue, M. J. O’Grady, and G. M. P. O’Hare, “Transient oscillations analysis and modified control strategy for seamless mode transfer in micro-grids: A wind-PV-ES hybrid system case study,” *Energies*, vol. 8, no. 12, pp. 13758–13777, 2015.

[40] D. Das, G. Gurrala, and U. J. Shenoy, “Transition from Grid Connected Mode to Islanded Mode in VSI fed Microgrids,” *Sādhanā*, pp. 1–2, 2016.

[41] S. Li and B. Ke, “Study of battery modeling using mathematical and circuit oriented approaches,” in *2011 IEEE Power and Energy Society General Meeting*, 2011, pp. 1–8.

[42] D. Fregosi, S. Bhattacharya, and S. Atcitty, “Empirical battery model characterizing a utility-scale carbon-enhanced VRLA battery,” in *2011 IEEE Energy Conversion Congress and Exposition*, 2011, pp. 3541–3548.

[43] H. Culcu, B. Verbrugge, N. Omar, P. van den Bossche, and J. van Mierlo, “Internal resistance of cells of lithium battery modules with FreedomCAR model,” *World Electr. Veh. J.*, vol. 3, no. 1, pp. 702–710, 2009.

[44] V. Ramadesigan, P. W. C. Northrop, S. De, S. Santhanagopalan, R. D. Braatz, and V. R. Subramanian, “Modeling and Simulation of Lithium-Ion Batteries from a Systems Engineering Perspective,” *J. Electrochem. Soc.*, vol. 159, no. 3, pp. R31–R45, 2012.

[45] R. Scharrenberg, “CSGriP – System dimensions: comparison of Burundi and the Netherlands,” 2016.

[46] DIgSILENT GmbH, “DIgSILENT PowerFactory Technical Reference Documentation PWM Converter.”

[47] M. Huang, F. Blaabjerg, Y. Yang, and W. Wu, “Step by step design of a high order power filter for three-phase three-wire grid-connected inverter in renewable energy system,” *2013 4th IEEE Int. Symp. Power Electron. Distrib. Gener. Syst. PEDG 2013 - Conf. Proc.*, 2013.

[48] Khaled H.Ahmed, “Passive filter design for three phase inverter interfacing in distributed generation,” *Electr. power Qual. uitilisation*, vol. XIII, no. 2, pp. 49–58, 2007.

[49] A. E. W. H. Kahlane, L. Hassaine, and M. Kherchi, “LCL filter design for photovoltaic grid connected systems,” *Third Int. Semin. new Renew. energies*, vol. 8, no. 2, pp. 227–232, 2014.

[50] M. Hojabri, M. Hojabri, and A. Toudeshki, “Passive damping filter design and application for three-phase pv grid-connected inverter 1,” vol. 2, no. 6, pp. 50–56, 2015.

[51] A. Reznik, M. G. Simoes, A. Al-Durra, and S. M. Muyeen, “LCL filter design and performance analysis for grid-interconnected systems,” *IEEE Trans. Ind. Appl.*, vol. 50, no. 2, pp. 1225–1232, 2014.

[52] M. Ben Sad-Romdhane, M. W. Naouar, I. S. Belkhodja, and E. Monmasson, “Simple and systematic LCL filter design for three-phase grid-connected power converters,” *Math. Comput. Simul.*, vol. 130, pp. 181–193, 2016.

[53] M. Liserre, F. Blaabjerg, and S. Hansen, “Design and control of an LCL-filter-based three-phase active rectifier,” *IEEE Trans. Ind. Appl.*, vol. 41, no. 5, pp. 1281–1291, 2005.

[54] T. C. Y. Wang, Z. Y. Z. Ye, G. S. G. Sinha, and X. Y. X. Yuan, “Output Filter Design for A Grid-Interconnected Three-Phase Inverter,” *IEEE 34th Annu. Conf. Power Electron. Spec. 2003 PESC 03*, vol. 2, pp. 779–784, 2003.

[55] D. Powerfactory, “DIgSILENT PowerFactory Technical Reference Documentation Static Generator,” vol. 1, pp. 1–40, 2015.

[56] H. (Cooper D. A. Markiewicz and A. (Wroclaw U. of T. Klajn, “Voltage Disturbances,” *Power Qual. Appl. Guid.*, vol. 5.4.2, pp. 4–11, 2004.

[57] P. (Prabha) Kundur, N. J. Balu, and M. G. Lauby, *Power system stability and control*. New York: McGraw-Hill, 1994.

[58] DIgSILENT GmbH, “DIgSILENT PowerFactory Technical Reference Documentation Low-Voltage Load and Partial LV-Load.”

[59] V. D. N. V. E.ON Netz GmbH, “TransmissionCode 2007. Network and System Rules of the German Transmission System Operators,” *August*, no. August, 2007.

[60] D. Powerfactory, “DIgSILENT PowerFactory Technical Reference Documentation - Lines,” 2015.

[61] Z. Miao *et al.*, “An SOC-Based Battery Management System for Microgrids,” *IEEE Trans. Smart Grid*, vol. 5, no. 2, pp. 966–973, 2014.

[62] D. Zhao, N. Zhang, and Y. Liu, “Micro-grid connected/islanding operation based on wind and PV hybrid power system,” *2012 IEEE Innov. Smart Grid Technol. - Asia, ISGT Asia 2012*, pp. 1–6, 2012.

[63] N. Bilidis, “Seamless Transitions of multiple Micro-grids between the Backbone Interconnected and the Islanded Operational Modes,” Delft University of Technology, 2016.

[64] R. Teodorescu, M. Liserre, and P. Rodríguez, *Grid converters for photovoltaic and wind power systems*. .

[65] B. B. Asare *et al.*, “Minutes CSGriP meeting September 2016,” no. 25, pp. 1–5, 2016.

[66] J. V. Ug. and B. V. Ug. Jan Desmet UGent , Colin Debruyne UGent and (2010), *Implementation of innovative renewable energy sources and their interaction on the distribution network*. Howest. Lemcko, 2010.

[67] N. Boccard, “Capacity factor of wind power realized values vs. estimates,” *Energy Policy*, vol. 37, no. 7, pp. 2679–2688, Jul. 2009.

[68] A. W. S. Kaas and P. Bauer, “Design approaches for a sustainable off-grid power system,” in *IECON 2011 - 37th Annual Conference of the IEEE Industrial Electronics Society*, 2011, pp. 3129–3133.

[69] C.-M. Young, C.-C. Liu, and C.-H. Liu, “New inverter-driven design and control method for two-phase induction motor drives,” *IEE Proc. - Electr. Power Appl.*, vol. 143, no. 6, p. 458, 1996.

[70] R. H. Bonn, “Developing a next generation PV inverter,” in *Conference Record of the Twenty-Ninth IEEE Photovoltaic Specialists Conference, 2002.*, pp. 1352–1355.

[71] R. J. Pasterczyk, J.-M. Guichon, J.-L. Schanen, and E. Atienza, “PWM Inverter Output Filter Cost-to-Losses Tradeoff and Optimal Design,” *IEEE Trans. Ind. Appl.*, vol. 45, no. 2, pp. 887–897, 2009.

[72] Vacon, “Technical Document: Grid Converter Application,” 2013.

# Appendices

# A

The connection control of a Cell to the EG was tested for varying SoC of BESS. The Table A.1 shows the various signals: Frequency before connection, Connection command, Frequency deviation and Converter overloading, linked with state change over from SA to GC, after trigger initiation at 10 s. Similarly, the disconnection control was evaluated for varying SoC, with initiation command at 30 s. The power flow to/from the EG at the moment of command trigger and the final disconnect signal for switching from GC to SA mode are represented in Table A.2.

***Table A.1:*** *Cell signals for Connection to EG at varying SoC*

| SoC (%) | Frequency before connection (Hz) | Connect Signal (s) | Maximum/minimum frequency deviation (Hz) | Converter Power limits |
|---|---|---|---|---|
| 10 | 48.62 | 15.3 | 50.24 | √ |
| 20 | 49.22 | 16.0 | 50.34 | √ |
| 30 | 49.82 | 18.5 | 50.44 | √ |
| 40 | 49.92 | 16.5 | 50.46 | √ |
| 50 | 50.02 | 14.5 | 50.48 | √ |
| 60 | 50.09 | 12.3 | 50.07 | √ |
| 70 | 50.15 | 21.4 | 49.67 | √ |
| 80 | 50.22 | 24 | 49.69 | √ |
| 90 | 51.53 | 13.9 | 49.90 | √ |

***Table A.2:*** *Cell signals for Disconnection to EG at varying SoC*

| SoC (%) | Disconnect Signal (s) | Active Power flow from EG for disconnection (kW) |
|---|---|---|
| 10 | 33.25 | 104.05 |
| 20 | 33.25 | 104.05 |
| 30 | 33.25 | 104.05 |
| 40 | 33.15 | 61.35 |
| 50 | 32.80 | -16.05 |
| 60 | 33.05 | -67.05 |
| 70 | 33.3 | -121.35 |
| 80 | 33.7 | -135.40 |
| 90 | 33.7 | -135.40 |

# B

Analogous to the simulations performed for a week in May, the MG in Figure 6.43, with the same parameters as specified in the Section 6.4.7, was simulated for a week in November. The Figure B.1 and Figure B.2 represent the State and SoC of the MG with and without decision-making algorithm.

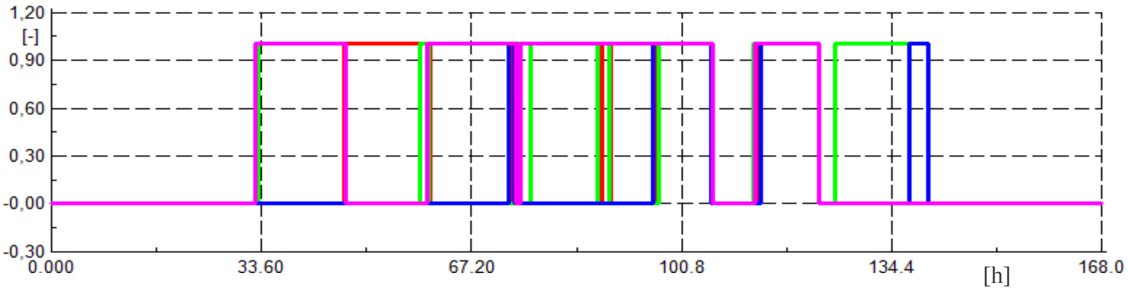


(a) State: 0 - Stand-alone, 1- Interconnected mode

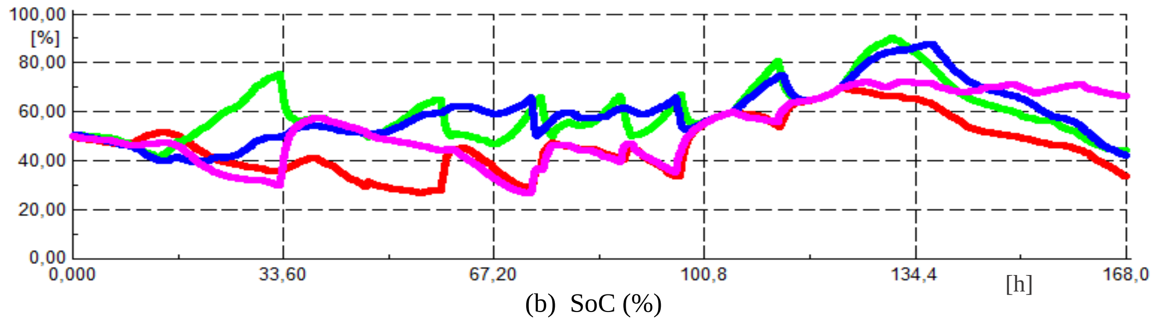


(b) SoC (%)

Cell 1 Cell 2 Cell 3 Cell 4

***Figure B.1:*** *Graphs for a week of November: State and SoC (with decision-making algorithm)*

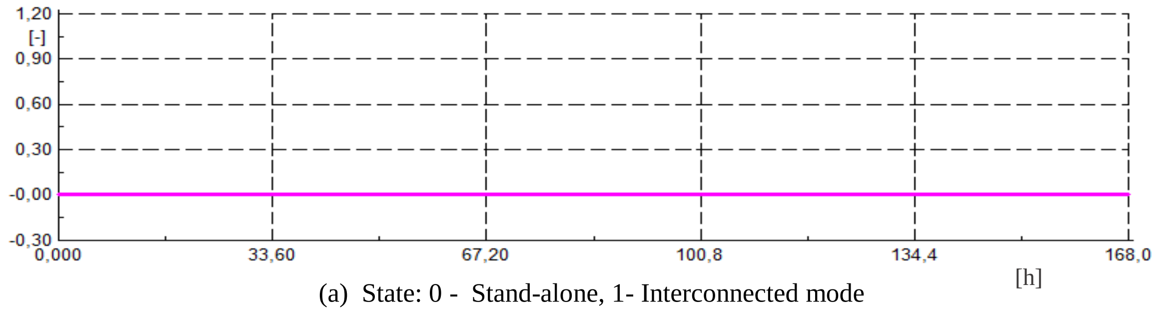


(a) State: 0 - Stand-alone, 1- Interconnected mode

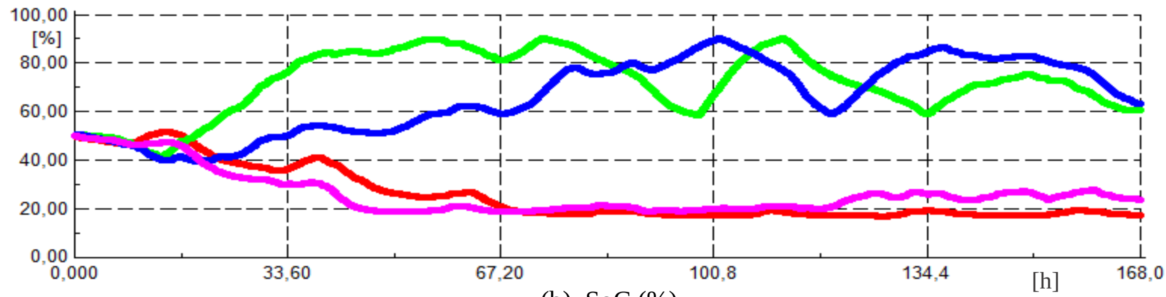


(b) SoC (%)

Cell 1 Cell 2 Cell 3 Cell 4

***Figure B.2:*** *Graphs for a week of November: State and SoC (w/o decision-making algorithm)*

The Table B.1 gives an overview of the results for both scenarios with and without Decision-making algorithm. As seen, the average SoC of the batteries in MG has improved in case of inclusion of decision-making algorithm has improved along with limiting the percentage of load shedding and curtailment.

***Table B.1:*** *Comparison of results with and without Decision-making algorithm - November*

| *Simulation* | *With Decision-making algorithm* | | | | *W/o Decision-making algorithm* | | | |
|---|---|---|---|---|---|---|---|---|
| *Cell* | 1 | 2 | 3 | 4 | 1 | 2 | 3 | 4 |
| SoC at start of week (%) | 50 | 50 | 50 | 50 | 50 | 50 | 50 | 50 |
| Curtailment (%) | 0 | 3.23 | 2.7 | 0 | 0 | 15.91 | 14.23 | 0 |
| Load Shedding (%) | 0 | 0 | 0 | 0 | 42.12 | 0 | 0 | 29.84 |
| Average SoC (%) | 46.63 | 59.51 | 58.90 | 52.84 | 25.61 | 72 | 66.05 | 26.20 |

# C

## Single Cell (Dis)Connection to External Grid - Stand-alone & Grid-connected modes

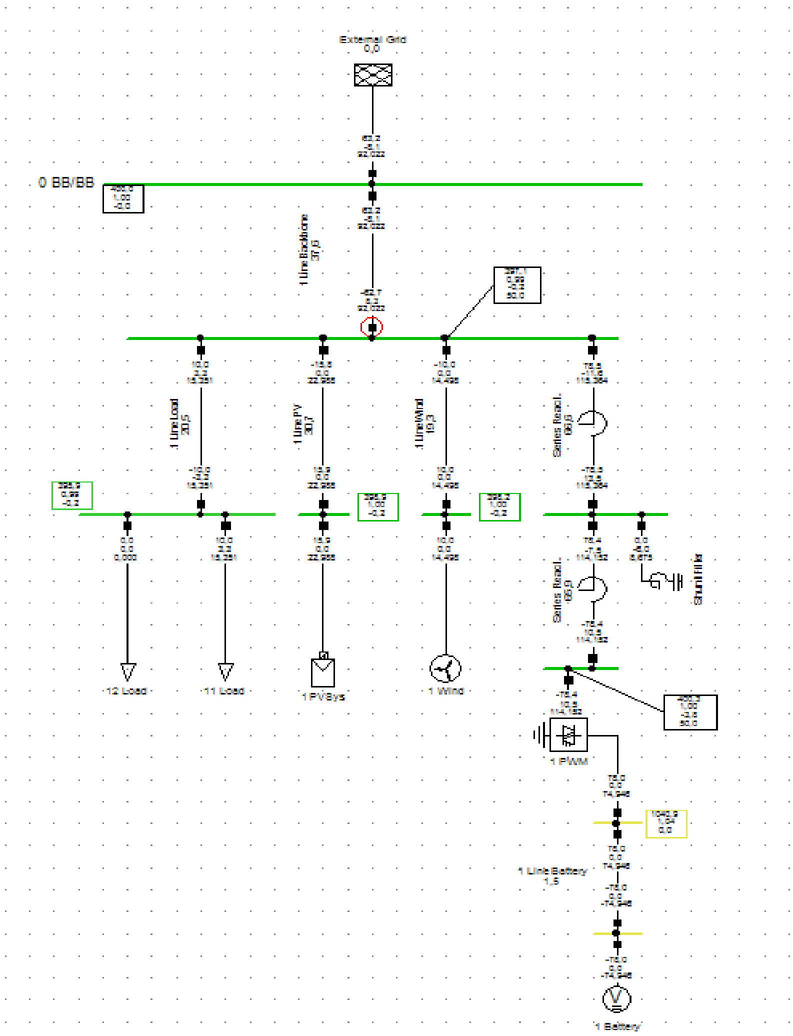


A Cell is a MG that can either operate in Stand-alone (SA) and Grid-connected (GC) modes. It comprises of the following components

1) Battery Energy Storage System (BESSS)
    a. Battery with base DC voltage of 1000 V and AC voltage of 400 V
    b. Converter (VSC) modelled as voltage source in all modes – Grid-forming element
2) Distributed Renewable Energy Resources (DRES)
    a. Solar modelled as current source – Grid-feeding element
    b. Wind modelled as current source – Grid-feeding element
3) Controllable loads
4) Backbone bus (BB)
5) External Grid (EG)

## Master Frame

The operation and control of Cell with the EG is performed through the Master Frame. It consists of

1) PLC Control – Formulates the frequency ($f_o$) and voltage ($U_o$) set-points to the converter, which is linked to PLC Controller frame.
2) VACON Inverter –This generates the voltage signal of desired magnitude and frequency, Linked to Inverter frame.
3) Measure Signals – Measures all the required signals for process in PLC control.

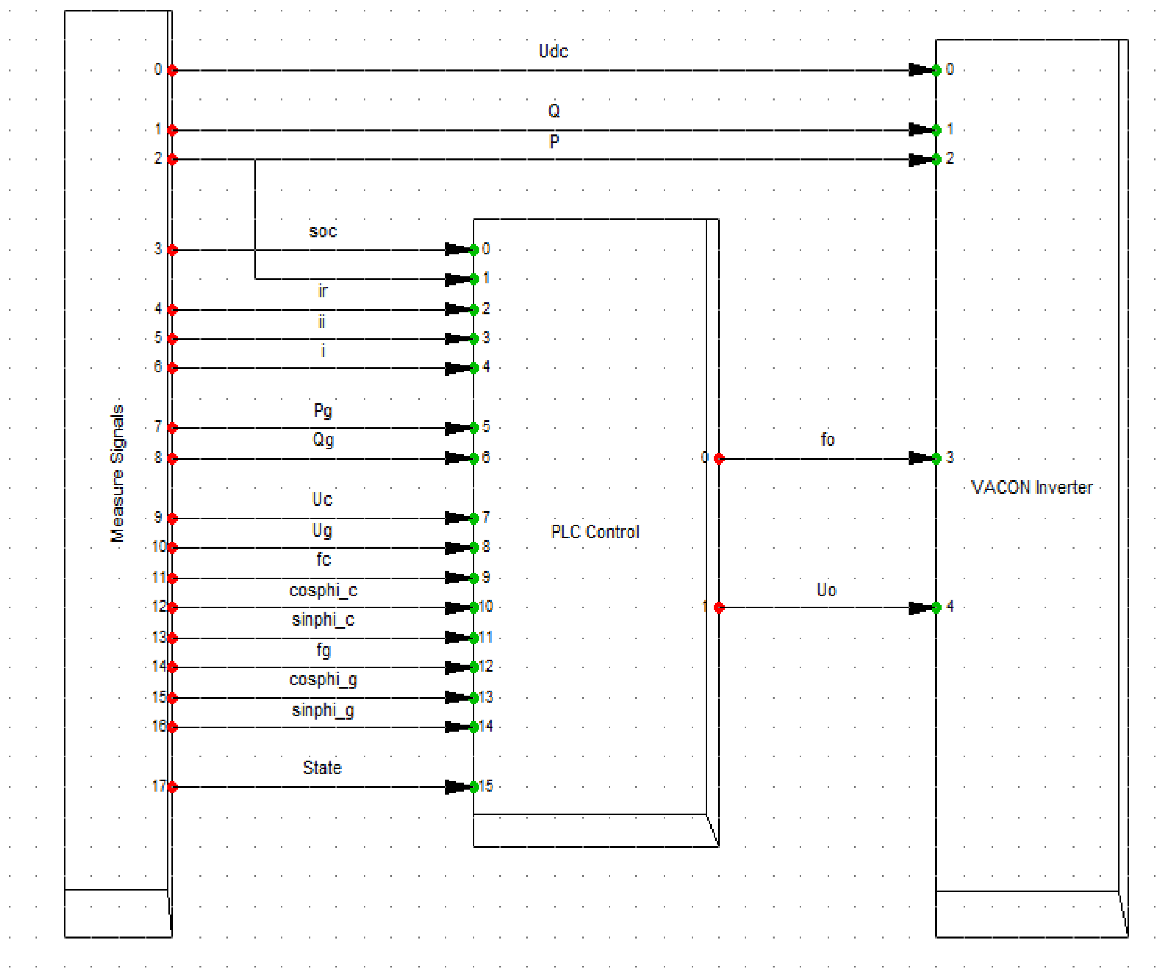

## *Inverter Frame*

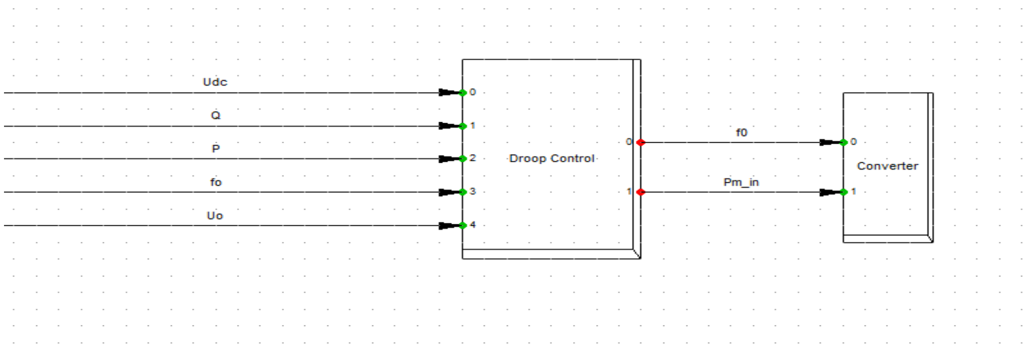


Droop Control is implemented in the Inverter frame and the final control inputs, Frequency of output voltage (f0) and Pulse Width Modulation index (Pm_in) are delivered to the PWM Converter.

| *Droop Control Parameters* | | |
|---|---|---|
| Active Power Droop coefficient (%) | $k_P$ | 0.3 |
| Reactive Power Droop coefficient (%) | $k_Q$ | 2 |

## *PLC Controller frame*

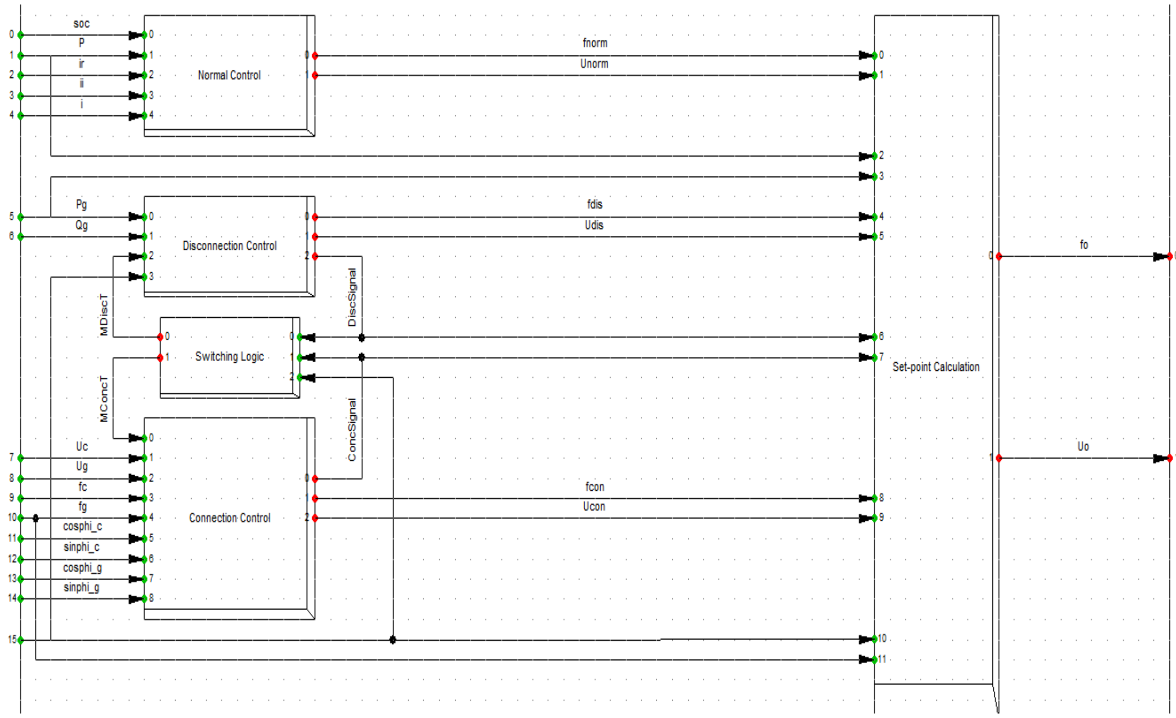


PLC Controller Frame comprises of

1) Normal Controller
2) Connection Controller
3) Disconnection Controller
4) Set-point calculation
5) Switching Logic

## *Normal Controller*

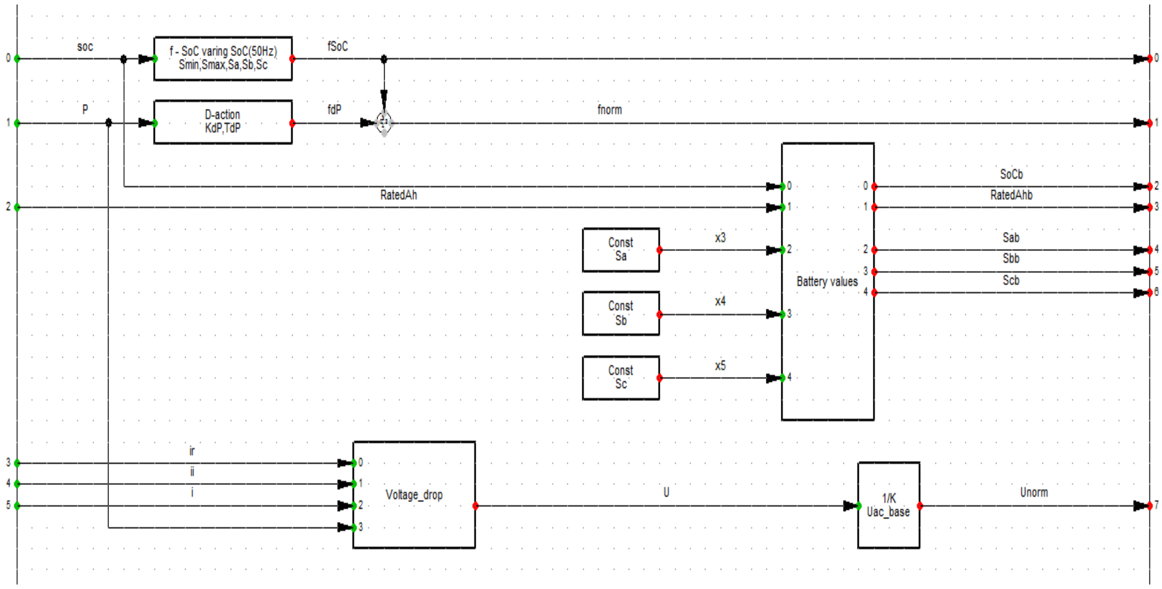


| Normal Controller Parameters | | |
|---|---|---|
| Frequency - SoC curve (%) | $SoC_{min}$ | 0 |
| | $S_a$ | 30 |
| | $S_c$ | 50 |
| | $S_b$ | 80 |
| | $SoC_{max}$ | 90 |
| Derivative gain | $K_{dP}$ | -0.001 |
| Derivative time | $T_{dp}$ | 1 |

## *Connection Controller*

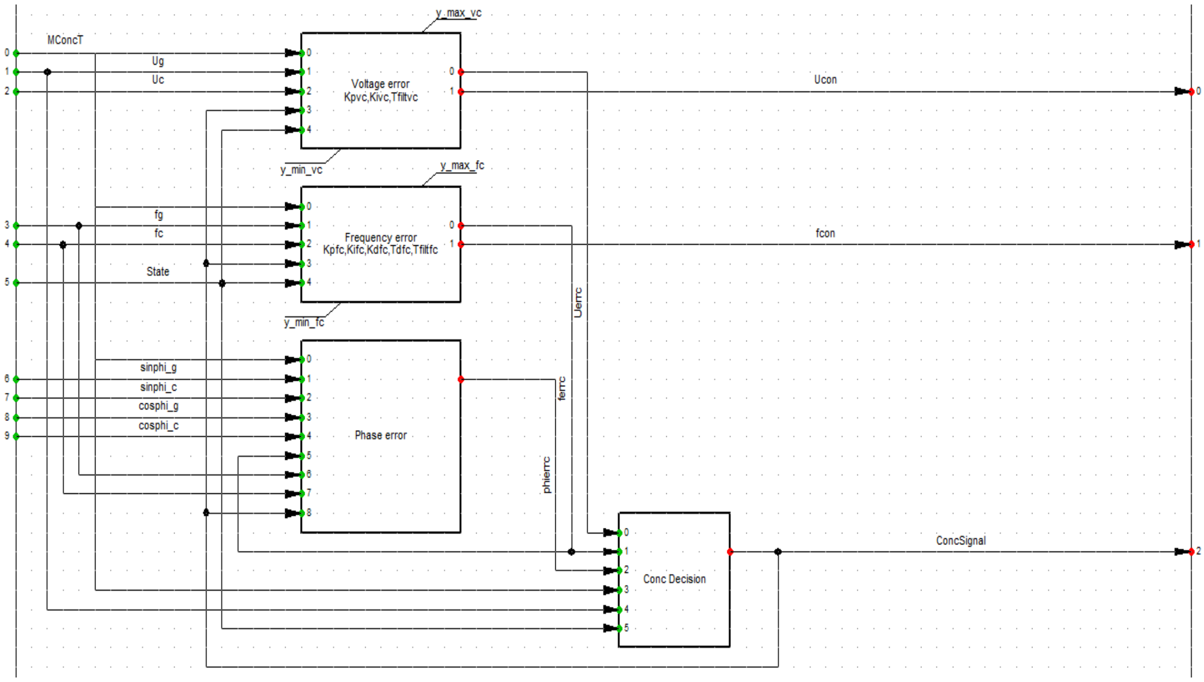

## Connection Controller – Frequency error

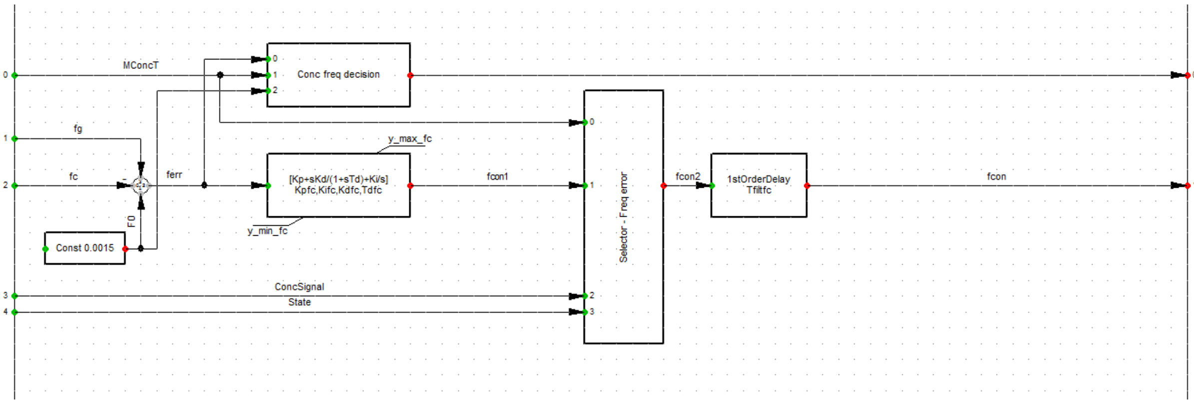


| *Connection Controller - Frequency Error Parameters* | | |
|---|---|---|
| Proportional gain | $K_{pfc}$ | 3 |
| Integral gain | $K_{ifc}$ | 5 |
| Derivative gain | $K_{dfc}$ | 1 |
| Derivative time | $T_{dfc}$ | 0.05 |
| Maximum anti -wind up limiter | $y\_max\_fc$ | 0.05 |
| Minimum anti- wind up limiter | $y\_min\_fc$ | -0.05 |
| Delay filter | $T_{filtfc}$ | 0.5 |

## Connection Controller – Voltage error

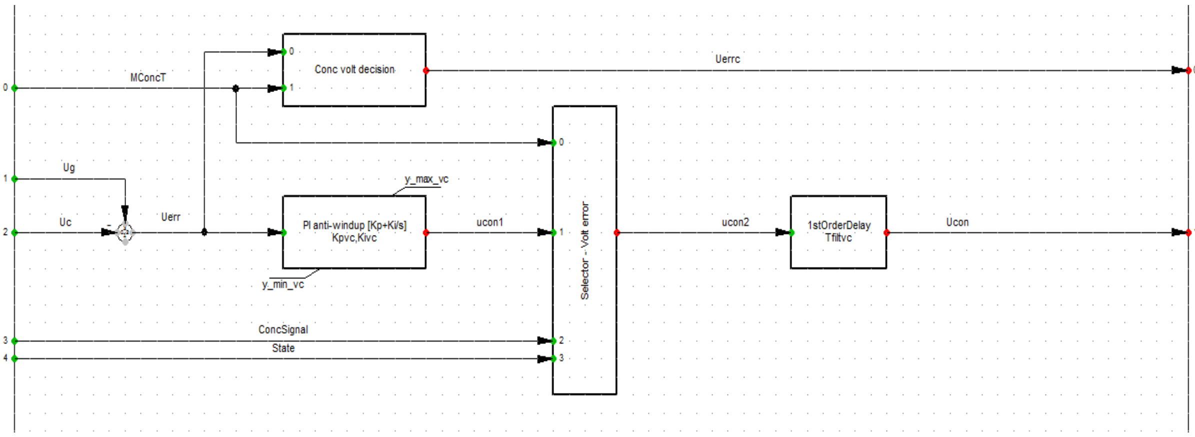


| *Connection Controller - Voltage Error Parameters* | | |
|---|---|---|
| Proportional gain | $K_{pvc}$ | 10 |
| Integral gain | $K_{ivc}$ | 0.5 |
| Maximum anti - wind up limiter | $y\_max\_vc$ | 0.02 |
| Minimum anti - wind up limiter | $y\_min\_vc$ | -0.02 |
| Delay filter | $T_{filtvc}$ | 0.5 |

## *Disconnection Controller*

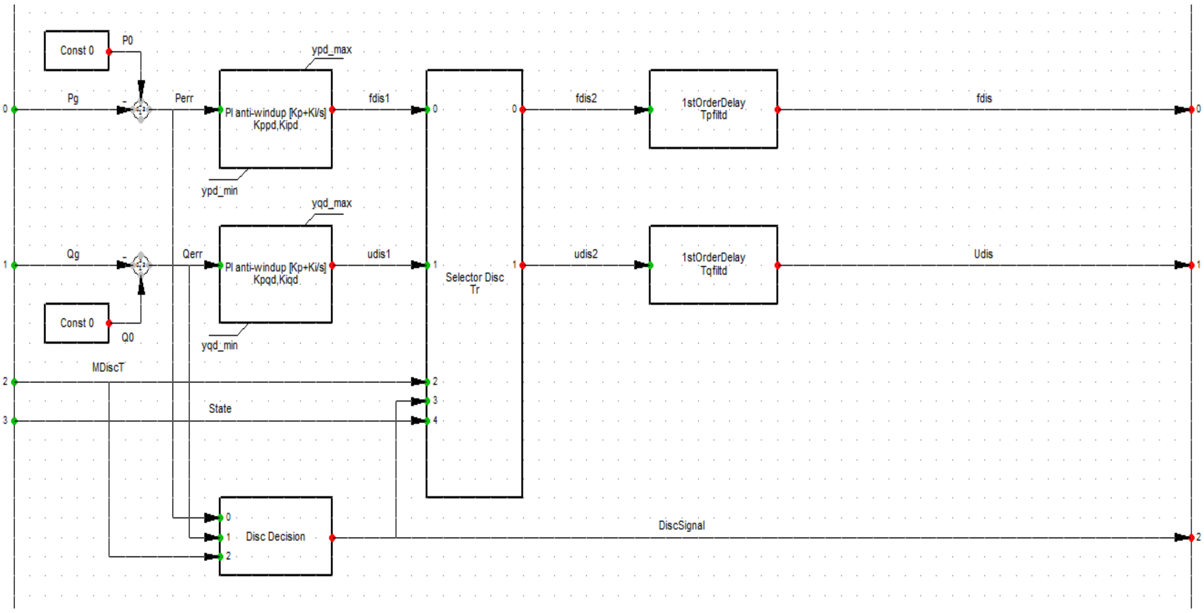


| *Disconnection Controller – P Error Parameters* | | |
|---|---|---|
| Proportional gain | $K_{ppd}$ | 0.05 |
| Integral gain | $K_{ipd}$ | 0.1 |
| Maximum anti - wind up limiter | $y\_max\_pd$ | 0.004 |
| Minimum anti - wind up limiter | $y\_min\_pd$ | -0.004 |
| Delay filter | $T_{filtpd}$ | 0.2 |

| *Disconnection Controller – Q Error Parameters* | | |
|---|---|---|
| Proportional gain | $K_{pqd}$ | 5 |
| Integral gain | $K_{iqd}$ | 20 |
| Maximum anti - wind up limiter | $y\_max\_qd$ | 0.01 |
| Minimum anti - wind up limiter | $y\_min\_qd$ | -0.01 |
| Delay filter | $T_{filtqd}$ | 0.2 |

# Multiple Cells with Decision-making Algorithm - Stand-alone & Interconnected modes

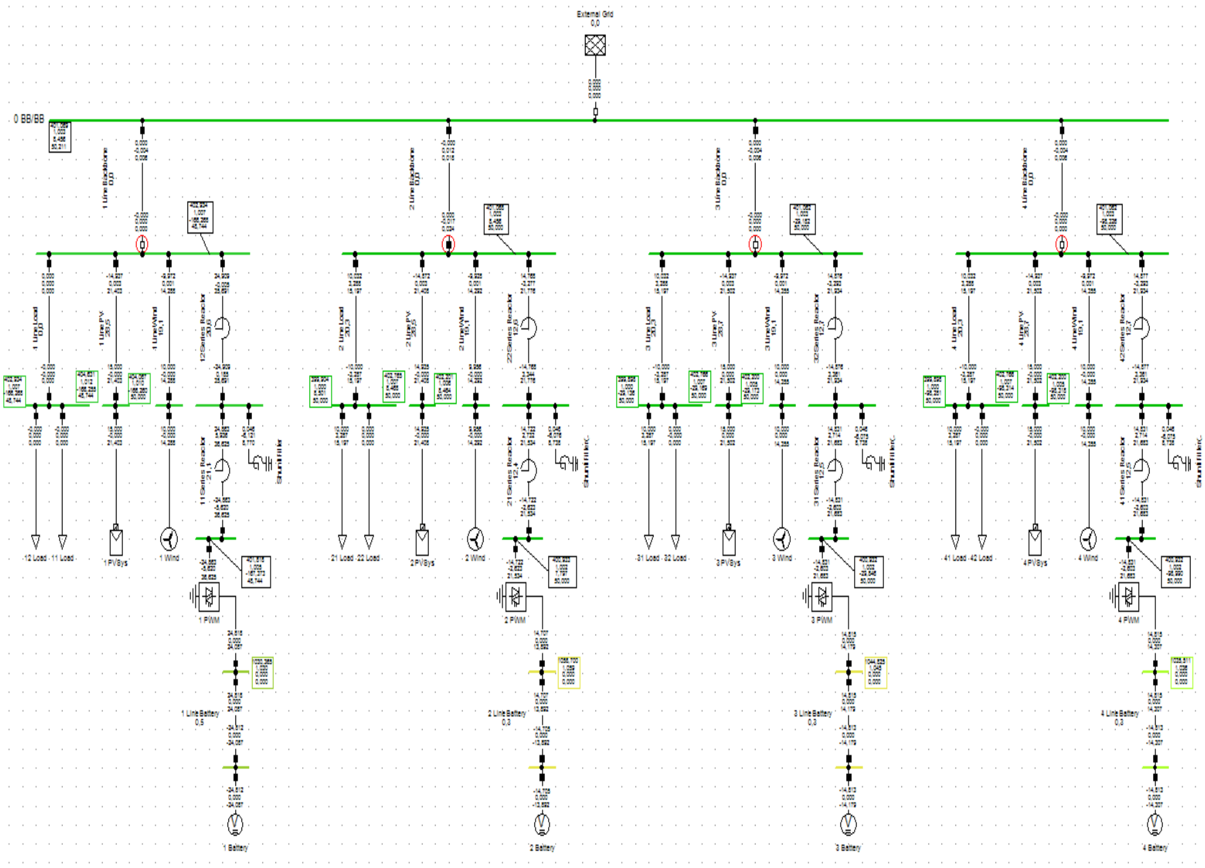

The MG consists of 4 Cells that can either operate in Stand-alone (SA) and Interconnected (IC) mode through Backbone (BB) bus. Each Cell comprises of the following components

1) Battery Energy Storage System (BESSS)
    a. Battery with base DC voltage of 1000 V and AC voltage of 400 V
    b. Converter (VSC) modelled as voltage source in all modes – Grid-forming element
2) Distributed Renewable Energy Resources (DRES)
    a. Solar modelled as current source – Grid-feeding element
    b. Wind modelled as current source – Grid-feeding element

## Master Frame

The operation and control of Cell with the EG is performed through the Master Frame. It consists of

1) PLC Control – Formulates the frequency $(f_o)$ and voltage $(U_o)$ set-points to the converter, which is linked to Controller frame.
2) VACON Inverter –This generates the voltage signal of desired magnitude and frequency, Linked to Inverter frame.
3) Decision Module – Generates the Connection Enable (MConcT) and Disconnection Enable (MDiscT) based on the devised decentralized decision-making algorithm. Linked to Decision frame.
4) Measure Signals – Measures all the required signals for process in PLC control.

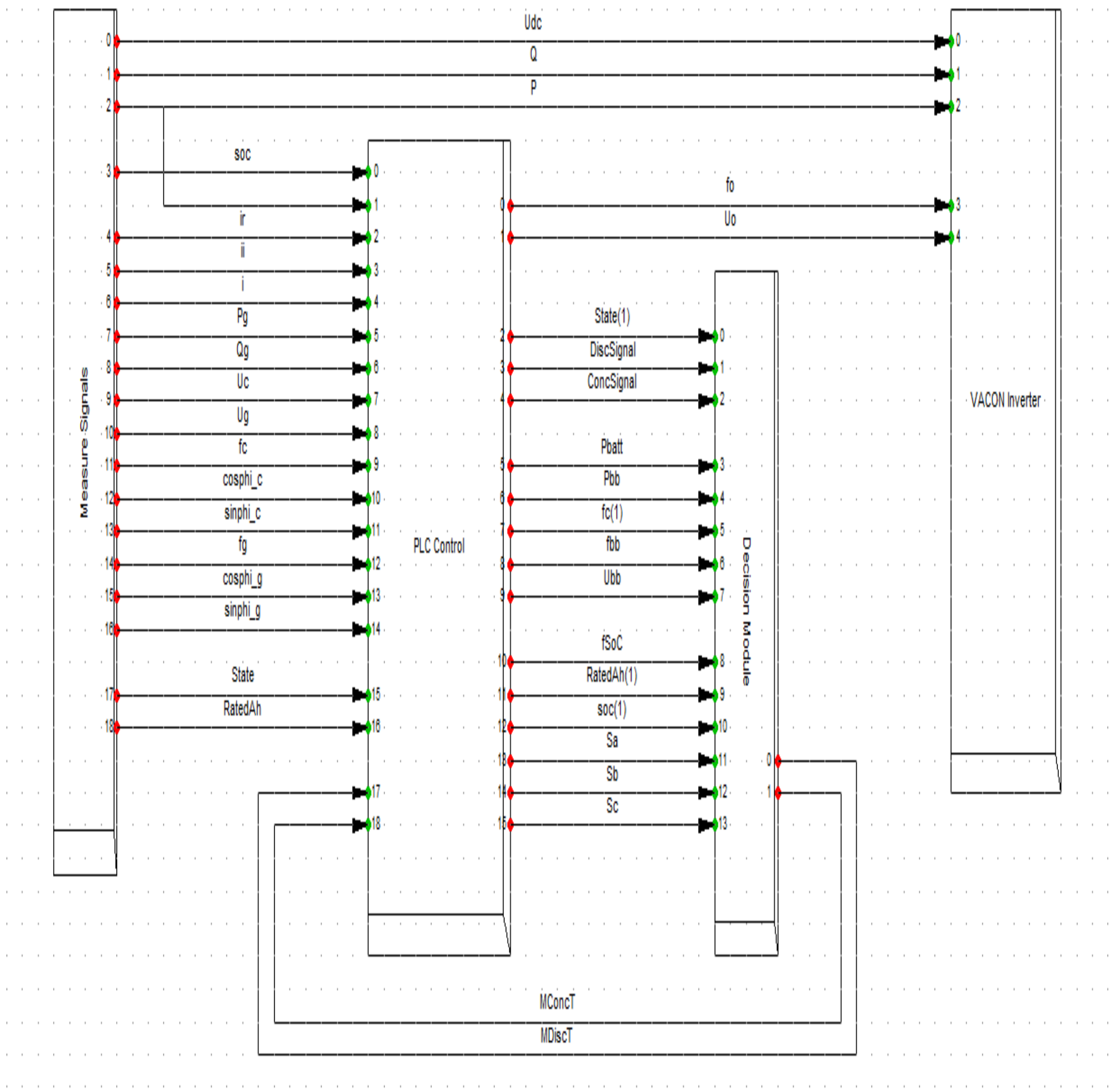

## Inverter Frame

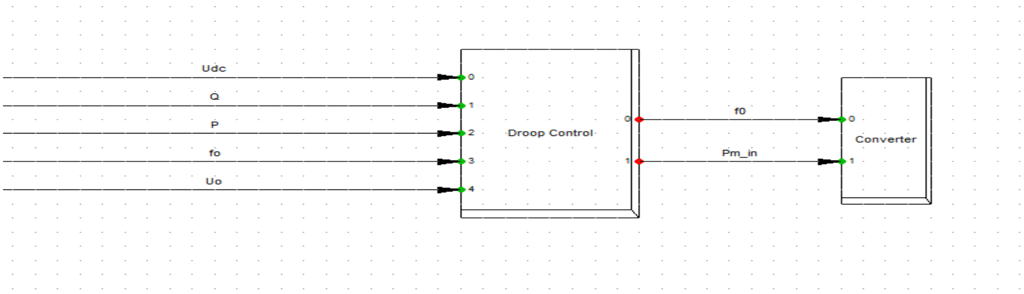


Droop Control is same as that of a Single Cell for all the 4 Cells with the same parameters.

## Controller frame

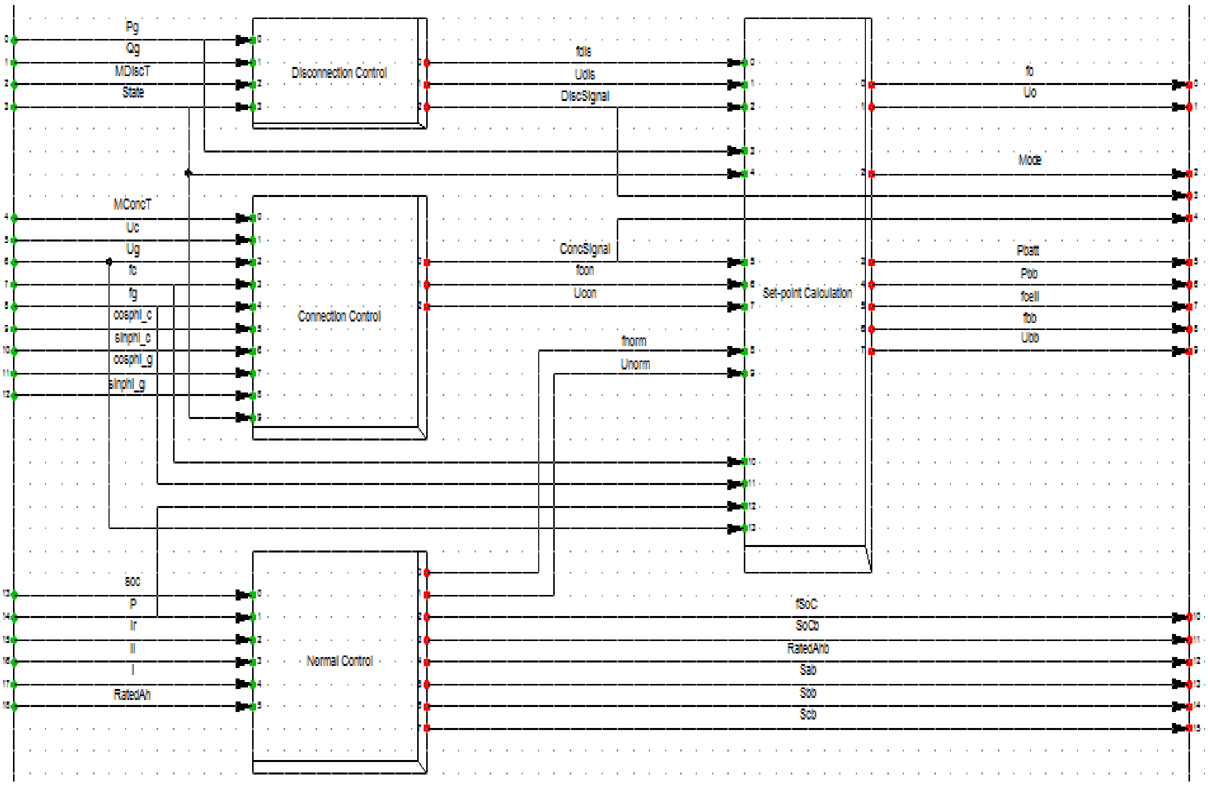


Controller frame comprises of

1) Normal Controller
2) Connection Controller
3) Disconnection Controller
4) Set-point calculation

The Normal, Connection and Disconnection controllers as similar to Single Cell are implemented in each of the 4 Cells with the same defined parameters.

## *Decision frame*

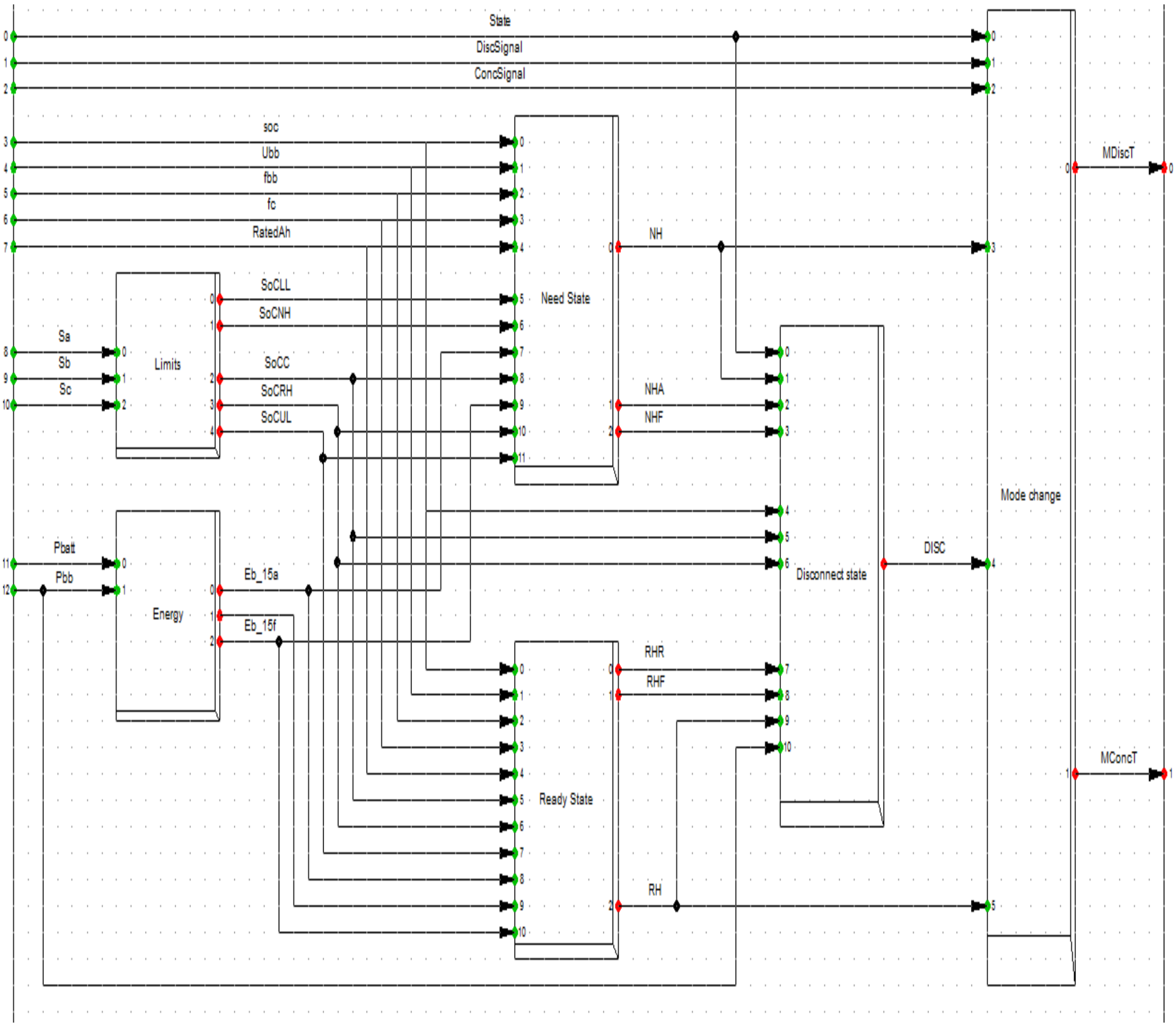


Decision frame comprises of

1) Limits – Defines all the required limits for defining the Need Help, Ready Help and Disconnect variables
2) Energy – Calculates the moving average of the past and forecasted energy absorbed/consumed by the BESS
3) Need State – Signifies the Need Help (NH) state of Cell with NH flow diagram
4) Ready State – Signifies the Ready Help (RH) state of Cell with RH flow diagram
5) Disconnect State – Signifies the Disconnect (DISC) state of Cell with DISC flow diagram
6) Mode Change – Creates ConcEnable (MConcT) signal for high NH and RH values and DiscEnable (MDiscT) signal for high DISC values. This triggers the Connection and Disconnection controllers in controller frame and prepares Cell for seamless transfer between SA and IC modes